Analysis of Dual Loop Parabolic Trough Concentrating Solar Power Plants

By

Joseph R. Shinners

A thesis submitting in partial fulfillment of

the requirements for the degree of

MASTER OF SCIENCE
(MECHANICAL ENGINEERING)

at the

UNIVERSITY OF WISCONSIN-MADISON

2014

Approved by

Professor Franklin Miller

December 15th, 2014

Abstract

Concentrating solar power plants utilizing parabolic troughs currently utilize organic heat transfer fluids, such as Dowtherm A, for thermal energy input to a steam Rankine power cycle. Organic heat transfer fluids have a temperature limit around 400°C because they begin to dissociate at higher temperatures. Molten salts are a potential substitute to organic heat transfer fluids, as they can reach higher temperatures without breaking down. Higher steam temperatures result in higher Rankine cycle efficiency. Although molten salts can reach higher temperatures, they also freeze at temperatures around 220°C. The time scale for freezing to occur in the heat collection element and other components connected to the heat collection element was modeled in EES (Engineering Equation Solver).

A proposal for a new parabolic trough power plant design is to utilize both Dowtherm A (an organic heat transfer fluid) and molten salt (60% $NaNO_3$ / 40% KNO_3). This system design would improve cycle efficiency through access to higher steam temperatures while mitigating the problems using molten salt by itself. To determine the viability of this system design this design was compared to two other systems, one that uses only Dowtherm A, and one that uses only molten salt (60% $NaNO_3$ / 40% KNO_3).

A design operating point for the Rankine was created for each of the three cycles in EES. After creating the design points for each cycle, off-design conditions were modeled in EES to account for performance changes in each cycle as a result of varying inputs including heat transfer fluid flow rate and temperature and cooling water flow rate and temperature. The off design models incorporated heat exchanger and turbine performance changes based on off design conditions. After creating off design models that captured these performance

changes, the inputs variables, including the heat transfer fluid flow rate and temperature and the cooling water flow rate and temperature, were correlated to the output variables, the net power, the heat transfer fluid return temperature, and the cooling water return temperature.

TRNSYS was used to simulate the annual performance of the three system designs (TRNSYS 2014). The location chosen for these simulations was Daggett, CA, which is the location of SEGs plant. The correlations for the power cycle models generated from EES were used to create components in TRNSYS to simulate the performance of the power cycles based on varying input values. Other components, such as a collector field model, a storage tank model, and cooling tower model, were used in conjunction with the power cycle. Annual simulations were run to compare the three cycles to determine the cycle with best performance.

Acknowledgements

I would first like to thank my two advisors, Dr. Franklin Miller and Dr. Sanford Klein. Your knowledge and your experience have been tremendously helpful and vital to my experience here. I have learned so much because of your dedication to teaching. I will always appreciate your willingness and openness to help me whenever I needed your advice. It has been an honor to be your student.

I want to thank the Dow Chemical Company for sponsoring my research. I have appreciated all of your input and insight into the project.

I would also like to thank all of my lab mates. My time in Madison has been amazing because I was able to spend it will all of you. I could not ask for better friends.

Finally, I want to thank my family. To my father Mike, my mother Lynne, and my brother Matthew, you are the inspiration for everything I do. I would not have made it here without your love and support.

This research was funded through Dow University Research Initiative Funding under project number 240705.

Table of Contents

List of Tables

x

List of Figures

Chapter 1 Introduction

1.1 Background and Literature Review

Concentrating solar thermal power plants utilize organic heat transfer fluids, such as Dowtherm A, to collect thermal energy in a collector field. The fluid is then heat exchanged with steam in a Rankine cycle to generate electrical energy. Organic fluids cannot tolerate temperatures above 400°C because hydrogen can dissociate from the fluid and migrate through the absorber pipe into the annular space between the absorber pipe and the glass envelope. Figure 1.1 is shown for reference (Solel UVAC 2004).

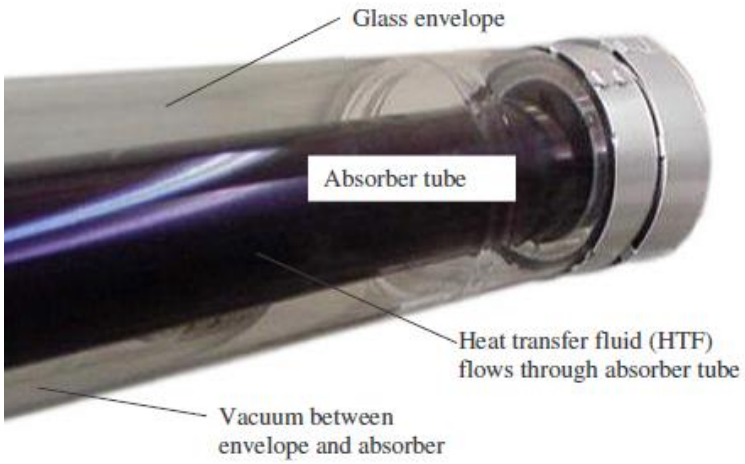

Figure 1.1 Heat Collection Element (HCE) (Solel UVAC 2004)

The presence of hydrogen in the annular space decreases the HCE performance significantly due to the free molecular flow that results from the presence of a minute amount of hydrogen in the vacuum space. A study of the effect of hydrogen in the vacuum space showed the efficiency of a heat collection element can decrease more than 15% (Forristall 2003). For this reason, it is important that organic heat transfer fluids operate at temperatures below

400°C in a parabolic trough collector field. Limiting the maximum temperature of the fluid limits the efficiency of the Rankine power cycle.

Molten salts can be used to reach higher temperatures than organic heat transfer fluids. They will not dissociate or break down at higher temperatures. However, molten salts freeze at relatively high temperatures (220°C). For this reason, the current literature states that the installation of resistance heat tracing is a permanent and necessary installation cost. Nitrate salts are the most popular choice for molten salts for collector field design because they have low corrosion rates with common piping materials, in addition to being thermally stable in higher temperature ranges (Kearney 2002). For this study, a nitrate salt (60% $NaNO_3$ / 40% KNO_3) is analyzed to see its viability as a heat transfer fluid. The mixture of sodium nitrate and potassium nitrate is chosen so that it has the lowest possible freezing temperature. This nitrate salt is ideal because it is low cost and available in large quantities ("Molten Salt Properties" 2014).

Due to the complications associated with both organic heat transfer fluids and molten salts, a system which utilizes both fluids has been proposed. The expectation of this system design is that the system could take advantage of the higher temperatures available to molten salt while mitigating the cost of heat tracing and corrosion resistance materials need when using molten salts.

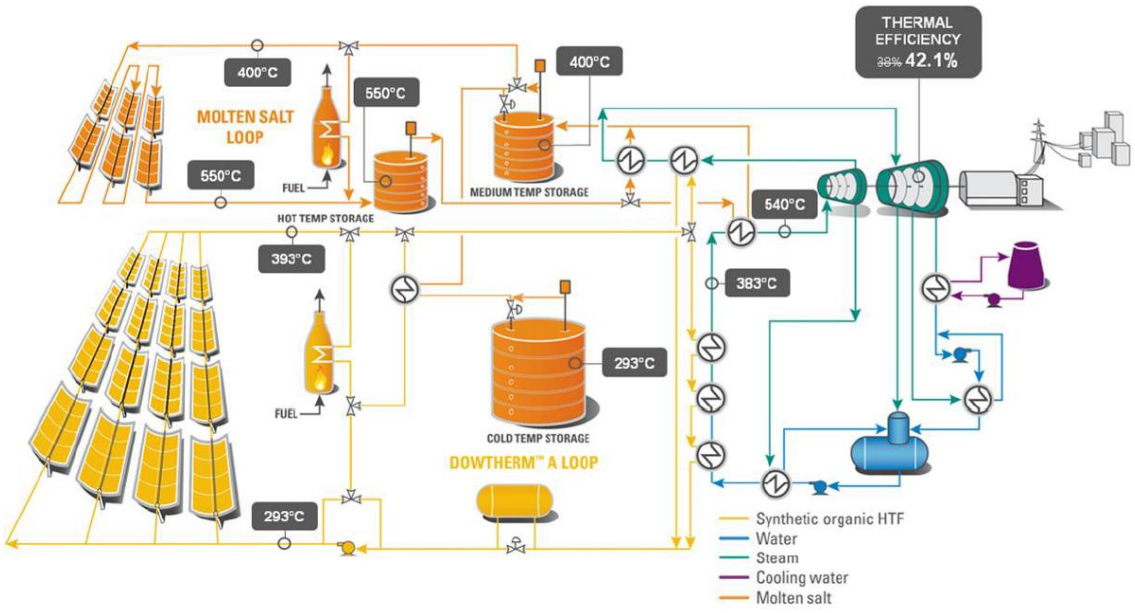

Figure 1.2 Dual Loop Design including molten salt thermal energy storage (Lang 2012)

Figure 1-2 is an example of the proposed dual loop system. The system was proposed by Lang and Cuthbert (2012). This system utilizes molten salt as thermal energy storage with no storage for the organic heat transfer fluid. Instead, the organic heat transfer fluid is heat exchanged with molten salt between the medium and cold storage tanks. In this case, molten salt is used as a thermal storage medium for both fluids. Natural gas is used as auxiliary heating to supplement the solar input. The study performed states that the thermal efficiency of the Rankine cycle can be increased to 42%. This is compared to the efficiency of a cycle that uses only organic heat transfer fluid, which is 38% (Lang 2012).

Another study analyzing the dual loop system corroborates the study by Lang and Cuthbert.

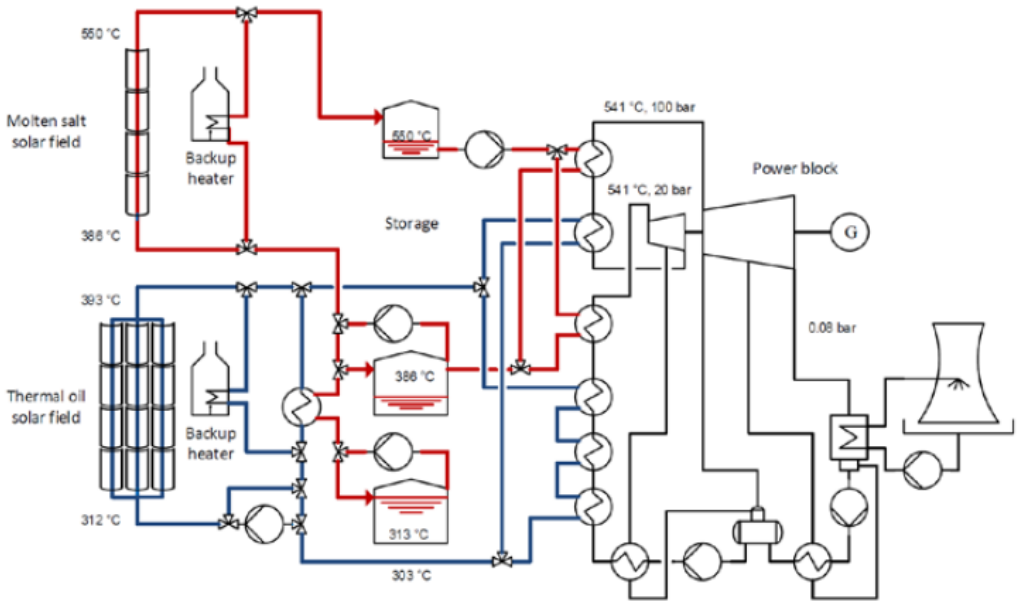

Figure 1.3 Schematic Flow Diagram of Dual Loop System (Vogel 2014)

The study by Vogel analyzing the dual loop system scores a mean power block efficiency of 41.87% compared to 37.21% for thermal oil (2014). The system design is similar to the design from Lang. The system utilizes three molten salt storage tanks, and natural gas auxiliary heating. Both of these studies claim an improvement to the power cycle efficiency to approximately 42%.

1.2 Objectives of current work

The use of molten salt as a heat transfer fluid in parabolic trough solar thermal power plants is the primary interest of this study. As stated in section 1.1, current literature claims that heat tracing is necessary in a parabolic trough system when utilizing molten salt. However, there is no estimate for the time scale for freezing to begin in the solar field. For this study, models were created in EES (Engineering Equation Solver) to determine the time scale for freezing to begin in components in the solar field. EES is a general equation solver that can solve thousands of coupled non-linear algebraic and differential equations and includes a

library of thermodynamic and transport properties of hundreds of substances (EES 2014). These models are described in Chapter 2.

The studies of dual loop systems utilizing molten salt and an organic heat transfer fluid claim a power cycle efficiency of approximately 42%. This is an improvement over the current systems utilizing only organic heat transfer fluids, which have a power cycle efficiency of approximately 38%. Models were created in EES to determine if these results could be replicated. Chapter 3 contains the description of a single loop of organic heat fluid system model and a dual loop system model at design conditions. The current studies do not analyze the power cycle efficiency associated with using a molten salt by itself; a single loop system utilizing only molten salt was also modeled to determine its power cycle efficiency at a design condition. In order to use these models in conjunction with a solar field, the performance of these cycles had to be analyzed for off-design conditions, which is described in Chapter 4.

Finally, the off-design models were used to create components in TRNSYS. TRNSYS is an extremely flexible graphically based software environment used to simulate the behavior of transient systems (2014). The power cycle components generated in Chapter 4 are coupled with a number of additional TRNSYS components, which are all described in Chapter 5. Using the entire solar field and power block models in TRNSYS, annual results were generated for the performance of each of the three cycles. These results are described in Chapter 6.

Chapter 2 Molten Salt Freezing

2.1 Introduction

An image of a parabolic trough concentrating solar collector is shown below in Figure 2.1.

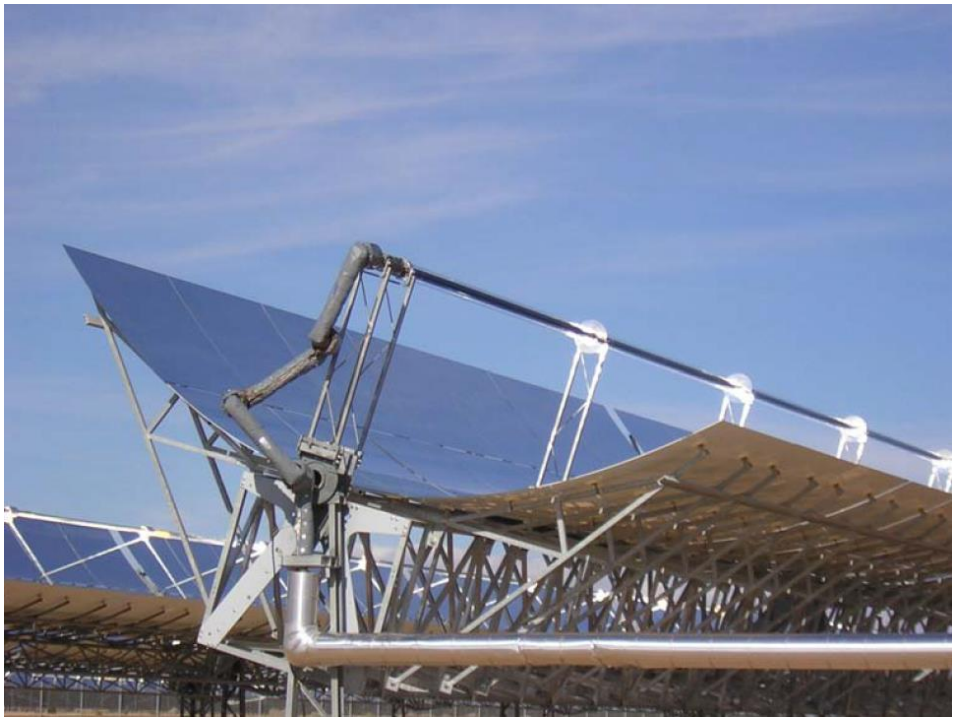

Figure 2.1 Parabolic Trough

A concern for using a molten salt as a Heat Transfer Fluid (HTF) is the potential of freezing during hours where there is no solar radiation. If molten salt froze inside the heat collection element (HCE), the salt would have to be melted before actual operation could resume. If freezing occurred inside any other element of the system, it would be much more difficult to melt the salt because it cannot be melted with solar radiation. For this reason, heat tracing is required on every element of the system other than the HCEs (Kearney 2002).

2.2 Freezing Model of Heat Collection Element

A model was created in order to generate a time scale for the freezing process, with the following assumptions. First, this cooling process occurs at night where no significant radiation will heat the HCE; therefore, there is no radiation transfer to the HCE. The HTF is not moving in the pipes, and the heat transfer in the direction of the flow is negligible. The heat transfer is uniform in the radial direction. A vacuum is present in the annular space between the glass and the absorber. The molten salt used for this model is a eutectic salt (60% $NaNO_3$ 40% KNO_3). This salt is specifically mixed to have a low freezing point at 220°C. Based on these assumptions, a diagram of the heat transfer model is shown in Figure 2.2.

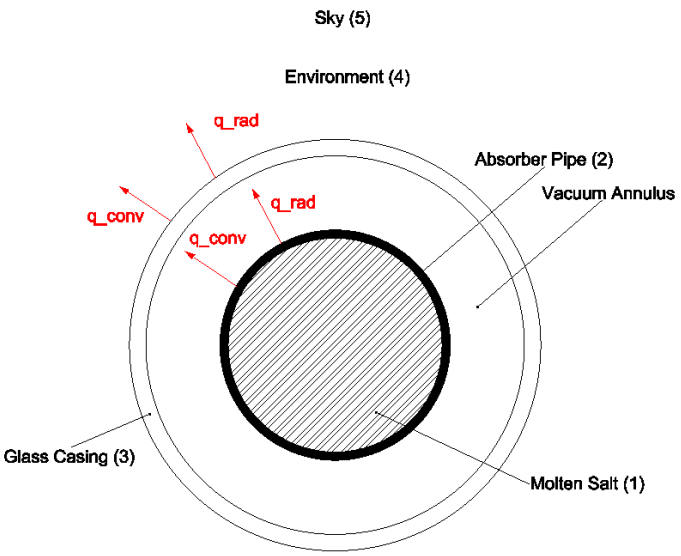

Figure 2.2 Cross-Section View of HCE

A numerical analysis was used to model the system in order to account for temperature-dependent property changes of the elements in the HCE. The density, conductivity, and specific heat capacity data for each element in the system are from EES (Engineering Equation Solver), and these data are found in Appendix A. The curve fits shown in the

Appendix are the curve fits used in the models described in this chapter. The molten salt was divided into elements in the radial direction, and an energy balance was carried out for each of the resulting nodes. The absorber pipe and glass casing were each considered to be one node. This assumption requires that the entire absorber pipe and the glass casing are spatially-uniform in temperature at any point in time. Therefore, this assumption neglects conduction resistance through the absorber pipe and the glass casing, which is justified due to the relatively high conductivity of each material. The derivation for the equations that determine the rate of temperature change of each node element is shown below.

The diagram representing the heat transfer control volume for the first node directly adjacent to the center of the molten salt is shown in Figure 2.3 For the simulations performed, the area of center is less than 0.07% of the total cross-sectional area of the salt. Therefore, the center of the molten salt is not included in this model. The center portion is small relative to the rest of the salt and, therefore, has low thermal energy relative to the rest of the salt. The radius of each node is the radius to the center of the node.

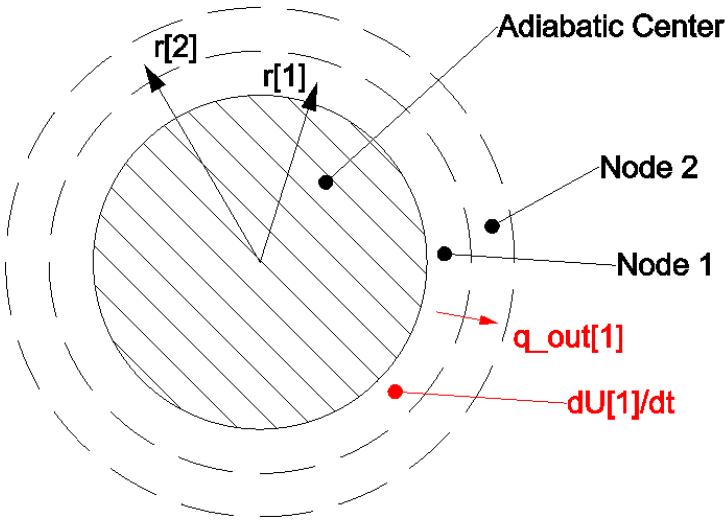

Figure 2.3 Node 1

The overall energy balance for all nodes is as follows:

$$\dot{q}_{in}[i] = \dot{q}_{out}[i] + \frac{dU[i]}{dt} \tag{2.1}$$

where "i" denotes the node, $\dot{q}_{in}[i]$ is the rate of heat transfer into the node, $\dot{q}_{out}[i]$ is the rate of heat transfer out of the node, and $\frac{dU[i]}{dt}$ is the rate of energy storage of the node.

For node 1, the following equations were used to find $\dot{q}_{in}[1]$, $\dot{q}_{out}[1]$, and $\frac{dU[1]}{dt}$:

$$\dot{q}_{in}[1] = 0 \tag{2.2}$$

$$\dot{q}_{out}[1] = 2\pi k_{salt}[1] \ln\left(\frac{r[1]}{r[2]}\right)(T[1] - T[2]) \tag{2.3}$$

$$\frac{dU[1]}{dt} = \rho_{salt}[1] c_{salt}[1] \left(\pi\left(r[1] + \frac{dr}{2}\right)^2 - \pi\left(r[1] - \frac{dr}{2}\right)^2\right)\left(\frac{dT[1]}{dt}\right) \tag{2.4}$$

where $k_{salt}[1]$, $\rho_{salt}[1]$, and $c_{salt}[1]$ are the conductivity, density, and specific heat capacity of the salt at node 1, respectively. These properties change with temperature and are calculated using the curve fits found in Appendix A.

A diagram representing the heat transfer for the control volume of node i, a node from 2 to the total number of nodes, N, minus 1 is shown below in Figure 2.4.

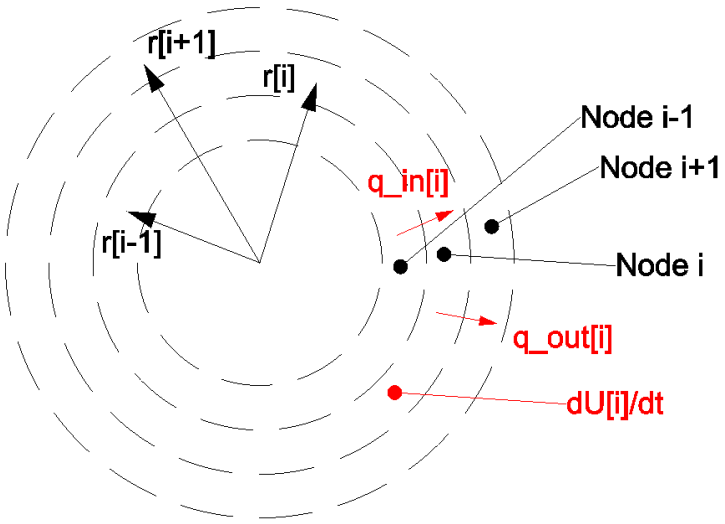

Figure 2.4 Node i

The equations to find the heat transfer in and out of node i, as well as the rate of energy storage in node i are as follows:

$$\dot{q}_{in}[i] = 2\pi k_{salt}[i] \ln\left(\frac{r[i-1]}{r[i]}\right)(T[i-1] - T[i]) \tag{2.5}$$

$$\dot{q}_{out}[i] = 2\pi k_{salt}[i] \ln\left(\frac{r[i]}{r[i+1]}\right)(T[i] - T[i+1]) \tag{2.6}$$

$$\frac{dU[i]}{dt} = \rho_{salt}[i] c_{salt}[i] \left(\pi\left(r[i] + \frac{dr}{2}\right)^2 - \pi\left(r[i] - \frac{dr}{2}\right)^2\right)\left(\frac{dT[i]}{dt}\right) \tag{2.7}$$

These terms are applied using Equation 2.1.

The outermost salt node, node N, and the absorber pipe are shown below in Figure 2.5.

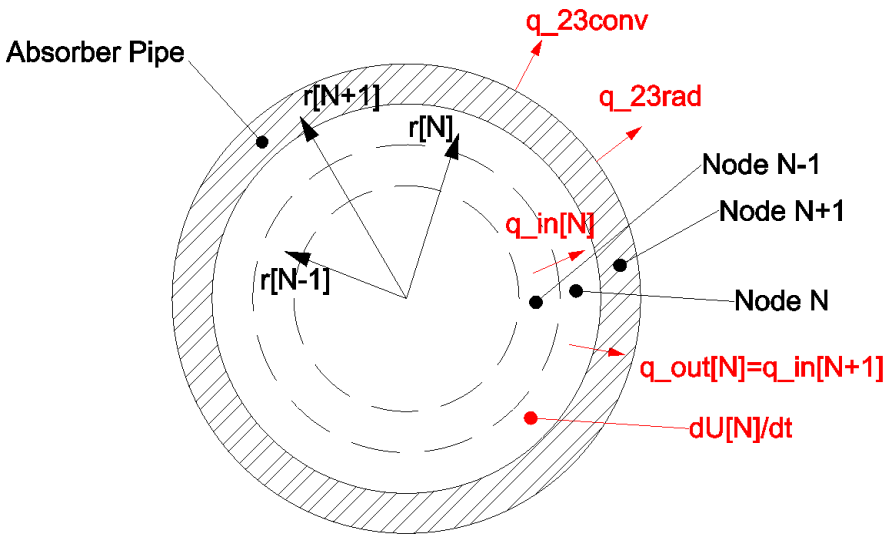

Figure 2.5 Node N and Absorber Pipe

The equations to find the heat transfer into and out of node N and N+1, the absorber pipe, as well as the rate of energy storage in each element are as follows:

$$\dot{q}_{in}[N] = 2\pi k_{salt}[N] \ln\left(\frac{r[N-1]}{r[N]}\right)(T[N-1] - T[N]) \tag{2.8}$$

$$\dot{q}_{in}[N+1] = \dot{q}_{out}[N] = \left(\frac{2\pi k_{salt}[N]}{\ln\left(\frac{r[N]+\frac{dr}{2}}{r[N]}\right)} + \frac{2\pi k_{abs}[N+1]}{\ln\left(\frac{r[N+1]}{r[N]+\frac{dr}{2}}\right)}\right)(T[N] - T[N+1]) \tag{2.9}$$

$$\frac{dU[N]}{dt} = \rho_{salt}[N]c_{salt}[N]\left(\pi\left(r[N]+\frac{dr}{2}\right)^2 - \pi\left(r[N]-\frac{dr}{2}\right)^2\right)\left(\frac{dT[N]}{dt}\right) \tag{2.10}$$

$$\frac{dU[N+1]}{dt} = \rho_{abs}[N+1]c_{abs}[N+1](\pi r_{out}^2 - \pi r_{in}^2)\left(\frac{dT[N+1]}{dt}\right) \tag{2.11}$$

$$\dot{q}_{out}[N+1] = \dot{q}_{23rad} + \dot{q}_{23conv} \tag{2.12}$$

k_{abs}, ρ_{abs}, and c_{abs} are the conductivity, density, and specific heat capacity of the absorber material, respectively. These properties are calculated using the thermophysical property data in EES for AISI302 stainless steel using the temperature of the node at the current time step. r_{out} and r_{in} are the outside and inside radii of the absorber pipe, respectively. q_{23rad} is the radiation heat transfer from the absorber pipe to the glass casing. q_{23conv} is the convective heat transfer from the absorber pipe to any gas that still may be present in the vacuum. Even with a vacuum, there is potential for some air to leak into the annular space. This effect is calculated using correlations found in Forristall (2002). The radiation heat transfer from the pipe to the glass is

$$\dot{q}_{23rad} = \frac{\sigma\pi D_{abs,out}\left(T_{abs}^4 - T_{glass}^4\right)}{\frac{1}{\varepsilon_{abs}} + \frac{\left(1-\varepsilon_{glass}\right)D_{abs,out}}{\varepsilon_{glass}D_{glass,in}}} \tag{2.13}$$

where T_{abs} is the absorber temperature, T_{glass} is the glass temperature, ε_{abs} is the emissivity of the absorber, ε_{glass} is the emissivity of the glass, $D_{abs,out}$ is the outside diameter of the absorber, and $D_{glass,in}$ is the inside diameter of the glass. The convective heat transfer from the absorber is defined by equation 2.14.

$$\dot{q}_{23conv} = \pi D_{abs,out} h_{vac}\left(T_{abs} - T_{glass}\right) \tag{2.14}$$

where h_{vac} is the heat transfer coefficient for the annulus gas present in the vacuum. The value for this coefficient was taken from Forristall's analysis and is included in Table 2.1 HCE parameters. It is the value for the heat transfer coefficient based on very small pressure present in the annulus (<0.0001 torr).

The diagram representing the heat transfer for the glass is shown below in Figure 2.6.

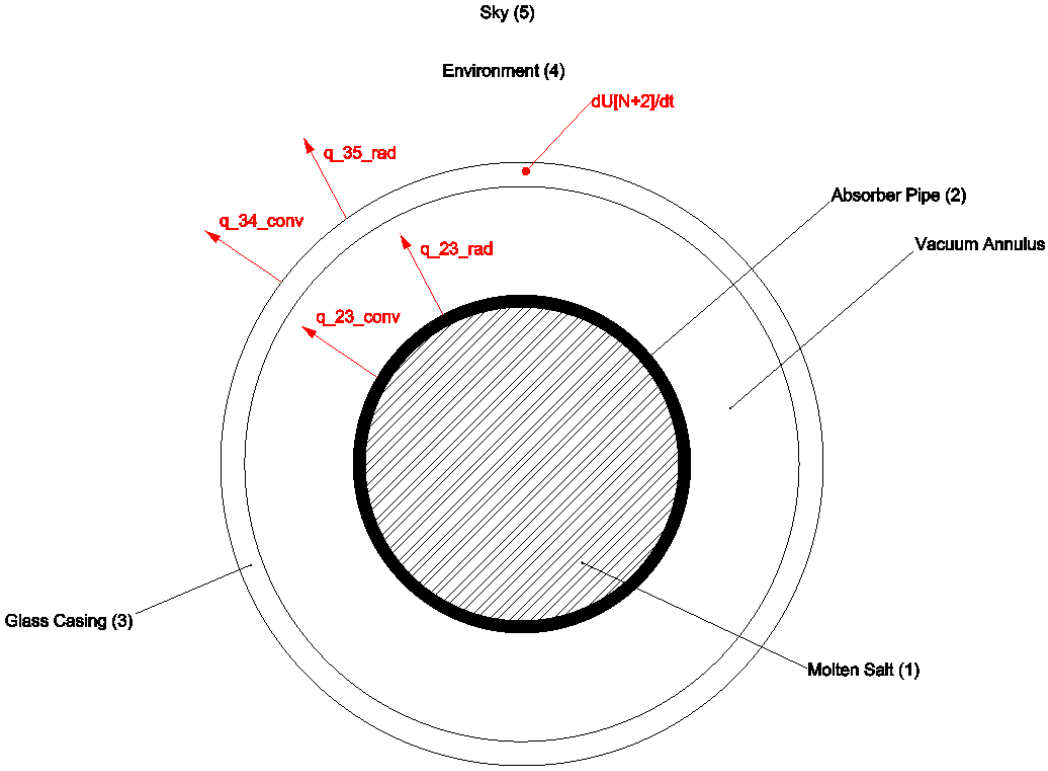

Figure 2.6 Heat Transfer for Glass Casing

The rate of heat transfer into and out of the glass, as well as the rate of thermal energy storage are provided in Equations 2.15-2.17.

$$\dot{q}_{in}[N+2] = \dot{q}_{23rad} + \dot{q}_{23conv} \tag{2.15}$$

$$\dot{q}_{out}[N+2] = \dot{q}_{34conv} + \dot{q}_{35rad} \tag{2.16}$$

$$\frac{dU[N+2]}{dt} = \rho_{glass}[N+2]c_{glass}[N+2]\left(\pi r_{glass,out}^2 - \pi r_{glass,in}^2\right)\left(\frac{dT[N+2]}{dt}\right) \tag{2.17}$$

k_{glass}, ρ_{glass}, and c_{glass} are the conductivity, density, and specific heat capacity of the glass casing, respectively. These properties are calculated using the thermophysical property data

in EES for Pyrex Glass using the temperature of the node at the current time step. $r_{glass,out}$ and $r_{glass,in}$ are the outside and inside radii of the glass casing, respectively. The values for the radii used are found in Table 2.1. q_{35rad} is the radiation heat transfer from the glass casing to the sky. q_{34conv} is the convective heat transfer from the glass casing to the surrounding air. The heat transfer rates q_{35rad} and q_{34conv} were calculated using the radiative and convective heat transfer relations given by Equations 2.18 and 2.19.

$$\dot{q}_{35rad} = \varepsilon_{glass}\sigma\pi D_{glass,out}\left(T_{glass}^4 - T_{sky}^4\right) \tag{2.18}$$

$$\dot{q}_{34conv} = h_{air}\pi D_{glass,out}\left(T_{glass} - T_{amb}\right) \tag{2.19}$$

T_{sky} is the effective sky temperature, and h_{air} is the heat transfer coefficient between the glass and the ambient air. This value was calculated using the heat transfer correlation for external flow around a cylinder found in EES. The external flow procedure in EES uses the Churchill and Bernstein correlation (1977). The heat transfer coefficient was calculated for various wind speeds. Different scenarios illustrating the effect with and without the presence of wind on the model will be shown in section 2.3.

The parameters for the HCE are tabulated in Table 2.1 (Buckholder 2009).

Table 2.1 HCE Parameters

Parameter	Description	Value	Additional Information
$D_{abs,in}$	Inside Absorber Diameter	.065 [m]	-
$D_{abs,out}$	Outside Absorber Diameter	.070 [m]	-
$D_{glass,in}$	Inside Glass Diameter	.115 [m]	-
$D_{glass,out}$	Outside Glass Diameter	.125 [m]	-
T_{amb}	Ambient Temperature	16.9 [°C]	-
T_{sky}	Effective Sky Temperature	8 [°C]	Parameter varied for Figure 2.7 and 2.8
T_{bulk}	Initial Bulk Temperature of Molten Salt	400 [°C]	Parameter varied for Figure 2.7 and 2.8
P_{atm}	Atmospheric Pressure	101.3 [kPa]	-
w_{speed}	Wind Speed	5 [m/s]	Parameter varied for Figure 2.7 and 2.8
h_{vac}	Heat Transfer coefficient between vacuum and absorber pipe	.0001115 [W/m^2-K]	-
ε_{glass}	Emissivity of glass	.9 [-]	-
ε_{abs}	Emissivity of absorber	.11 [-]	-

Other values, such as conductivity, density, specific heat capacity, etc. were assumed to change with temperature. These values were found using the thermophysical property data found in EES. In the case of the molten salt, the temperature range of the property data did not include values slightly above freezing. Therefore, the data were curve fit, and these values were extrapolated from the curve fit. The curve fits can be found in Appendix A.

2.3 HCE Freezing Model Plots

Using this model, the temperature of the molten salt at the inside surface of the absorber pipe (Node N) was plotted against time. This temperature was critical because the salt closest to the edge of the pipe would be the first to freeze. The first plot is shown in Figure 2.7.

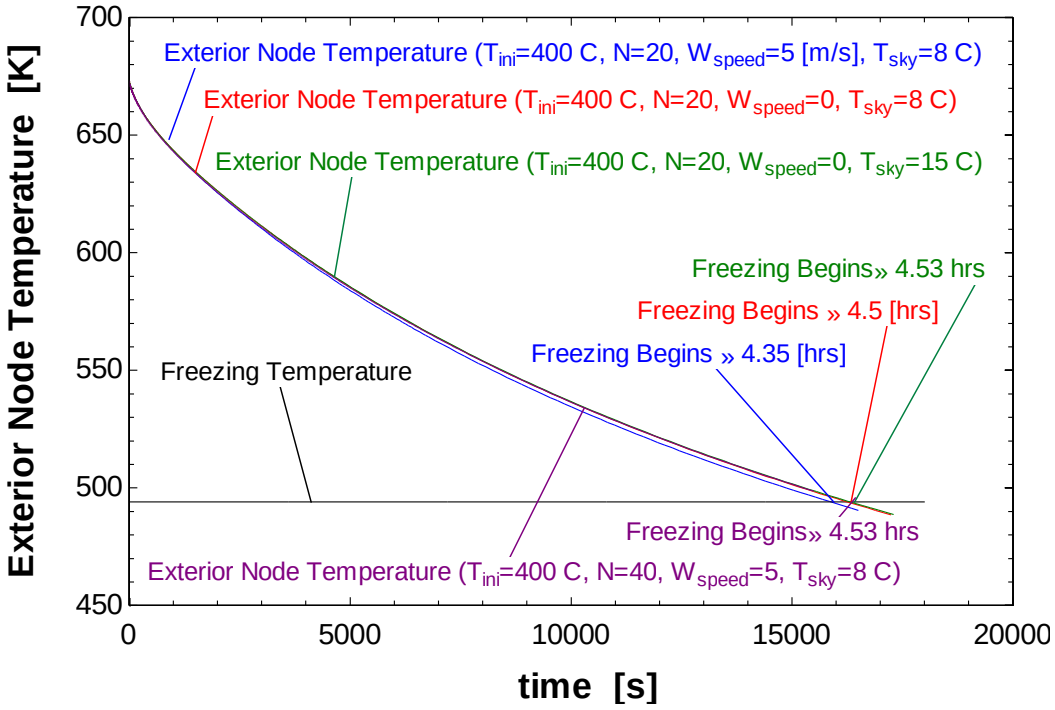

Figure 2.7 Exterior Node Temperature vs. Time with Initial Temperature of 400°C (HCE)

Four curves have been plotted together in this figure. In every case, the initial temperature was 400°C. The first curve is the temperature of the exterior node with the wind speed at 5 m/s and an effective sky temperature of 8°C, and the time it takes for freezing to begin is approximately 4.35 hours. The second curve is the temperature of the exterior node with no wind and an effective sky temperature of 8°C, and the time it takes for freezing to begin is approximately 4.5 hours. The third curve is the temperature of the exterior node with the no wind and an effective sky temperature of 15°C, and the time it takes for freezing to begin is approximately 4.53 hours. The final curve is the temperature of the exterior node with the wind speed at 5 m/s and an effective sky temperature of 8°C. The final curve represents a simulation with 40 nodes instead of 20, and the time it takes for freezing to begin is approximately 4.53 hours. Figure 2.8 shows the same conditions with an initial molten salt temperature of 550°C. The curves superimpose over one another because varying the

conditions and number of nodes does not strongly affect the time to reach the freezing temperature.

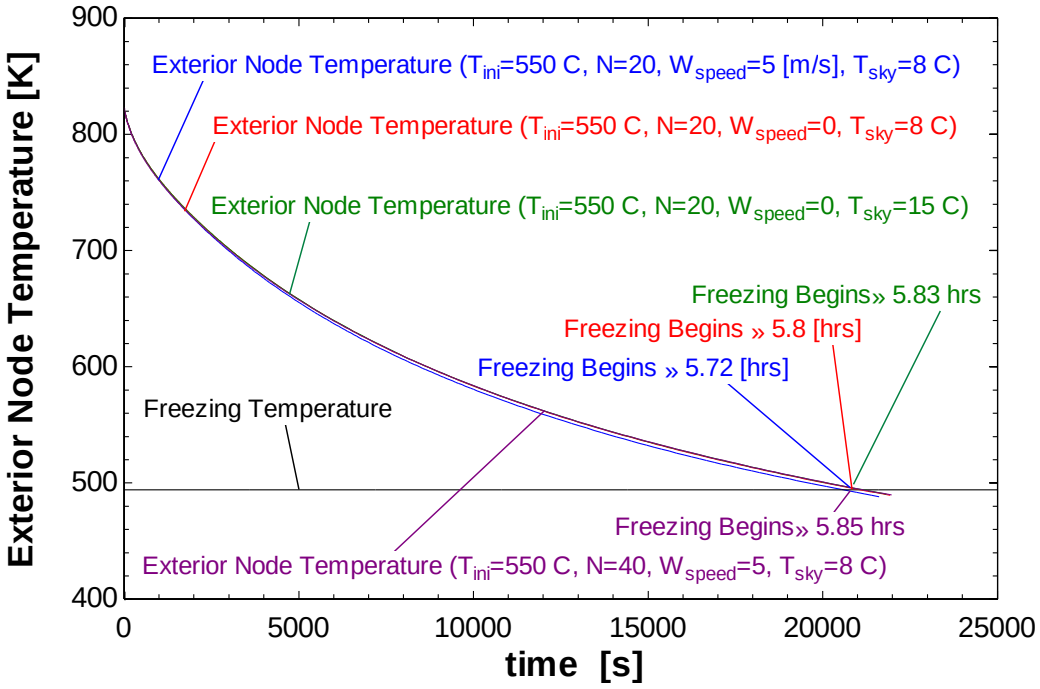

Figure 2.8 Exterior Node Temperature vs. Time with Initial Temperature of 550°C (HCE)

As with Figure 2.7, the wind speed and effective sky temperature were altered to generate three separate curves. The approximate amount of time needed for freezing to begin is 5.8 hours when the initial temperature is 550°C. In both cases, it is probable that molten salt will freeze in the HCE overnight. The initial temperature, wind speed, and sky conditions are all unimportant factors.

It is important to note that this model is not designed to determine temperatures once freezing begins due to latent heat effects and substantial property changes of the salt. However, for most salts in the solid phase, their thermal conductivity is on the order of 10^1. For (60% $NaNO_3$ 40% KNO_3) in the liquid phase, the thermal conductivity is roughly 0.5 [W/m-K], which means that the conductivity will increase by at least one order of magnitude.

Therefore, once freezing begins in the pipe, the temperature of the salt should decreases more rapidly.

2.4 Freezing Model of Return Pipe

Another element in the system where freezing is a concern is the return pipe shown in Figure 2.1. Since the HTF does not need to absorb energy in this element of the system, the advantage for this element is the presence of insulation between the absorber tube and the outside casing. This advantage also creates an issue because, unlike the HCE, if the molten salt freezes overnight, it cannot be melted by solar radiation.

A diagram of the heat transfer mechanisms acting on the pipe are shown below in Figure 2.9.

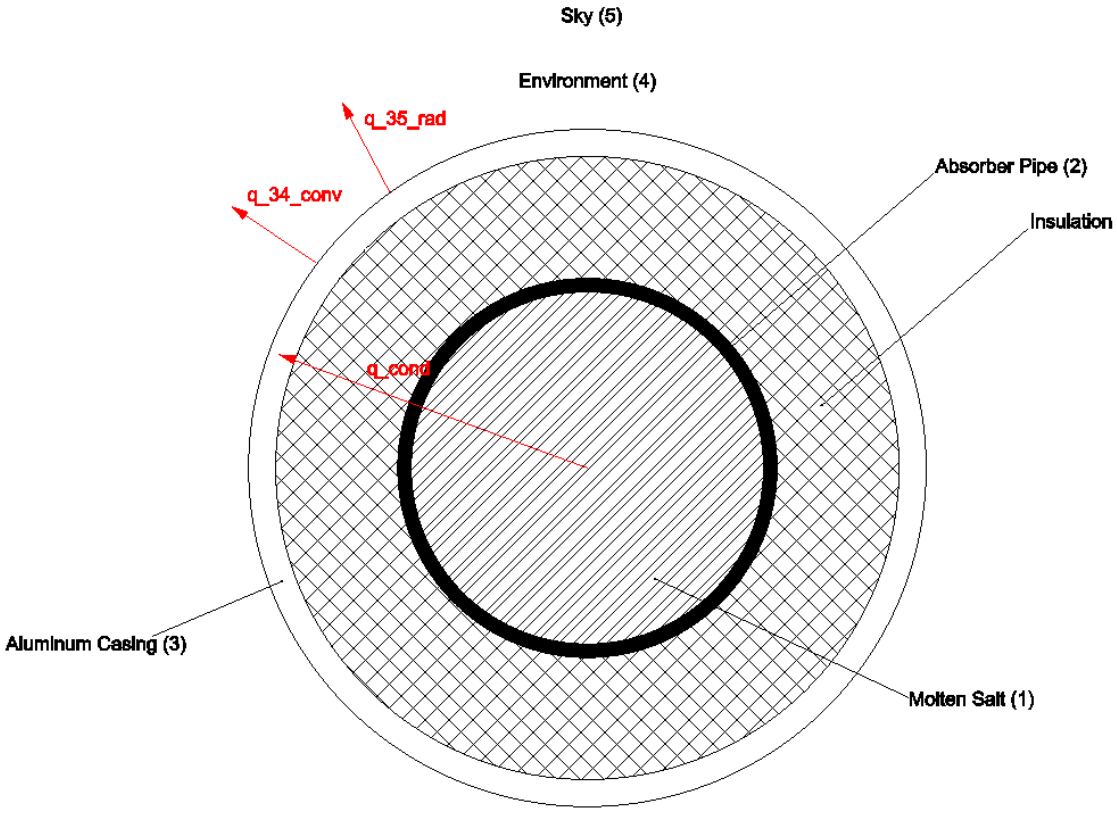

Figure 2.9 Return Pipe

A model for this element of system was created that was similar to the model for the HCE. The pipe was broken into nodes. Much like the HCE, the absorber pipe and the aluminum casing were both assigned one node, so the conduction through the absorber pipe and conduction through the aluminum casing were both ignored. The model assumes that the cooling process occurs at night when there is no significant radiation absorbed by the pipe. In addition, just as in the HCE model, the molten salt is not moving in the pipe.

The overall energy balance found in Equation 2.1 is applicable to this model. In addition, Equations 2.2 through 2.11 are also used for this model. The first change occurs for the heat transfer from node N+1, the absorber pipe to node N+2, the first insulation node. A diagram illustrating the heat transfer between these two nodes is shown in Figure 10.

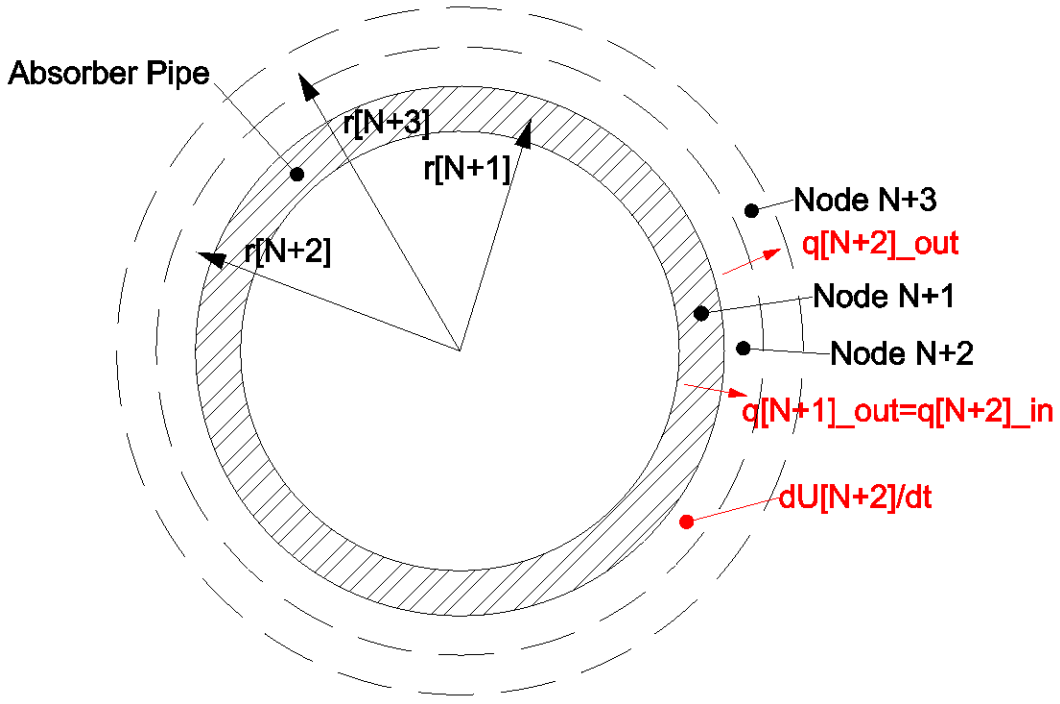

Figure 2.10 Insulation Node N+2

The equations for the heat transfer rates in and out of node N+2, as well as, the rate of thermal energy storage are as follows:

$$\dot{q}_{in}[N+2] = \dot{q}_{out}[N+1] = \left(\frac{2\pi k_{abs}[N+1]}{\ln\left(\frac{r_{abs,out}}{r[N+1]}\right)} + \frac{2\pi k_{ins}[N+2]}{\ln\left(\frac{r[N+2]}{r_{abs,out}}\right)} \right) (T[N+1] - T[N+2]) \tag{2.20}$$

$$\dot{q}_{out}[N+2] = \frac{2\pi k_{ins}[N+2]}{\ln\left(\frac{r[N+3]}{r[N+2]}\right)} (T[N+2] - T[N+3]) \tag{2.21}$$

$$\frac{dU[N+2]}{dt} = \pi \rho_{ins}[N+2] c_{ins}[N+2] \left(\left(r[N+2] + \frac{dr}{2} \right)^2 - \left(r[N+2] - \frac{dr}{2} \right)^2 \right) \left(\frac{dT[N+2]}{dt} \right) \tag{2.22}$$

k_{ins}, ρ_{ins}, and c_{ins} are the conductivity, density, and specific heat capacity of the insulation, respectively. The data and curve fit to the data for the conductivity of the insulation is found in Appendix A. The density of the insulation and specific heat are assumed to be constant at 145 kg/m^3 and 840 J/kg-K, respectively (EES 2014). The distance between nodes, dr, is not necessarily the same for the insulation as the molten salt, which is accounted for in the model. The distance between the nodes for molten salt and insulation depends on the number of nodes in each substance.

The heat transfer rates and the rate of thermal energy storage of the interior nodes for the insulation are characterized by equations 2.5 through 2.7, except that the conductivity, density, and specific heat capacity are that of the insulation rather than the salt. The diagram

for the heat transfer mechanisms for final insulation node and the aluminum casing is shown below in Figure 2.11.

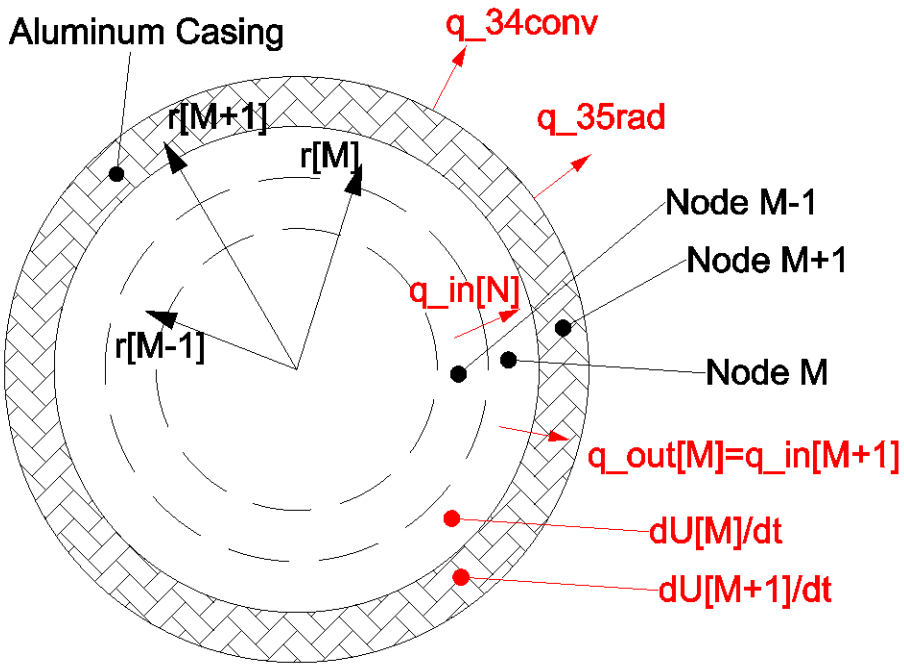

Figure 2.11 Exterior Insulation Node and Aluminum Casing

The equations that characterize each of the heat transfer rates shown in Figure 2.11 follow.

$$\dot{q}_{in}[M] = \frac{2\pi k_{ins}[M]}{\ln\left(\frac{r[M]}{r[M-1]}\right)}(T[M-1] - T[M]) \tag{2.23}$$

$$\dot{q}_{in}[M+1] = \dot{q}_{out}[M] = \left(\frac{2\pi k_{ins}[M]}{\ln\left(\frac{r[M]+\frac{dr}{2}}{r[M]}\right)} + \frac{2\pi k_{cas}[M+1]}{\ln\left(\frac{r[M+1]}{r[M]+\frac{dr}{2}}\right)}\right)(T[M] - T[M+1]) \tag{2.24}$$

$$\frac{dU[M]}{dt} = \rho_{ins}[M]c_{ins}[M]\left(\pi\left(r[M]+\frac{dr}{2}\right)^2 - \pi\left(r[M]-\frac{dr}{2}\right)^2\right)\left(\frac{dT[M]}{dt}\right) \tag{2.25}$$

$$\frac{dU[M+1]}{dt} = \rho_{cas}[M+1]c_{cas}[M+1]\left(\pi r_{cas,out}^2 - \pi r_{cas,in}^2\right)\left(\frac{dT[M+1]}{dt}\right) \quad (2.26)$$

$$\dot{q}_{out}[M+1] = \dot{q}_{35rad} + \dot{q}_{34conv} \quad (2.27)$$

where k_{cas}, ρ_{cas}, and c_{cas} are the conductivity, density, and specific heat capacity of the aluminum casing, respectively. The data and curve fits to the data for the aluminum casing are found in Appendix A. $\dot{q}_{35rad}$ is the radiation heat transfer from the aluminum casing to the sky, and $\dot{q}_{34conv}$ is the convective heat transfer from the aluminum casing to the surroundings, which are characterized by the following equations:

$$\dot{q}_{35rad} = \varepsilon_{cas}\sigma\pi D_{cas,out}\left(T_{cas}^4 - T_{sky}^4\right) \quad (2.28)$$

$$\dot{q}_{34conv} = h_{air}\pi D_{cas,out}(T_{cas} - T_{amb}) \quad (2.29)$$

T_{sky} is the effective sky temperature, and h_{air} is the heat transfer coefficient between the glass and the ambient air. This value was calculated using the heat transfer correlation for external flow around a cylinder found in EES. The external flow procedure in EES uses the Churchill and Bernstein correlation (1977). This value was varied based on wind speed. Different scenarios illustrating the effect with and without the presence of wind on the model are shown in Figure 2.12 and Figure 2.13.

The parameters for the HCE are tabulated below in Table 2.2 Return Pipe Parameters.

Table 2.2 Return Pipe Parameters

Parameter	Description	Value	Additional Information
$D_{abs,in}$	Inside Absorber Diameter	.065 [m]	Parameter varied for Figure 2.12 and 2.13
$D_{abs,out}$	Outside Absorber Diameter	.070 [m]	Parameter varied for Figure 2.12 and 2.13
$D_{cas,in}$	Inside Case Diameter	.115 [m]	Parameter varied for Figure 2.12
$D_{cas,out}$	Outside Case Diameter	.125 [m]	Parameter varied for Figure 2.12
T_{amb}	Ambient Temperature	16.9 [°C]	-
T_{sky}	Effective Sky Temperature	8 [°C]	Parameter varied for Figure 2.12 and 2.13
T_{bulk}	Initial Bulk Temperature of Molten Salt	400 [°C]	Parameter varied for Figure 2.12 and 2.13
P_{atm}	Atmospheric Pressure	101.3 [kPa]	-
w_{speed}	Wind Speed	5 [m/s]	Parameter varied for Figure 2.12 and 2.13
ε_{cas}	Emissivity of case	.1 [-]	-

Other values, such as conductivity, density, specific heat capacity, etc. were assumed to change with temperature. These values were found using the thermophysical property data found in EES. The insulation chosen for this model was cellular glass.

2.5 Return Pipe Freezing Model Plots

Using this model, the temperature of the molten salt at the inside surface of the absorber pipe was plotted against time, which was designated by node N. Just as in the previous model, this temperature was critical because the salt closest to the edge of the pipe would be the first to freeze. The first plot is shown below in Figure 2.12.

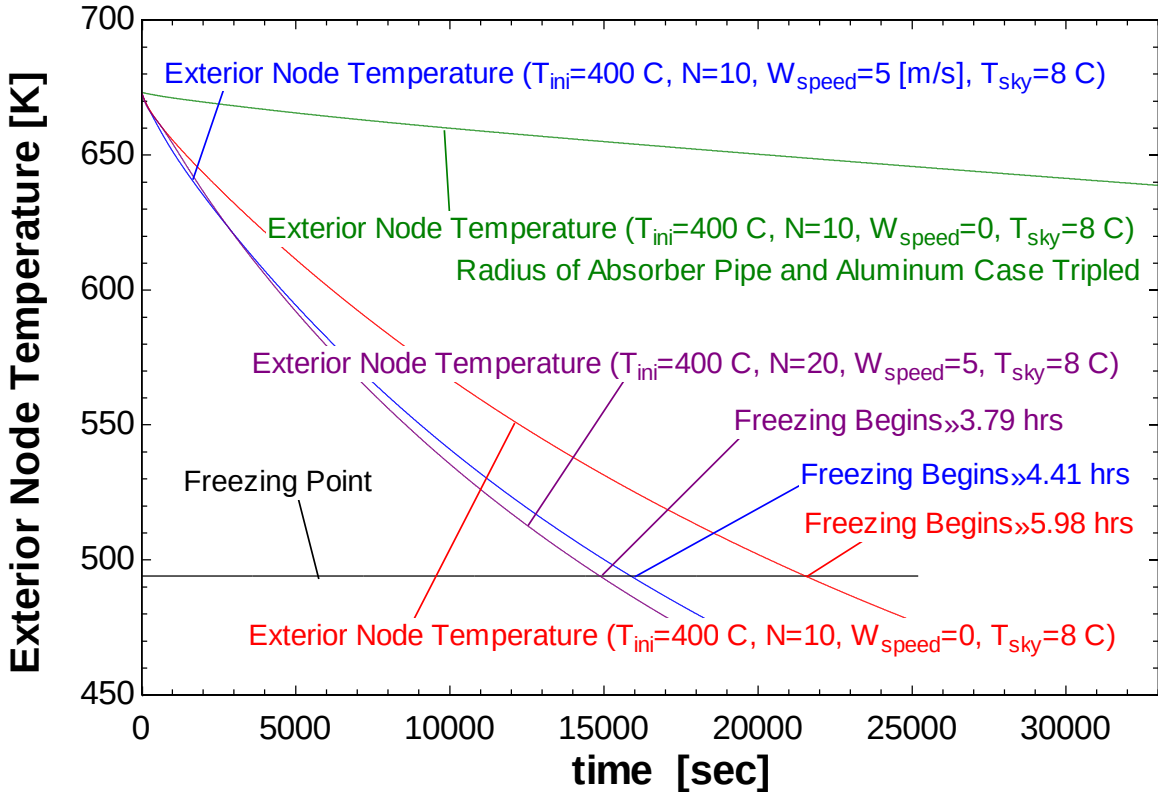

Figure 2.12 Exterior Node Temperature vs. Time with Initial Temperature of 400°C

Four curves have been plotted together in this figure. In every case, the initial temperature was 400°C. The first curve is the temperature of the exterior node with the wind speed at 5 m/s and an effective sky temperature of 8°C, and the time it takes for freezing to begin is approximately 4.41 hours. The second curve is the temperature of the exterior node with no wind and an effective sky temperature of 8°C, and the time it takes for freezing to begin is approximately 5.98 hours. The third curve is the temperature of the exterior node with the no wind and an effective sky temperature of 8°C, but the diameters of the absorber pipe and the aluminum casing are tripled. In this case, freezing does not occur overnight. The final curve shows the exterior node temperature when the number of nodes is doubled with the wind speed at 5 m/s and an effective sky temperature of 8°C. The time for freezing to begin is 3.79 hours.

Figure 2.13 shows the same conditions with an initial molten salt temperature of 550°C.

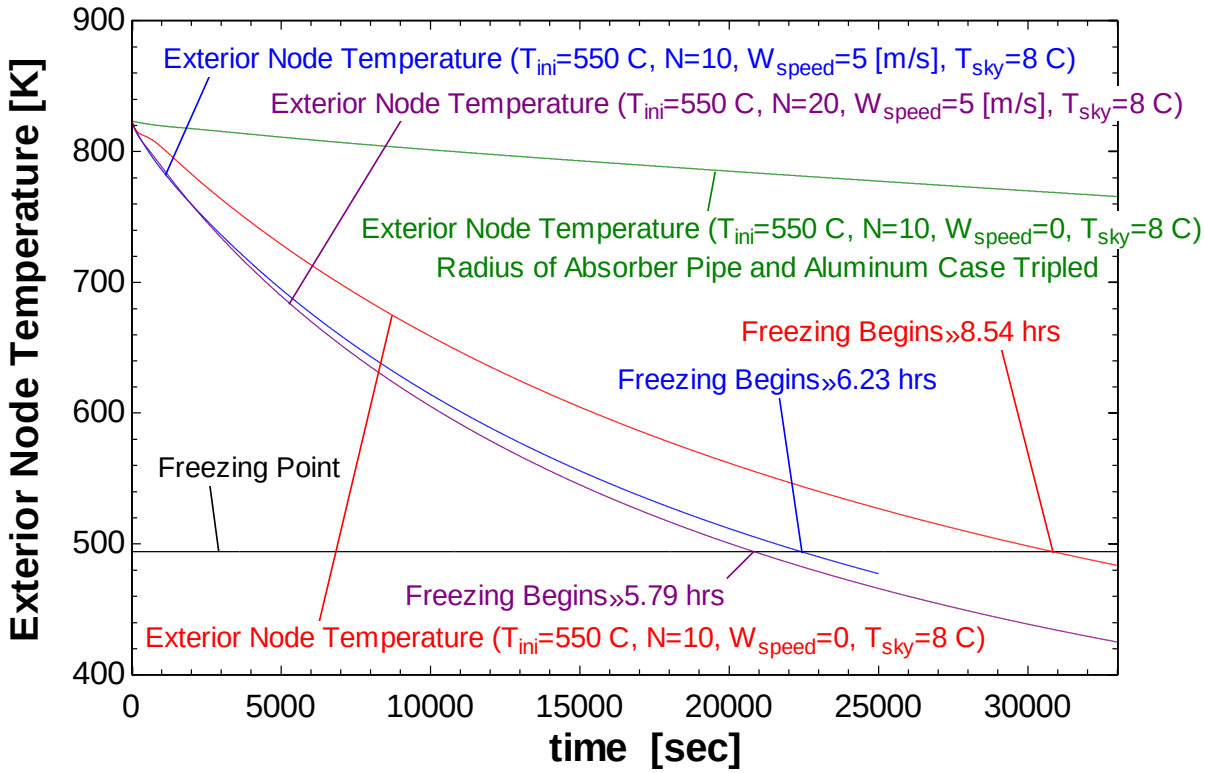

Figure 2.13 Exterior Node Temperature vs. Time with Initial Temperature of 550°C (Return Pipe)

As with Figure 2.12, the wind speed and effective sky temperature were altered to generate three separate curves. The approximate amount of time needed for freezing to begin is 6.23 hours when the initial temperature is 550°C. In both cases, it is probable that molten salt will freeze in the HCE overnight. From the return pipe model, it is clear that wind speed has a higher impact than in the HCE model. However, the change is not enough to disregard concern of overnight freezing. The pipe diameters, however, do play an extremely important role. As shown in Figure 2.12 and Figure 2.13, the molten salt did not begin to freeze when the diameters were tripled. In addition, increasing the number of nodes decreases the time to reach the freezing temperature. For the same conditions, the time to reach the freezing temperature decreases. The number of nodes could be increased for the other simulations,

but the conclusion remains the same. The time scale for freezing to begin for molten salt is only a matter of hours. This result confirms previous findings, which is that heat tracing or other means of melting solidified salt is an unavoidable cost when utilizing molten salt as a heat transfer fluid in a collector field.

Chapter 3 Rankine Power Cycle

3.1 Introduction

The standard power cycle used for electrical generation in both conventional and solar thermal power plants is the steam Rankine cycle. A schematic for the power cycle is shown in Figure 3.1. The heat transfer fluid that supplies energy to this cycle is Dowtherm A, which is a commercially available high temperature heat transfer fluid. This cycle will be used as a baseline comparison with a single loop cycle of molten salt and a dual loop cycle, which utilizes both Dowtherm A and molten salt.

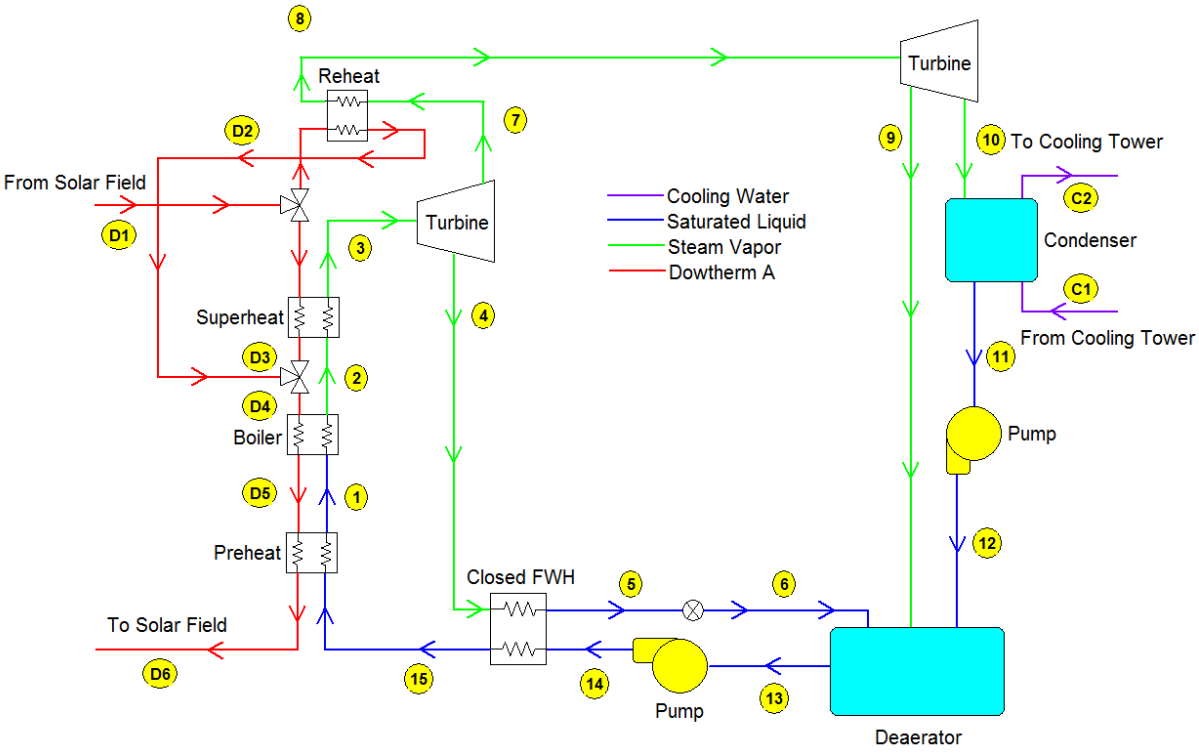

Figure 3.1 Rankine Power Cycle

3.2 Power Cycle Assumptions

The chapter describes the design point for the three cycles being analyzed. It does not include information about the performance of each cycle at conditions deviating from the design point. Off-design analysis will be shown in the next chapter. Several assumptions were made for the standard operational point for each cycle. These assumptions, which are commonly made in first-order analyses of these cycles (Patnode 2006) are as follows:

- The water exiting the preheater (closed feed water heater in the case of the single loop of molten salt or dual loop) is saturated liquid (x=0).
- The water exiting the boiler is saturated vapor (x=1).
- The water exiting the deaerator is saturated liquid (x=0).
- The water exiting the condenser is saturated liquid (x=0).
- The water exiting the closed feed water heater is saturated liquid (x=0).
- The pressure drop across any heat exchanger is negligible.

A design condition for a nominal 30 MW plant was identified by selecting a set temperature and mass flow rate for the heat transfer fluid as well as a set temperature and mass flow rate for the cooling liquid. These values are shown in Table 3.1. The values for the mass flow rate and boiler pressure and all other pressures are determined by varying the boiler pressure to find an optimum efficiency, which will be discussed later. The design inlet temperature of the Dowtherm A is the same value used in the analysis by the Lang (2012). At any state for the cycle, the properties of steam and Dowtherm A are calculated using the governing equations discussed in the following sections. Additional properties are calculated using the 'Steam_IAPWS' properties relations in EES (Engineering Equation Solver). The programs

used to generate these design points are included in the electronic supplement to this document.

Table 3.1 Design Points

Parameter	Description	Value
T_{HTF}	Inlet Dowtherm A Temperature	393 [°C]
$\dot{m}_{HTF}$	Inlet Dowtherm A mass flow rate	384 [kg/s]
P_{HTF}	Dowtherm A Pressure	150 [kPa]
T_{cw}	Inlet cold water Temperature	25 [°C]
$\dot{m}_{cw}$	Inlet cold water mass flow rate	1400 [kg/s]
P_{boiler}	Boiler Pressure	11000 [kPa]
P_{bleed_1}	1st Turbine Bleed Off Pressure	3125 [kPa]
P_{out}	Pressure at outlet of Turbine 1	2800 [kPa]
P_{bleed_2}	2nd Turbine Bleed Off Pressure	650 [kPa]
$\varepsilon_{turbine}$	Isentropic Turbine Efficiency	0.85
ε_{pump}	Isentropic Pump Efficiency	0.65
f_{super}	Mass fraction of HTF sent to superheater	0.60
PPT_{super}	Pinch point Temperature Difference at hot end of superheater	20 [K]
PPT_{re}	Pinch point Temperature Difference at hot end of reheater	40 [K]
PPT_{boiler}	Pinch point Temperature Difference at cold end of boiler	10 [K]
PPT_{CFWH}	Pinch point Temperature Difference at hot end of closed feed water heater	20 [K]
$PPT_{Condense}$	Pinch point Temperature Difference at cold end of Condenser	10 [K]
$\dot{W}_{net}$	Design Power Output	30 [MW]

3.3 Superheater

The heat transfer fluid (HTF) stream coming from the solar field is split in two streams. One stream goes to the superheater and the other goes to the reheater after the first turbine, as shown in Figure 3.1. All of the heat exchangers are assumed to be counterflow heat exchangers. Using the design mass flow rate and temperature of the HTF, as well as the

conditions after the boiler (assuming saturated vapor at the boiler pressure), the heat transfer in the superheater was determined. The transport properties of steam are assumed to be constant in the superheater at the average temperature of the steam determined with Equation 3.1.

$$T_{avg,steam} = \frac{T_2 + T_3}{2} \tag{3.1}$$

The transport properties of the Dowtherm A are also assumed to be constant in the superheater; therefore, the average temperature is calculated to evaluate the properties in the superheater.

$$T_{avg,HTF} = \frac{T_{D1} + T_{D3}}{2} \tag{3.2}$$

The capacitance rate of the steam is the product of the mass flow rate of the steam and the specific heat capacity of the steam. The mass flow rate of steam is determined from the equations in the boiler, which is shown in section 3.6. The specific heat capacity of the steam in the superheater is determined using the "CP" function in EES.

$$\dot{C}_{cold} = \dot{m}_{steam} c_p\left('Steam_{IAPWS}', T = T_{avg,steam}, P = P_{boiler}\right) \tag{3.3}$$

Similar to equation 3.3, the capacitance rate of the Dowtherm A is calculated from the mass flow rate of the Dowtherm A and the specific heat capacity of the Dowtherm A. The mass flow rate of the Dowtherm A is specified in Table 3.1, and the specific heat capacity is calculated using the "CP" function in EES.

$$\dot{C}_{hot} = \dot{m}_{HTF} c_p\left('Dowtherm'_A, T = T_{avg,HTF}, P = P_{HTF}\right) \tag{3.4}$$

The minimum capacitance rate in the superheater is defined as the lowest capacitance of the two fluids in the superheater.

$$\dot{C}_{min} = Minimum\left(\dot{C}_{cold}, \dot{C}_{hot}\right) \tag{3.5}$$

The maximum capacitance rate in the superheater is defined as the highest capacitance of the two fluids in the superheater.

$$\dot{C}_{max} = Maximum\left(\dot{C}_{cold}, \dot{C}_{hot}\right) \tag{3.6}$$

$\dot{C}_r$ is the heat capacity ratio in the superheater, which is calculated as the ratio between the minimum and maximum capacitance rate.

$$\dot{C}_r = \frac{\dot{C}_{min}}{\dot{C}_{max}} \tag{3.7}$$

An overall UA (heat transfer coefficient-area product) for the superheater was determined as well as the design heat transfer rate, $\dot{Q}_{super}$, using a specified pinch point temperature difference at the outlet of the superheater,

$$PPT_{super} = T_{D1} - T_3 \tag{3.8}$$

The pinch point temperature difference is defined as the difference in temperature between the two fluids in a heat exchanger on the side of the heat exchanger where the temperatures are closest together. The pinch point temperature differences specified in Table 3.1 determine the value of the effectiveness of each heat exchanger, which must be between 0 and 1. The pinch point temperature differences also determine the value of the overall heat transfer coefficient for each heat exchanger. The overall heat transfer coefficients for the

single loop of Dowtherm A cycle will be compared to the values from Patnode (2006) model in Chapter 4. For the superheater, the pinch point temperature difference, PPT_{super}, is defined as the difference between the temperature of the inlet Dowtherm A and the steam exiting the superheater. The heat transfer in the superheater, $\dot{Q}_{super}$, is defined as the product of the mass flow rate of the steam and the specific enthalpy difference between the outlet and inlet steam. The values for the specific enthalpy of the steam at the inlet and outlet are calculated using the "ENTHALPY" function in EES.

$$\dot{Q}_{super} = \dot{m}_{steam}(h_3 - h_2) \tag{3.9}$$

The rate of heat transfer in the superheater is also the product of the mass flow rate of the Dowtherm A and the specific enthalpy difference between the inlet and outlet Dowtherm A.

$$\dot{Q}_{super} = \dot{m}_{HTF}(h_{D1} - h_{D3}) \tag{3.10}$$

The heat transfer in the superheater is also defined as the product of the heat exchanger effectiveness, the minimum capacitance rate, and the difference between the temperature of the hot inlet fluid and the temperature of the cold inlet fluid.

$$\dot{Q}_{super} = \varepsilon_{super}\dot{C}_{min}(T_{D1} - T_2) \tag{3.11}$$

The effectiveness of a counter flow heat exchanger is calculated using equation 3.12, if the heat capacity ratio is less than 1, which is the case for the superheater.

$$\varepsilon_{super} = \frac{1 - e^{-NTU_{super}(1-C_r)}}{1 - C_r e^{-NTU_{super}(1-C_r)}} \tag{3.12}$$

The number of transfer units for the superheater, NTU_{super}, is calculated using equation 3.13, which is the ratio of the overall heat transfer coefficient, UA_{super}, and the minimum capacitance rate.

$$NTU_{super} = \frac{UA_{super}}{\dot{C}_{min}} \tag{3.13}$$

3.4 1st Turbine

The steam exiting the superheater enters the first turbine. Each turbine in this design has two stages. At the end of the first stage of each turbine, a fraction of the steam is bled off for preheating liquid water in feedwater heaters. The power outputs from each stage of the first turbine as well as the properties after each stage of the turbine were calculated. For an ideal turbine, the specific entropy of the steam is constant.

$$s_{4,s} = s_3 \tag{3.14}$$

For an ideal turbine, the power is the product of the mass flow rate of the steam and the change in the specific enthalpy.

$$\dot{W}_{ideal} = \dot{m}_{steam}(h_3 - h_{4,s}) \tag{3.15}$$

An actual turbine does not perform with 100% efficiency and is not ideal. Therefore, the actual power is the product of the isentropic efficiency and the ideal power. $\varepsilon_{turbine}$ is the isentropic efficiency of the turbine, which is assumed to be 0.85. Fernandez lists turbine efficiencies as large as 90% in concentrating solar plants (2013). The only important factor in assuming a turbine efficiency in these systems is that the efficiency is the same for each of the three power cycles modeled.

$$\dot{W}_{actual} = \varepsilon_{turbine} W_{ideal} \tag{3.16}$$

The actual power can be used to calculate the actual enthalpy of the steam after the turbine using equation 3.17. Since the pressure on each side of the turbine is predetermined in Table 3.1, the properties of steam can be determined using the pressure and the enthalpy calculated from the turbine equations. These properties can be found using the thermophysical property functions in EES.

$$\dot{W}_{actual} = \dot{m}_{steam}(h_3 - h_4) \tag{3.17}$$

3.5 Reheat and Mix

The equations used to define the states after the reheater are the same as the equations used for the superheater. The outlet HTF from the reheater is reintroduced to the HTF (Heat Transfer Fluid) outlet from the super heater, which continues on to the boiler, as shown in Figure 3.1. The state points after the reheater and superheater are D2 and D3, respectively. These two HTF streams are mixed to state D4. Mass and energy balances are employed to find the outlet state properties of the mixer. Equation 3.18 is a mass balance on the heat transfer fluid entering the boiler. The sum of the mass flow rate coming from the superheater and the mass flow rate coming from the reheater is equal to the mass flow rate into the boiler, which is also equal to the mass flow rate incoming from the solar field.

$$\dot{m}_{HTF,out} = \dot{m}_{HTF,super} + \dot{m}_{HTF,re} \tag{3.18}$$

Equation 3.19 is an energy balance on the fluid streams previously described with the system being the control volume where streams D_2 and D_3 enter and D_4 exits. It is assumed that there are no sources of heat transfer to or from the system. Therefore, the energy of the fluid leaving must equal the energy of the fluids entering.

$$\dot{m}_{HTF,out} h_{D4} = \dot{m}_{HTF,super} h_{D3} + \dot{m}_{HTF,re} h_{D2} \tag{3.19}$$

After finding the enthalpy of the mixed Dowtherm A stream and assuming a negligible pressure drop, the temperature of the mixed Dowtherm A stream was determined using thermophysical property functions in EES.

3.6 Boiler

The stream of Dowtherm A from the superheater and reheater enters the boiler where the saturated liquid water is converted to saturated steam. Based on the assumptions listed in Section 3.2, there is only a phase change in the boiler at the design point; therefore, the temperature and pressure are constant as the water changes from liquid to vapor. Since the effective capacitance rate of the steam in the boiler is infinite, the minimum capacitance rate is due to the Dowtherm A. The properties of the Dowtherm A are assumed to be constant in the boiler; therefore, the average temperature is calculated to evaluate the properties in the boiler.

$$T_{avg,HTF} = \frac{T_{D4} + T_{D5}}{2} \tag{3.20}$$

The capacitance rate is calculated as the product of the mass flow rate of the Dowtherm A and the specific heat capacity of the Dowtherm A in the boiler.

$$\dot{C}_{min} = \dot{C}_{hot} = \dot{m}_{HTF} c_{p,Dowtherm} \tag{3.21}$$

A pinch point temperature difference was used for the boiler in the same fashion as before with the superheater and reheater. Since this temperature difference was fixed, and the states before and after the boiler are also fixed, the mass flow rate for the design condition is determined from standard counterflow heat exchanger relations. The pinch point temperature

difference is set on the cold end of the boiler. The value of the pinch point temperature difference is set based on the same characteristics described in section 3.3.

$$PPT_{boiler} = T_{D5} - T_1 \tag{3.22}$$

The rate of heat transfer in the boiler, $\dot{Q}_{boiler}$, is defined as the product of the mass flow rate of the steam and the specific enthalpy difference between the outlet and inlet steam. Since the pressure and temperature are not independent in a phase change process, the properties were determined using the pressure and

$$\dot{Q}_{boiler} = \dot{m}_{steam}(h_2 - h_1) \tag{3.23}$$

The heat transfer in the boiler is also defined as the product of the mass flow rate of the Dowtherm A and the specific enthalpy difference between the inlet and outlet Dowtherm. Since the specific enthalpy of the Dowtherm entering the boiler is determined from the superheater and the specific enthalpy of the Dowtherm A exiting is determined from the pinch point temperature difference, the heat transfer rate in the boiler, $\dot{Q}_{boiler}$, is determined directly from equation 3.24. In equation 3.23, the specific enthalpy of the water entering and exiting is known from the quality conditions specified in Table 3.1. Therefore, the mass flow rate of steam in the cycle is determined from this known information in equation 3.23.

$$\dot{Q}_{boiler} = \dot{m}_{HTF}(h_{D4} - h_{D5}) \tag{3.24}$$

The heat transfer rate in the boiler is also defined as the product of the heat exchanger effectiveness, the minimum capacitance rate, and the difference between the temperature of the hot inlet fluid and the temperature of the cold inlet fluid.

$$\dot{Q}_{boiler} = \varepsilon_{boiler}\dot{C}_{min}(T_{D4} - T_1) \tag{3.25}$$

The effectiveness of a heat exchanger with a heat capacity ratio equal to zero is calculated using equation 3.26. The heat capacity ratio is equal to zero for the boiler because the maximum capacitance rate is infinite because the water is undergoing a phase change.

$$\varepsilon_{boiler} = 1 - e^{-NTU_{boiler}} \tag{3.26}$$

The number of transfer units for the boiler, NTU_{boiler}, is calculated using equation 3.27, which is the ratio of the overall heat transfer coefficient, UA_{boiler}, and the minimum capacitance rate.

$$NTU_{boiler} = \frac{UA_{boiler}}{\dot{C}_{min}} \tag{3.27}$$

3.7 Preheater

After exiting the boiler, the Dowtherm A passes through the last heat exchanger, the preheater. The preheater is designed to heat the sub-cooled liquid water to saturation. The governing equations for the preheater are energy balances and heat exchanger rate equations. The transport properties of water are assumed to be constant in the preheater at the average temperature of the water. Equation 3.28 is used to find the average temperature of the water in order to determine those properties.

$$T_{avg,liquid} = \frac{T_1 + T_{15}}{2} \tag{3.28}$$

The transport properties of the Dowtherm A are also assumed to be constant in the preheater; therefore, the average temperature is calculated to evaluate the properties in the preheater.

$$T_{avg,HTF} = \frac{T_{D5} + T_{D6}}{2} \tag{3.29}$$

The capacitance rate is calculated based on the mass flow rate of the water and the specific heat capacity of the water. The mass flow rate of water is determined from the equations in the boiler.

$$\dot{C}_{cold} = \dot{m}_{steam} c_{p,steam} \tag{3.30}$$

The capacitance rate of the Dowtherm A is calculated from the mass flow rate of the Dowtherm A and the specific heat capacity of the Dowtherm A.

$$\dot{C}_{hot} = \dot{m}_{HTF} c_{p,Dowtherm} \tag{3.31}$$

The minimum capacitance rate in the superheater is defined as the lowest capacitance of the two fluids in the superheater.

$$\dot{C}_{min} = Minimum\left(\dot{C}_{cold}, \dot{C}_{hot}\right) \tag{3.32}$$

The maximum capacitance rate in the superheater is defined as the highest capacitance of the two fluids in the superheater.

$$\dot{C}_{max} = Maximum\left(\dot{C}_{cold}, \dot{C}_{hot}\right) \tag{3.33}$$

$\dot{C}_r$ is the heat capacity ratio in the superheater, which is calculated as the ratio between the minimum and maximum capacitance rate.

$$\dot{C}_r = \frac{\dot{C}_{min}}{\dot{C}_{max}} \tag{3.34}$$

The mass flow rate and outlet condition are predetermined for the preheater by the relations used to model the boiler and superheater. No pinch point temperature difference is used for the preheater due to the fact that the heat exchanger properties are restricted by the condition

that the water exiting the preheater has a quality equal to 1 at design conditions. Using the heat exchanger relations, an overall heat transfer coefficient for the preheater was determined for the preheater. The rate of heat transfer in the preheater, $\dot{Q}_{pre}$, is defined as the product of the mass flow rate of the water and the specific enthalpy difference between the outlet and inlet water.

$$\dot{Q}_{pre} = \dot{m}_{steam}(h_1 - h_{15}) \tag{3.35}$$

Assuming negligible jacket losses, the rate of heat transfer in the preheater is also defined as the product of the mass flow rate of the Dowtherm A and the specific enthalpy difference between the inlet and outlet Dowtherm A.

$$\dot{Q}_{pre} = \dot{m}_{HTF}(h_{D5} - h_{D6}) \tag{3.36}$$

The rate of heat transfer in the preheater is also defined as the product of the heat exchanger effectiveness, the minimum capacitance rate, and the difference between the temperature of the hot inlet fluid and the temperature of the cold inlet fluid.

$$\dot{Q}_{pre} = \varepsilon_{pre}\dot{C}_{min}(T_{D5} - T_{15}) \tag{3.37}$$

The effectiveness of a counter flow heat exchanger is calculated using equation 3.38, if the heat capacity ratio is less than 1, which is the case for the preheater.

$$\varepsilon_{pre} = \frac{1 - e^{-NTU_{pre}(1-C_r)}}{1 - C_r e^{-NTU_{pre}(1-C_r)}} \tag{3.38}$$

The number of transfer units for the preheater, NTU_{pre}, is calculated using equation 3.39, which is the ratio of the overall heat transfer coefficient, UA_{pre}, and the minimum capacitance rate.

$$NTU_{pre} = \frac{UA_{pre}}{\dot{C}_{min}} \tag{3.39}$$

3.8 2nd Turbine

The equations used for the second turbine are the same as the equations listed in Section 3.4. This turbine is assumed to have the same efficiency as the first, and there is one bleed-off line from the turbine containing steam that routes directly to the deaerator, as shown in Figure 3.1.

3.9 Condenser

The steam that continues through the second stage of the second turbine exits to the condenser. The fluid on the cooling side of the condenser is water. The temperature and mass flow rate of the cooling water are set for the design condition as specified in Table 3.1. These values were chosen to be the same as those used for the design condition for the SEGs plant in Daggett, CA (Patnode 2006). The overall heat transfer coefficient is calculated knowing these design criteria and the state of the saturated liquid based on the assumptions found in Section 3.2. The transport properties of the cooling water are assumed to be constant in the condenser at the average temperature of the water. Equation 3.40 is used to find the average temperature of the water in order to determine those properties.

$$T_{avg,cw} = \frac{T_{C1} + T_{C2}}{2} \tag{3.40}$$

The capacitance rate of the condensing steam is infinite. Therefore, the capacitance rate of the cooling water is the minimum capacitance rate in the condenser. The capacitance rate is calculated as the product of the mass flow rate of the cooling water and the specific heat capacity of the cooling water in the condenser.

$$\dot{C}_{min} = \dot{C}_{cold} = \dot{m}_{cw} c_p\left('Water', T = T_{avg,cw}, x = 0\right) \tag{3.41}$$

The pinch point temperature difference is set on the hot end of the condenser. The value of the pinch point temperature difference is set based on the same characteristics described in section 3.3.

$$PPT_{condense} = T_{11} - T_{C1} \tag{3.42}$$

The rate of heat transfer in the condenser, $\dot{Q}_{condense}$, is defined as the product of the mass flow rate of the steam and the specific enthalpy difference between the outlet and inlet steam. Since the pressure and temperature are not independent in a phase change process, only one of those properties can be used in the condenser. The other property used is the quality.

$$\dot{Q}_{condense} = \dot{m}_{steam}(h_{10} - h_{11}) \tag{3.43}$$

The rate of heat transfer in the condenser is also defined as the product of the mass flow rate of the cooling water and the specific enthalpy difference between the inlet and outlet cooling water. Since the temperature of the cooling water entering the condenser is determined from the Table 3.1 and the temperature of the cooling water exiting is determined from the pinch point temperature difference, the heat transfer rate in the condenser, $\dot{Q}_{condenser}$, is determined directly from equation 3.44. In equation 3.43, the quality of the water entering

and exiting is known from Table 3.1. Therefore, the only unknown variable is the condenser pressure, which is calculated from equations 3.43 and 3.44.

$$\dot{Q}_{condense} = \dot{m}_{cw}(h_{C2} - h_{C1}) \tag{3.44}$$

The heat transfer rate in the condenser is also defined as the product of the heat exchanger effectiveness, the minimum capacitance rate, and the difference between the temperature of the hot inlet steam and the temperature of the cold inlet cooling water.

$$\dot{Q}_{condense} = \varepsilon_{condense}\dot{C}_{min}(T_{10} - T_{C1}) \tag{3.45}$$

The effectiveness of a heat exchanger with a heat capacity ratio equal to zero is calculated using equation 3.46. The heat capacity ratio is equal to zero for the condenser because the maximum capacitance rate is infinite because the water is undergoing a phase change.

$$\varepsilon_{condense} = 1 - e^{-NTU_{condense}} \tag{3.46}$$

The number of transfer units for the condenser, $NTU_{condense}$, is calculated using equation 3.47, which is the ratio of the overall heat transfer coefficient, $UA_{condenser}$, and the minimum capacitance rate.

$$NTU_{condense} = \frac{UA_{condense}}{\dot{C}_{min}} \tag{3.47}$$

3.10 Pump

In order to prevent back-pressure on the condenser, the water exiting the condenser must be pumped to the pressure exiting the first stage of turbine 2. The equations for a non-isentropic pump are used to find the specific enthalpy of the liquid water exiting the pump as well as the power required to pump the liquid. Power is defined as positive when being done by the

system; in this case, the power will be negative because power is being done on the system. For an ideal pump, the specific entropy of the liquid water is constant.

$$s_{12,s} = s_{11} \tag{3.48}$$

For an ideal pump, the work is the product of the mass flow rate of the liquid water and the change in the specific enthalpy.

$$W_{ideal} = \dot{m}_{water}\left(h_{11} - h_{12,s}\right) \tag{3.49}$$

An actual pump does not perform with 100% efficiency and is not ideal. The product of the efficiency and the actual power is equal to the ideal work. $\varepsilon_{turbine}$ is the isentropic efficiency of the pump, which is assumed to be 0.65. This value for pump efficiency is reasonable based on actual plant operation (Patnode 2006). However, it is more important that the pump efficiency is consistent between the three cycle designs.

$$W_{actual} = \frac{W_{ideal}}{\varepsilon_{pump}} \tag{3.50}$$

The actual work can be used to calculate the actual enthalpy of the liquid water at the exit of the pump using equation 3.51. Since the pressure on each side of the pump is predetermined in Table 3.1, the properties of liquid water can be determined using the pressure and the enthalpy calculated from the pump equations. These properties can be found using the thermophysical property functions in EES.

$$W_{actual} = \dot{m}_{water}(h_{11} - h_{12}) \tag{3.51}$$

3.11 Closed Feed Water Heater

The steam bled off from the first stage of turbine 1 is used to heat the liquid water before the preheater. The water coming from the turbine exiting the closed feed water heater is assumed to be saturated liquid. Using this design criterion and the other design criteria specified in Table 3.1, the properties of each fluid were calculated using mass and energy balances and heat exchanger correlations. The specific heat of the liquid water is assumed to be constant in the closed feed water heater at the average temperature of the water. Equation 3.52 is used to find the average temperature of the water in order to determine those properties.

$$T_{avg,liquid} = \frac{T_{14} + T_{15}}{2} \tag{3.52}$$

The capacitance rate of the condensing steam is infinite. Therefore, the capacitance rate of the liquid water is the minimum capacitance rate in the closed feed water heater. The capacitance rate is calculated as the product of the mass flow rate of the liquid water and the specific heat capacity of the liquid water in the closed feed water heater.

$$\dot{C}_{min} = \dot{C}_{cold} = \dot{m}_{cw} c_p\left('Water', T = T_{avg,liquid}, P = P_{cw}\right) \tag{3.53}$$

The pinch point temperature difference is set on the cold end of the closed feed water heater. The value of the pinch point temperature difference is set based on the same characteristics described in section 3.3.

$$PPT_{CFWH} = T_4 - T_{15} \tag{3.54}$$

The heat transfer rate in the closed feed water heater, $\dot{Q}_{CFWH}$, is defined as the product of the mass flow rate of the steam and the specific enthalpy difference between the outlet and inlet

steam. Since the pressure and temperature are not independent in a phase change process, only one of those properties can be used in the closed feed water heater. The quality is used as the second property to determine the state.

$$\dot{Q}_{CFWH} = \dot{m}_{steam}(h_4 - h_5) \tag{3.55}$$

The heat transfer rate in the closed feed water heater is also defined as the product of the mass flow rate of the liquid water and the specific enthalpy difference between the inlet and outlet liquid water.

$$\dot{Q}_{CFWH} = \dot{m}_{liquid}(h_{15} - h_{14}) \tag{3.56}$$

The heat transfer rate in the closed feed water heater is also defined as the product of the heat exchanger effectiveness, the minimum capacitance rate, and the difference between the temperature of the hot inlet fluid and the temperature of the cold inlet fluid.

$$\dot{Q}_{CFWH} = \varepsilon_{CFWH}\dot{C}_{min}(T_4 - T_{14}) \tag{3.57}$$

The effectiveness of a heat exchanger with a heat capacity ratio equal to zero is calculated using equation 3.58. The heat capacity ratio is equal to zero for the closed feed water heater because the maximum capacitance rate is infinite because the bleed off steam is undergoing a phase change.

$$\varepsilon_{CFWH} = 1 - e^{-NTU_{CFWH}} \tag{3.58}$$

The number of transfer units for the closed feed water heater, NTU_{CFWH}, is calculated using equation 3.59, which is the ratio of the overall heat transfer coefficient, UA_{CFWH}, and the minimum capacitance rate.

$$NTU_{CFWH} = \frac{UA_{CFWH}}{\dot{C}_{min}} \tag{3.59}$$

3.12 Throttling

The saturated steam exiting the closed feed water heater must be throttled in order to reduce the pressure to the pressure of the steam bleeding off of turbine 2 in order to prevent back pressure on the turbine. The throttle step occurs between state 5 and 6, referring to Figure 3.1. Mass and energy balances are used to find the properties of the water after throttling. The mass flow rate into the throttling section is equal to the mass flow rate out of the throttling section.

$$\dot{m}_{in} = \dot{m}_{out} \tag{3.60}$$

Throttling is a constant enthalpy process. Using this condition and knowing the pressure after throttling, the temperature of the water after throttling can be determined since the specific enthalpy at state 5 and 6 are known.

$$h_5 = h_6 \tag{3.61}$$

3.13 Deaerator

The deaerator for this system is modeled as an open feed-water heater. Typically, deaerators include a small makeup water stream, which accounts for any steam removed at this step. This is done to remove the noncondensable gases that accumulate in the system. These gases can manifest due to leaks in the system or other gases created from decomposition. However, if leaks are kept to a minimum and if water impurities are minimal, the amount of steam that needs to be removed from the system is small (El-Wakil 2002). For this reason, the deaerator can be modeled as a mixing process with the saturated steam exiting the closed

feed water heater, the bleed-off steam from the first stage of the second turbine, and the water coming from the condenser. It is assumed that the water exiting the deaerator is saturated liquid. Mass and steady state energy balances are provided in Equations 3.53 and 3.54. Equation 3.62 is a mass balance on the heat transfer fluid entering the deaerator. The sum of the mass flow rate coming from the bleed off from the two turbines and the mass flow rate coming from the condenser is equal to the mass flow rate into the pump, which is also equal to the total mass flow rate of steam in the system.

$$\dot{m}_{out} = \dot{m}_{sat.liquid} + \dot{m}_{steam} + \dot{m}_{cw} \tag{3.62}$$

Equation 3.63 is an energy balance on the fluid streams previously described. Selecting the deaerator as the system, it is assumed that there are no sources of heat transfer to or from the system. Therefore, the energy of the fluid leaving must equal the energy of the fluids entering. The last pump, which operates between states 13 and 14, increases the pressure of the fluid to the boiler pressure uses the same equations found in 3.10.

$$\dot{m}_{out}h_{13} = \dot{m}_{sat.liquid}h_6 + \dot{m}_{steam}h_9 + \dot{m}_{cw}h_{12} \tag{3.63}$$

3.14 Overall Values

The overall cycle values are calculated using the following equations.

$$\dot{W}_{net} = \dot{W}_{t11} + \dot{W}_{t12} + \dot{W}_{t21} + \dot{W}_{t22} + \dot{W}_{p1} + \dot{W}_{p2} \tag{3.64}$$

$\dot{W}_{t11}$ is the turbine work done in turbine one in the first stage; $\dot{W}_{t12}$ is the turbine work done in turbine one in the second stage, etc. $\dot{W}_{p1}$ is the work done on pump one, which is negative. The first law efficiency is calculated two ways, as shown in Equation 3.65. It is calculated from the net work divided by the sum of heat transfer rates in each heat exchanger

with the HTF. It can also be calculated by the net work divided by the mass flow rate of the HTF multiplied by the difference between the enthalpy of the HTF coming from the solar field and the enthalpy of the HTF returning to the solar field. These two efficiencies are identical and provide a check on the coding of the model.

$$\eta_{first} = \frac{\dot{W}_{net}}{\dot{Q}_{pre} + \dot{Q}_{boiler} + \dot{Q}_{super} + \dot{Q}_{re}} = \frac{\dot{W}_{net}}{\dot{m}_{HTF}(h_{D1} - h_{D6})} \tag{3.65}$$

The second law efficiency of the system is also calculated based on the exergy of the Dowtherm A coming from the solar field and returning to the solar field.

$$\Delta\dot{X}_D = \dot{m}_d\big(h_{D1} - h_{dead} - T_{dead}(s_{D1} - s_{dead}) - h_{D6} - h_{dead} - T_{dead}(s_{D6} - s_{dead})\big)$$

$$\Delta\dot{X}_D = \dot{m}_d\big(h_{D1} - h_{D6} - T_{dead}(s_{D1} - s_{D6})\big) \tag{3.66}$$

The change in exergy of the Dowtherm A, $\Delta\dot{X}_D$, is the product of the mass flow rate of the Dowtherm A and the change in specific exergy of the Dowtherm. The enthalpy and entropy of the dead states cancel one another, and the equation can be reduced as shown in Equation 3.66. The temperature of the dead state is assumed to be 25°C. The second law efficiency of this system is the ratio of the net work to the change in exergy of the Dowtherm. The efficiencies at design for each cycle can be found in Table 3.2.

$$\eta_{second} = \frac{\dot{W}_{net}}{\Delta\dot{X}_D} \tag{3.67}$$

3.14 T-s Diagram

The T-s Diagram for this cycle is shown in Figure 3.2. Refer to Figure 3.1 for the state points in the power cycle diagram.

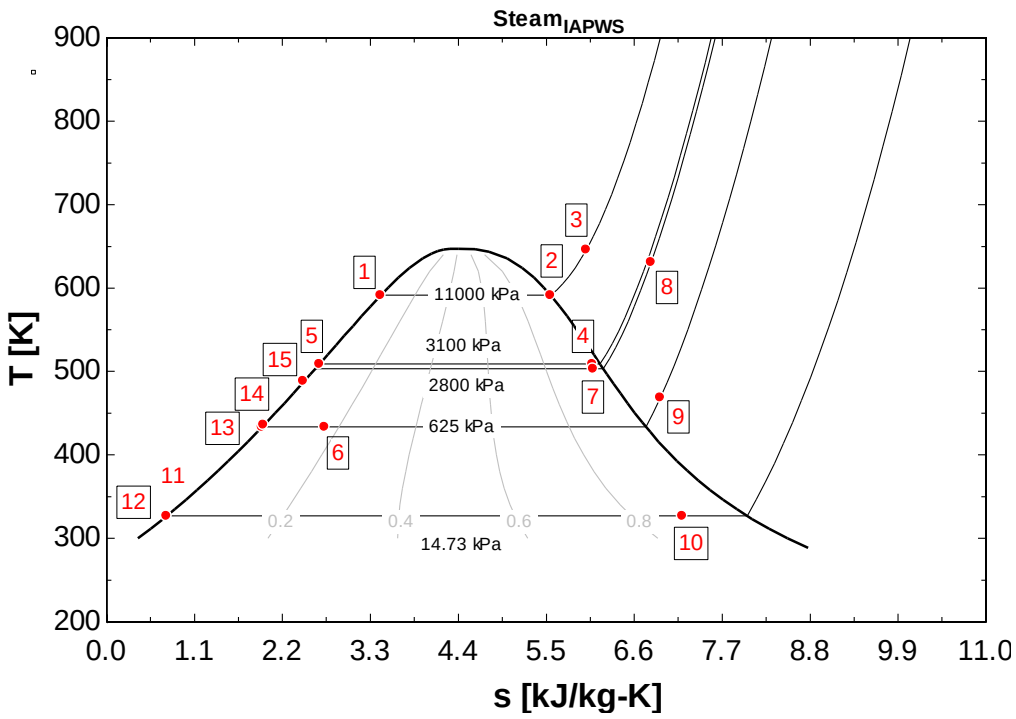

Figure 3.2 T-s Diagram Single Loop Dowtherm

3.15 Design Values

The design values for the single loop Dowtherm A cycle are shown below in Table 3.2. The boiler pressure (State 1), the first turbine bleed off pressure (State 4), the intermediate pressure (State 8), and the second turbine bleed off pressure (State 9) were all optimized to determine the design point with the highest efficiency. Plots of the effect of the different pressures on cycle efficiency are shown in Section 3.19. Using the pinch point temperature differences along with the other design criteria, the overall heat transfer coefficients for the heat exchangers are calculated. These values are found in Table 3.2.

Table 3.2 Design Results of Dowtherm Single Loop

Parameter	Description	Value
ε_{pre}	Effectiveness of Preheater	.94
ε_{boiler}	Effectiveness of Boiler	.82
ε_{super}	Effectiveness of Superheater	.78
ε_{re}	Effectiveness of Reheater	.94
ε_{cond}	Effectiveness of Condenser	.48
ε_{CFWH}	Effectiveness of Closed Feed Water Heater	.72
UA_{pre}	Overall Heat Transfer Coefficient for Preheater	533 [kW/K]
UA_{boiler}	Overall Heat Transfer Coefficient for Boiler	1643 [kW/K]
UA_{super}	Overall Heat Transfer Coefficient for Superheater	280.5 [kW/K]
UA_{re}	Overall Heat Transfer Coefficient for Reheater	240 [kW/K]
UA_{cond}	Overall Heat Transfer Coefficient for Condenser	3691 [kW/K]
UA_{CFWH}	Overall Heat Transfer Coefficient for Closed Feed Water Heater	191.5 [kW/K]
b_{T_1}	Mass fraction of Steam bled off from Turbine 1	.13
b_{T_2}	Mass fraction of Steam bled off from Turbine 2	.17
η_{first}	First Law Efficiency	36.8%
η_{second}	Second Law Efficiency	70.3%
$P_{condense}$	Condenser Pressure	9.013 [kPa]
$\dot{m}_{steam}$	Mass flow rate of steam	34.06 [kg/s]
T_{D6}	Dowtherm Return Temperature	582.3 [K]

One of the conditions arbitrarily set was the fraction of HTF going to the superheater and reheater, which is listed in Table 3.1. This parameter does not change overall cycle efficiency when varied from 0.4 to 0.8 because the pinch point temperature differences set for each heat exchanger are maintained. This means that the output from the heat exchangers will be the same regardless of the fraction, but will be larger or smaller depending on the fraction. Therefore, the exact value of this variable is unimportant for design. The pinch

point temperature differences are maintained for the superheater and the reheater; therefore, the cycle efficiency and net work are unaffected. However, the overall heat transfer coefficients for both of these heat exchangers change when the fraction of the flow rate sent to the superheater, described in Table 3.1, is changed as shown in Figure 3.3.

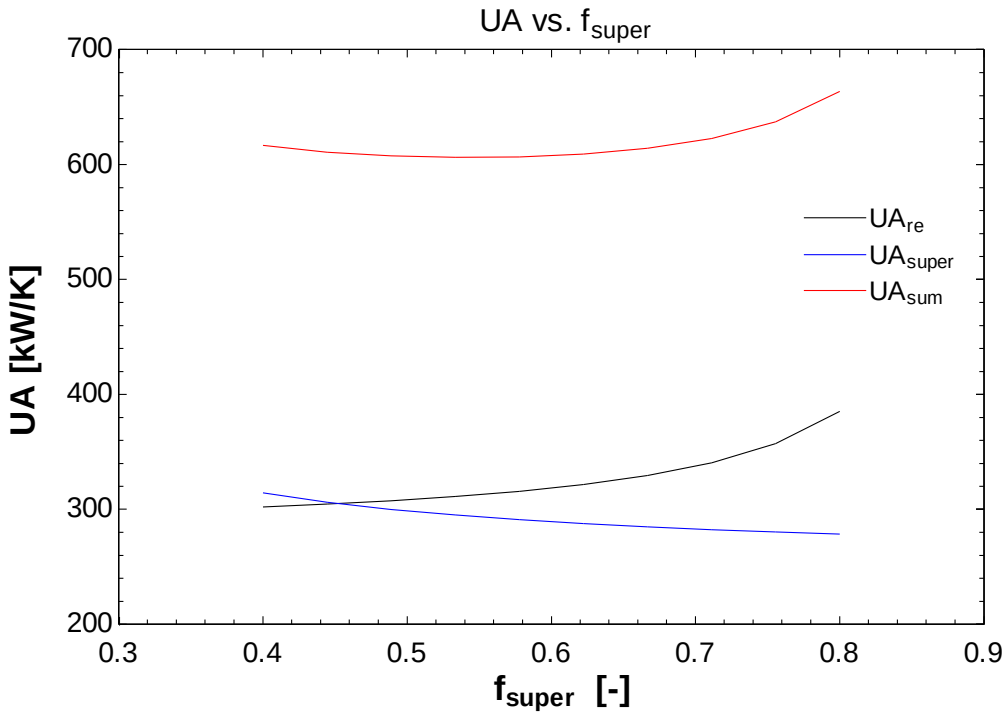

Figure 3.3 UA vs. f_{super}

The overall heat transfer-area (UA)-coefficient is the product of the heat transfer coefficient and heat exchanger surface area. The value of the coefficient correlates to the physical size of the heat exchanger surface area. It can be compared to other values from an existing solar thermal power plant that uses an organic HTF comparable to Dowtherm A. Table 3-3 lists the values of the overall heat transfer coefficients for the heat exchangers from the SEGs plant in Kramer Junction, CA, which is also 30 MW output (Patnode 2006).

Table 3.3 Overall Heat Transfer Coefficients for Components of SEGs plant

	Effectiveness [-] (SEGs)	UA [kW/K] (SEGs)	Effectiveness [-] (Model)	UA [kW/K] (Model)
Preheater	0.97	891.1	0.94	533
Boiler	0.93	2371	0.82	1643
Superheater	0.81	356.9	0.78	280.5
Reheater	0.58	149.1	0.94	240

Comparing the values in this table indicates that the heat exchanger sizes needed for the system design are within reason.

3.16 Alternate Designs

The cycle described in the previous sections will be compared to two different cycles: a single loop of molten salt and a dual loop system utilizing both Dowtherm A and molten salt. The cooling water temperature and mass flow rate are held constant across each system design. Other factors, such as boiler, intermediate, and bleed off pressures, are optimized for each design.

3.17 Power Cycle with Single Loop of Molten Salt

Molten salts can tolerate higher temperatures than organic heat transfer fluids, such as Dowtherm A, because organic heat transfer fluids begin to break down at temperatures above 400°C. This cycle will utilize a single loop of molten salt with a temperature coming from the solar field of 550°C. Other than the change in HTF, this cycle is similar to the cycle described in sections 3.2 to 3.14 with the only difference being the lack of a preheater.

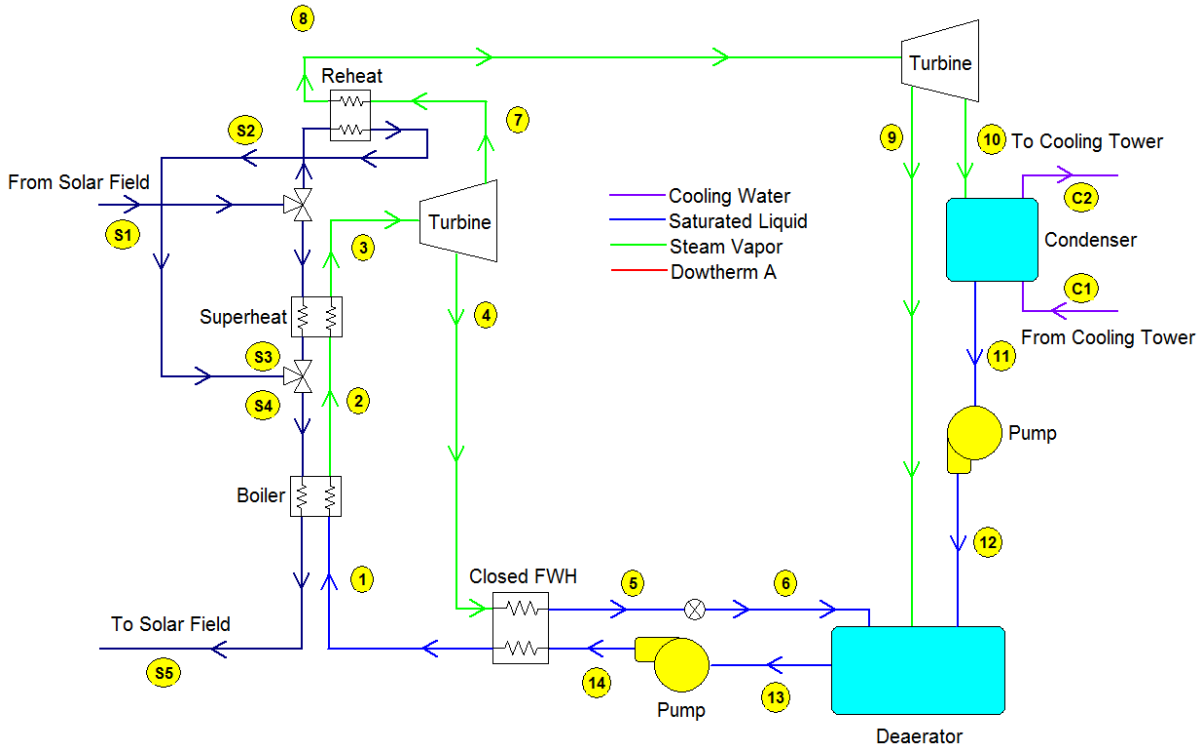

Figure 3.4 Rankine Cycle with Molten Salt HTF

The bleed off steam from turbine 1 (between states 3 and 4/7) is at a higher temperature than the system with the single loop of Dowtherm A. Since the liquid water returning to the boiler can be heated using bleed off steam, the molten salt can return to the solar field at higher temperature, which results in a higher first law efficiency for the power plant. The T-s Diagram for this cycle is shown in Figure 3.5. Refer to Figure 3.4 for the state points in the power cycle diagram.

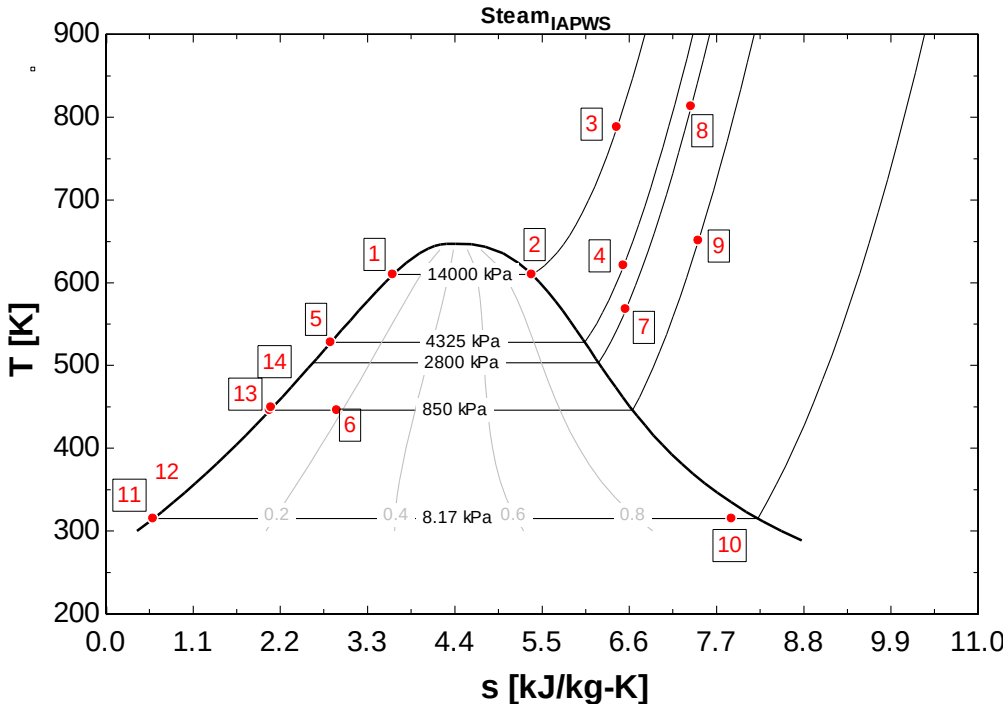

Figure 3.5 T-s Diagram Single Loop Molten Salt

The results for this design are shown in Table 3.4. Refer to descriptions from Table 3.2.

Table 3.4 Design Results of Molten Salt Single Loop

Parameter	Value	Parameter	Value
ε_{boiler}	0.87	UA_{boiler}	720.2 [kW/K]
ε_{super}	0.99	UA_{super}	1003 [kW/K]
ε_{re}	0.98	UA_{re}	272.2 [kW/K]
ε_{cond}	0.41	UA_{cond}	3075 [kW/K]
ε_{CFWH}	0.99	UA_{CFWH}	750.5 [kW/K]
b_{T_1}	0.41	P_{boiler}	14000 [kPa]
b_{T_2}	0.09	P_{bleed_1}	4325 [kPa]
η_{first}	42.6%	P_{out}	2800 [kPa]
η_{second}	72.8%	P_{bleed_2}	850 [kPa]
T_{S5}	625 [K]	$P_{condense}$	8.17 [kPa]
f_{super}	0.76	$\dot{m}_{steam}$	33.2 [kg/s]

The efficiency of the single loop molten salt cycle is greater than the single loop of Dowtherm A cycle previously described, due to the higher temperatures available with molten salt.

3.18 Power Cycle with Dual Loop of Dowtherm and Molten Salt

The last cycle design is a Rankine power cycle that utilizes both Dowtherm A and molten salt as heat transfer fluids. In this case, the cycle is the same as the one described in 3.2 to 3.14. However, after the superheater, the steam passes through another heat exchanger where the heat transfer fluid is molten salt. The same is true with the reheater. The cooling water temperature and mass flow rate are the same in this design as the previous systems in section 3.2 and 3.17. Similar to the design with the single loop of molten salt, the dual loop system does not have a preheater, due to the fact that the water can be heated to near saturation in the closed feed water heater. The boiler pressure, intermediate pressure, and bleed off pressures were optimized to maximize the first law efficiency, which is shown in section 3.20.

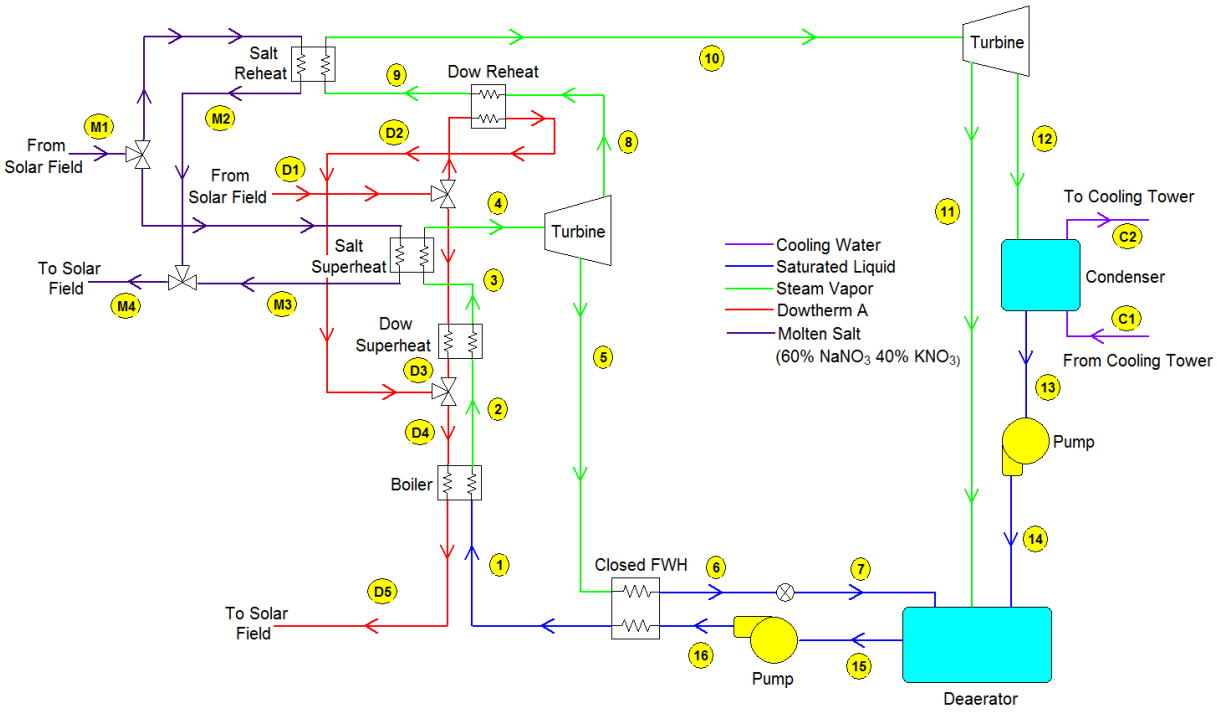

Figure 3.6 Rankine Cycle with Dowtherm and Molten Salt

The T-s Diagram for this cycle is shown in Figure 3.7. Refer to Figure 3.6 for the state points in the power cycle diagram.

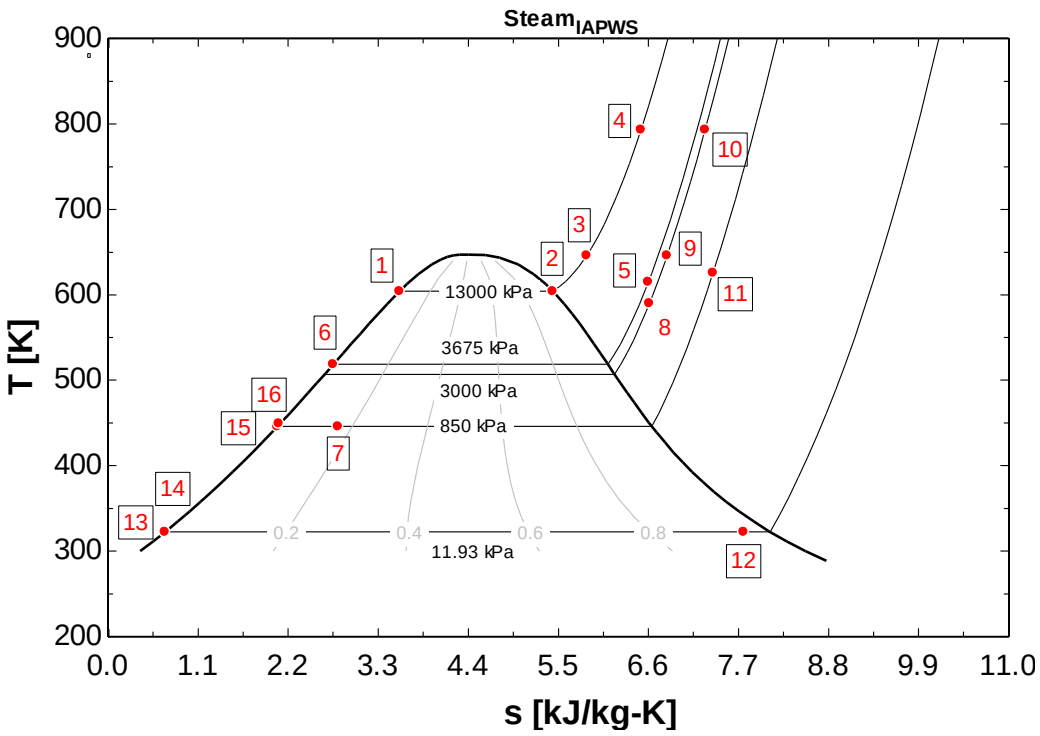

Figure 3.7 T-S Diagram for Dual Loop Cycle

The design performance parameters for this design after optimization of the intermediate pressure between turbine 1 and 2 and the bleed off pressure from each turbine, are shown in Table 3.5. Refer to descriptions from Table 3.2.

Table 3.5 Design Results of Dual Loop

Parameter	Value	Parameter	Value	Parameter	Value
ε_{boiler}	.81	UA_{boiler}	1496 [kW/K]	P_{bleed_1}	3600 [kPa]
ε_{super}	.73	UA_{super}	273.4 [kW/K]	P_{out}	3000 [kPa]
$\varepsilon_{super_{salt}}$	.87	$UA_{super_{salt}}$	315 [kW/K]	P_{bleed_2}	850 [kPa]
ε_{re}	.74	UA_{re}	71.02 [kW/K]	$P_{condense}$	8.17 [kPa]
$\varepsilon_{re_{salt}}$	.83	$UA_{re_{salt}}$	171.7 [kW/K]	b_{T_1}	.39
ε_{cond}	.41	UA_{cond}	3065 [kW/K]	b_{T_2}	.12
ε_{CFWH}	.99	UA_{CFWH}	829.3 [kW/K]	η_{first}	42.7%
T_{D5}	614 [K]	T_{M4}	726.9 [K]	η_{second}	74.9%
$\dot{m}_{steam}$	32.75 [kg/s]	P_{boiler}	13000 [kPa]		

3.19 Pinch Point Temperature Sensitivity

The pinch point temperatures for each cycle were arbitrarily chosen. A sensitivity analysis was performed to determine the effect of changing the pinch point temperature differences on the system design. Table 3.6 contains the results from the sensitivity analysis.

Table 3.6 Pinch Point Temperature Sensitivity Analysis

Single Loop of Dowtherm A Heat Exchangers	**Pinch Point Temperature Difference (K)**	**UA Value (kW/K)**	**Cycle Efficiency (-)**	**Net Power (MW)**	**HTF Return Temperature (K)**
Boiler	10±5	1643±464	0.3684±0.0008	30±2.1440	582.3±6.396
Superheater	20±5	280.5±59.86	0.3684±0.0009	30±0.0530	582.3±0.061
Reheater	40±5	240±47.94	0.3684±0.0003	30±0.0077	582.3±0.102
Condenser	10±5	3691±1392	0.3684±0.0069	30±0.5583	582.3±0
Single Loop of Molten Salt Heat Exchangers					
Boiler	15±5	720.2±111.3	0.4263±0.0002	30±0.7355	624.8±5.000
Superheater	35±5	1003±1929	0.4263±0.0008	30±0.0529	624.8±0.000
Reheater	10±5	272.2±79.33	0.4263±0.0003	30±0.0241	624.8±0.000
Condenser	10±5	3075±1220	0.4263±0.0061	30±0.4305	624.8±0.000
Dual Loop Heat Exchangers					**Dowtherm A /Molten Salt**
Boiler	10±5	1496±447.2	0.4270±0.0008	30±2.6810	614.0±5.000/ 726.9±8.831
Dow Superheater	20±5	273.4±60.29	0.4270±0.0001	30±0.4435	614±0.000/ 726.9±4.636
Dow Reheater	20±5	71.02±13.88	0.4270±0.00004	30±0.1422	614±0.000/ 726.9±1.487
Salt Superheater	30±5	315±52.7	0.4270±0.0006	30±0.2911	614±0.000/ 726.9±2.422
Salt Reheater	30±5	171.7±27.34	0.4270±0.0003	30±0.1175	614±0.000/ 726.9±0.990
Condenser	10±5	3065±1217	0.4270±0.0061	30±0.4293	614±0.000/ 726.9±0.000

The sensitivity analysis shows that decreasing the pinch point temperature difference on the boiler has the largest effect on the net power output. Note that these values provide a reference for the rate of change of variables relative to a change in the pinch point

temperature difference. An actual change in pinch point temperature difference would not result in an exact change in the net power, overall heat transfer, or efficiency. This is evident in the change in UA value for the single loop of salt superheater. Increasing the pinch point temperature difference by 5 [K] would not decrease the UA value by 1929 [kW/K]. This would result in a negative value for the overall heat transfer coefficient, which does not make sense. What this actually indicates is that small changes around the current value of the pinch point temperature difference result in large changes in the overall heat transfer coefficient. The pinch point temperature difference on the boiler could be decreased for each cycle to increase the power output. The heat transfer fluid flow rate could then be decreased such that the net power would remain at design (30 MW), which increase the cycle efficiency. However, for this study, it is more important that the heat exchanger area available to each cycle is consistent for each three cycles. In the case of the single loop of Dowtherm A cycle and the dual loop cycle, Dowtherm A is used as the heat transfer fluid in the boiler. Both of these heat exchangers have an overall conductance value of approximately 1500 [kW/K]. The single loop of salt boiler has an overall conductance value of approximately 720 [kW/K]. In the boiler, the heat transfer coefficient for the boiling steam is orders of magnitude bigger than the heat transfer coefficient on the heat transfer fluid side of the heat exchanger. For Dowtherm A and molten salt, the Prandtl numbers at the average temperature of the heat transfer fluids in the boiler are 4.78 and 4.72, respectively. Assuming that the pipes are designed such that the Reynolds numbers are the same, as well as the pipe diameter, the Nusselt number for each heat transfer fluid in the boiler will be the same. Equation 3.68 shows the calculation for the convective heat transfer coefficient.

$$h = \frac{Nu \cdot k}{D} \tag{3.68}$$

The Nusselt number and diameter will be the same for each heat transfer fluid in the boiler. Therefore, the heat transfer coefficient only differs based on the conductivity of each fluid. For Dowtherm A and molten salt, the conductivities at the average temperature of the heat transfer fluids in the boiler are 0.0856 [W/m-K] and 0.5237 [W/m-K], respectively. The salt heat transfer coefficient is approximately 6 times larger than the Dowtherm A heat transfer coefficient. Since the heat transfer coefficient of the heat transfer fluid is the only factor in determining the size of heat exchanger, the single loop of Dowtherm and dual loop boilers will be 12 times the size of the molten salt boiler based the fact that they overall heat transfer coefficient for the single loop of Dowtherm A boiler and the dual loop boiler are already double that of the single loop of molten salt boiler. Therefore, the single loop of Dowtherm and dual loop pinch point temperatures should not be decreased any further since the size of their heat exchangers are already much larger than the heat exchangers in the single loop of salt cycle. The pinch point temperatures for the single loop of salt cycle could be reduced further to improve the cycle; however, based on the results in Chapter 6, the single loop of salt cycle is already advantageous based on the current pinch point temperature differences.

3.20 System Optimization

In order to find the optimum design condition for these cycles, the design parameters, such as boiler and intermediate pressure, were varied to find the operating point with the highest efficiency. However, real world effects also have to been considered when choosing the design points such that the system designs are realistic and operate at realistic conditions.

The figure shown below is a plot of cycle efficiency vs. boiler pressure for the single loop of Dowtherm A.

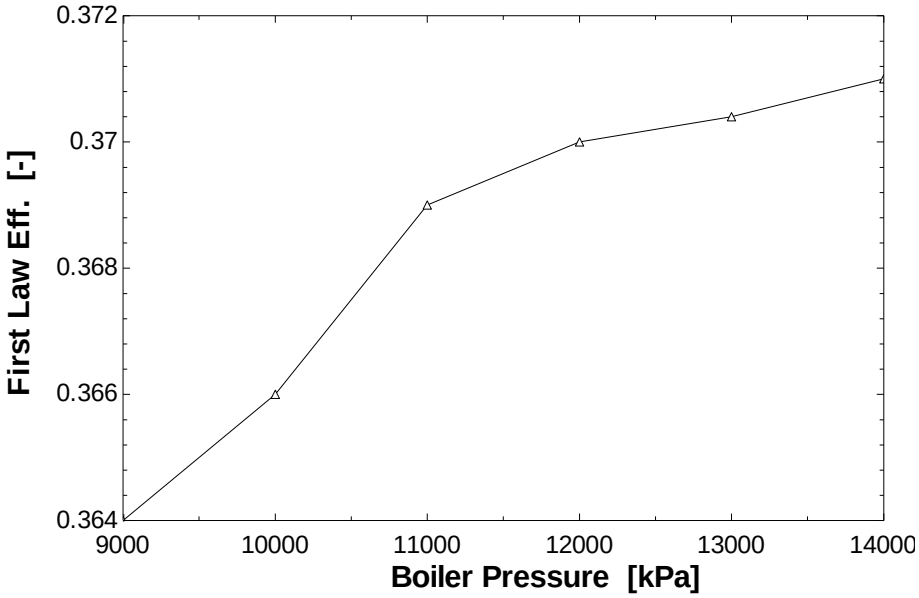

Figure 3.8 Cycle Efficiency vs. Boiler Pressure (Single Loop Dowtherm)

As shown in Figure 3.8, the first law efficiency increases as boiler pressure increases. Using this trend as a basis for design, it seems that the system with a high boiler pressure would be the optimum design. However, raising the boiler pressure increases the cost of the boiler and affects the quality at the outlet of the first turbine, as shown in Figure 3.9.

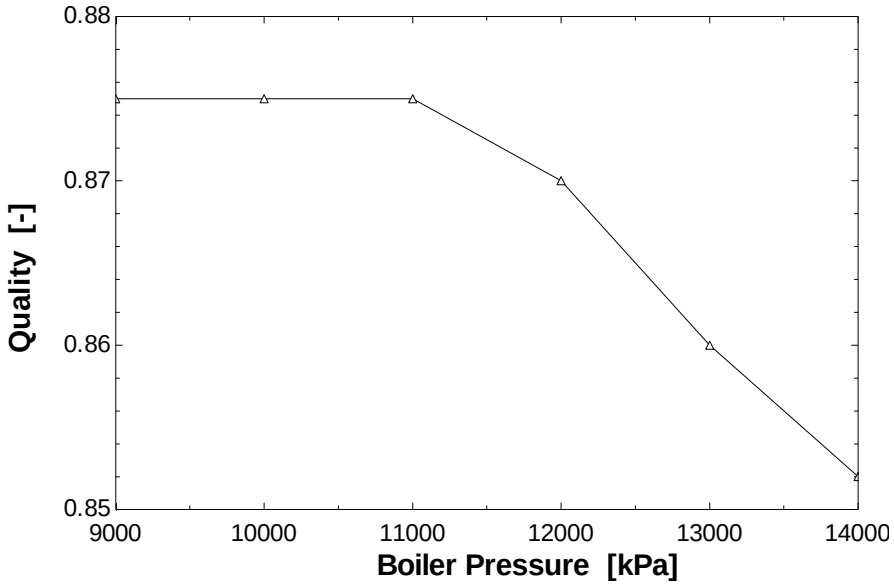

Figure 3.9 Quality vs. Boiler Pressure (Single Loop Dowtherm)

Condensing steam in a turbine can result in erosion of the turbine blades; therefore, the quality of the steam must be maintained at an acceptable level. Most turbine manufactures specify that the steam quality cannot drop below .85 (Logan 2003). For the design condition of this cycle, the quality is limited to .875 in order to ensure that the quality is not out of range for off-design conditions. Since the boiler pressure is limited by this condition, the cycle efficiency is limited to 36.8%.

For the other two cycles, the boiler pressure was also changed to find the optimum operating point. A plot of cycle efficiency vs. boiler pressure is shown below in Figure 3.10.

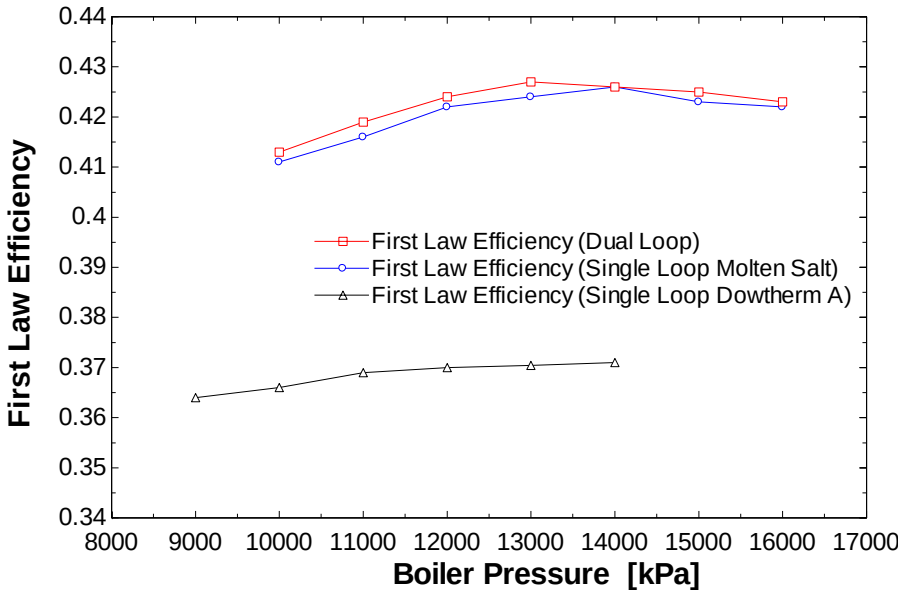

Figure 3.10 First Law Efficiency vs. Boiler Pressure (All Cycles)

Figure 3.10 shows that the single loop of molten salt cycle has a maximum efficiency around at a boiler pressure around 14000 kPa. The dual loop system has a maximum efficiency around 13000 kPa. The maximum efficiency in these two cycles is unlike the single loop of Dowtherm A because the other two cycles do not have a preheater. Since the liquid water is heated to saturation in the closed feed water heater, the bleed off pressure must increase as the boiler pressure increases. After the boiler pressure is increased more than 14000 kPa, the bleed off pressure from turbine 1 increases at a faster rate. The pressure ratio between the boiler and the first stage of the turbine decreases, and the cycle efficiency decreases.

The intermediate pressure between the first and second turbine is also varied to determine the optimum design point.

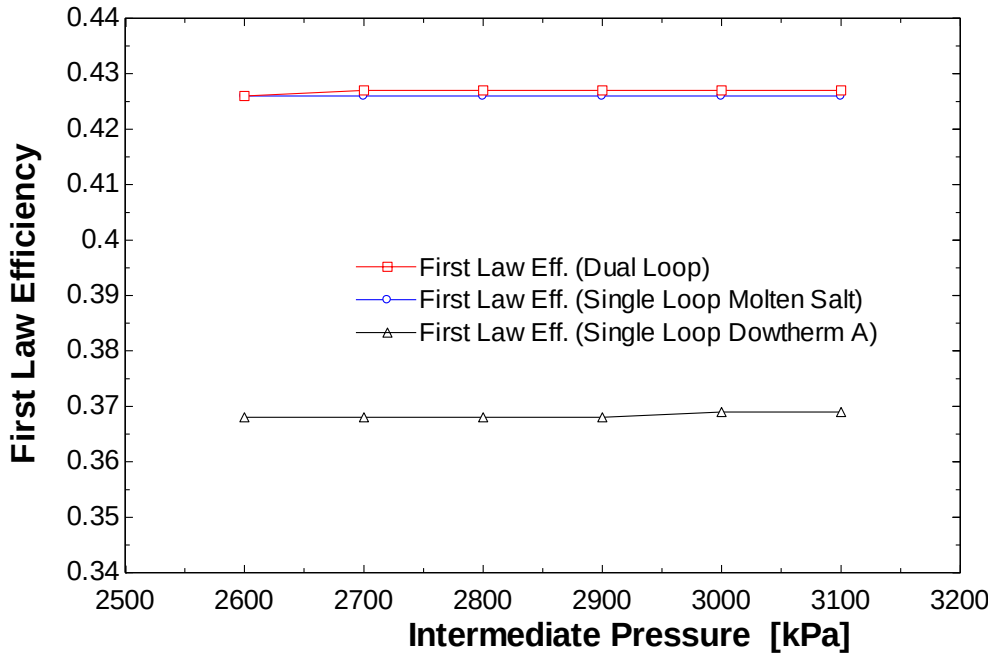

Figure 3.11 First Law Efficiency vs. Intermediate Pressure (All Cycles)

Figure 3.11 shows that intermediate pressure does not affect cycle efficiency as much as boiler pressure. For each cycle, the optimum boiler pressure was held constant for each cycle. The bleed off pressures from each turbine were also varied to find the highest possible efficiency. Figure 3.11 shows that the efficiency of each cycle does not depend on the intermediate pressure between the two turbines or the bleed off pressures for each turbine. That is to say, for a given intermediate pressure, there are two corresponding bleed off pressures from the first stages of the turbines that result in an optimum efficiency close to or equal to a different intermediate pressure with different corresponding bleed off pressures.

Design points for each cycle are shown in Table 3.7 based on the model data shown in the previous two figures and the design criteria in Table 3.1.

Table 3.7 Design Points

Design Value	Single Loop Dowtherm	Single Loop Molten Salt	Dual Loop
Boiler Pressure	11000 [kPa]	14000 [kPa]	13000 [kPa]
Mass Flow Rate	384 [kg/s]	233 [kg/s]	358 [kg/s] Dow 150 [kg/s] Salt
First Law Efficiency	36.8%	42.6%	42.7%
Second Law Efficiency	70.3%	72.8%	76.3%

The first law efficiency for the single loop of molten salt cycle and the dual loop cycle are comparable. This result is expected since they have access to the same temperatures. Each cycle has outputs based on these design conditions. Throughout a typical year, these conditions will not remain constant due to variations in solar radiation, ambient temperature, etc. Therefore, the system will not operate at the design conditions continuously. The next chapter will describe the methodology for determining the performance of each cycle based on variations of the input values.

Chapter 4 Off-Design Modeling

4.1 Introduction

A solar power cycle will not operate at its design condition continuously. Parameters including, the heat transfer fluid (HTF) mass flow rate, the HTF inlet temperature, the cooling water mass flow rate, and the cooling water inlet temperature, will vary based on the performance of the solar field. This chapter explains how the off-design performance of the power cycle is simulated.

4.2 Assumptions

All of the assumptions used in Chapter 3 are employed for off-design, except for one.

- The water exiting the boiler is saturated vapor (x=1).
- The water exiting the deaerator is saturated liquid (x=0).
- The water exiting the condenser is saturated liquid (x=0).
- The water exiting the closed feed water heater is saturated liquid (x=0).
- The pressure drop across any heat exchanger is negligible.

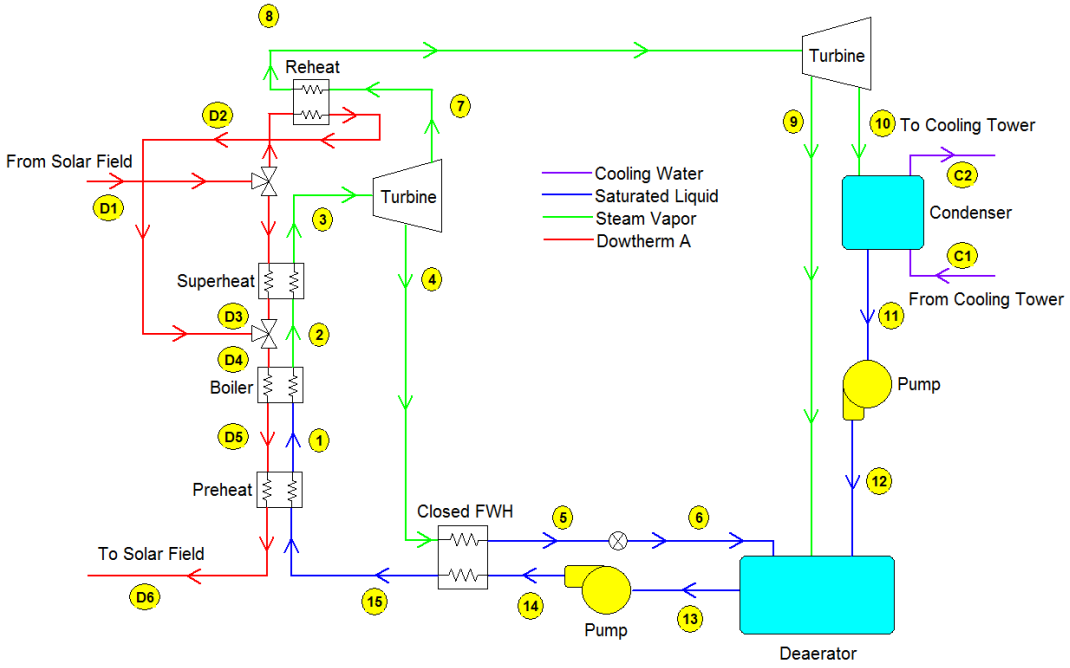

Figure 4.1 Single Loop of Dowtherm A

The water exiting the preheater (state 1) may not be a saturated liquid. At off-design, if this constraint is held, the system would be over defined due to the fact that the heat exchanger sizes are set at values based on the design condition. For a majority of the off-design conditions, the water exiting the preheater has a quality greater than zero. When the quality is greater than zero, the heat exchanger relationship used in the preheater (Equation 3.38) would be invalid for a portion of the preheater because the water could start boiling at the hot end of the preheater.

$$\varepsilon_{pre} = \frac{1 - e^{-NTU_{pre}(1-C_r)}}{1 - C_r e^{-NTU_{pre}(1-C_r)}} \qquad \text{(From Chapter 3: 3.38)}$$

The plot below shows the quality entering the boiler at state 1 for a range of heat transfer fluid inlet temperatures and flow rates for the single loop of Dowtherm A.

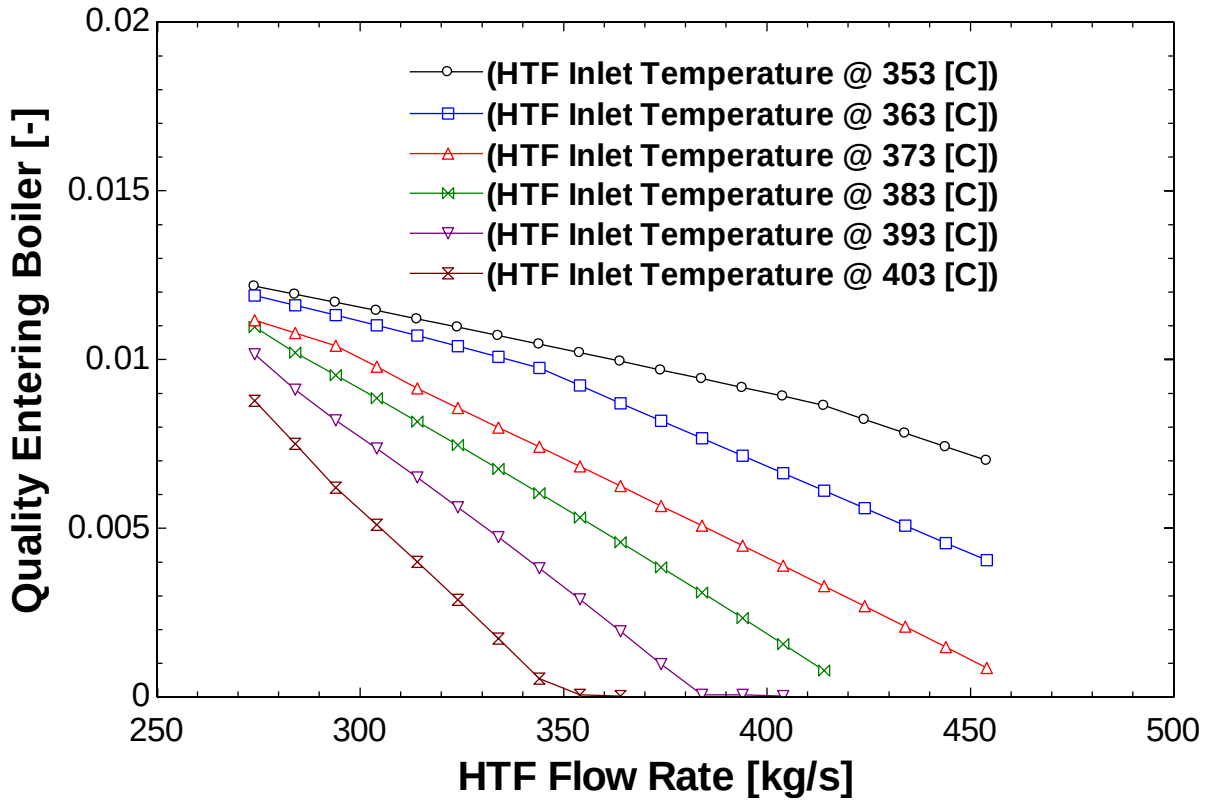

Figure 4.2 Quality Entering Boiler vs. HTF Flow Rate

As shown in Figure 4.2, the quality entering the boiler is low for a range of temperature and heat transfer fluid mass flow rates. Therefore, the effect of boiling in the preheater is neglected because the minute amount of boiling that takes place. The effects of boiling in the closed feed water heater are also small for the single loop of molten salt and the dual loop cycle. Therefore, equation 3.38 can still be used for the preheater.

4.3 Heat Exchangers

The overall heat transfer coefficient or UA value changes with different values of the mass flow rates on each side of the heat exchanger. The mass flow rate of the heat transfer fluid may vary with time. In addition, the amount of steam generated will change based on the flow rate and temperature of the heat transfer fluid coming from the solar field. The UA

value of an unfinned, tubular heat exchanger can be defined as the inverse of the total resistance to heat transfer between the two fluids (Nellis and Klein 2009):

$$\frac{1}{UA} = \frac{1}{h_i A_i} + \frac{R''_{fi}}{A_i} + \frac{ln\left(\frac{D_o}{D_i}\right)}{2\pi kL} + \frac{R''_{fo}}{A_o} + \frac{1}{h_o A_o} \tag{4.1}$$

where h is the convective heat transfer coefficient, A is the surface area, R'' is the fouling factor per unit area, D is the diameter, k is the conductivity of the tube material, and L is the length of the heat exchanger. However, the fouling factor and conduction through the tube should be relatively insignificant when compared to the convective heat transfer in well-designed plants. Based on this assumption, equation 4.1 can be reduced to:

$$\frac{1}{UA} \cong \frac{1}{h_i A_i} + \frac{1}{h_o A_o} \tag{4.2}$$

The convective heat transfer coefficients are functions of the Nusselt number:

$$h = \frac{Nu \cdot k_{fluid}}{D} \tag{4.3}$$

where Nu is the Nusselt number, k_{fluid} is the thermal conductivity of the fluid, and D is the hydraulic diameter. Assuming the flow for both fluids is fully developed hydrodynamically and thermally and turbulent flow, the Nusselt number can be expressed as a function of the Reynolds number and the Prandtl number using the Dittus-Boelter equation:

$$Nu_D = 0.023 \cdot Re_D^{0.8} \cdot Pr^n \tag{4.4}$$

where n=0.4 for a heating fluid and n=0.3 for a cooling fluid. This correlation is not valid for a fluid that is undergoing a phase change. The Dittus-Boelter equation is only valid for situations where

- $0.6 \leq Pr \leq 160$
- $Re > 10000$
- $\frac{L}{D} > 10$

The Reynolds number is defined by the following equation:

$$Re_D = \frac{4\dot{m}}{\pi D \mu} \tag{4.5}$$

where μ is the dynamic fluid viscosity. The Prandtl number is defined by the following equation:

$$Pr = \frac{\mu c}{k_{fluid}} \tag{4.6}$$

If constant fluid properties are assumed, the Prandtl number is constant for both fluids. The Reynolds will change if the mass flow rate changes. Therefore, the convective heat transfer coefficient is proportional to the mass flow rate of the fluid raised to the 0.8 power:

$$h \propto Nu \propto Re^{0.8} \propto \dot{m}^{0.8} \tag{4.7}$$

For the boiler, condenser, and closed feed water heater, it is assumed that the thermal resistance of the steam undergoing a phase change is negligible. Therefore, equation 4.2 can be modified as shown:

$$\frac{1}{UA} \cong \frac{1}{h_o A_o} \tag{4.8}$$

Applying the assumption that the heat transfer coefficient scales with the mass flow rate equation 4.8 is reduced to:

$$\frac{1}{UA} \propto \frac{1}{\dot{m}^{0.8}} \tag{4.9}$$

This equation can also be used to describe the relationship between the mass flow rate of the fluid not undergoing a phase change and the overall heat transfer coefficient at the design condition:

$$\frac{1}{UA_{REF}} \propto \frac{1}{\dot{m}_{REF}{}^{0.8}} \tag{4.10}$$

Combining equations 4.9 and 4.10 gives:

$$\frac{UA}{UA_{REF}} = \frac{\dot{m}^{0.8}}{\dot{m}_{REF}{}^{0.8}} \tag{4.11}$$

Equation 4.11 applies to any heat exchanger where a phase change takes place, which includes the boiler, condenser, and closed feed water heater. Equation 4.11 can be validated by creating a model for an actual heat exchanger and observing the effect of changing the heat transfer fluid mass flow rate. The model created was a simple model with steam boiling in a pipe and the heat transfer fluid flowing in an annular pipe around the steam. The number of pipes and length of pipe required were determined using the heat flux found from the Single Loop of Dowtherm A cycle. For the design condition, the properties of the heat exchanger were found:

- $Re_{Dow} \cong 40000$
- $\mathrm{Pr}_{Dow} = 4.78$
- $\frac{L}{D}\ (Dow) \cong 20000$
- $h_{Dow} \cong 200\ \left[\frac{W}{m^2-K}\right]$
- $h_{steam} \cong 10000\ \left[\frac{W}{m^2-K}\right]$

Since the heat transfer coefficient on the steam side is expected to be much greater than the heat transfer coefficient on the Dowtherm A side, the assumption that the steam heat transfer coefficient can be ignored in equation 4.8 is valid. The mass flow rate of the Dowtherm A was varied to find the overall heat transfer coefficient at different values of flow rate. Equation 4.11 was used to predict the value of the overall heat transfer coefficient. A comparison between the calculation and the model is shown below.

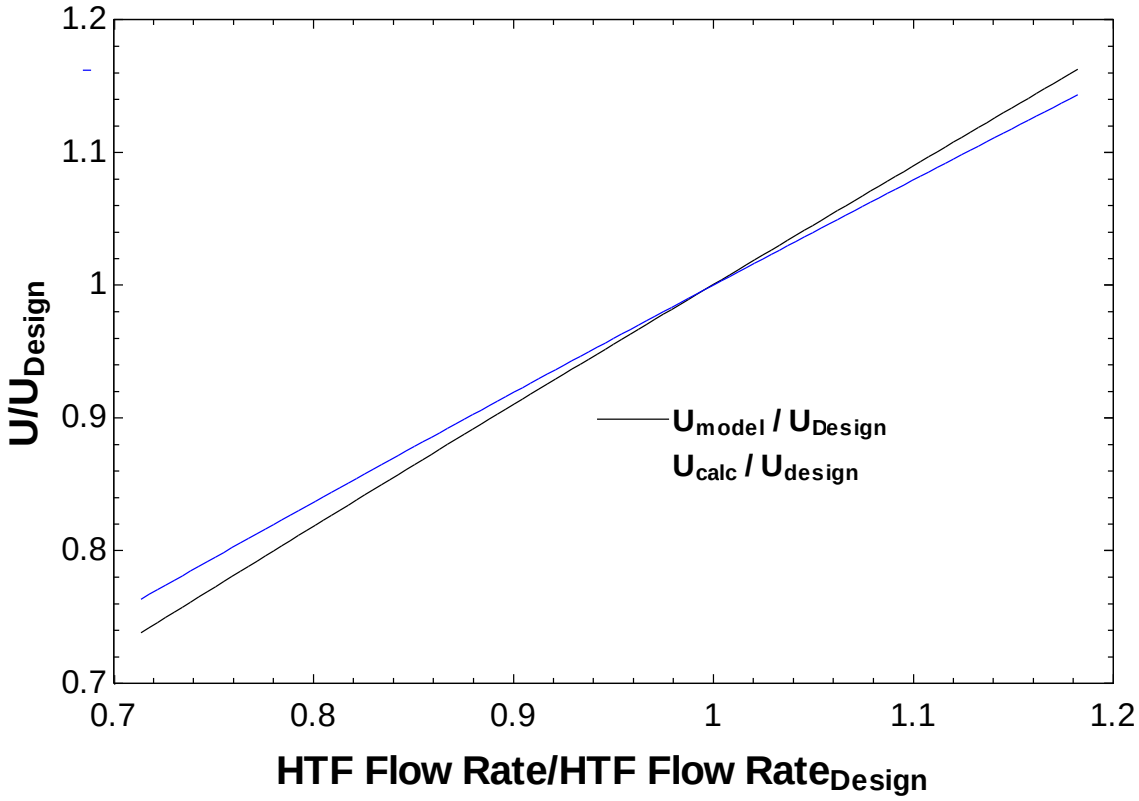

Figure 4.3 Non-Dimensional Overall Heat Transfer Coefficient vs. Non-Dimensional Mass Flow Rate in Boiler

The error between the model value and calculation was found using the following equation:

$$Percent\ Error = \frac{|U_{model} - U_{calc}|}{U_{model}} * 100\ [\%] \tag{4.12}$$

The maximum error was found to be 3.5%. This model applies only to the heat exchangers where a phase change takes place. Therefore, additional analysis is required to determine the effect of mass flow rate in the heat exchangers where a phase change does not occur. Combing equation 4.2 with the assumptions listed in equations 4.3 to 4.7, the equation 4.13 applies to a heat exchanger where a phase change does not take place.

$$\frac{1}{UA} \propto \frac{1}{\dot{m}_i{}^{0.8}} + \frac{1}{\dot{m}_o{}^{0.8}} \tag{4.13}$$

This equation can also be used to describe the relationship between the mass flow rate of each fluid and the overall heat transfer coefficient at the design condition.

$$\frac{1}{UA_{ref}} \propto \frac{1}{\dot{m}_{i,REF}{}^{0.8}} + \frac{1}{\dot{m}_{o,REF}{}^{0.8}} \tag{4.14}$$

Combining equations 4.13 and 4.14, the UA at varying mass flow rate is found using the following equation:

$$\frac{UA}{UA_{REF}} = \frac{\frac{1}{\dot{m}_{i,REF}{}^{0.8}} + \frac{1}{\dot{m}_{o,REF}{}^{0.8}}}{\frac{1}{\dot{m}_{\iota}{}^{0.8}} + \frac{1}{\dot{m}_{o}{}^{0.8}}} = \left(\frac{\dot{m}_{\iota}{}^{0.8}\dot{m}_{o}{}^{0.8}}{\dot{m}_{i,REF}{}^{0.8}\dot{m}_{o,REF}{}^{0.8}}\right)\left(\frac{\dot{m}_{o,REF}{}^{0.8} + \dot{m}_{i,REF}{}^{0.8}}{\dot{m}_{o}{}^{0.8} + \dot{m}_{\iota}{}^{0.8}}\right) \tag{4.15}$$

It is assumed that the steam and heat transfer fluid remain in the same proportion at off-design conditions.

$$\frac{\dot{m}_i}{\dot{m}_o} = \frac{\dot{m}_{i,REF}}{\dot{m}_{o,REF}} = K \tag{4.16}$$

A plot of the ratio of the mass flow rate of the heat transfer fluid to the mass flow rate of steam is shown.

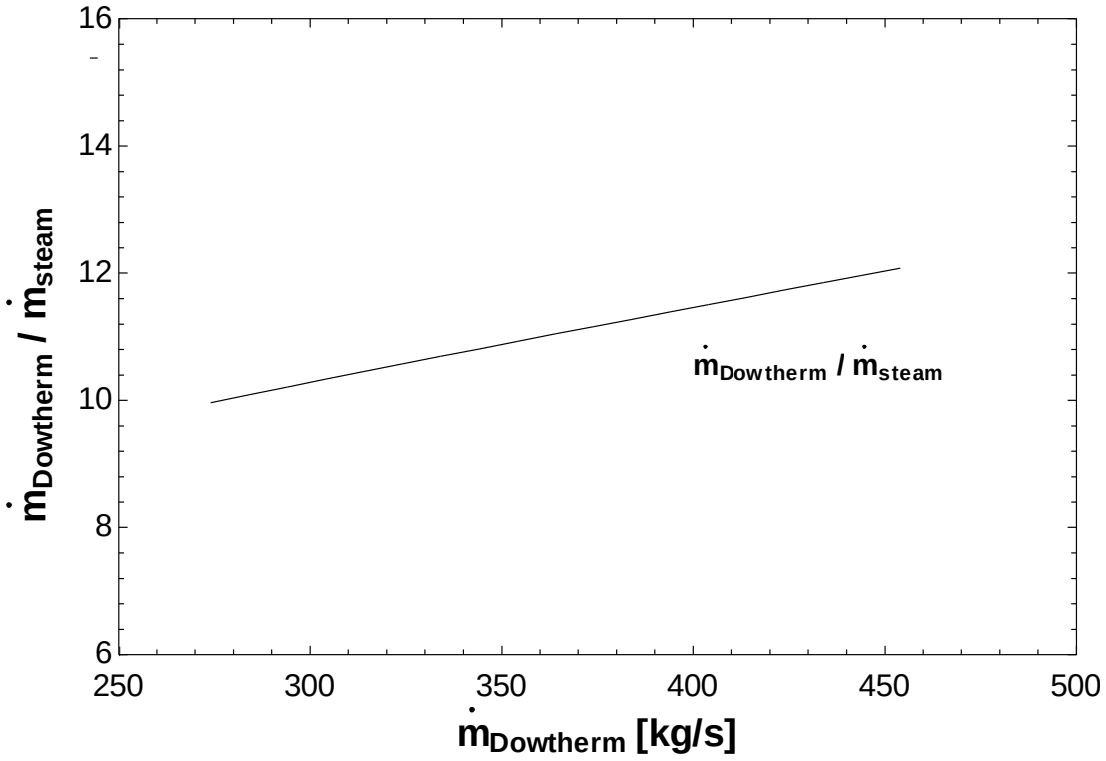

Figure 4.4 Ratio of Dowtherm A Flow Rate to Steam Flow Rate vs. Dowtherm A Flow Rate at Design Temperature (393 [C]).

Applying equation 4.16 to equation 4.15 leads to

$$\frac{UA}{UA_{REF}} = \frac{\frac{1}{K \cdot \dot{m}_{o,REF}{}^{0.8}} + \frac{1}{\dot{m}_{o,REF}{}^{0.8}}}{\frac{1}{K \cdot \dot{m}_{o}{}^{0.8}} + \frac{1}{\dot{m}_{o}{}^{0.8}}} = \left(\frac{\cancel{K \cdot \dot{m}_{o}{}^{0.8}}\dot{m}_{o}{}^{0.8}}{\cancel{K \cdot \dot{m}_{o,REF}{}^{0.8}}\dot{m}_{o,REF}{}^{0.8}}\right)\left(\frac{\cancel{\dot{m}_{o,REF}{}^{0.8}}(\cancel{K+1})}{\cancel{\dot{m}_{o}{}^{0.8}}(\cancel{K+1})}\right)$$

$$= \left(\frac{\dot{m}_{o}}{\dot{m}_{o,REF}}\right)^{0.8} \tag{4.17}$$

A heat exchanger model was created to analyze the validity of equation 4.17. Equation 4.17 is the same equation used in Patnode's modeling approach (2006). The model created was a simple model with liquid water flowing in a pipe and the heat transfer fluid flowing in an

annular pipe around the water. The number of pipes and length of pipe required were determined using the heat flux in the Preheater found from the Single Loop of Dowtherm A cycle. The mass flow rate of the liquid water corresponding to the mass flow rate of the Dowtherm A was determined from the Boiler. The flow rates of each fluid are the same in the boiler as they are in the preheater. Since the boiler model has been validated, the same flow rate of water based on the Dowtherm A flow rate was used. Two different model configurations were created to test equation 4.17. In the first scenario, the heat transfer coefficient of the steam was assumed to be equal to the Dowtherm A heat transfer coefficient.

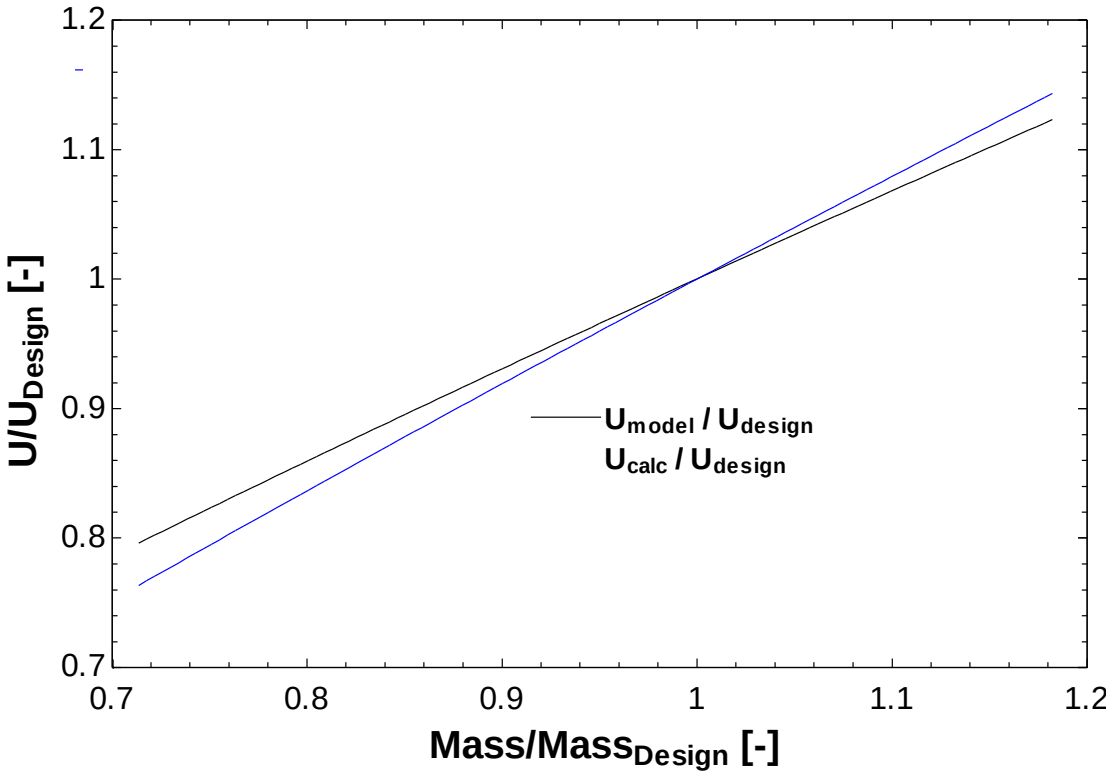

Figure 4.5 Non-Dimensional Overall Heat Transfer Coefficient vs. Non-Dimensional Mass Flow Rate in Preheater ($h_{steam}=h_{Dowtherm}$)

The model and calculation value of the overall heat transfer coefficient show agreement. Using equation 4.12, the maximum error between the model value and the calculation value is 2.5%. The next plot shows the second configuration where the heat transfer coefficient of the steam is six times larger than the heat transfer coefficient of the heat transfer fluid.

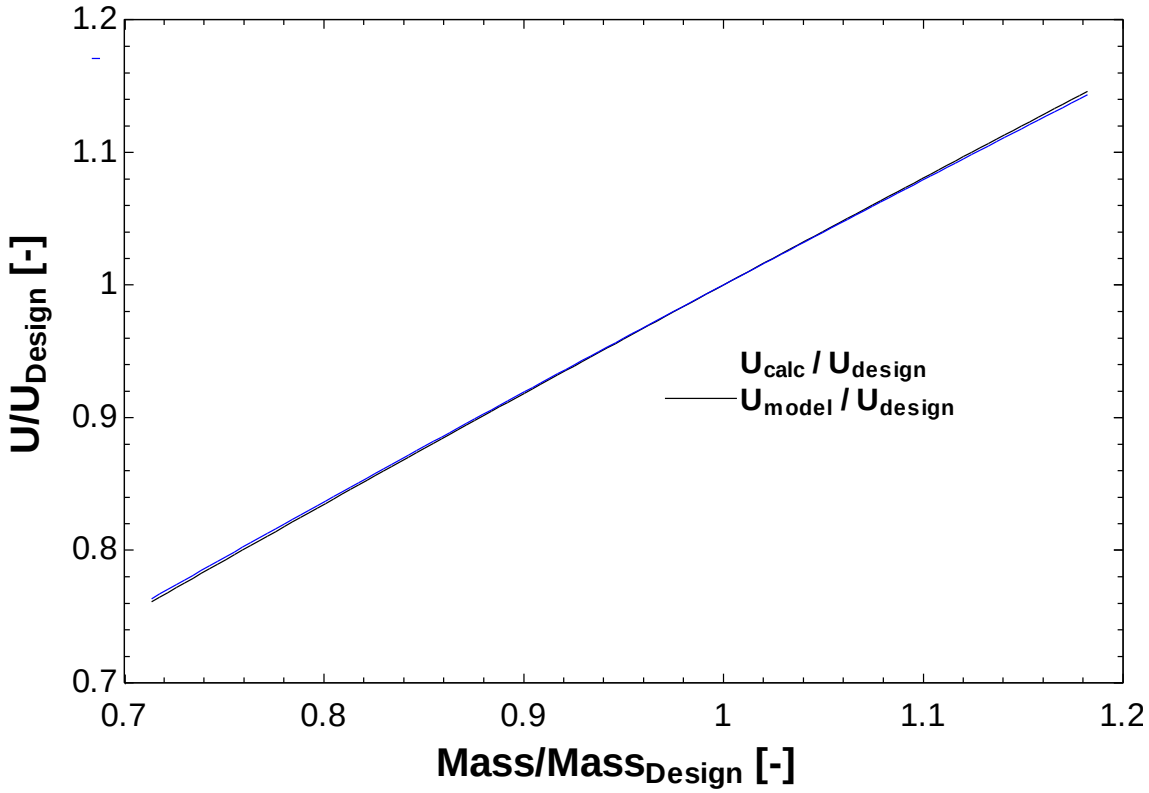

Figure 4.6 Non-Dimensional Overall Heat Transfer Coefficient vs. Non-Dimensional Mass Flow Rate in Preheater ($h_{steam}=6*h_{Dowtherm}$)

As shown in Figure 4.6, the model and calculated values for the overall heat transfer coefficient show even better agreement when the steam heat transfer coefficient is much larger than the heat transfer coefficient of the heat transfer fluid.

4.4 Stodola's Law

The pressure drop over each turbine will also vary based on the mass flow rate of steam. The law of the ellipse governs the relationship between turbine inlet pressure, outlet pressure, and mass flow rate when compared to the reference states (Stodola and Lowenstein 1945). The following equation is used to describe the relationship between turbine inlet pressure (P_1) , outlet pressure (P_2), and mass flow rate (Patnode 2006).

$$\frac{P_1^2 - P_2^2}{P_{1,ref}^2 - P_{2,ref}^2} = \left(\frac{\dot{m}}{\dot{m}_{ref}}\right)^2 \tag{4.18}$$

As before, the mass flow rate of steam is determined in the boiler. The pressure in the condenser is determined based on the cooling water input parameters. Using the known mass flow rate and the condensing pressure, the bleed off pressure from the second turbine can be determined using equation 4.18. Each pressure at off-design conditions can be determined using equation 4.18.

4.5 Turbine Efficiency

The isentropic efficiency of a turbine varies with changes in steam mass flow rates. The figure below shows the reduction in efficiency for a 3600-rpm condensing turbine with one governing stage as a function of throttle flow ratio (Bartlett 1958).

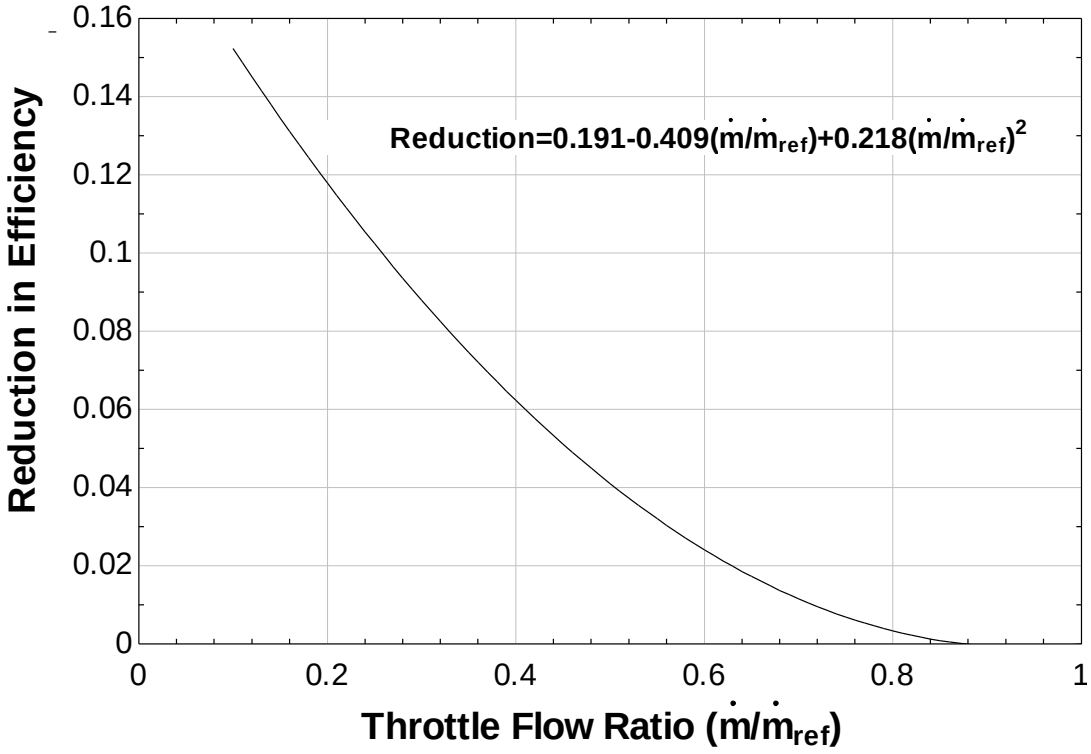

Figure 4.7 Turbine Efficiency Reduction vs. Throttle Flow Ratio

Each stage of the turbine is treated individually. The throttle flow ratio is the ratio of the mass flow rate through a stage to the design value of the mass flow rate through the stage. The turbine efficiency for each of the two stages in each of the two turbines is calculated using the following equation:

$$\eta = (1 - Reduction) \cdot \eta_{ref} \tag{4.19}$$

4.6 Output Variables

The purpose of modeling the Rankine cycles in EES is to determine a relationship between output parameters and input parameters over a range of values. If empirical relationships between these variables can be obtained, another program, such as TRNSYS, can be used to model the performance of the entire system over a year in a computationally efficient manner. The input variables that change during system operation are the heat transfer fluid

flow rate, the heat transfer fluid inlet temperature, the cooling water mass flow rate, and the cooling water inlet temperature. The output variables needed for cycle calculations are the heat transfer fluid outlet temperature, the cooling water outlet temperature, and the net power. These output variables were plotted against each of the input variables in order to determine their effect.

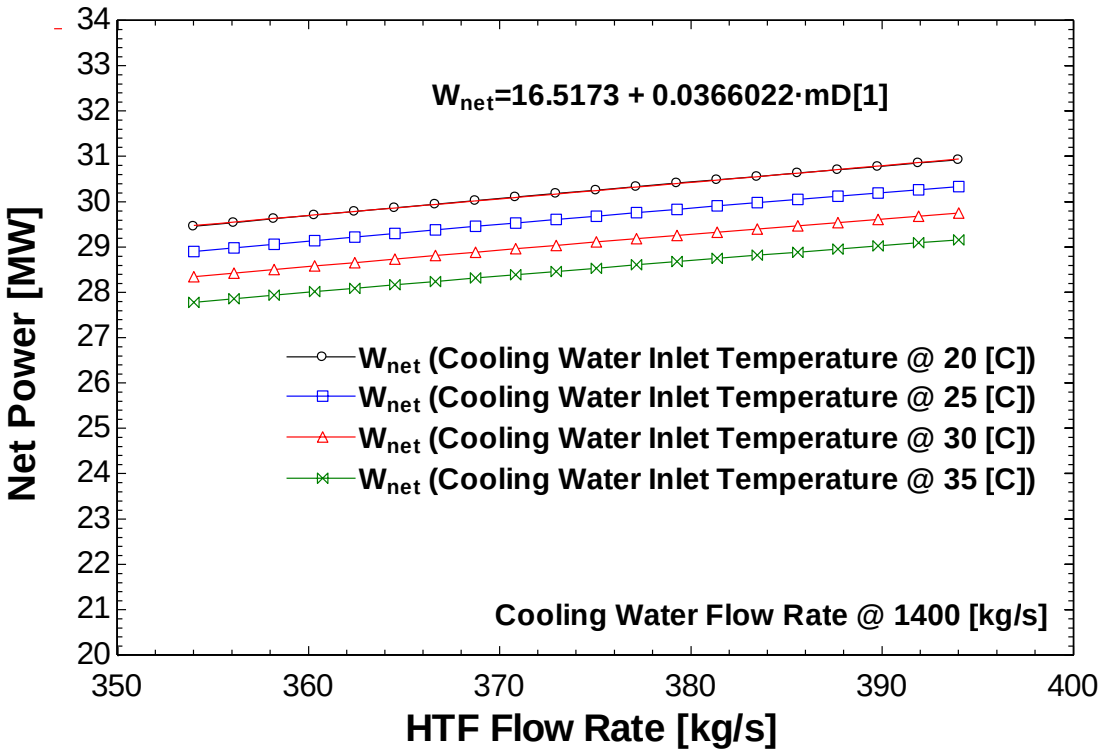

Figure 4.8 Net Power vs. HTF Flow Rate (HTF Inlet Temperature @ 393 [C])

Figure 4.8 is a plot of net power vs. heat transfer fluid mass flow rate. The four curves represent four different cooling water temperatures entering the condenser. For each case, the cooling water flow rate is held constant at 1400 [kg/s]. As shown in Figure 4.8, the net power reacts to changes in input parameters in the way one would expect. As the mass flow rate of the heat transfer fluid increases, the net power increases. As the cooling water inlet temperature increases, the net power decreases. The net power would decrease with

increasing cooling water temperature because of the direct relationship between the inlet cooling water temperature and the condensing pressure. If the inlet cooling water temperature increases, the condensing pressure increases, which, in turn, decreases the pressure drop between the second stage of the second turbine and the condenser.

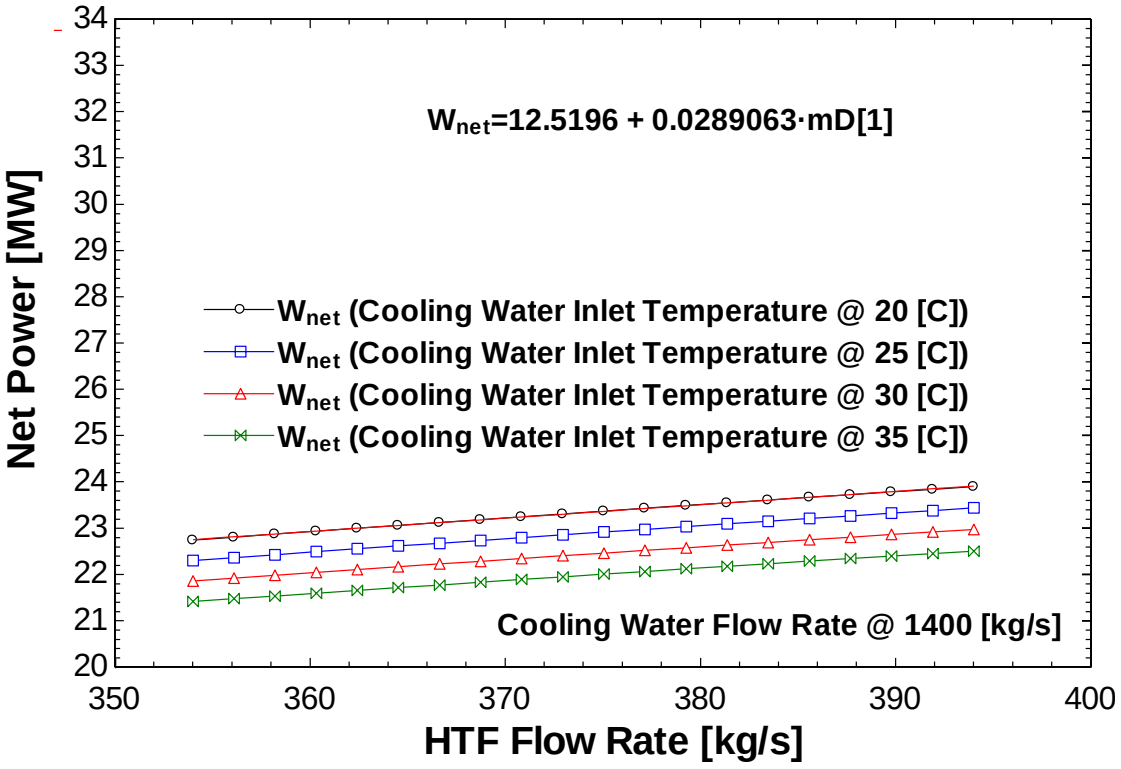

Figure 4.9 Net Power vs. HTF Flow Rate (HTF Inlet Temperature @ 363 [C])

Figure 4.9 is the same as Figure 4.8 except that the heat transfer fluid inlet temperature has decreased by 30 degrees. As shown, the net power decreases as the temperature of the heat transfer fluid inlet temperature decreases. In addition, a first order polynomial fit of one of the curves is shown on each figure. The slope decreases by 23.5 %. The slope of the curve decreases with decreasing temperature, which implies the relationship between net power and the heat transfer fluid mass flow rate and between net power and heat transfer fluid inlet temperature are not independent of one another.

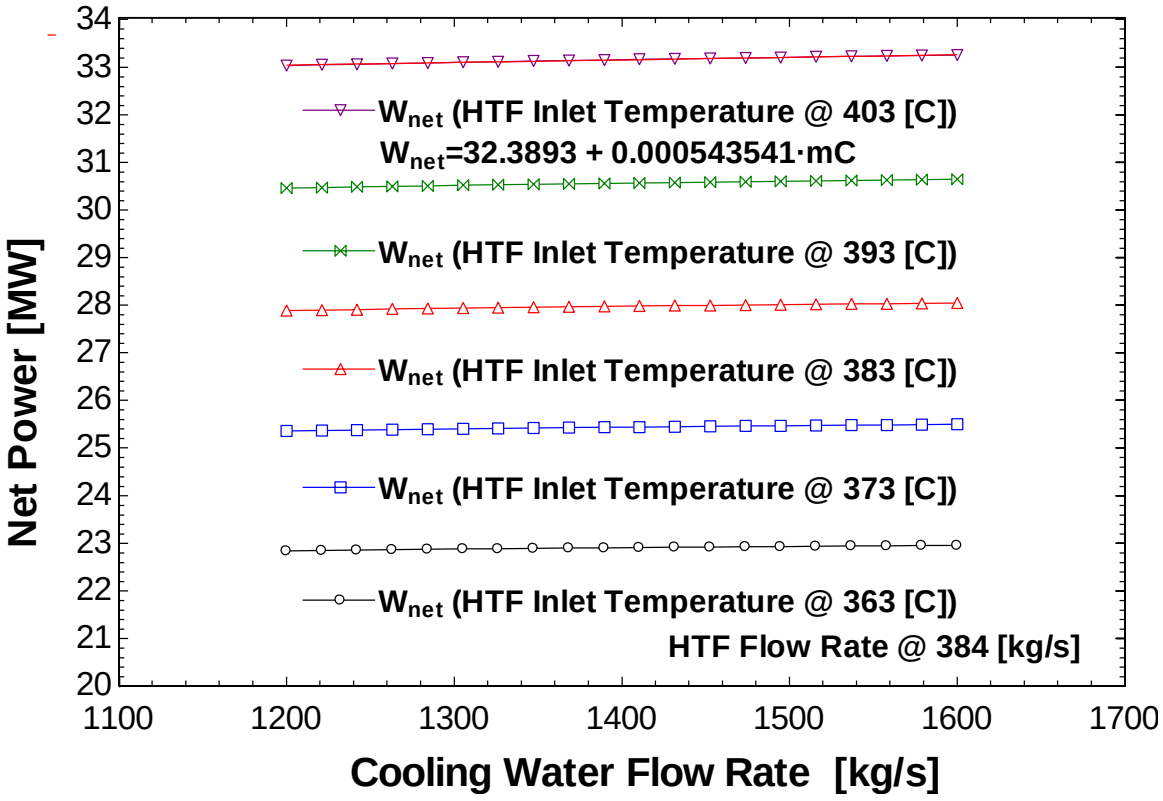

Figure 4.10 Net Power vs. Cooling Water Flow Rate (Cooling Water Inlet Temperature @ 20 [C])

Figure 4.10 shows the relationship between net power and cooling water flow rate. Each curve represents a different heat transfer fluid inlet temperature. As shown in Figure 4.10, the net power of the cycle is more sensitive to changes in heat transfer fluid inlet temperature than to cooling water flow rate.

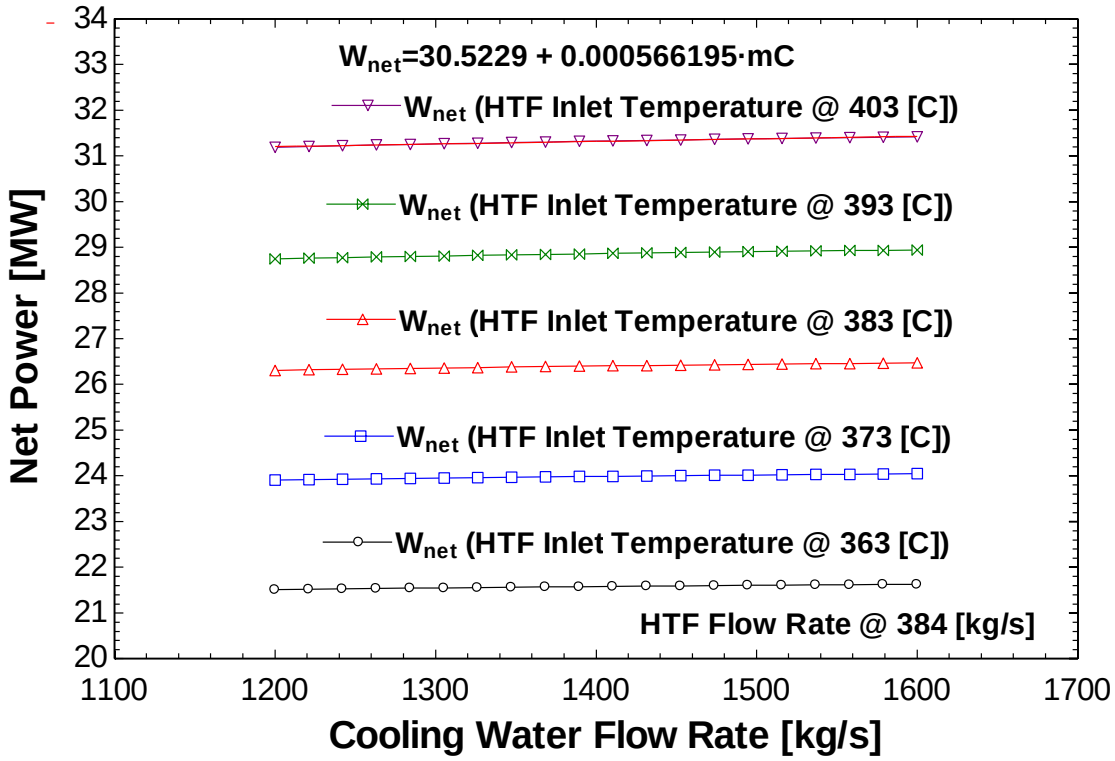

Figure 4.11 Net Power vs. Cooling Water Flow Rate (Cooling Water Inlet Temperature @ 35 [C])

Figure 4.11 is the same as Figure 4.10 except that the cooling water inlet temperature has increased by 15 degrees. As shown, the net power decreases as the temperature of the cooling water inlet temperature. In addition, a first order polynomial fit of one of the curves is shown on each figure. The slope of the curve does not change with cooling water inlet temperature, which implies the relationship between net power and the cooling water flow rate and between net power and cooling water inlet temperature are independent of one another.

The final parameter that was varied for the off-design model is the turbine efficiency. This parameter was varied to show the effect of using a turbine with better performance in each system. A plot of the effect of changing the turbine efficiency for each system is shown in Figure 4.12.

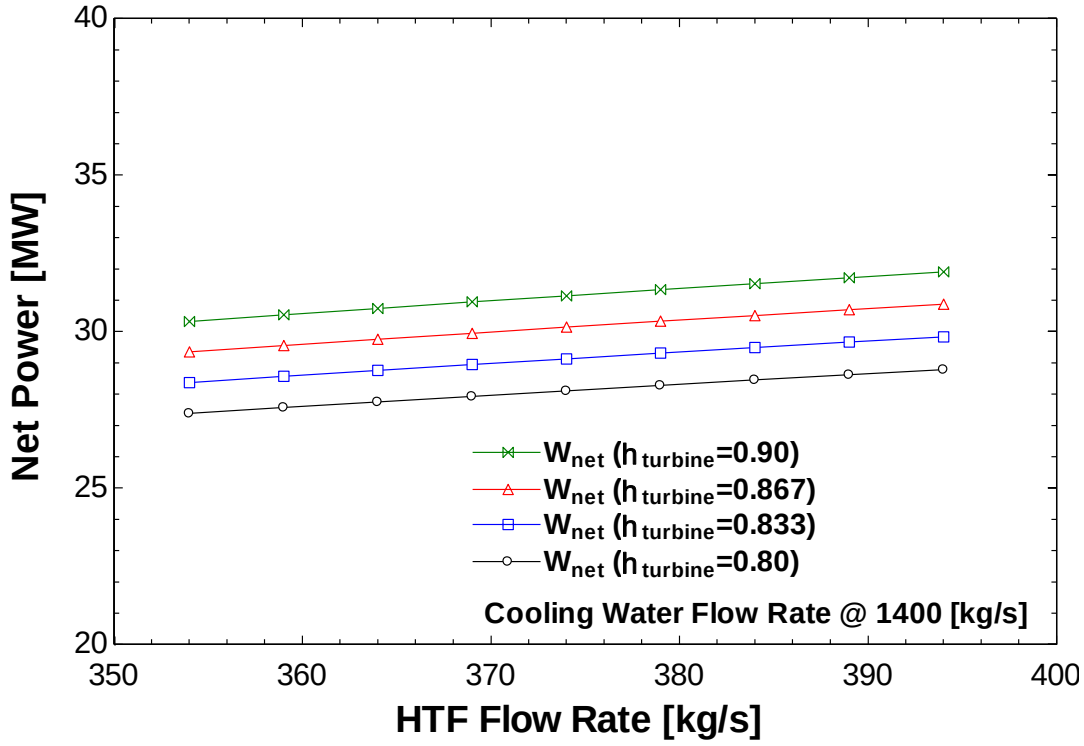

Figure 4.12 Net Power vs. HTF Flow Rate (Cooling Water Flow Rate @ 1400 [kg/s])

The effect of the turbine efficiency on the overall efficiency is shown in Figure 4.13.

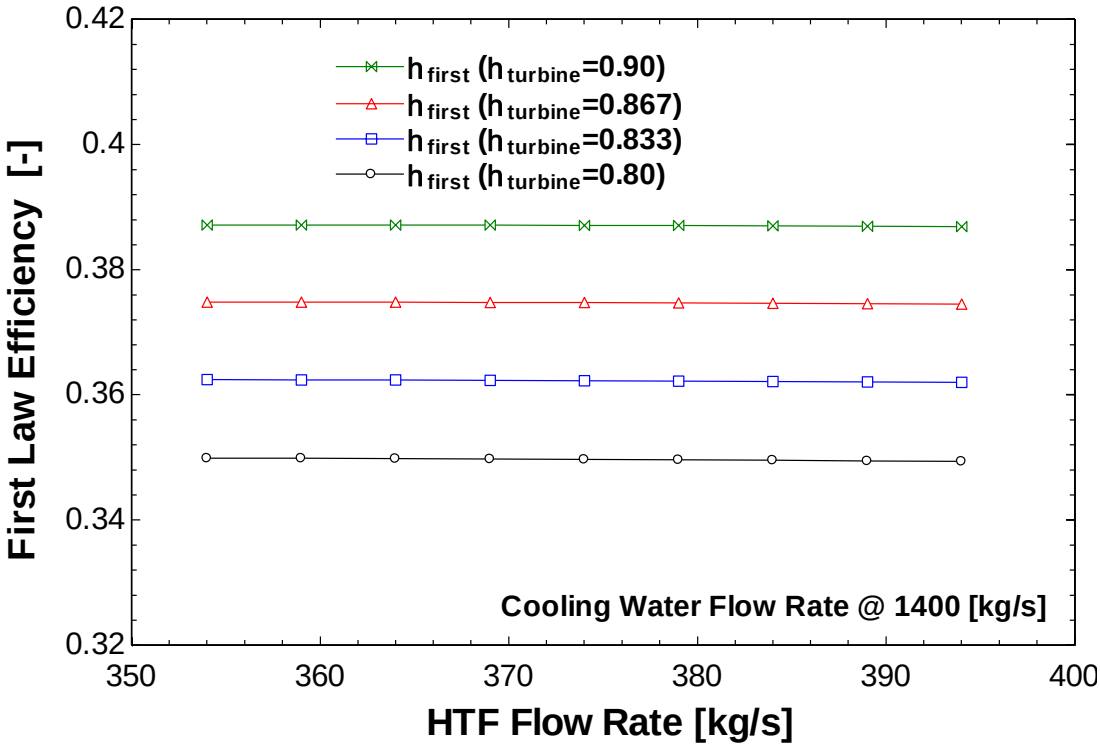

Figure 4.13 First Law Efficiency vs. HTF Flow Rate (Cooling Water Flow Rate @ 1400 [kg/s])

The turbine efficiency has a linear effect of the net power and the first law efficiency.

These figures show the relationship between input and output parameters in the single loop Rankine cycle with Dowtherm A. Figures 4.8 through 4.13 show the relationships that exist between the operating variables. Since this is the case with each one of the three cycles, a method of describing the relationships between the input and output variables must be obtained by including the effect of input variables on each other.

4.7 Multivariable Regression

The first step of regressing the dependent variables (Net Power, HTF return temperature, and cooling water return temperature), is to create tables that capture the outcomes for the expected range of input values (HTF flow rate, HTF inlet temperature, cooling water flow rate, and cooling water inlet temperature). The reference turbine efficiency is also a parameter which was varied. The ranges of input values are shown in Table 4.1.

Table 4.1 Input Variable Ranges

Variable	Single Loop Dowtherm A	Single Loop Molten Salt	Dual Loop
HTF Mass Flow Rate	354-394 [kg/s]	203-243 [kg/s]	328-368 [kg/s] Dowtherm A 120-160 [kg/s] Molten Salt
HTF Inlet Temperature	363-403 [C]	520-560 [C]	363-403 [C] 520-560 [C]
Cooling Water Mass Flow Rate	1200-1600 [kg/s]	1200-1600 [kg/s]	1200-1600 [kg/s]
Cooling Water Inlet Temperature	15-30 [C]	15-30 [C]	15-30 [C]
Turbine Efficiency	0.80-0.90	0.80-0.90	0.80-0.90

The variable ranges for the cycle have been chosen to be relatively small considering the variability in available solar energy throughout a year or even a day. However, if storage and

auxiliary heating are used effectively, the plant should be able to maintain the operating variables relatively constant during periods of plant operation. The ranges chosen should account for the relationships between input and output variables.

An example of a section table run in EES is shown in Figure 4.14. The EES files used to generate the results in this chapter are provided in an electronic supplement which is indexed in Appendix 2. The pattern is applied in such a way that all combinations of variables are accounted for in the table, which yields 1620 runs.

1..1620	1 mD_1 [kg/s]	2 TD_{in} [C]	3 mC [kg/s]	4 TC_{in} [C]	5 η_{first} [-]	6 η_{second} [-]	7 W_{net} [MW]	8 m_1 [kg/s]	9 TD_6 [K]	10 TC_2 [K]
Run 1	354	363	1200	20	0.3642	0.7246	22.56	25.63	564.5	301
Run 2	359	363	1200	20	0.3644	0.7245	22.71	25.83	565.1	301
Run 3	364	363	1200	20	0.3645	0.7244	22.86	26.03	565.7	301.1
Run 4	369	363	1200	20	0.3647	0.7242	23.01	26.22	566.3	301.1
Run 5	374	363	1200	20	0.3648	0.724	23.15	26.41	566.8	301.2
Run 6	379	363	1200	20	0.365	0.7238	23.29	26.6	567.4	301.2
Run 7	384	363	1200	20	0.3651	0.7236	23.43	26.79	567.9	301.3
Run 8	389	363	1200	20	0.3652	0.7234	23.57	26.98	568.5	301.3
Run 9	394	363	1200	20	0.3653	0.7232	23.7	27.16	569	301.4
Run 10	354	373	1200	20	0.3677	0.72	24.75	27.86	569.3	301.6
Run 11	359	373	1200	20	0.3678	0.7197	24.92	28.08	569.9	301.7
Run 12	364	373	1200	20	0.3679	0.7194	25.08	28.3	570.6	301.7
Run 13	369	373	1200	20	0.368	0.719	25.24	28.52	571.2	301.8
Run 14	374	373	1200	20	0.3681	0.7187	25.4	28.74	571.8	301.8
Run 15	379	373	1200	20	0.3681	0.7183	25.55	28.95	572.4	301.9
Run 16	384	373	1200	20	0.3682	0.7179	25.7	29.16	573	301.9
Run 17	389	373	1200	20	0.3683	0.7175	25.85	29.37	573.5	302
Run 18	394	373	1200	20	0.3683	0.7171	26	29.58	574.1	302
Run 19	354	383	1200	20	0.3704	0.7158	26.94	30.08	574.1	302.3
Run 20	359	383	1200	20	0.3704	0.7152	27.12	30.33	574.7	302.3
Run 21	364	383	1200	20	0.3704	0.7147	27.3	30.58	575.4	302.4
Run 22	369	383	1200	20	0.3704	0.7142	27.47	30.83	576	302.5
Run 23	374	383	1200	20	0.3704	0.7136	27.64	31.07	576.7	302.5
Run 24	379	383	1200	20	0.3704	0.713	27.8	31.31	577.3	302.6
Run 25	384	383	1200	20	0.3704	0.7124	27.97	31.55	577.9	302.6
Run 26	389	383	1200	20	0.3704	0.7121	28.13	31.79	578.5	302.7
Run 27	394	383	1200	20	0.3704	0.7119	28.29	32.03	579.1	302.7
Run 28	354	393	1200	20	0.3722	0.7118	29.17	32.41	578.5	303
Run 29	359	393	1200	20	0.3722	0.7115	29.37	32.69	579.2	303
Run 30	364	393	1200	20	0.3721	0.7112	29.55	32.97	579.8	303.1
Run 31	369	393	1200	20	0.372	0.7109	29.74	33.25	580.5	303.2
Run 32	374	393	1200	20	0.3719	0.7105	29.92	33.52	581.1	303.2
Run 33	379	393	1200	20	0.3718	0.7102	30.1	33.79	581.7	303.3

Figure 4.14 Table Run for Single Loop of Dowtherm A

The single loop of molten salt and the dual loop cycle both have tables with the same pattern applied to account for each possible combination of input variables over the ranges specified in Table 4.1.

Using these data sets, the "Linear Regression" tool in EES is used to create correlations between the input variables and output variables. This function creates second order polynomial correlations between the input and output variables with cross terms. The function also gives the standard error of each term in the correlation. Using this information, terms that have a standard error higher than the coefficient of the term can be eliminated in order to simplify the correlation. An example correlation for the single loop of Dowtherm A is shown below.

$$TD_{return} = 212 + 1.160 \cdot \dot{m}_{HTF} - 0.000193 \cdot \dot{m}_{HTF}^2 + 1.197 \cdot TD_{in} - 0.00113 \cdot TD_{in}^2 - .0000388 \cdot \dot{m}_{HTF} \cdot TD_{in} + 0.00000964 \cdot TC_{in} \cdot TD_{in} \quad (4.20)$$

where TD_{return} is the Dowtherm A return temperature, $\dot{m}_{HTF}$ is the Dowtherm A mass flow rate, TD_{in} is the Dowtherm A inlet temperature, and TC_{in} is the cooling water inlet temperature. Note that there are terms in this equation that have been eliminated because they did not significantly improve the regression. There is no dependence of the return temperature on the cooling water flow rate. In addition, there is no second order dependence of the return temperature on the cooling water flow rate or temperature. Also, all cross terms with the cooling water flow rate have been eliminated.

A table with the correlations for the single loop of Dowtherm A is shown in Table 4.2.

Table 4.2 Single Loop of Dowtherm A Correlations

Variable	Correlation	RMS	R^2
W_{net}	$W_{net} = 12.0 - 0.0523 \cdot \dot{m}_{HTF} - 0.0000590 \cdot \dot{m}_{HTF}^2 - 0.0318 \cdot TD_{in} - 0.0000590 \cdot TD_{in}^2 - 0.00450 \cdot \dot{m}_{cw} - 0.000000803 \cdot \dot{m}_{cw}^2 + 0.329 \cdot TC_{in} - 0.0000252 \cdot TC_{in}^2 - 69.4 \cdot \eta_{turbine} - 3.810 \cdot \eta_{turbine}^2 + 0.000247 \cdot \dot{m}_{HTF} \cdot TD_{in} + 0.00000292 \cdot \dot{m}_{HTF} \cdot \dot{m}_{cw} - 0.000135 \cdot \dot{m}_{HTF} \cdot TC_{in} + 0.0419 \cdot \dot{m}_{HTF} \cdot \eta_{turbine} + 0.0000167 \cdot TD_{in} \cdot \dot{m}_{cw} - 0.000791 \cdot TD_{in} \cdot TC_{in} + 0.235 \cdot TD_{in} \cdot \eta_{turbine} + 0.00000314 \cdot \dot{m}_{cw} \cdot TC_{in} + 0.000410 \cdot \dot{m}_{cw} \cdot \eta_{turbine} - 0.100 \cdot TC_{in} \cdot \eta_{turbine}$	.0809	100.00%
TD_{return}	$TD_{return} = 212 + 1.160 \cdot \dot{m}_{HTF} - 0.000193 \cdot \dot{m}_{HTF}^2 + 1.197 \cdot TD_{in} - 0.00113 \cdot TD_{in}^2 - .0000388 \cdot \dot{m}_{HTF} \cdot TD_{in} + 0.00000964 \cdot TC_{in} \cdot TD_{in}$	.0576	99.99%
TC_{return}	$TC_{return} = 269 - 0.0126 \cdot \dot{m}_{HTF} - 0.0000111 \cdot \dot{m}_{HTF}^2 + 0.0279 \cdot TD_{in} + 0.000102 \cdot TD_{in}^2 - 0.000967 \cdot \dot{m}_{cw} + 0.00000448 \cdot \dot{m}_{cw}^2 + 0.965 \cdot TC_{in} - 0.0000403 \cdot TC_{in}^2 + 7.85 \cdot \eta_{turbine} + 0.000123 \cdot \dot{m}_{HTF} \cdot TD_{in} - 0.00000781 \cdot \dot{m}_{HTF} \cdot \dot{m}_{cw} + 0.0000224 \cdot \dot{m}_{HTF} \cdot TC_{in} - 0.00672 \cdot \dot{m}_{HTF} \cdot \eta_{turbine} - 0.0000450 \cdot TD_{in} \cdot \dot{m}_{cw} + 0.000134 \cdot TD_{in} \cdot TC_{in} - 0.0395 \cdot TD_{in} \cdot \eta_{turbine} - 0.0000136 \cdot \dot{m}_{cw} \cdot TC_{in} + 0.00334 \cdot \dot{m}_{cw} \cdot \eta_{turbine} + 0.0170 \cdot TC_{in} \cdot \eta_{turbine}$	.0105	100.00%

The first law efficiency is calculated using the net power and the return temperature correlations.

$$\eta_{first} = \frac{\dot{W}_{net}}{\dot{m}_{HTF} h_{Dow}(TD_{in}) - \dot{m}_{HTF} h_{Dow}(TD_{return})} \tag{4.21}$$

where h is the specific enthalpy of Dowtherm A, which is determined in EES using the temperature, and the net power and return temperature are calculated using the correlations from table 4.2.

A table with the correlations for the single loop of Molten Salt is shown in Table 4.3.

Table 4.3 Single Loop of Molten Salt Correlations

Variable	Correlation	RMS	R^2
W_{net}	$W_{net} = 32.0 - 0.101 \cdot \dot{m}_{salt} - 0.000154 \cdot \dot{m}_{salt}^2 - 0.107 \cdot TS_{in} + 0.0000581 \cdot TS_{in}^2 - 0.00195 \cdot \dot{m}_{cw} - 0.000000559 \cdot \dot{m}_{cw}^2 + 0.193 \cdot TC_{in} - 0.0000118 \cdot TC_{in}^2 - 41.8 \cdot \eta_{turbine} - 6.62 \cdot \eta_{turbine}^2 + 0.000315 \cdot \dot{m}_{salt} \cdot TS_{in} + 0.00000530 \cdot \dot{m}_{salt} \cdot \dot{m}_{cw} - 0.000278 \cdot \dot{m}_{salt} \cdot TC_{in} + 0.0998 \cdot \dot{m}_{salt} \cdot \eta_{turbine} + 0.00000515 \cdot TS_{in} \cdot \dot{m}_{cw} - 0.000268 \cdot TS_{in} \cdot TC_{in} + 0.0110 \cdot TS_{in} \cdot \eta_{turbine} + 0.00000207 \cdot \dot{m}_{cw} \cdot TC_{in} + 0.000373 \cdot \dot{m}_{cw} \cdot \eta_{turbine} - 0.0858 \cdot TC_{in} \cdot \eta_{turbine}$	.00541	100.00%
TS_{return}	$TS_{return} = 303 + 0.318 \cdot \dot{m}_{salt} - 0.000619 \cdot \dot{m}_{salt}^2 + 0.655 \cdot TS_{in} - 0.000372 \cdot TS_{in}^2 + 0.0000000225 \cdot \dot{m}_{cw}^2 - 0.00188 \cdot TC_{in} - 4.04 \cdot \eta_{turbine} + 4.56 \cdot \eta_{turbine}^2 + 0.000395 \cdot \dot{m}_{salt} \cdot TS_{in} - 0.000000127 \cdot \dot{m}_{salt} \cdot \dot{m}_{cw} + 0.00000498 \cdot \dot{m}_{salt} \cdot TC_{in} + 0.00520 \cdot \dot{m}_{salt} \cdot \eta_{turbine} - 0.000000112 \cdot TS_{in} \cdot \dot{m}_{cw} + 0.00000503 \cdot TS_{in} \cdot TC_{in} - 0.0399 \cdot TS_{in} \cdot \eta_{turbine} - 0.000000138 \cdot \dot{m}_{cw} \cdot TC_{in} + 0.00143 \cdot TC_{in} \cdot \eta_{turbine}$	.00397	100.00%
TC_{return}	$TC_{return} = 274 - 0.00184 \cdot \dot{m}_{salt} - 0.000000547 \cdot \dot{m}_{salt}^2 + 0.0172 \cdot TS_{in} + 0.0000135 \cdot TS_{in}^2 - 0.00468 \cdot \dot{m}_{cw} + 0.00000356 \cdot \dot{m}_{cw}^2 + 0.983 \cdot TC_{in} - 0.0000416 \cdot TC_{in}^2 + 2.68 \cdot \eta_{turbine} + 0.874 \cdot \eta_{turbine}^2 + 0.000107 \cdot \dot{m}_{salt} \cdot TS_{in} - 0.0000160 \cdot \dot{m}_{salt} \cdot \dot{m}_{cw} + 0.0000497 \cdot \dot{m}_{salt} \cdot TC_{in} - 0.0131 \cdot \dot{m}_{salt} \cdot \eta_{turbine} - 0.0000157 \cdot TS_{in} \cdot \dot{m}_{cw} + 0.0000485 \cdot TS_{in} \cdot TC_{in} - 0.0165 \cdot TS_{in} \cdot \eta_{turbine} - 0.0000112 \cdot \dot{m}_{cw} \cdot TC_{in} + 0.00260 \cdot \dot{m}_{cw} \cdot \eta_{turbine} + 0.0142 \cdot TC_{in} \cdot \eta_{turbine}$	.00603	100.00%

The first law efficiency is calculated using the net power and the return temperature correlations.

$$\eta_{first} = \frac{W_{net}}{\dot{m}_{salt} h(TS_{in}) - \dot{m}_{salt} h(TS_{return})} \tag{4.21}$$

where h is the specific enthalpy, and the net power and return temperature are calculated using the correlations from Table 4.3. The salt used in the specific enthalpy function is a 60/40 mixture of sodium and potassium nitrate. Properties for this fluid are provided in EES, which refers to this fluid as Salt (60% $NaNO_3$ / 40% KNO_3). A table with the correlations for the dual loop is shown in Table 4.4.

Table 4.4 Dual Loop Correlations

Variable	Correlation	RMS	R^2
W_{net}	$W_{net} = 60.8 - 0.0256 \cdot \dot{m}_{Dow} - 0.0000572 \cdot \dot{m}_{Dow}^2 - 0.0826 \cdot TD_{in} - 0.000182 \cdot TD_{in}^2 - 0.00323 \cdot \dot{m}_{cw} - 0.000000538 \cdot \dot{m}_{cw}^2 + 0.254 \cdot TC_{in} - 0.00000788 \cdot TC_{in}^2 - 0.175 \cdot \dot{m}_{salt} - 0.000151 \cdot \dot{m}_{salt}^2 - 0.131 \cdot TS_{in} + 0.0000303 \cdot TS_{in}^2 - 70.0 \cdot \eta_{turbine} - 4.97 \cdot \eta_{turbine}^2 + 0.000133 \cdot \dot{m}_{Dow} \cdot TD_{in} + 0.00000189 \cdot \dot{m}_{Dow} \cdot \dot{m}_{cw} - 0.0000968 \cdot \dot{m}_{Dow} \cdot TC_{in} + 0.0000563 \cdot \dot{m}_{Dow} \cdot \dot{m}_{salt} + 0.00000148 \cdot \dot{m}_{Dow} \cdot TS_{in} + 0.0403 \cdot \dot{m}_{Dow} \cdot \eta_{turbine} + 0.0000106 \cdot TD_{in} \cdot \dot{m}_{cw} - 0.000550 \cdot TD_{in} \cdot TC_{in} + 0.000352 \cdot TD_{in} \cdot \dot{m}_{salt} + 0.000248 \cdot TD_{in} \cdot TS_{in} + 0.195 \cdot TD_{in} \cdot \eta_{turbine} + 0.00000190 \cdot \dot{m}_{cw} \cdot TC_{in} + 0.000000317 \cdot \dot{m}_{cw} \cdot \dot{m}_{salt} + 0.000000590 \cdot \dot{m}_{cw} \cdot TS_{in} + 0.000458 \cdot \dot{m}_{cw} \cdot \eta_{turbine} - 0.0000137 \cdot TC_{in} \cdot \dot{m}_{salt} - 0.0000290 \cdot TC_{in} \cdot TS_{in} - 0.0890 \cdot TC_{in} \cdot \eta_{turbine} + 0.000135 \cdot \dot{m}_{salt} \cdot TS_{in} + 0.0116 \cdot \dot{m}_{salt} \cdot \eta_{turbine} + 0.0327 \cdot TS_{in} \cdot \eta_{turbine}$	.0108	100.00%

TD_{return}	$TD_{return} = 264 + 0.0426 \cdot \dot{m}_{Dow} - 0.000169 \cdot \dot{m}_{Dow}^2 + 1.00 \cdot TD_{in} - 0.000922 \cdot TD_{in}^2 + 0.000113 \cdot \dot{m}_{cw} + 0.0000000208 \cdot \dot{m}_{cw}^2 - 0.00840 \cdot TC_{in} + 0.00000401 \cdot TC_{in}^2 - 0.168 \cdot \dot{m}_{salt} - 0.000186 \cdot \dot{m}_{salt}^2 + 0.00967 \cdot TS_{in} + 0.00000813 \cdot TS_{in}^2 + 9.58 \cdot \eta_{turbine} + 4.07 \cdot \eta_{turbine}^2 + 0.000457 \cdot \dot{m}_{Dow} \cdot TD_{in} - 0.0000000218 \cdot \dot{m}_{Dow} \cdot \dot{m}_{cw} - 0.00000157 \cdot \dot{m}_{Dow} \cdot TC_{in} + 0.0000478 \cdot \dot{m}_{Dow} \cdot \dot{m}_{salt} - 0.0000696 \cdot \dot{m}_{Dow} \cdot TS_{in} + 0.0203 \cdot \dot{m}_{Dow} \cdot \eta_{turbine} - 0.000000402 \cdot TD_{in} \cdot \dot{m}_{cw} + 0.0000206 \cdot TD_{in} \cdot TC_{in} + 0.000421 \cdot TD_{in} \cdot \dot{m}_{salt} + 0.000227 \cdot TD_{in} \cdot TS_{in} - 0.0173 \cdot TD_{in} \cdot \eta_{turbine} - 0.000000143 \cdot \dot{m}_{cw} \cdot TC_{in} - 0.0000000482 \cdot \dot{m}_{cw} \cdot \dot{m}_{salt} - 0.0000000547 \cdot \dot{m}_{cw} \cdot TS_{in} + 0.00000427 \cdot TC_{in} \cdot \dot{m}_{salt} + 0.00000453 \cdot TC_{in} \cdot TS_{in} + 0.00134 \cdot TC_{in} \cdot \eta_{turbine} + 0.000175 \cdot \dot{m}_{salt} \cdot TS_{in} - 0.0336 \cdot \dot{m}_{salt} \cdot \eta_{turbine} - 0.0480 \cdot TS_{in} \cdot \eta_{turbine}$	.0133	100.00%
TS_{return}	$TS_{return} = 12.2 + 0.0144 \cdot \dot{m}_{Dow} + 0.000187 \cdot \dot{m}_{Dow}^2 + 0.805 \cdot TD_{in} + 0.00128 \cdot TD_{in}^2 - 0.000255 \cdot \dot{m}_{cw} - 0.0000000349 \cdot \dot{m}_{cw}^2 + 0.0202 \cdot TC_{in} + 0.583 \cdot \dot{m}_{salt} - 0.00129 \cdot \dot{m}_{salt}^2 + 1.58 \cdot TS_{in} - 0.000208 \cdot TS_{in}^2 - 41.0 \cdot \eta_{turbine} - 6.60 \cdot \eta_{turbine}^2 + 0.0000915 \cdot \dot{m}_{Dow} \cdot TD_{in} + 0.0000000394 \cdot \dot{m}_{Dow} \cdot \dot{m}_{cw} - 0.000196 \cdot \dot{m}_{Dow} \cdot \dot{m}_{salt} - 0.000416 \cdot \dot{m}_{Dow} \cdot TS_{in} - 0.0186 \cdot \dot{m}_{Dow} \cdot \eta_{turbine} + 0.000000534 \cdot TD_{in} \cdot \dot{m}_{salt} - 0.0000194 \cdot TD_{in} \cdot TC_{in} - 0.00263 \cdot TD_{in} \cdot \dot{m}_{salt} - 0.00307 \cdot TD_{in} \cdot TS_{in} - 0.0200 \cdot TD_{in} \cdot \eta_{turbine} + 0.000000165 \cdot \dot{m}_{cw} \cdot \dot{m}_{salt} + 0.000000298 \cdot \dot{m}_{cw} \cdot TS_{in} - 0.0000156 \cdot TC_{in} \cdot \dot{m}_{salt} - 0.0000293 \cdot TC_{in} \cdot TS_{in} + 0.00231 \cdot \dot{m}_{salt} \cdot TS_{in} + 0.0381 \cdot \dot{m}_{salt} \cdot \eta_{turbine} + 0.132 \cdot TS_{in} \cdot \eta_{turbine}$	.0998	99.99%

TC_{return}	$TC_{return} = 283 - 0.0117 \cdot \dot{m}_{Dow} - 0.00000884 \cdot \dot{m}_{Dow}^2 - 0.0362 \cdot TD_{in} + 0.000121 \cdot TD_{in}^2 + 0.00000704 \cdot \dot{m}_{cw} + 0.00000346 \cdot \dot{m}_{cw}^2 + 0.972 \cdot TC_{in} - 0.0000412 \cdot TC_{in}^2 - 0.0108 \cdot \dot{m}_{salt} - 0.0000118 \cdot \dot{m}_{salt}^2 - 0.00959 \cdot TS_{in} + 0.00000271 \cdot TS_{in}^2 + 7.35 \cdot \eta_{turbine} + 0.502 \cdot \eta_{turbine}^2 + 0.0000965 \cdot \dot{m}_{Dow} \cdot TD_{in} - 0.00000586 \cdot \dot{m}_{Dow} \cdot \dot{m}_{cw} + 0.0000166 \cdot \dot{m}_{Dow} \cdot TC_{in} + 0.00000338 \cdot \dot{m}_{Dow} \cdot \dot{m}_{salt} - 0.00000200 \cdot \dot{m}_{Dow} \cdot TS_{in} - 0.00345 \cdot \dot{m}_{Dow} \cdot \eta_{turbine} + 0.0000336 \cdot TD_{in} \cdot \dot{m}_{cw} + 0.0000985 \cdot TD_{in} \cdot TC_{in} + 0.0000335 \cdot TD_{in} \cdot \dot{m}_{salt} + 0.0000376 \cdot TD_{in} \cdot TS_{in} - 0.0303 \cdot TD_{in} \cdot \eta_{turbine} - 0.0000108 \cdot \dot{m}_{cw} \cdot TC_{in} - 0.00000116 \cdot \dot{m}_{cw} \cdot \dot{m}_{salt} - 0.00000195 \cdot \dot{m}_{cw} \cdot TS_{in} - 0.00000577 \cdot TC_{in} \cdot TS_{in} + 0.0147 \cdot TC_{in} \cdot \eta_{turbine} + 0.00000766 \cdot \dot{m}_{salt} \cdot TS_{in} - 0.00121 \cdot \dot{m}_{salt} \cdot \eta_{turbine} - 0.00348 \cdot TS_{in} \cdot \eta_{turbine}$	.00773	100.00%

The first law efficiency is calculated using the net power and the return temperature correlations.

$$\eta_{first} = \frac{W_{net}}{\dot{m}_{salt}(h_{salt}(TS_{in}) - h_{salt}(TS_{return})) + \dot{m}_{Dow}(h_{Dow}(TD_{in}) - h_{Dow}(TD_{return}))} \tag{4.22}$$

where h is the specific enthalpy, and the net power and return temperature are calculated using the correlations from table 4.4. The salt used in the specific enthalpy function is $'Salt(60NaNO3\_40KNO3)'$.

Correlations between the inputs variables and the output variables are obtained using the linear regression tool in EES for each cycle. In order to determine the effectiveness of these correlations, the error between the model and the correlations is found at various operating

points. The percent error is calculated using equation 4.23, which is used for each correlation value and its corresponding model value.

$$Percent\ Error = \frac{|Value_{correlation} - Value_{model}|}{Value_{model}} \cdot 100\ [\%] \qquad (4.23)$$

Table 4.5 Error between Model and Correlation Values (Single Loop Dowtherm A)

HTF Mass Flow Rate [kg/s]	HTF Inlet Temperature [C]	Cooling Water Inlet Temperature [C]	Cooling Water Mass Flow Rate [kg/s]	Error in Net Power [%]	Error in HTF Return Temperature [%]	Error in Cooling Water Return Temperature [%]	Error in First Law Efficiency [%]
354	363	30	1200	0.001	0.013	0.003	0.100
354	363	15	1600	0.117	0.009	0.012	0.208
384	393	30	1200	0.003	0.002	0.005	0.017
384	393	15	1600	0.016	0.001	0.001	0.006
394	403	30	1200	0.116	0.001	0.016	0.121
394	403	15	1600	0.011	0.005	0.002	0.046

The error associated with the correlations is low for the operating points shown. A table with the error for the single loop molten salt cycle for selected operating points is shown in Table 4.6.

Table 4.6 Error between Model and Correlation Values (Single Loop Molten Salt)

HTF Mass Flow Rate [kg/s]	HTF Inlet Temperature [C]	Cooling Water Inlet Temperature [C]	Cooling Water Mass Flow Rate [kg/s]	Error in Net Power [%]	Error in HTF Return Temperature [%]	Error in Cooling Water Return Temperature [%]	Error in First Law Efficiency [%]
203	520	30	1200	0.012	0.0004	0.0003	0.013
203	520	15	1600	0.079	0.0003	0.009	0.080
233	550	30	1200	0.002	0.0008	0.005	0.0004
233	550	15	1600	0.016	0.0008	0.0009	0.018
243	560	30	1200	0.074	0.0003	0.010	0.075
243	560	15	1600	0.012	0.0005	0.0003	0.013

The final table with the dual loop error between the model values and the correlations is shown in Table 4.7.

Table 4.7 Error between Model and Correlation Values (Dual Loop)

HTF Mass Flow Rate [kg/s] Dow/Salt	HTF Inlet Temperature [C] Dow/Salt	Cooling Water Inlet Temperature [C]	Cooling Water Mass Flow Rate [kg/s]	Error in Net Power [%]	Error in HTF Return Temperature [%] Dow/Salt	Error in Cooling Water Return Temperature [%]	Error in First Law Efficiency [%]
328/120	363/520	30	1200	0.037	0.003/0.016	0.001	0.021
328/120	363/520	15	1600	0.074	0.003/0.017	0.015	0.090
358/150	393/550	30	1200	0.044	0.003/0.005	0.004	0.053
358/150	393/550	15	1600	0.060	0.002/0.004	0.001	0.069
368/160	403/560	30	1200	0.082	0.003/0.018	0.017	0.103
368/160	403/560	15	1600	0.013	0.003/0.017	0.001	0.008

The error for each one of the correlations used to calculate output variables is small. Therefore, these correlations can be used to approximate the Rankine cycle model at off-design conditions.

4.8 Model Justification

The model created in EES is based on assumptions that have been described in the previous two chapters. Therefore, the model has to be justified with real data from a solar power plant and/or compared with results of other models. The power output from the single loop of Dowtherm A is compared to another solar power plant that utilizes an organic heat transfer fluid. Figures 4.15 and 4.16 are plots of the power output throughout a typical day in the summer and winter (Patnode 2006).

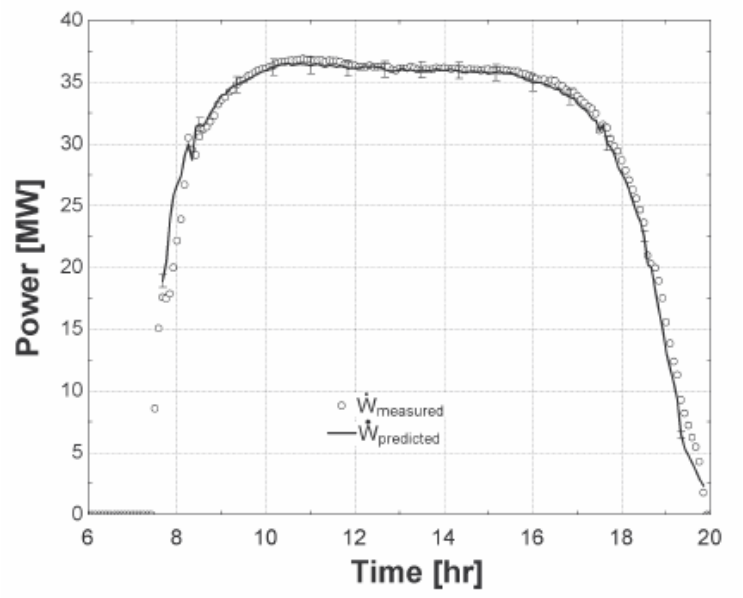

Figure 4.15 Gross power predicted by the power cycle model as compared to measured gross electric power for June 20, 1998 from Patnode 2006.

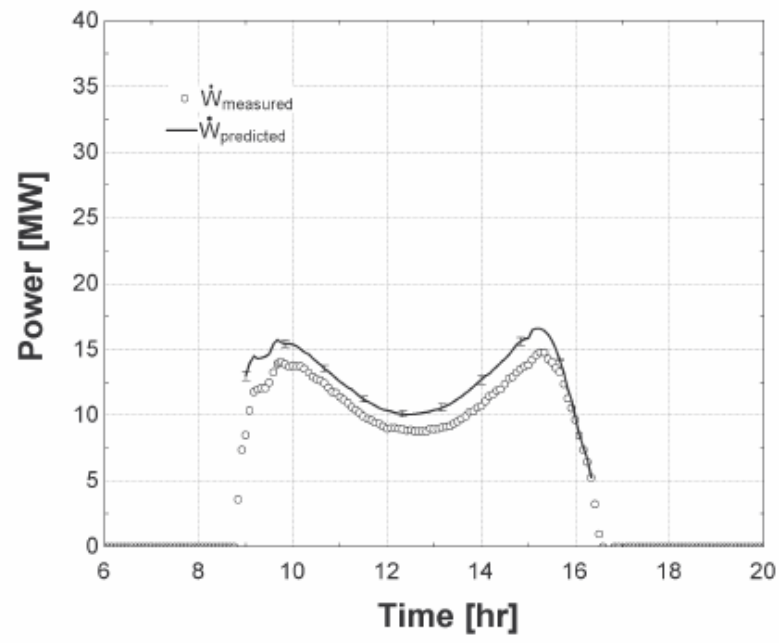

Figure 4.16 Gross power output predicted by the power cycle model as compared to measure gross electric power for December 16, 1998 from Patnode 2006.

The EES model used to predict the actual power output shows agreement with experimental data from the plant to within (+/- 1%) on the summer day, and 10% higher at most on the winter day (Patnode 2006). Since Patnode's model has been shown to compare well with experimental measurements, the power cycle model described in the previous two chapters will be compared to this power cycle model. In order to compare these two models, adjustments are made to the model in Chapter 3 to make the operating conditions and physical sizes of the equipment similar to those used in the Patnode model. The Patnode model does not take in the cooling water flow rate and cooling water temperature as inputs. The condensing pressure is a direct input of the model. Therefore, the first adjustment is changing the condenser to have a fixed pressure to match the Patnode model. A table with the old, new, and Patnode overall heat transfer coefficient values is shown in Table 4.8.

Table 4.8 Overall Heat Transfer Coefficient Values

Heat Exchanger	Previous Value (kW/K)	Adjusted Value (kW/K)	Patnode Value (kW/K)
Preheater	533	667	724
Boiler	1643	2054	2051
Superheater	280.5	311	292
Reheater	240	178.7	149.1
Closed Feed Water Heater	191.5	214.2	217.1 (AVERAGE)

The average overall heat transfer coefficient is listed for the closed feed water heater for the Patnode model, since the Patnode cycle has six closed feed water heaters.

A plot of the total turbine work vs. the flow rate of the heat transfer fluid is shown below which contains curves generated from the model described in Chapter 3 and the Patnode model described above.

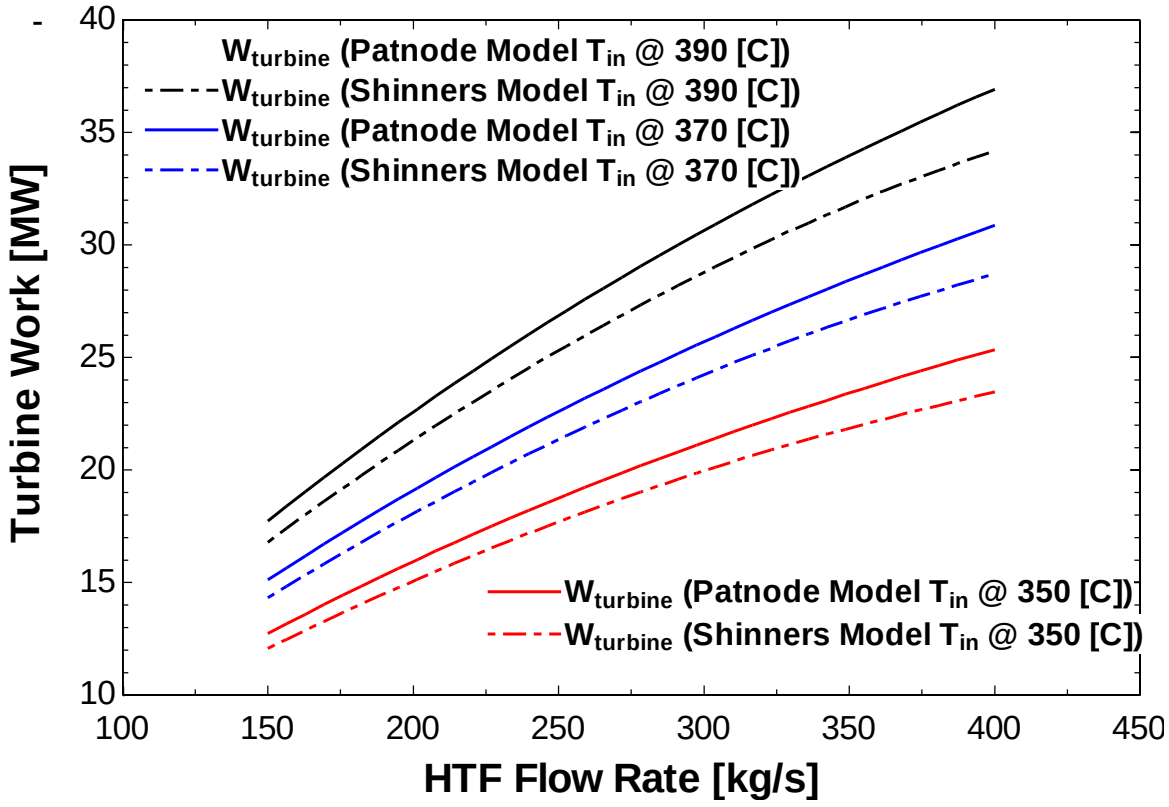

Figure 4.17 Turbine Work vs. HTF mass flow, at various HTF temperatures entering the power cycle. Condensing pressure=0.08 [bar]

The maximum difference from the Patnode is 7.5%. The reasons for this discrepancy are provided below. Despite a difference in between the curves, both models follow the same trend with varying temperature and flow rate of the heat transfer fluid.

The two models are also compared at different condenser pressures to determine whether or not the trends are constant. A plot of the turbine work vs. mass flow rate at 12 kPa is shown in Figure 4.18.

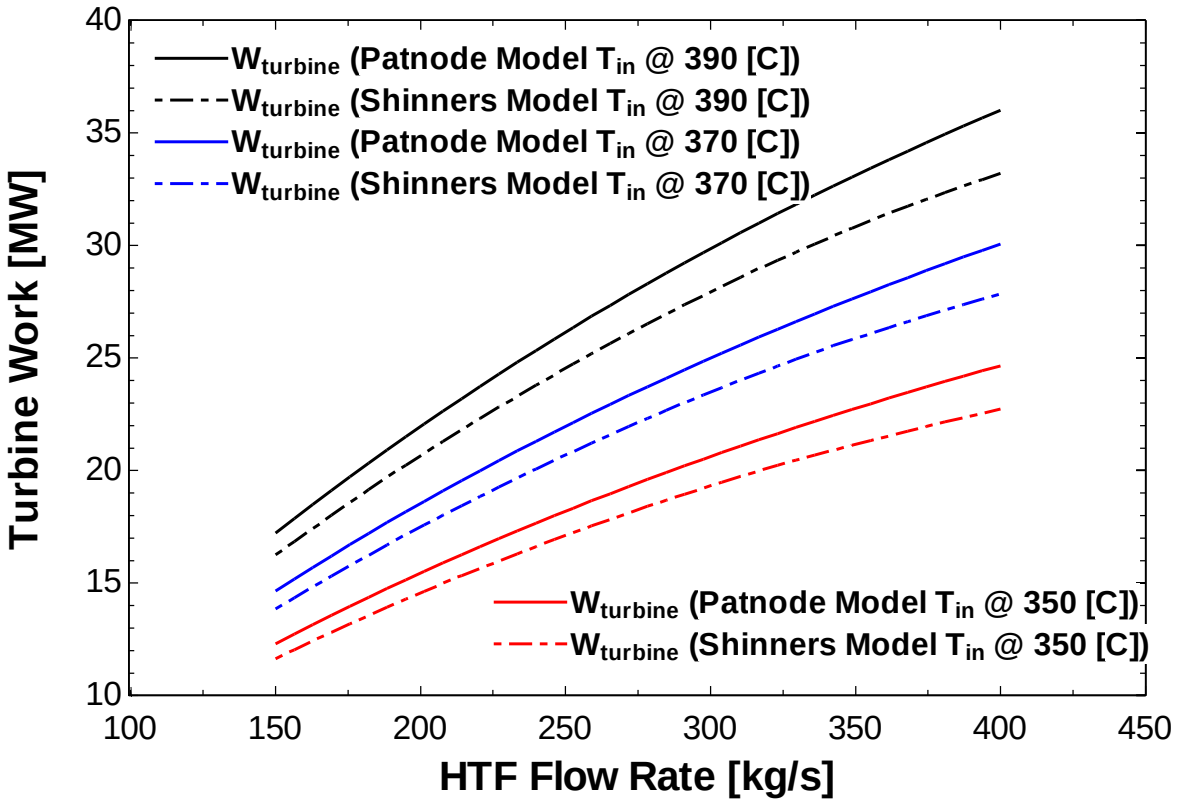

Figure 4.18 Turbine Work vs. HTF mass flow, at various HTF temperatures entering the power cycle. Condensing pressure=0.12 [bar]

The trends shown in figure 4.17 are the same shown in figure 4.18. Even with varying condenser pressure, the models follow the same trend, and the difference from the Patnode model is less than 7.5%. The first law efficiencies of each cycle are also compared. The efficiencies do not account for parasitic power losses; the efficiency compared is the ratio of the total turbine work to the heat input.

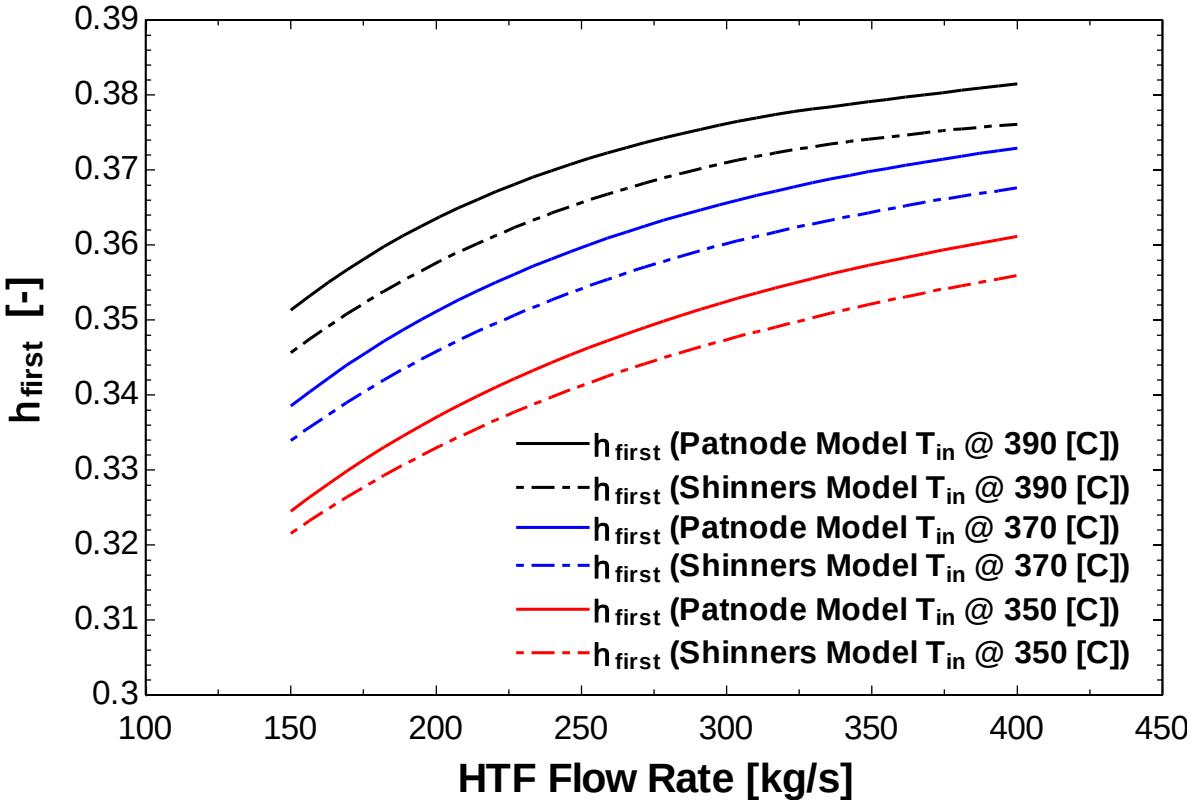

Figure 4.19 First Law Efficiency vs. HTF mass flow, at various HTF temperatures entering the power cycle. Condensing pressure=0.08 [bar]

The efficiencies of each cycle follow similar trends for the same temperatures. The model described in Chapter 3 differs from the Patnode model by less than 1.5%. The efficiencies are also plotted at a higher condenser pressure shown in Figure 4.20.

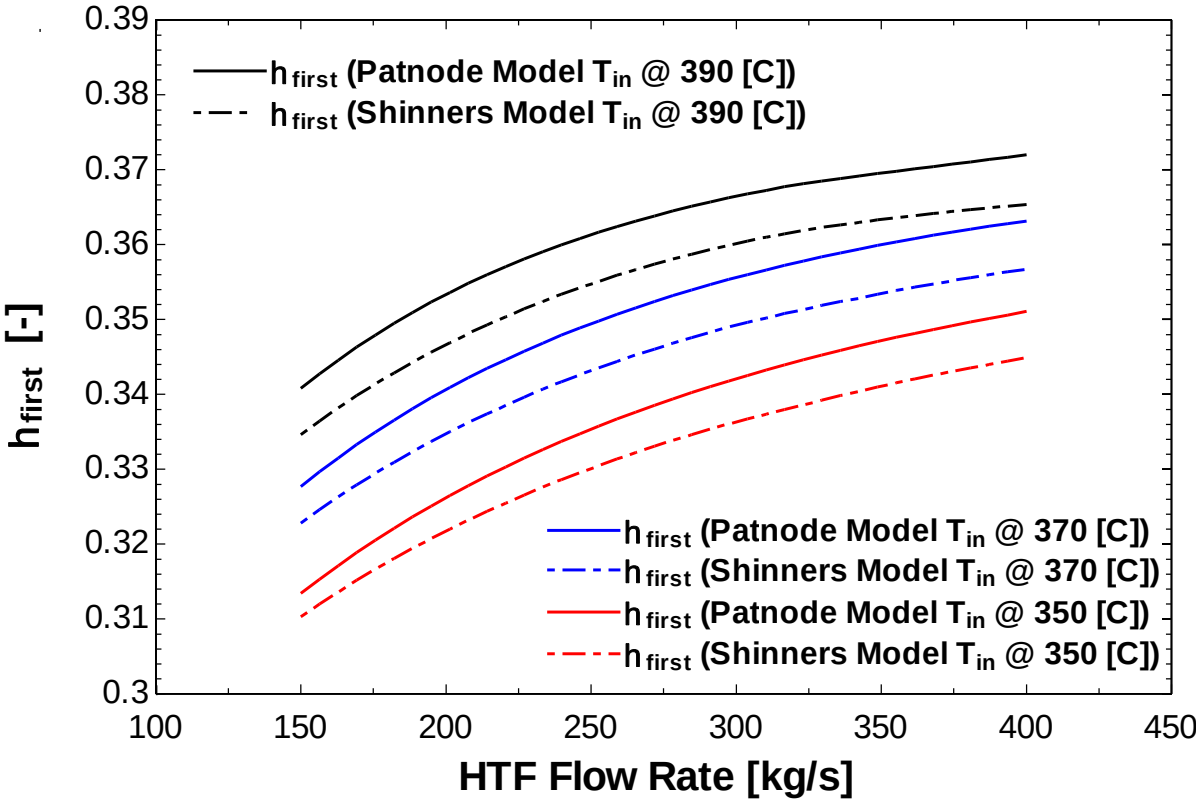

Figure 4.20 First Law Efficiency vs. HTF mass flow, at various HTF temperatures entering the power cycle. Condensing pressure=0.12 [bar]

For a higher condenser pressure, the efficiency differs from the Patnode model by less than 2%. The last parameter compared between the two models is the heat transfer fluid return temperature.

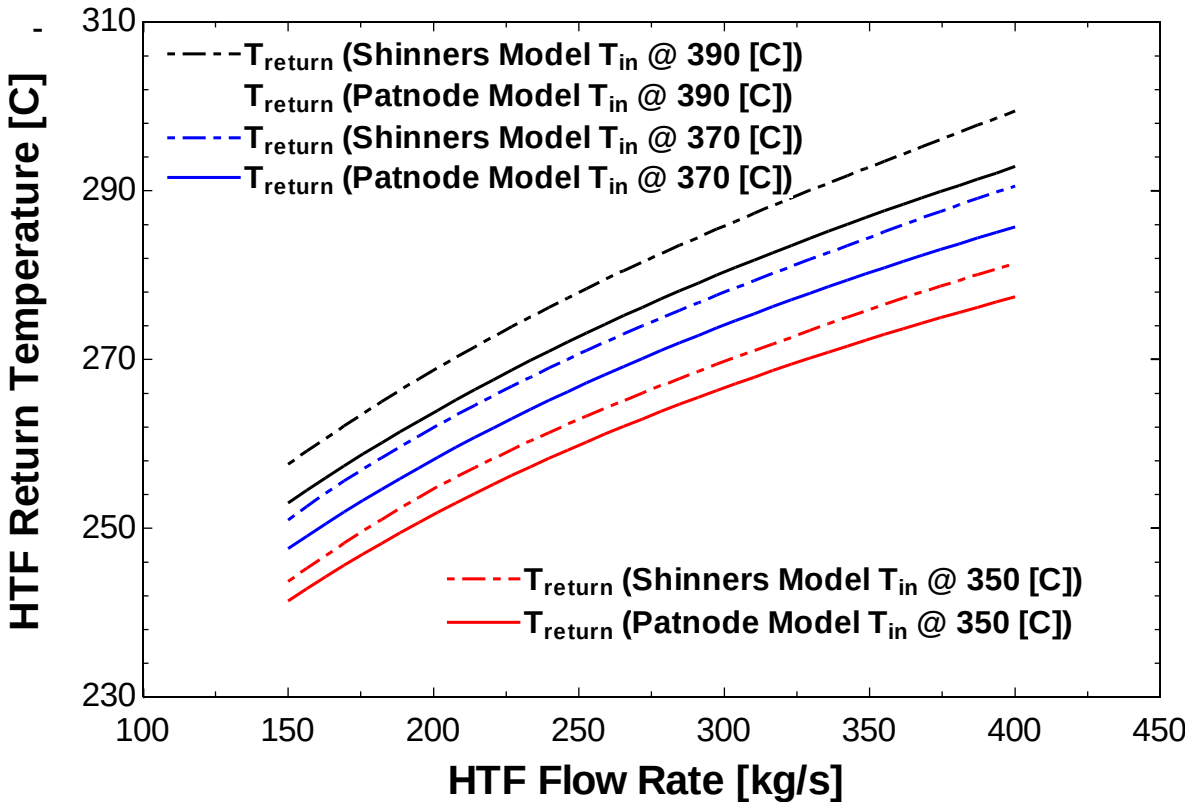

Figure 4.21 HTF Return Temperature vs. HTF mass flow, at various HTF temperatures entering the power cycle. Condensing pressure=0.08 [bar]

The Chapter 3 model return temperature is higher than the Patnode model by a maximum of 2.5%. The efficiencies of both cycles are close, but the total turbine work for the Patnode model is higher. The temperature curves shown in figure 4.21 do not change for different condenser pressures. The two models will never completely agree because the Patnode model has varying turbine efficiencies for each turbine stage, and there are 3 stages on the first turbine and 5 on the second. These efficiencies range from 0.84 to 0.94, as opposed to this model, which has a turbine efficiency constant at 0.85. The turbine power is higher for the Patnode model because the turbine efficiency is higher for most stages in the Patnode model. Though this difference exists, Figures 4.17 through 4.21 show that the model described in this Chapter and Chapter 3 follow the same trends and closely agree to a model

successfully used to predict the output parameters of a Rankine cycle utilizing and a single loop of an organic heat transfer fluid. The purpose of this model is to compare the three systems using Dowtherm A and molten salt heat transfer fluids. The same assumptions (condenser inputs, turbine and pump efficiencies, etc.) are used for both fluids, which tends to cancel their effects with regard to how the systems perform with fluids.

Chapter 5 TRNSYS Components

5.1 Introduction

In addition to the Rankine cycle models adapted to TRNSYS, there are several other TRNSYS components required to model the entire system. This section will describe the additional TRNSYS components used for the system and any modifications required. Figure 5.1 shows the basic system setup for the TRNSYS system.

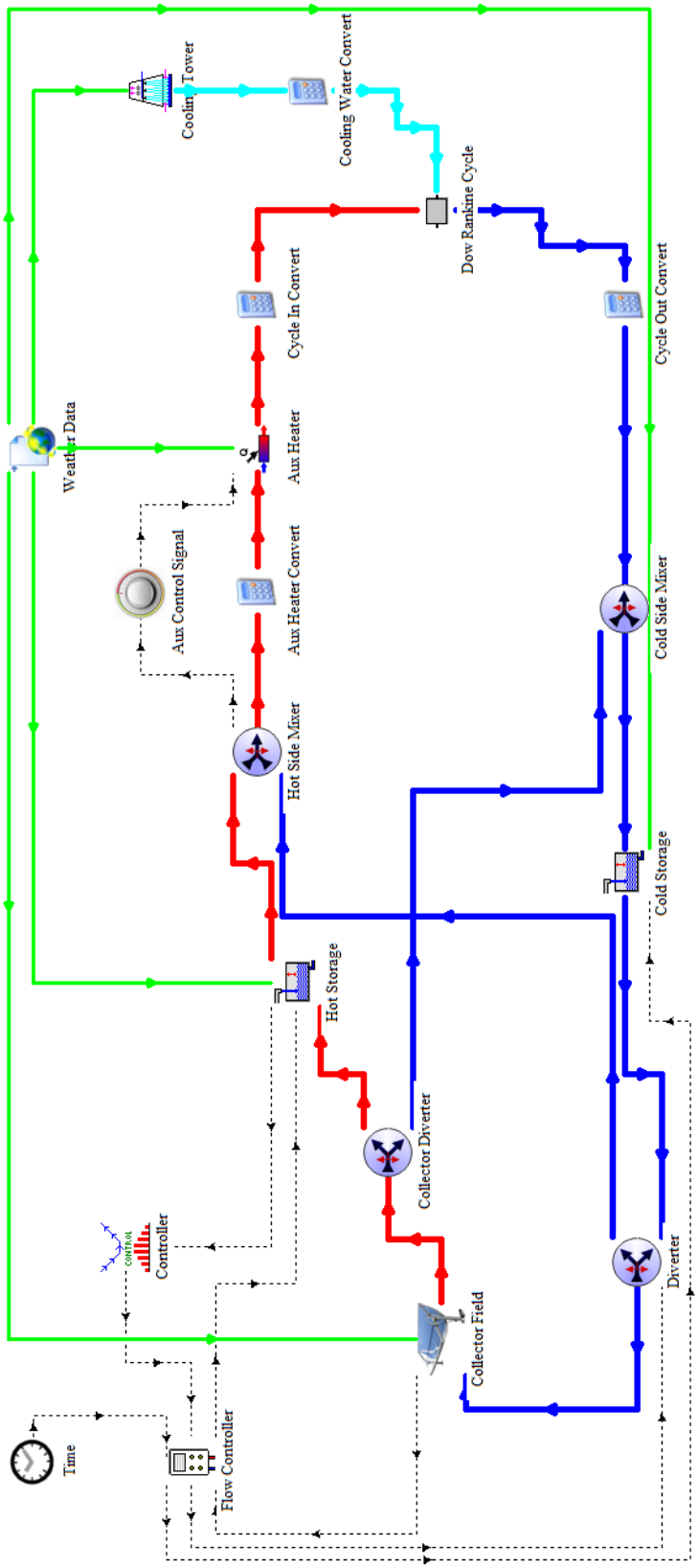

Figure 5.1 TRNSYS System Layout

5.2 Time Values (Type 21-Existing)

Type 21 is a component that outputs the time in various forms. Table 5.1 shows the parameters and outputs for Type 21.

Table 5.1 Type 21 Parameters and Outputs

Parameters	Name	Dimension	Unit	Type	Range	Default
1	Mode	Dimensionless	[-]	Integer	[1]	1
2	Relative Time	Dimensionless	[-]	Boolean	[0;1]	0
Outputs						
1	Simulation Year	Dimensionless	[-]	Real	[-inf;inf]	0
2	Simulation Month	Dimensionless	[-]	Real	[-inf;inf]	0
3	Simulation Day	Dimensionless	[-]	Real	[-inf;inf]	0
4	Calendar Month	Dimensionless	[-]	Real	[-inf;inf]	0
5	Day of the Year	Dimensionless	[-]	Real	[-inf;inf]	0
6	Day of the Month	Dimensionless	[-]	Real	[-inf;inf]	0
7	Day of the Week	Dimensionless	[-]	Real	[-inf;inf]	0
8	Hour of the Year	Dimensionless	[-]	Real	[-inf;inf]	0
9	Hour of the Month	Dimensionless	[-]	Real	[-inf;inf]	0
10	Hour of the Week	Dimensionless	[-]	Real	[-inf;inf]	0
11	Hour of the Day	Dimensionless	[-]	Real	[-inf;inf]	0

The only output used from this type is the hour of the day, which is used in the flow controller, Type 860.

5.3 Collector Model (Type 850-Updated)

The collector field model used for the TRNSYS system is based on Excelergy (Price 2005), which was modified for the analysis of the SEGs power plants by Patnode (2006). The model calculates the outlet temperature from a collector field, as well as parasitic heat and power requirements, based on a number of parameters and inputs. A list of the parameters for the collector field model is shown in Table 5.2.

Table 5.2 Collector Parameters

Number	Name	Dimension	Unit	Type	Range	Default Value
1	$\dot{W}_{gross}$	Power	[MW]	Real	[-inf;inf]	35
2	η_{gross}	Dimensionless	[-]	Real	[-inf;inf]	0.375
3	$NumHCEType$	Dimensionless	[-]	Real	[-inf;inf]	4
4	$NumColType$	Dimensionless	[-]	Real	[-inf;inf]	1
4+2n-1	$HCEType(n)$	Dimensionless	[-]	Real	[-inf;inf]	1
4+2n	$HCEFrac(n)$	Dimensionless	[-]	Real	[-inf;inf]	1
4+2n+6i-5	$ColType(i)$	Dimensionless	[-]	Real	[-inf;inf]	1
4+2n+6i-4	$ColFrac(i)$	Dimensionless	[-]	Real	[-inf;inf]	1
4+2n+6i-3	$TrkTwstErr(i)$	Dimensionless	[-]	Real	[-inf;inf]	0.994
4+2n+6i-2	$GeoAcc(i)$	Dimensionless	[-]	Real	[-inf;inf]	0.98
4+2n+6i-1	$MirRef(i)$	Dimensionless	[-]	Real	[-inf;inf]	0.93
4+2n+6i	$MirCln(i)$	Dimensionless	[-]	Real	[-inf;inf]	0.95
4+2n+6i+1	$ConcFac$	Dimensionless	[-]	Real	[-inf;inf]	1

$\dot{W}_{gross}$ and $\eta_{gross}$are two parameters used to calculate the rated energy absorbed by the collector field.

$$\dot{Q}_{sf,rated} = \frac{\dot{W}_{gross}}{\eta_{gross}} \tag{5.1}$$

Parasitic power requirements are calculated as a function of the energy absorbed in the collector field and the rated energy absorbed by the collector field (Price 2005).

$$SfTotPar = SfPar \cdot SfParPF + C_{HTF}Par \cdot C_{HTF}ParPF(C_{HTF}ParF_0 + C_{HTF}ParF_1 \cdot \frac{\dot{Q}_{col}}{\dot{Q}_{sf,rated}} + C_{HTF}ParF_2 \left(\frac{\dot{Q}_{col}}{\dot{Q}_{sf,rated}}\right)^2 \tag{5.2}$$

$SfTotPar$ is the total parasitic power requirement from the collector field. $\dot{Q}_{col}$ is the energy collected by the collector field. $SfPar$, $SfParPF$, $C_{HTF}Par$, $C_{HTF}ParPF$, $C_{HTF}ParF_0$, $C_{HTF}ParF_1$, $C_{HTF}ParF_2$, and $AntiFrPar$ are all coefficients associated with motor and pump losses through the solar field based on load conditions. The pump parasitic losses calculated by the collector field will not be used for the simulations. The pump parasitic losses will be calculated with another method describe in the next section. $NumHCEType$ is the parameter that determines the number of HCE types in the collector field based on the working condition of the collector and type of collector. $HCEType$ has five options for collector types, which include Schott collectors with a vacuum, UVAC collectors with lost vacuum, UVAC collectors with broken envelopes, UVAC collectors with hydrogen in the annulus, and Schott 2008 collectors with vacuum. The 2008 Schott collector model was added to the collector model. $HCEFrac$ determines the fraction of each of the collector types in the field. $NumColType$, $ColType$, and $ColFrac$ are dummy variables that are not used in the program calculations and do not affect the program outputs. $TrkTwstErr$ is the collector field twist and tracking error. $GeoAcc$ is the collector geometric accuracy. $MirRef$ and $MirCln$ are the mirror reflectiveness and mirror cleanliness, respectively. $ConcFac$ is the concentration factor. These parameters are set as the same as the SEGs plant modeled by Patnode (Patnode 2006). The product of these parameters is used to calculate the field error.

$$ColFieldErr = TrkTwstErr \cdot GeoAcc \cdot MirRef \cdot MirCln \cdot ConcFac \qquad (5.3)$$

Table 5.3 Collector Model Inputs

	Name	Dimension	Unit	Type	Range	Default
1	$T_{HTF,in}$	Temperature	[C]	Real	[-inf;inf]	80
2	DNI	Power/Area	[W/m^2]	Real	[-inf;inf]	0
3	$T_{ambient}$	Temperature	[C]	Real	[-inf;inf]	15
4	$WndSpd$	Velocity	[m/s]	Real	[-inf;inf]	0
5	$SFMode$	Dimensionless	[-]	Real	[-inf;inf]	0
6	$\dot{V}_{HTF}$	Flow Rate	[m^3/s]	Real	[-inf;inf]	0.15
7	Lat_{site}		[deg]	Real	[-inf;inf]	37
8	$Long_{site}$		[deg]	Real	[-inf;inf]	-117.022
9	$Long_{standard}$		[deg]	Real	[-inf;inf]	-120
10	SF_{Area}	Area	[m^2]	Real	[-inf;inf]	182000
11	HTF_{type}	Dimensionless	[-]	Real	[-inf;inf]	4
12	$IAMF_0$	Dimensionless	[-]	Real	[-inf;inf]	1
13	$IAMF_1$	Dimensionless	[-]	Real	[-inf;inf]	0.0506
14	$IAMF_2$	Dimensionless	[-]	Real	[-inf;inf]	-0.1763
15	$FocalLength$	Length	[m]	Real	[-inf;inf]	5
16	$SCA_{spacing}$	Length	[m]	Real	[-inf;inf]	5
17	$Distance_{Rows}$	Length	[m]	Real	[-inf;inf]	5
18	$Width$	Length	[m]	Real	[-inf;inf]	4.83
19	$SFAvail$	Dimensionless	[-]	Real	[-inf;inf]	0.99
20	$ColTilt$		[deg]	Real	[-inf;inf]	0
21	$ColAz$		[deg]	Real	[-inf;inf]	0
22	$NumSCAs$	Dimensionless	[-]	Real	[-inf;inf]	8
23	SCA_{length}	Length	[m]	Real	[-inf;inf]	50
24	$T_{HTF,min}$	Temperature	[C]	Real	[-inf;inf]	50
25	$SfPar$	Dimensionless	[-]	Real	[-inf;inf]	0.1357
26	$SfParPF$	Dimensionless	[-]	Real	[-inf;inf]	1
27	$C_{HTF}Par$	Dimensionless	[-]	Real	[-inf;inf]	5.3664
28	$C_{HTF}ParPF$	Dimensionless	[-]	Real	[-inf;inf]	1
29	$C_{HTF}ParF_0$	Dimensionless	[-]	Real	[-inf;inf]	-0.036
30	$C_{HTF}ParF_1$	Dimensionless	[-]	Real	[-inf;inf]	0.242
31	$C_{HTF}ParF_2$	Dimensionless	[-]	Real	[-inf;inf]	0.794
32	$AntiFrPar$	Dimensionless	[-]	Real	[-inf;inf]	0.5366
33	$DSTadjust$	Time	[hr]	Real	[-inf;inf]	0
34	$Mode_{Shadow}$	Dimensionless	[-]	Real	[-inf;inf]	1
35	$T_{out,design}$	Temperature	[C]	Real	[-inf;inf]	400
36	$\dot{m}_{HTF,min}$	Flow Rate	[kg/s]	Real	[-inf;inf]	50
37	$\dot{m}_{HTF,max}$	Flow Rate	[kg/s]	Real	[-inf;inf]	550

The inlet temperature is connected to the cold storage tank. Direct normal insolation, ambient temperature, and wind speed are taken from the weather data in Type 15. The collector model has two operating modes. In mode one, the flow rate to the collector is specified, and the model calculates the outlet temperature. The opposite is true for mode two, which is used for all simulations. Input six changes based on the mode; in mode two, input six is the collector outlet temperature. The latitude and longitude of the site are from Daggett, CA. The standard longitude is the standard meridian for the local time zone. The solar field area is the total collector mirror area. This input will be varied for the different simulation configurations. There are ten different heat transfer fluids that can be used. The only two heat transfer fluids used for the simulations are Dowtherm A and molten salt (60% $NaNO_3$ / 40% KNO_3). The property data for these two fluids were added to the collector model. $IAMF_0$, $IAMF_1$, and $IAMF_2$ are curve fit coefficients to calculate the incidence angle modifier. These exponents are based on the testing of the LS-2 collector by Sandia (Kearny 1994). The focal length is the average trough focal length for the collector. The collector spacing, row distance, mirror width, and solar field availability are taken from the values of the SEGs plant modeled by Patnode. The collector tilt is assumed to be zero and the azimuth angle is also set to be zero, which indicates that the collectors are oriented due south for east-west tracking. Input 26, $NumSCAs$, indicates the number of collectors per row and the SCA_{length} is the length of a single collector. For the single loop of Dowtherm, these parameters are the same as the SEGs plant. The number of collectors is 8 and the collector length is 50 meters, which results in a total row length of 400 meters. The minimum heat transfer fluid temperature is used to calculate the required antifreeze protection in the collector field. For Dowtherm A, this is not a concern because the freezing point is 12°C, but

is a concern for molten salt with the freezing point being 220°C. The shadow mode has two potential inputs. For mode one, the collectors track the sun continuously, and, for mode two, the collectors do not adjust their position until the sun sensor is shaded. In mode two, the absorbed radiation will be zero for several instances throughout the day. Mode one is used for all simulations. The design outlet temperature is an input that is used to calculate potential loss in energy or energy that could be transferred to storage, which is unused for these simulations. The minimum collector flow rate is left at the default value for all simulations. The maximum collector flow rate is set to twice the design Rankine cycle flow rate.

The simulations for this analysis use the 2008 Schott collector type. The collector component did not include this collector model, so it was added. The collector field error is a product of several parameters specific to the collector type, which are shown in Table 5.4.

Table 5.4 2008 Schott Collector Optical Properties (Buckholder 2009)

Parameter	Value
Dust Correction	0.98
Bell Shading	0.971
Transmittance	0.963
Absorptivity	0.96

These parameters were taken from the Heat Loss Testing performed by NREL (Burkholder 2009). These parameters are used to calculate the field error of the solar field.

$$HCEFieldErr = Dust_{correction} \cdot Bell\ Shading \cdot Transmittance \cdot Absorptivity \quad (5.4)$$

The field error is then used to calculate the optical efficiency.

$$Optical\ Efficiency = ColFieldErr \cdot HCEFieldErr \cdot RowShadow \cdot EndLoss \quad (5.5)$$

The optical efficiency is used to find the energy absorbed by the collector field.

$$Q''_{abs} = DNI \cdot SfAvail \cdot Cos(\theta) \cdot IAM \cdot OpticalEfficiency \quad (5.6)$$

The heat loss from the collector is dependent on collector type. The heat loss for the 2008 Schott collector is modeled after the heat loss testing performed by NREL. A plot of the heat loss vs. temperature from this test is shown in Figure 5.2.

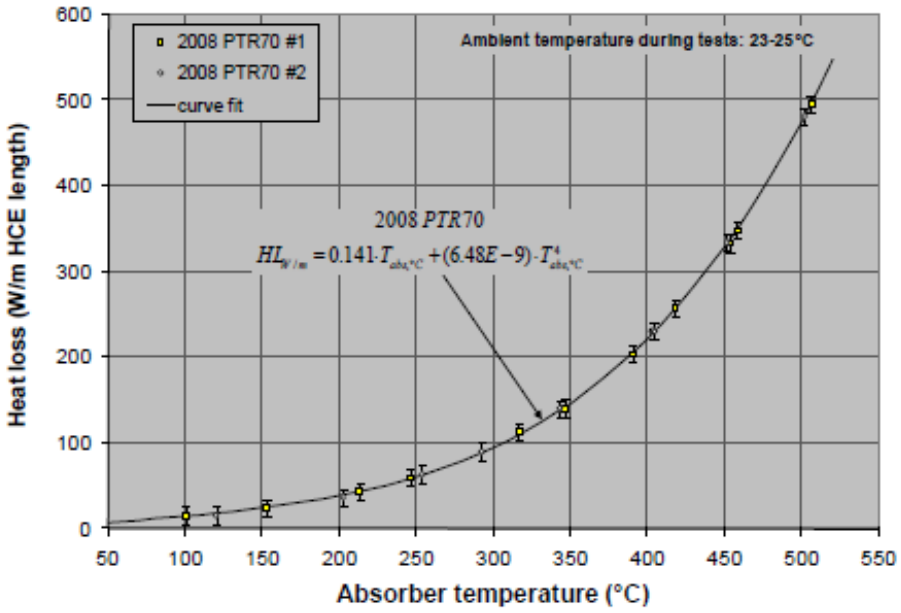

Figure 5.2 Heat Loss vs. Temperature for 2008 Schott Collector (Buckholder 2009)

It is important to note that the heat loss for the collector increases drastically after 400°C, which poses a problem for molten salt as a working fluid since the design outlet temperature of molten salt from the collector field is 550°C. Using this information, the heat loss in the collector is calculated based on the following equations from Buckholder (2009).

$$HL = \frac{HL_1 + HL_2 + HL_3 + HL_4}{T_o - T_i} \tag{5.7}$$

$$HL_1 = \left(A_0 + A_5 \cdot \sqrt{V_w}\right)(T_o - T_i) \tag{5.8}$$

$$HL_2 = \left(A_1 + A_6 \cdot \sqrt{V_w}\right)\left(\frac{T_o^2 - T_i^2}{2} - T_{amb} \cdot (T_o - T_i)\right) \tag{5.9}$$

$$HL_3 = \frac{A_2 + A_4 \cdot I_b \cdot IAM \cdot Cos(\theta)}{3}(T_o^3 - T_i^3) \tag{5.10}$$

$$HL_4 = \frac{A_3}{4}(T_o^4 - T_i^4) \tag{5.11}$$

T_o and T_i are the collector field outlet and inlet temperatures, respectively. V_w is the wind speed, and T_{amb} is the ambient temperature. I_b is the beam radiation, which is radiation from the sun that has not been scattered by the atmosphere. Theta is the angle of incidence. IAM stands for incidence angle modifier. The coefficients for this equation, A_1 through A_6 were determined from the heat loss testing performed by NREL (2009). These coefficients are shown in Table 5.5.

Table 5.5 Heat Loss Coefficients 2008 Schott Collector (Buckholder 2009)

Heat Loss Coefficient	2008 PTR70 Collector
A_0	4.05
A_1	0.247
A_2	-0.00146
A_3	5.65E-06
A_4	7.62E-08
A_5	-1.70
A_6	0.0125

With the heat loss and other collector performance criteria, the 2008 Schott collectors were added to the collector component in TRNSYS. However, Dowtherm A and molten salt (60% $NaNO_3$ / 40% KNO_3) were not included as working fluids in the collector component. The property data had to be curve fit and added in order to model these fluids. Plots of the property curve fits and relative statistics for both fluids are shown below. The property data are determined using EES (Engineering Equation Solver 2009).

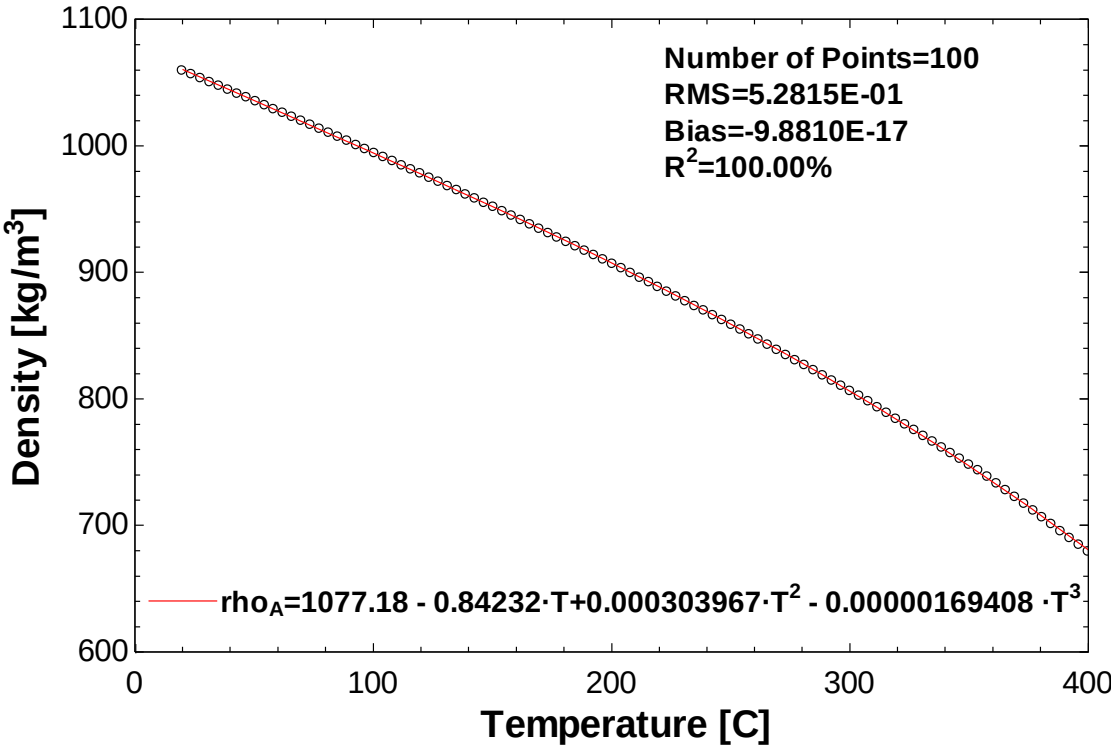

Figure 5.3 Curve fit for Density of Dowtherm A

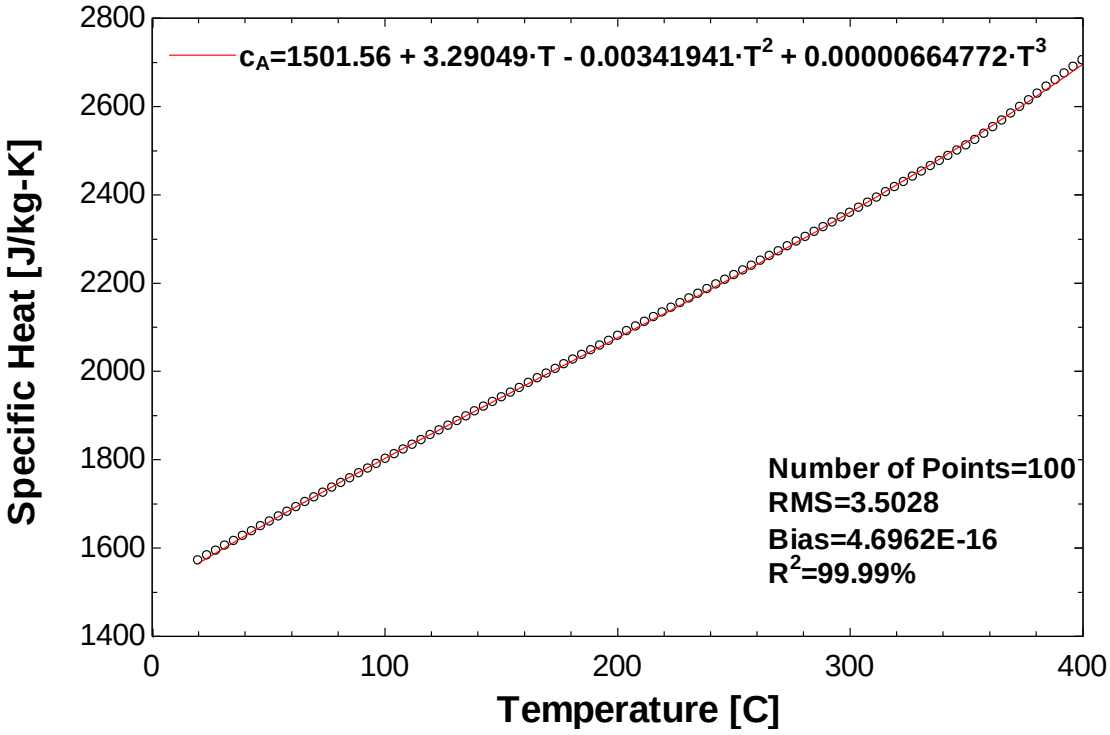

Figure 5.4 Curve fit for Specific Heat of Dowtherm A

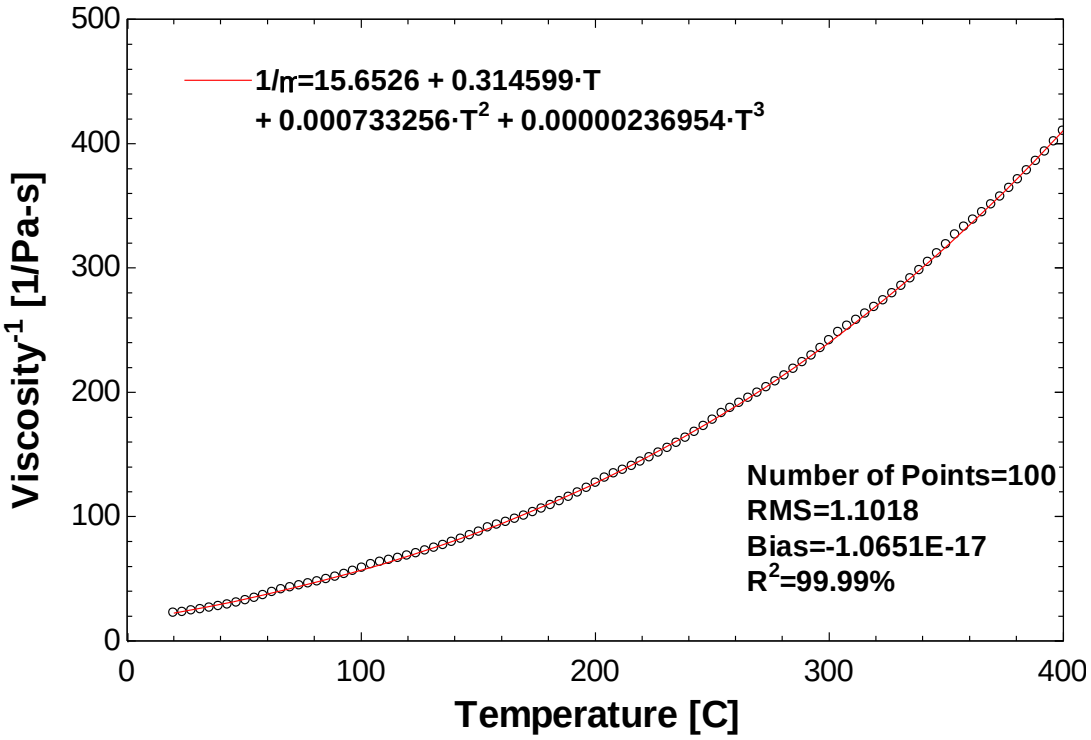

Figure 5.5 Curve fit for Inverse of Dynamic Viscosity of Dowtherm A

The inverse of the dynamic viscosity is used for the curve fit because the root mean square error and coefficient of determination are lower than a fit to the viscosity directly. The inverse is calculated in the program using the curve fit above, and then the viscosity is determined by taking the inverse of the calculated value.

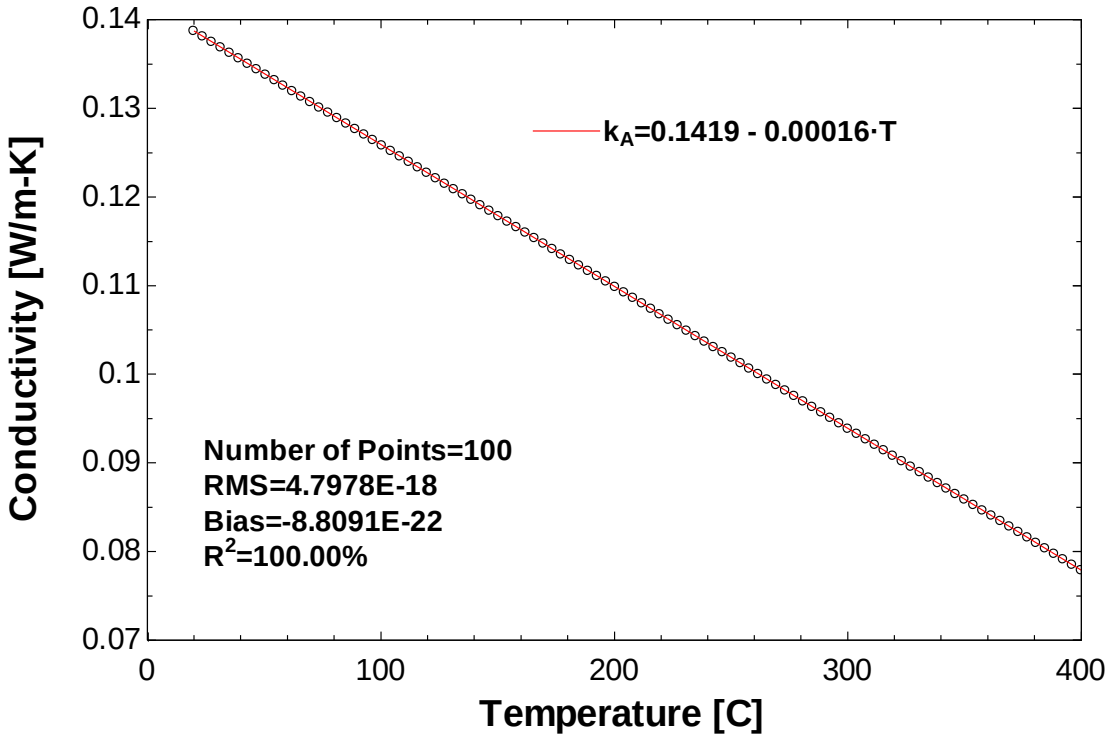

Figure 5.6 Curve fit for Thermal Conductivity of Dowtherm A

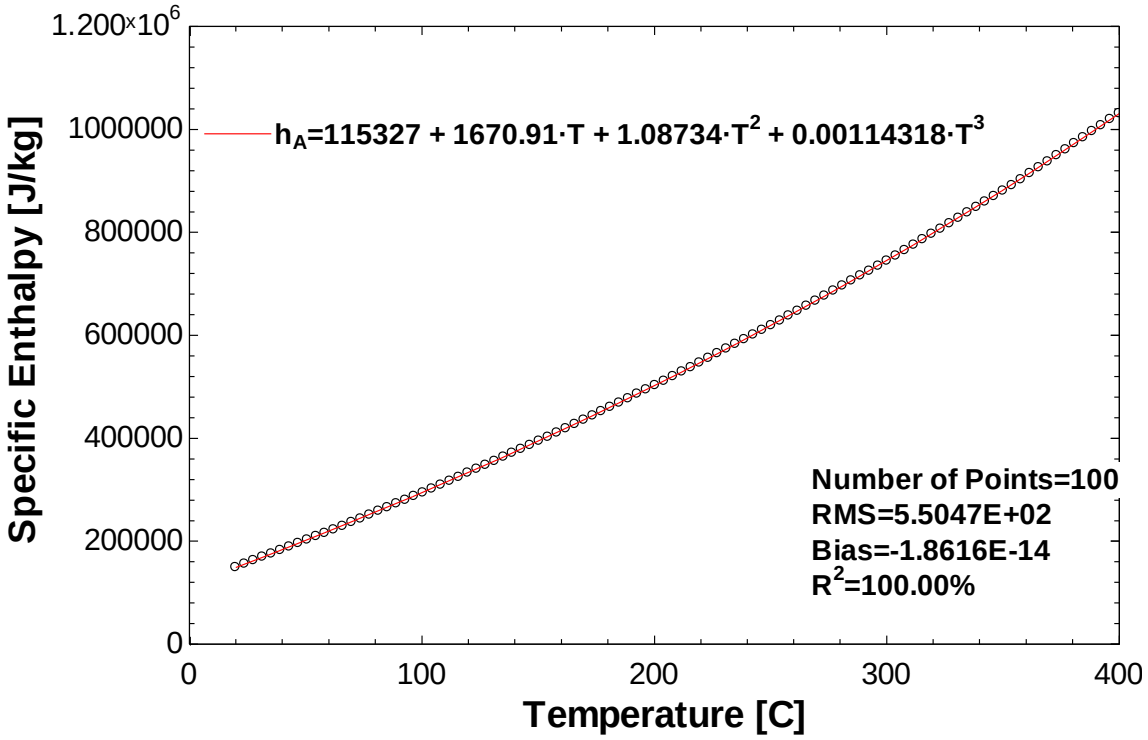

Figure 5.7 Curve fit for Specific Enthalpy of Dowtherm A

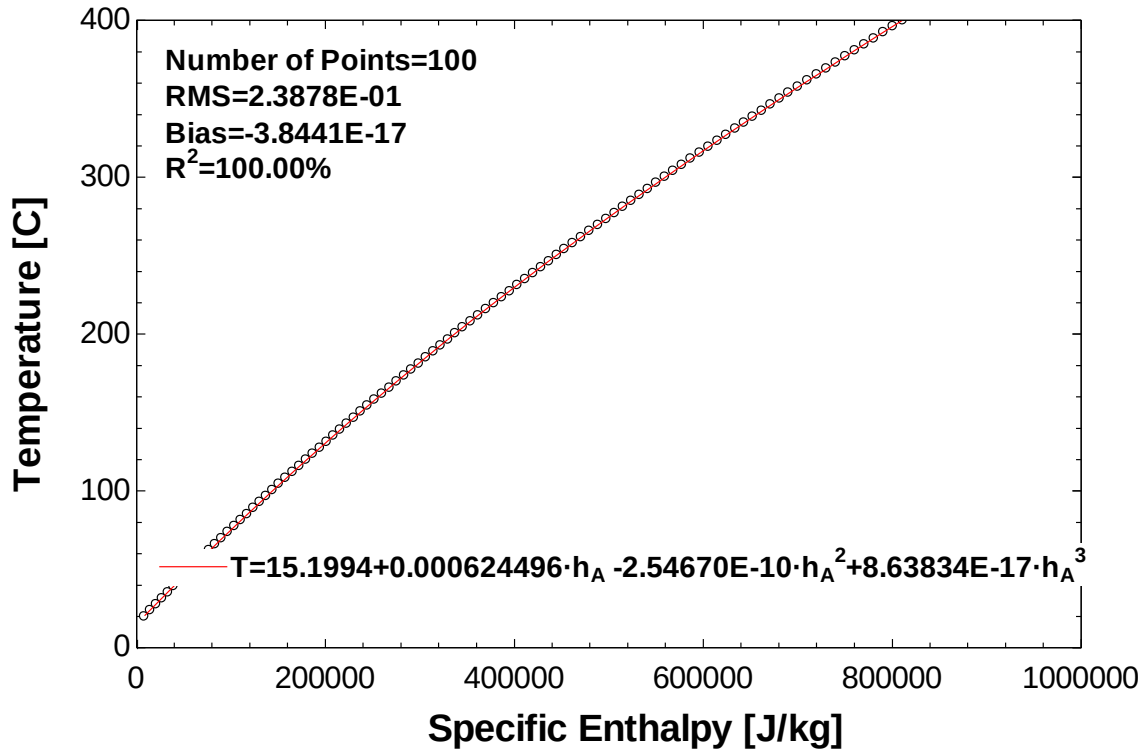

Figure 5.8 Curve fit for Temperature of Dowtherm A

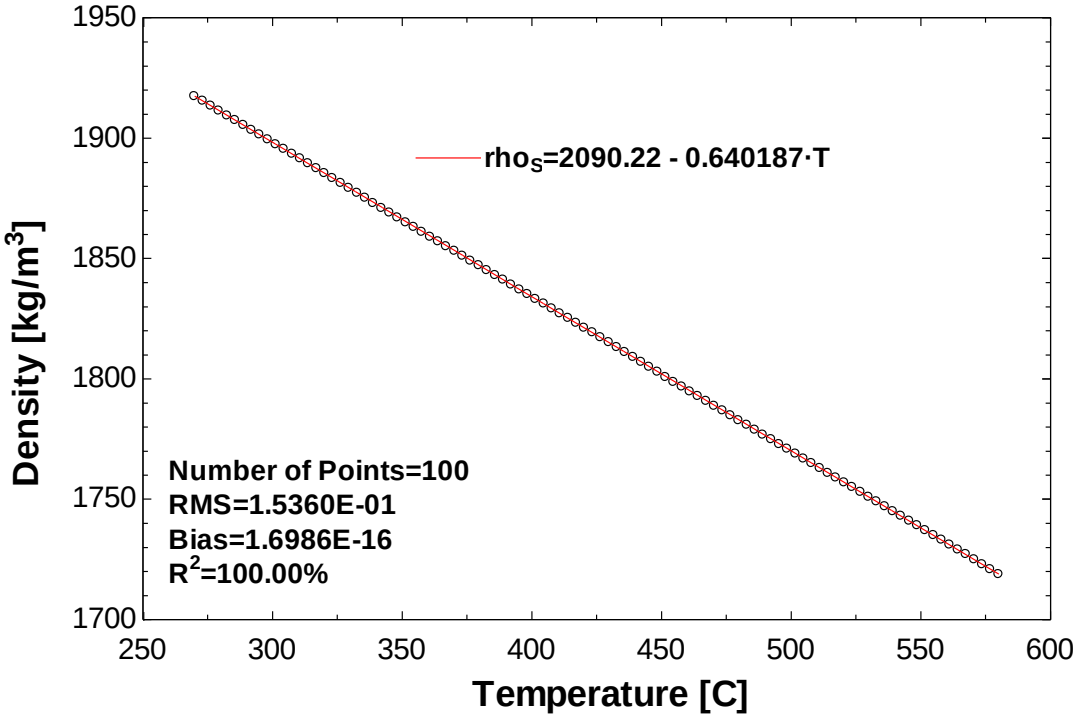

Figure 5.9 Curve fit for Density of Molten Salt (60% $NaNO_3$ / 40% KNO_3)

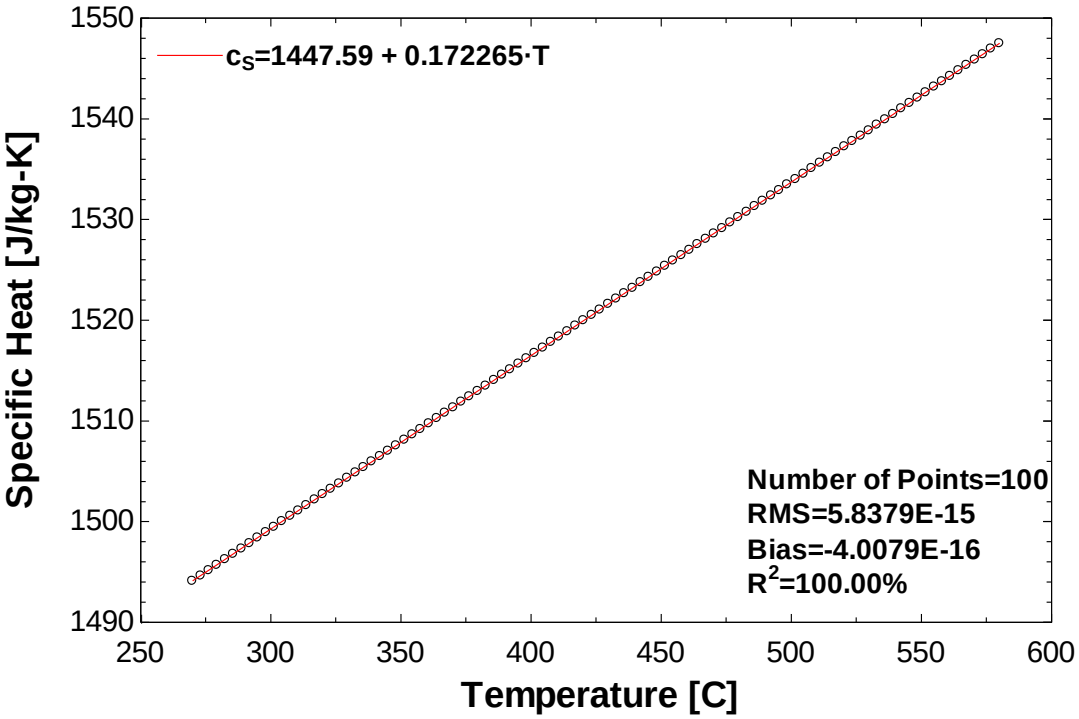

Figure 5.10 Curve fit for Specific Heat of Molten Salt (60% $NaNO_3$ / 40% KNO_3)

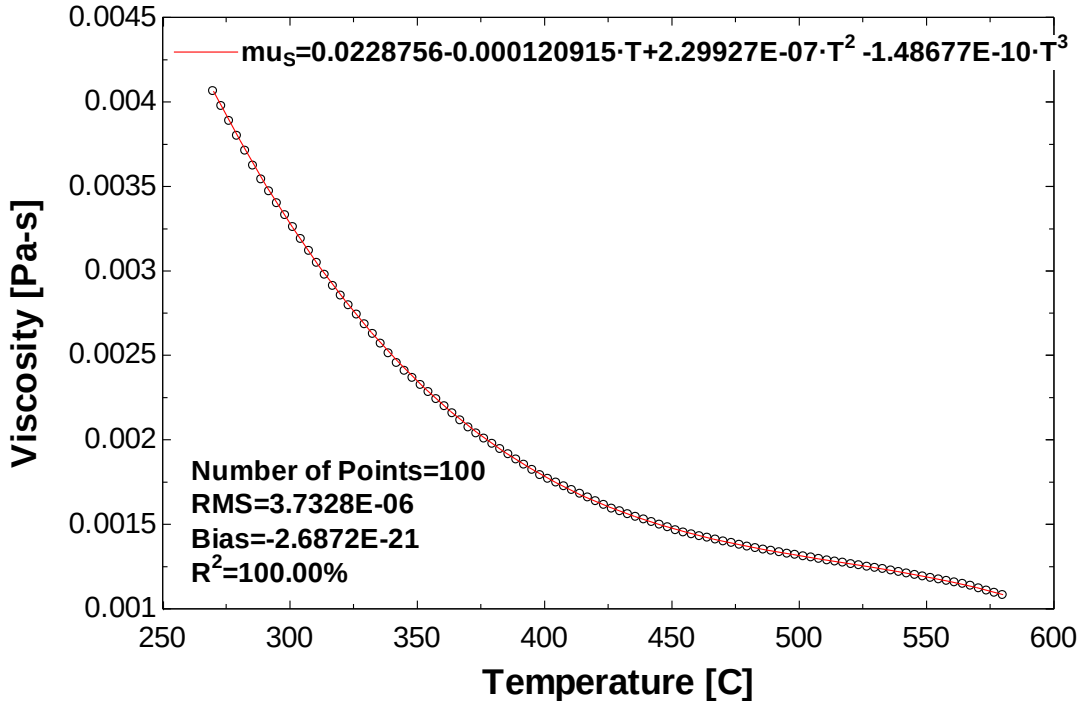

Figure 5.11 Curve fit for Dynamic Viscosity of Molten Salt (60% $NaNO_3$ / 40% KNO_3)

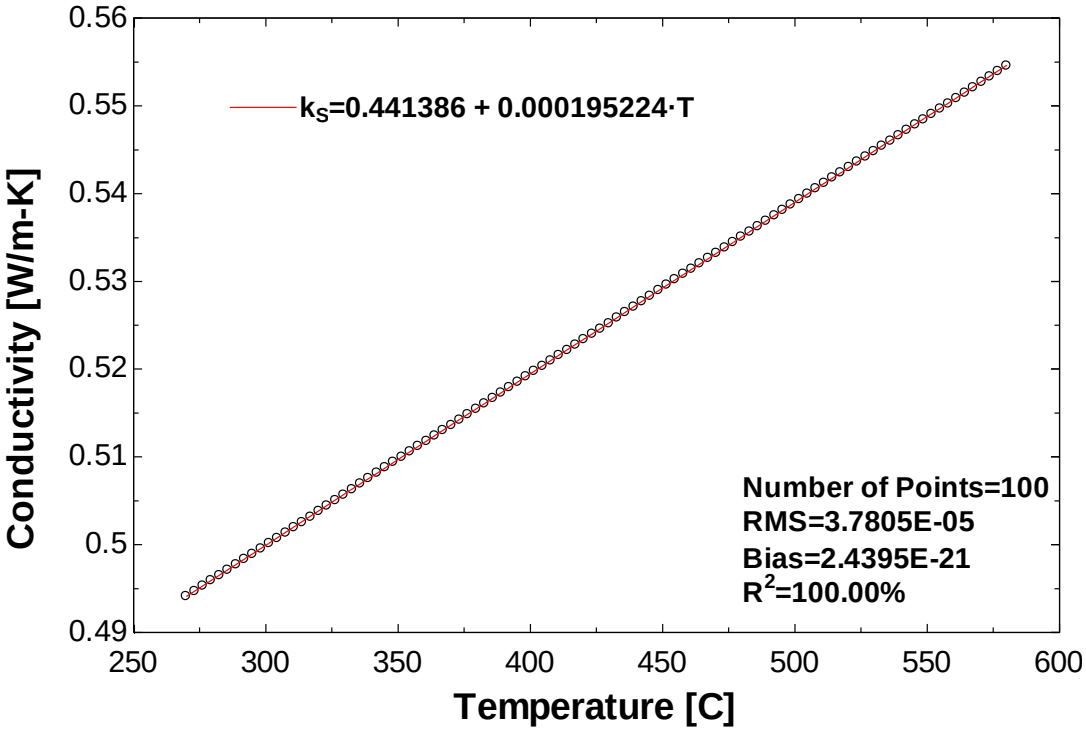

Figure 5.12 Curve fit for Thermal Conductivity of Molten Salt (60% $NaNO_3$ / 40% KNO_3)

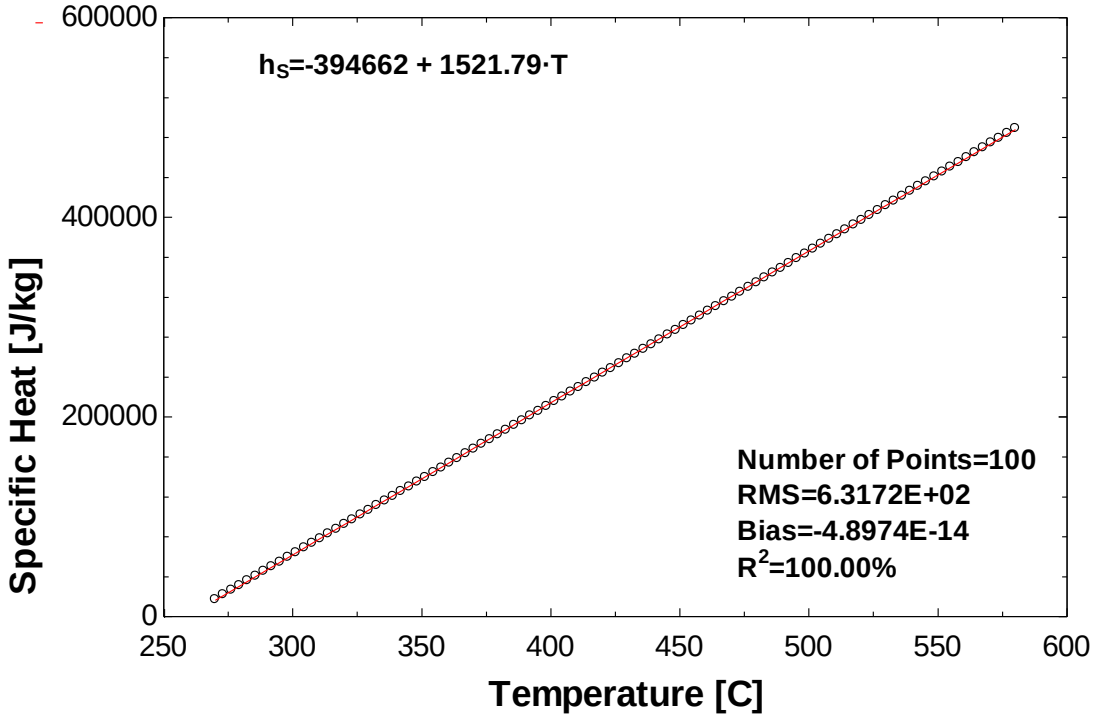

Figure 5.13 Curve fit for Specific Enthalpy of Molten Salt (60% $NaNO_3$ / 40% KNO_3)

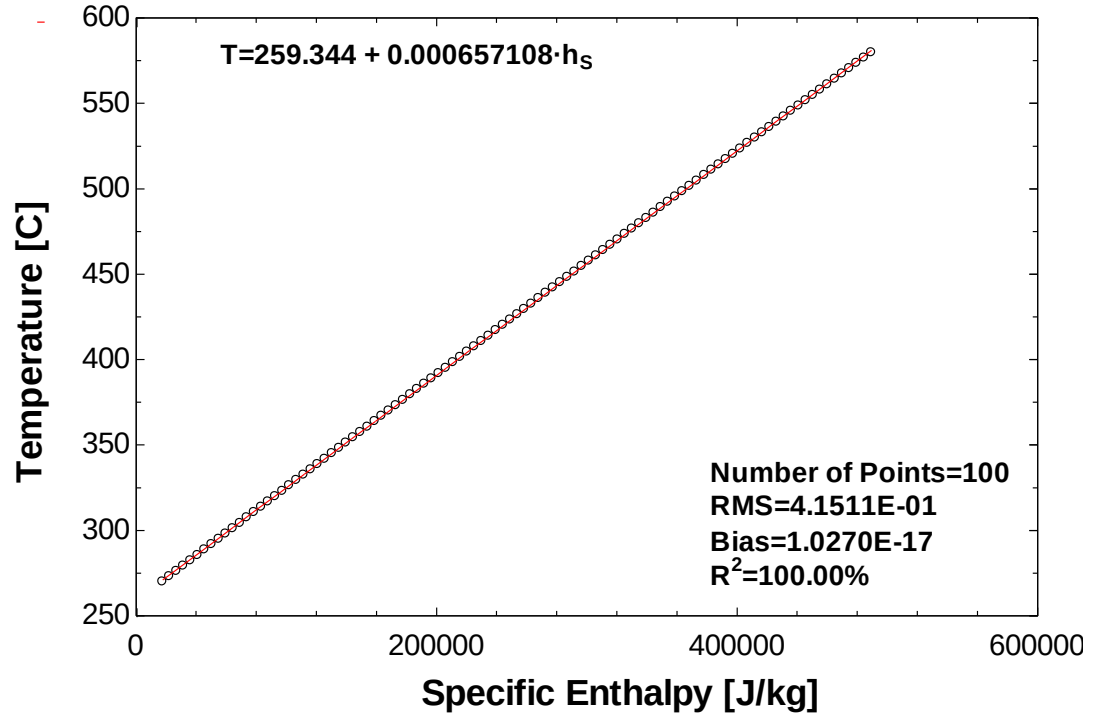

Figure 5.14 Curve fit for Temperature of Molten Salt (60% $NaNO_3$ / 40% KNO_3)

With the property curves shown above, the collector component in TRNSYS can be used to simulate the performance of both the new working fluids in the new 2008 Schott collector.

5.4 Pump Parasitics (Type 920-New)

The pumping requirement for the collector field is determined using data from the SEGs plant in southern California. The design flow of the heat transfer fluid (Therminol VP-1) is 7590 gal/min at 293°C. For this design condition, the pump power required for the collector field is 1.6 MWe (Patnode 2006) for a plant that has a net power output of 30 MW. It is assumed that, for Dowtherm A, the pumping power for the same volumetric flow rate would be the same due to the fact that Therminol VP-1 and Dowtherm A have similar fluid properties, as shown in Table 5.6.

Table 5.6 Property Comparison between Dowtherm A (Dow) and Therminol VP-1 (TVP-1)

Temp [C]	$C_{p,Dow}$ [kJ/kg-K]	$C_{p,TVP-1}$ [kJ/kg-K]	k_{Dow} [W/m-K]	k_{TVP-1} [W/m-K]	μ_{Dow} [Pa-s]	μ_{TVP-1} [Pa-s]	ρ_{Dow} [kg/m^3]	ρ_{TVP-1} [kg/m^3]
50	1.658	1.634	0.1339	0.1333	0.002606	0.00213	1036	1040
68.42	1.711	1.689	0.131	0.1313	0.001523	0.001539	1021	1025
86.84	1.763	1.735	0.128	0.1292	0.001214	0.001173	1006	1010
105.3	1.815	1.79	0.1251	0.127	0.000908	0.000927	990.5	994.4
123.7	1.866	1.843	0.1221	0.1247	0.000779	0.000755	974.7	979.5
142.1	1.918	1.89	0.1192	0.1223	0.00065	0.000629	958.9	963.9
160.5	1.969	1.946	0.1162	0.1197	0.00054	0.000535	942.8	948.2
178.9	2.021	1.991	0.1133	0.117	0.000474	0.000461	926.1	931.7
197.4	2.072	2.041	0.1103	0.1142	0.000408	0.000402	909.4	915.2
215.8	2.123	2.091	0.1074	0.1113	0.000356	0.000355	892	898.6
234.2	2.174	2.137	0.1044	0.1082	0.000316	0.000316	874.2	882
252.6	2.224	2.191	0.1015	0.1051	0.000275	0.000283	856.3	864.4
271.1	2.277	2.237	0.09853	0.1018	0.000248	0.000256	837.1	846.9
289.5	2.329	2.285	0.09558	0.09838	0.000222	0.000233	817.7	827.8
307.9	2.382	2.338	0.09264	0.09488	0.000198	0.000213	797.9	808.5
326.3	2.439	2.383	0.08969	0.09124	0.000183	0.000196	776.1	788.3
344.7	2.495	2.438	0.08674	0.08753	0.000168	0.000181	754.4	767
363.2	2.559	2.493	0.08379	0.08366	0.000154	0.000168	730.9	744.5
381.6	2.632	2.558	0.08085	0.07969	0.000139	0.000156	705.2	720.5
400	2.705	2.63	0.0779	0.0756	0.000124	0.000146	679.5	694

At design conditions, the parasitic pumping power (1.6 MWe) is over 5% the design power output of the system. The pumping power requirement for each of these fluids must be

analyzed to determine their effect on system outputs. The System Advisor Model (SAM) was used to determine the piping layout and pumping power requirement for each system at various conditions. This software optimizes a collector field layout based on fluid type, collector area, design power output, and plant location. Based on this information, the System Advisor Model calculates a plants performance, which includes field flow rate and the pumping power associated with that flow rate. The points generated by SAM were fit to a curve. The points above the curve are associated with system startup. The data from the System Advisor Model for Dowtherm A and molten salt are shown in Figures 5.15 and 5.16.

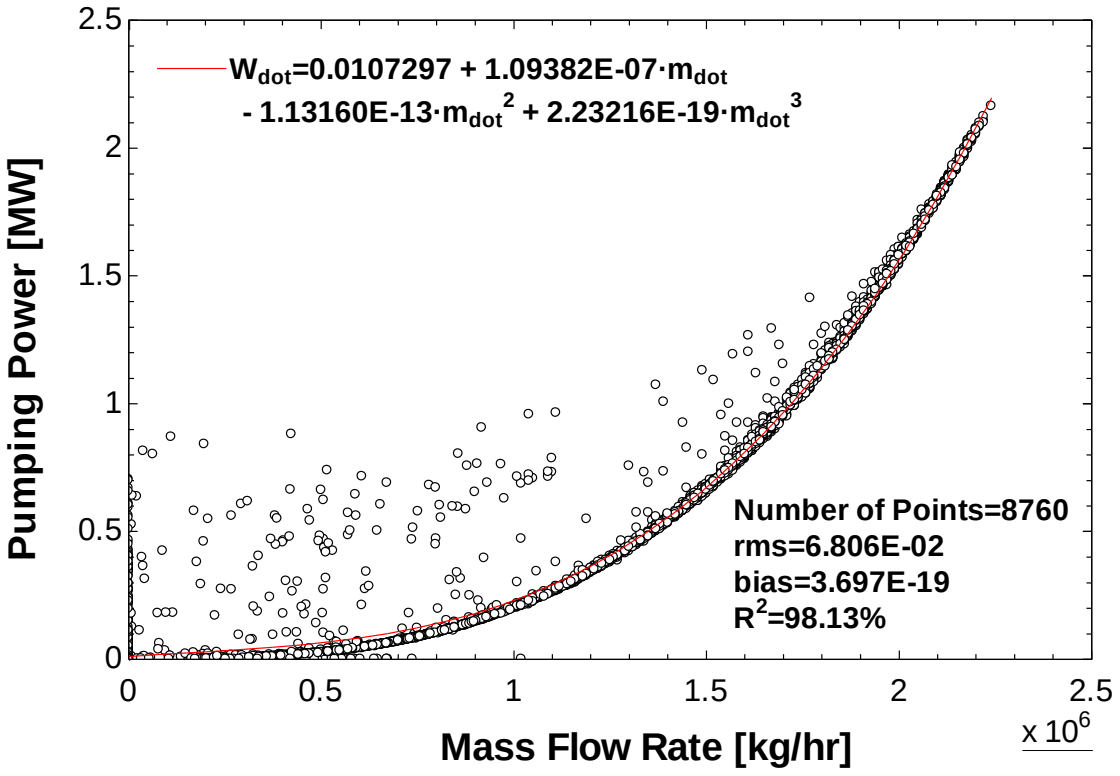

Figure 5.15 Pumping Power vs. Mass Flow Rate Dowtherm A

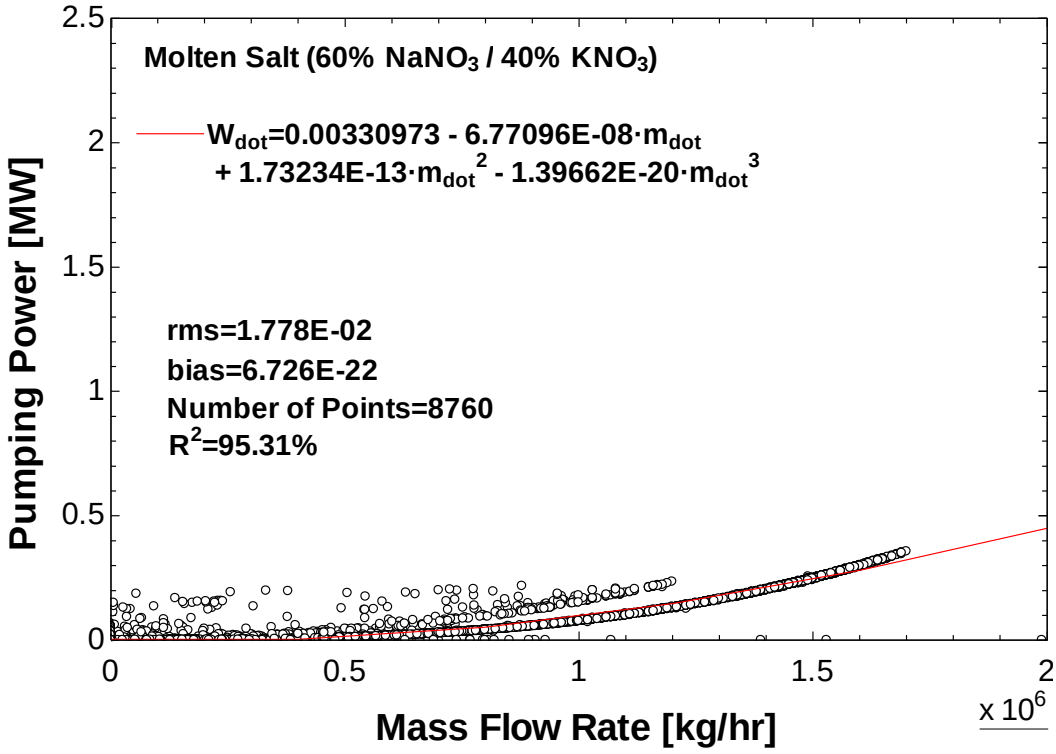

Figure 5.16 Pumping Power vs. Mass Flow Rate Molten Salt (60% $NaNO_3$ / 40% KNO_3)

The initial results from SAM show reveal that the pumping power for Dowtherm A is significantly higher than the pumping power for molten salt at the same mass flow rate, primarily due to the significant density difference between the two fluids. The ratio of the pumping powers for the organic and salt solutions is defined in Equation 5.12 where $\dot{W}_{Dow}$ and $\dot{W}_{Salt}$ are the pumping power requirements for Dowtherm A and molten salt, respectively. The mass flow rate is assumed to be the same for both fluids. ΔP_{Dow} and ΔP_{Salt} are the pressure drops associated with Dowtherm A and molten salt, respectively.

$$\frac{\dot{W}_{Dow}}{\dot{W}_{Salt}} = \frac{\frac{\Delta P_{Dow}\left(\frac{\dot{m}}{\rho_{Dow}}\right)}{\eta_{pump}}}{\frac{\Delta P_{Salt}\left(\frac{\dot{m}}{\rho_{Salt}}\right)}{\eta_{pump}}} \tag{5.12}$$

Equation 5.12 can be simplified as shown in equation 5.13

$$\frac{\dot{W}_{Dow}}{\dot{W}_{Salt}} = \frac{\Delta P_{Dow}}{\Delta P_{Salt}}\left(\frac{\rho_{Salt}}{\rho_{Dow}}\right) \tag{5.13}$$

The pressure drop for each fluid can be simplified using equation 5.14.

$$\frac{\Delta P_{Dow}}{\Delta P_{Salt}} = \frac{f_{Dow}\left(\frac{L}{D}\right)^{\frac{1}{2}}\rho_{Dow}\left(\frac{\dot{m}}{\rho_{Dow}}\right)^{2}}{f_{Salt}\left(\frac{L}{D}\right)^{\frac{1}{2}}\rho_{Salt}\left(\frac{\dot{m}}{\rho_{Salt}}\right)^{2}} = \frac{f_{Dow}}{f_{Salt}}\left(\frac{\rho_{Salt}}{\rho_{Dow}}\right) \tag{5.14}$$

Assuming that the piping has the same geometry for both fluids, the length and diameter terms cancel out, so the pressure drop ratio is equal to the ratio of the friction factors, f_{Dow} and f_{Salt}, multiplied by the inverse ratio of the densities.

$$f = f_{fd}\left(1 + \left(\frac{L}{D}\right)^{0.7}\right) \tag{5.15}$$

The friction factor is calculated using equation 5.15. By substituting this equation back into 5.14, the only term that remains is f_{fd} because the length and diameter are assumed to be the same.

$$f_{fd} = 4\left(-\frac{0.001570232}{ln(Re)} + \frac{0.394203137}{ln(Re)^2} + \frac{2.534153311}{ln(Re)^3}\right) \tag{5.16}$$

Equation 5.16 uses the friction factor correlation from Li and Seem (2011).

$$\frac{\dot{W}_{Dow}}{\dot{W}_{Salt}} = \frac{f_{fd,Dow}}{f_{fd,Salt}}\left(\frac{\rho_{Salt}}{\rho_{Dow}}\right)^{2} \tag{5.17}$$

Finally, by substituting equation 5.14 and 5.15 into equation 5.13, the ratio of the pump work between the two fluids can be determined using equation 5.17. In order to calculate the ratio

of the pump work, the Reynolds number must be calculated for each fluid to determine the friction factor. Using the 2008 Schott collector properties and typical average temperatures for each fluid (350 [C] for Dowtherm A and 475 [C] for molten salt) to determine the properties, the pump work for salt was calculated using equation 8 and the correlation for Dowtherm pumping power in figure 5.17.

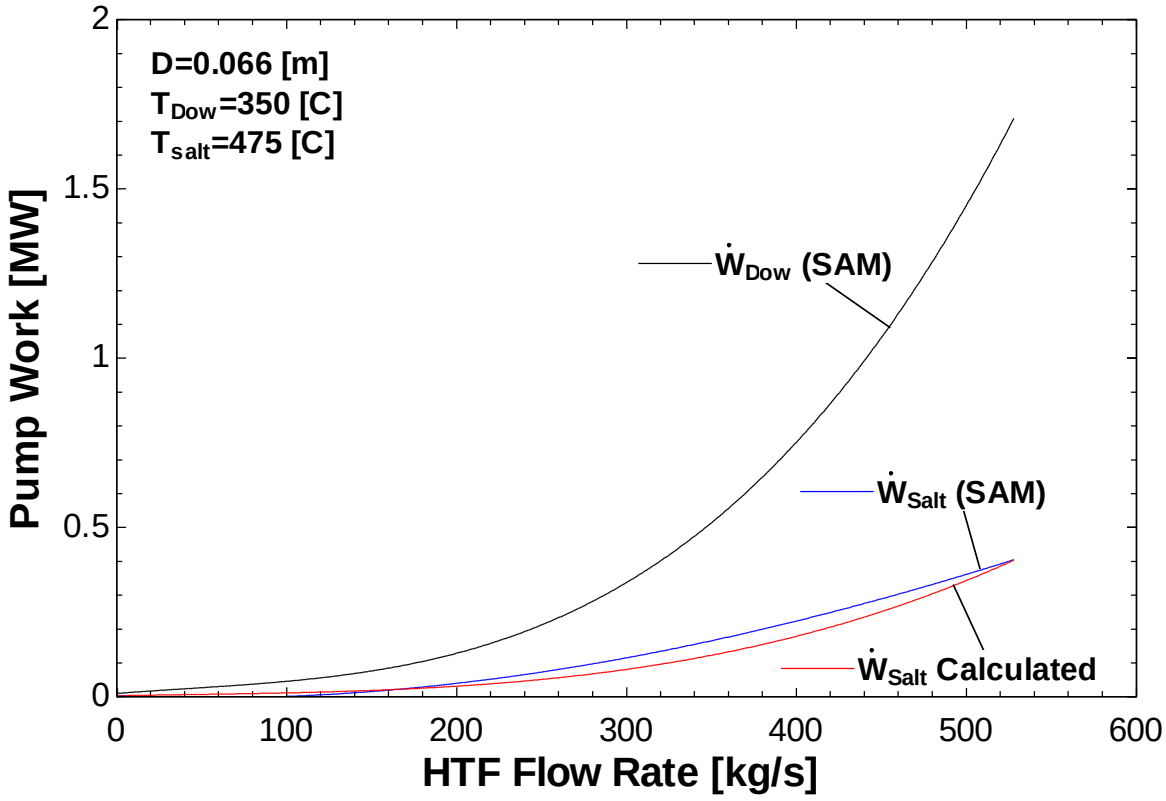

Figure 5.17 Pump Work vs. Mass Flow Rate

As shown, the pump work for salt calculated using equation 5.17 based on the Dowtherm pump work closely agrees with the curve generated by the System Advisor Model. Based on equation 5.17, it is clear that the density of the fluid dominates the value of the pump work. The density of molten salt is approximately 1800 kg/s and the density of Dowtherm A is approximately 800 kg/s, so it is clear why the parasitic pumping power for Dowtherm is

higher for the same mass flow rate. The study by Kearney (2003) corroborates this result. It states that the pumping parasitics are relatively low compared to a Therminol VP-1 (an organic heat transfer fluid) solar field. The pump work type component is created based on the curve fits from Figures 5.15 and 5.16.

Table 5.7 Pump Parasitics Parameters, Inputs, and Outputs

Parameters	Name	Dimension	Unit	Type	Range	Default
1	Fluid Select	Dimensionless	[-]	Integer	[-inf;inf]	0
Inputs						
1	Mass Flow	Flow Rate	[kg/hr]	Real	[-inf;inf]	0
2	Cycle Flow	Flow Rate	[kg/hr]	Real	[-inf;inf]	0
Output						
1	W_{pump}	Dimensionless	[-] (MW)	Real	[-inf;inf]	0

The two fluids that can be selected are Dowtherm A and molten salt. The mass flow is the flow rate through the collector field, and the cycle flow is the flow through the Rankine cycle. The component uses the maximum of these two values to calculate the pump power required for the cycle based on the curve fit equations from Figure 5.15 and 5.16. The pump work is dimensionless in the proforma because TRNSYS does not have MW units, but the pump work units are in MW.

5.5 N-Stage Differential Controller (Type 973-Exisiting)

Type 973 is an N-stage set point differential controller with a deadband and time delay. For this system, this component is used to control the volume in the hot storage tank; therefore, for this simulation, the tank volume is the only setting being controlled. The model outputs an ON/OFF control function based on the tank volume that can be used to control other components in the system. The model turns on the stage when the volume falls below the set point volume minus one-half of the deadband volume difference and remains on until the

volume rises above the set point plus one half of the dead band volume difference. However, the model will stay on or off for a predetermined time regardless of the tank volume based on a time delay input specified by the user. Table 5.8 is a list of all the parameters, inputs, and outputs for Type 973.

Table 5.8 Volume Controller Parameters, Inputs, and Outputs

Para.	Name	Dimension	Unit	Type	Range	Default
1	Number of Levels	Dimensionless	[-]	Integer	[1;25]	1
2	Number of Oscillations Permitted	Dimensionless	[-]	Integer	[1;99]	5
3	On-time Delay	Time	[hr]	Real	[0;inf]	0.25
4	Off-time Delay	Time	[hr]	Real	[0;24]	0.25
5	Controller Dead Band	Any	Any	Real	[-inf;inf]	2.0
6	Mode	Dimensionless	[-]	Integer	[1;2]	1
Inputs						
1	Value to Watch	Any	Any	Real	[-inf;inf]	20.0
2	Set Point	Any	Any	Real	[-inf;inf]	20.0
3	On/off Signal	Dimensionless	[-]	Real	[0;1]	0
Output						
1	Control Signal	Dimensionless	[-]	Real	[0;1]	0
2	Conditioning Signal	Dimensionless	[-]	Real	[0;1]	0

The number of levels for these simulations will always be one. The number of oscillations of the controller state allowed in one time step before the output is fixed and the solution found for this situation. If the number of oscillations is set to an odd number, the control may bounce between two control states for successive time steps. If the number of oscillations is set to an even number, the control system may stay longer in one regime than actually intended. The on-time delay and off-time delay parameters are overrides that will keep the control signal at a fixed on or off value for the specified time based each value, respectively.

The dead band is the range where the controller will turn on for the simulation. The range is symmetric about the set point. Mode is an unused parameter in this component.

The value to watch for the controller would be the volume of the hot storage tank for this system. The set point is the median value in the range of the dead band. Setting the On/Off signal input to a value greater than 0.5 allows the controller to modulate the stage in an attempt to meet the set point. If this input is less than 0.5, all output signals from this controller will be set to zero. For this system, the value is set to one.

5.6 Flow Controller (Type 860-New)

The flow controller is a component that adjusts the flow for the entire system based on storage tank volume, time of day, and direct normal insolation. A table with the parameters, inputs, and outputs is shown in Table 5.9.

Table 5.9 Flow Controller Parameters, Inputs, and Outputs

Parameters	Name	Dimension	Unit	Type	Range	Default
1	$Hour_{Start}$	Time	[hr]	Real	[0;24]	6
2	$Hour_{End}$	Time	[hr]	Real	[0;24]	21
3	$Set\ Flow$	Flow Rate	[kg/s]	Real	[0;inf]	384.0
Inputs						
1	$Hour$	Time	[hr]	Real	[0;24]	0
2	$Control_{Signal}$	Dimensionless	[-]	Real	[0;1]	0
3	$Collector_{Flow}$	Flow Rate	[kg/hr]	Real	[0;inf]	0
Outputs						
1	$Flow_{Demand,CT}$	Flow Rate	[kg/hr]	Real	[0;inf]	0
2	$Bypass\ Flow$	Flow Rate	[kg/hr]	Real	[0;inf]	0
3	$Flow_{Demand,HT}$	Flow Rate	[kg/hr]	Real	[0;inf]	0
4	$Time\ Signal$	Dimensionless	[-]	Real	[0;1]	0

The parameters $Hour_{Start}$ and $Hour_{End}$ correspond to the times between which the power cycle is in operation. Between these two hours, the flow rate to the power cycle is the design flow rate for the power cycle. For all other hours during the day, the flow rate to the power

cycle is zero. The set flow is the mass flow rate sent to the power block. The hour input is the hour of the day output from Type 21. The control signal input is the signal output from the volume controller, Type 973. The collector flow is the flow rate specified by the collector model, Type 850.

The flow demand from the storage tanks are determined from the time of day and control signal from the volume controller. The bypass flow is the amount of flow required to bypass the collector field to be heated by an auxiliary heater, Type 6, to meet the cycle demand. If the control signal is one, meaning the volume of the hot storage tank is depleted, the flow demand from the tanks is as follows

$$Flow_{Demand,CT} = Set\ Flow + Collector\ Flow \tag{5.18}$$

$$Flow_{Demand,HT} = 0 \tag{5.19}$$

$$Bypass\ Flow = Set\ Flow \tag{5.20}$$

If the control signal is zero, there is sufficient volume in the hot storage tank to supply the cycle flow, and the flow demand from the tanks is a follows

$$Flow_{Demand,CT} = Collector\ Flow \tag{5.21}$$

$$Flow_{Demand,HT} = Set\ Flow \tag{5.22}$$

$$Bypass\ Flow = 0 \tag{5.23}$$

The time signal is an output that indicates whether or not the cycle flow is non-zero based on the time of day; an output of one indicates that the cycle flow is non-zero, and an output of zero indicates that the cycle flow is zero.

5.7 Mixer (Type 870-New)

Type 870 was created to determine the outlet properties of a stream from two mixing flows of either Dowtherm A or molten salt (60% $NaNO_3$ / 40% KNO_3). The component does a mass and energy balance on a system that includes the two incoming fluid streams and the single outlet stream. Any heat losses or gains from the environment are assumed to be negligible. The parameters, inputs, and outputs are shown in Table 5.10.

Table 5.10 Mixer Parameters, Inputs, and Outputs

Para.	Name	Dimension	Unit	Type	Range	Default
1	Fluid Select	Dimensionless	[-]	Integer	[1;2]	1
Inputs						
1	$Temperature_1$	Temperature	[C]	Real	[-inf;inf]	0
2	$Flow_1$	Flow Rate	[kg/hr]	Real	[-inf;inf]	0
3	$Temperature_2$	Temperature	[C]	Real	[-inf;inf]	0
4	$Flow_2$	Flow Rate	[kg/hr]	Real	[-inf;inf]	0
Outputs						
1	Outlet Temperature	Temperature	[C]	Real	[-inf;inf]	0
2	Outlet Flow	Flow Rate	[kg/hr]	Real	[-inf;inf]	0

In order to perform an energy balance on the system, the specific enthalpy of the fluid must be determined from the temperature. EES was used to find a correlation between the temperature and the enthalpy for Dowtherm A and molten salt (60% $NaNO_3$ / 40% KNO_3). Plots of enthalpy vs. temperature for Dowtherm A and molten salt are shown below. Curve fits correlating temperature to enthalpy are included on each plot with relevant statistics.

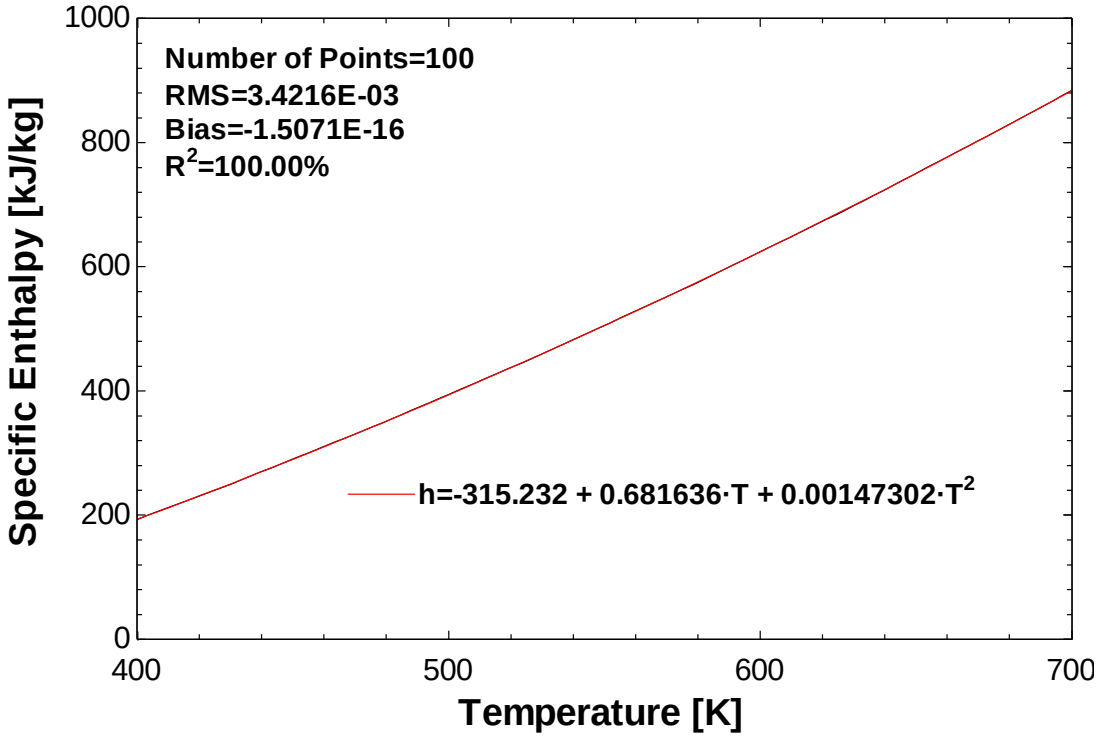

Figure 5.18 Specific Enthalpy vs. Temperature (Dowtherm A)

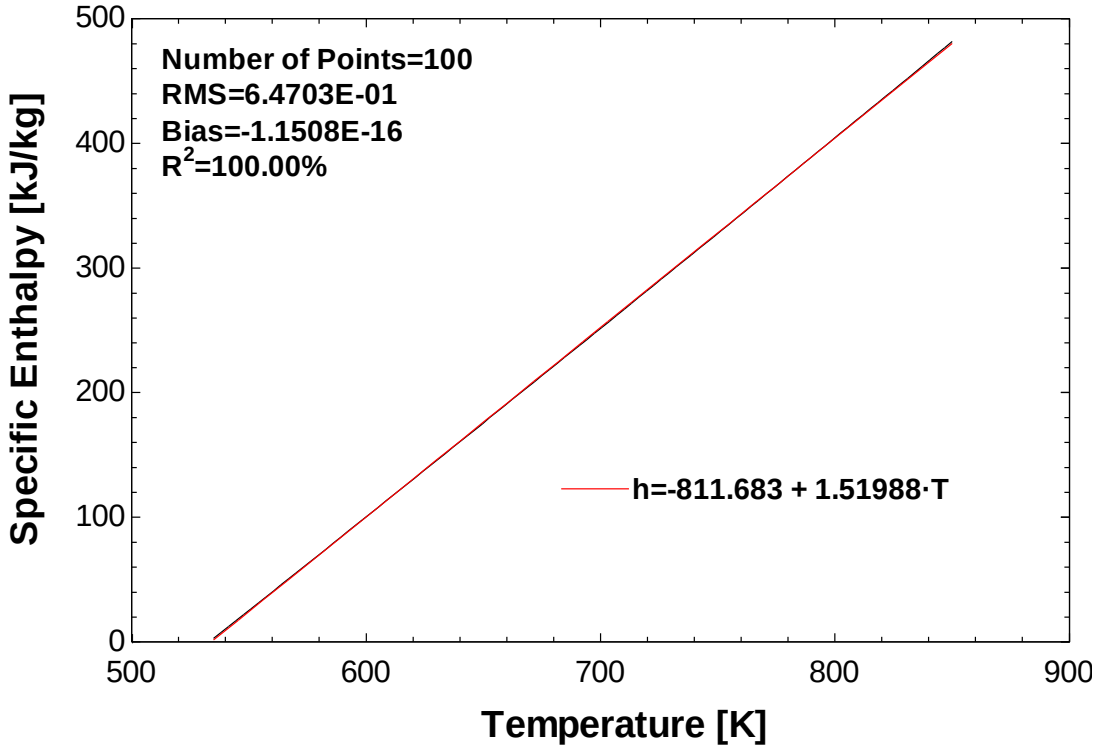

Figure 5.19 Specific Enthalpy vs. Temperature (Molten Salt 60% $NaNO_3$ / 40% KNO_3)

The flow exiting the system is determined from a mass balance on the system using equation 5.24.

$$\dot{m}_{out} = \dot{m}_1 + \dot{m}_2 \tag{5.24}$$

The enthalpy of the fluid exiting the system is determined from an energy balance on the system using equation 5.25. Note that the inputs have units of Celsius, but the curve fit equations are in units of Kelvin. The temperature inputs are converted to Kelvin in the component.

$$h_{out} = \frac{(\dot{m}_1 h_1 + \dot{m}_2 h_2)}{\dot{m}_{out}} \tag{5.25}$$

Once the enthalpy of the exiting fluid stream is determined, the temperature of the exiting fluid stream must be calculated. A plot of temperature as a function of enthalpy for Dowtherm A is shown below, as well as a curve fit of the data with relevant statistics.

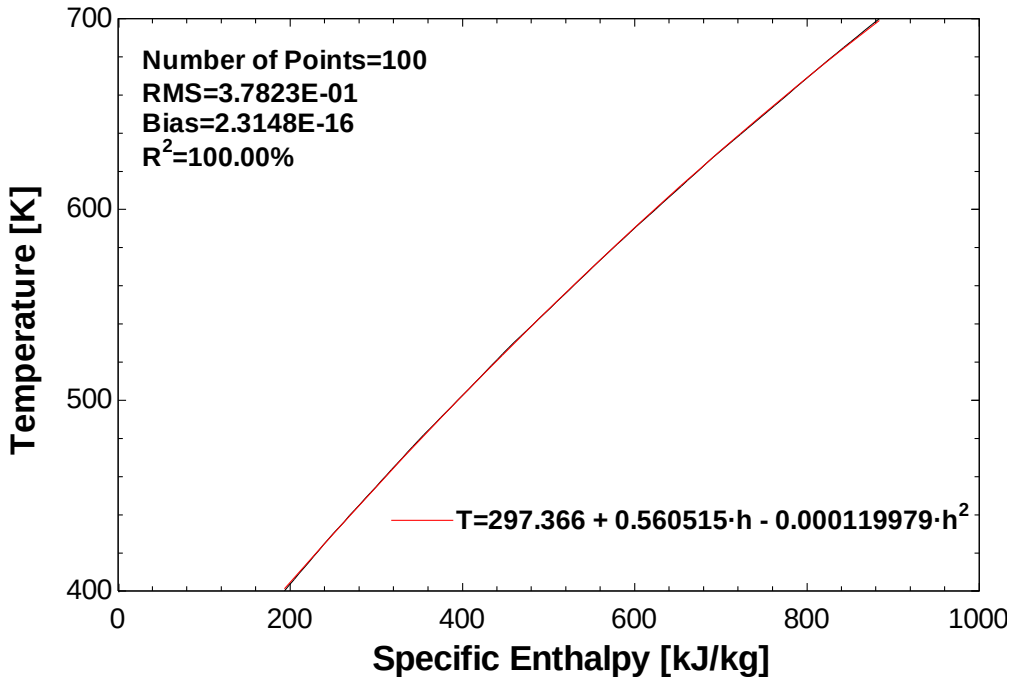

Figure 5.20 Temperature vs. Specific Enthalpy (Dowtherm A)

The outlet temperature for a molten salt stream can be determined from the specific enthalpy by solving the curve fit equation from figure 5.19 for temperature, which gives:

$$T = 534.048 + 0.657934 \cdot h \tag{5.26}$$

5.8 Diverter (Type 880-New)

The diverter component directs flow based on the signals from the flow controller (Type 860). The inputs and outputs for the diverter are shown in Table 5.11.

Table 5.11 Diverter Parameters, Inputs, and Outputs

Inputs	Name	Dimension	Unit	Type	Range	Default
1	Flow Demand	Flow Rate	[kg/hr]	Real	[-inf;inf]	0
2	Bypass Flow	Flow Rate	[kg/hr]	Real	[-inf;inf]	0
3	Inlet Temperature	Temperature	[C]	Real	[-inf;inf]	0
Outputs						
1	Collector Flow	Flow Rate	[kg/hr]	Real	[-inf;inf]	0
2	Bypass Flow	Flow Rate	[kg/hr]	Real	[-inf;inf]	0
3	Outlet Temperature	Temperature	[C]	Real	[-inf;inf]	0

The flow demand and bypass flow are determined from the flow controller. The inlet temperature is the temperature from the cold storage tank. The collector flow is an output from the diverter model, but it is not an input to the collector model. The collector model determines its own flow rate to meet the temperature requirement, as described before. The collector flow is tracked for mass conservation purposes. The bypass flow connects to a mixer after the hot storage tank. The outlet temperature is equal to the inlet temperature.

5.9 Collector Diverter (Type 910-New)

The collector diverter component directs flow based on the outlet temperature from the collector field. The inputs and outputs for the diverter are shown in Table 5.12.

Table 5.12 Collector Diverter Parameters, Inputs, and Outputs

Inputs	Name	Dimension	Unit	Type	Range	Default
1	Design Temperature	Temperature	[kg/hr]	Real	[-inf;inf]	0
2	Collector Flow	Flow Rate	[kg/hr]	Real	[-inf;inf]	0
3	Collector Temperature	Temperature	[C]	Real	[-inf;inf]	0
Outputs						
1	Hot Tank Flow	Flow Rate	[kg/hr]	Real	[-inf;inf]	0
2	Cold Tank Flow	Flow Rate	[kg/hr]	Real	[-inf;inf]	0
3	Outlet Temperature	Temperature	[C]	Real	[-inf;inf]	0

This diverter regulates flow based on the outlet temperature of the collector field. The collector field model has minimum flow rate requirement regardless of the presence of radiation. At hours where no radiation is present, the heat transfer fluid will cool as it passes through the collector field due to thermal losses in the field. The collector diverter recirculates this flow back to the cold storage tank to ensure that lower temperature fluid is not being mixed with higher temperature fluid in the hot storage tank. The model diverts flow back to the cold storage tank when the outlet temperature from the collector field is less than a specified design temperature.

5.10 Variable Volume Tank (Type 39-Existing)

The hot and cold storage tanks on each side of the collector field are both variable volume tanks. The parameters, inputs, and outputs are shown in Table 5.13.

Table 5.13 Variable Volume Tank Parameters, Inputs, and Outputs

Para.	Name	Dimension	Unit	Type	Range	Default
1	Tank Operation Mode	Dimensionless	[-]	Integer	[1;2]	2
2	Overall Tank Volume	Volume	[m^3]	Real	[0;inf]	20.0
3	Minimum Fluid Volume	Volume	[m^3]	Real	[0;inf]	1.0
4	Maximum Fluid Volume	Volume	[m^3]	Real	[0;inf]	18.0
5	Tank Circumference	Length	[m]	Real	[0;inf]	15.0
6	Cross-Sectional Area	Area	[m^2]	Real	[0;inf]	4.0
7	Wetted Loss Coefficient	Heat Transfer Coefficient	[kJ/hr-m^2]	Real	[0;inf]	6.0
8	Dry Loss Coefficient	Heat Transfer Coefficient	[kJ/hr-m^2]	Real	[0;inf]	4.0
9	Fluid Specific Heat	Specific Heat	[kJ/kg-K]	Real	[0;inf]	4.190
10	Fluid Density	Density	[kg/m^3]	Real	[0;inf]	1000.0
11	Initial Fluid Temperature	Temperature	[C]	Real	[-inf;inf]	22.0
12	Initial Fluid Volume	Volume	[m^3]	Real	[0;inf]	5.0
Inputs						
1	Inlet Temperature	Temperature	[C]	Real	[-inf;inf]	25.0
2	Inlet Flow Rate	Flow Rate	[kg/hr]	Real	[0;inf]	100.0
3	Flow Rate to Load	Flow Rate	[kg/hr]	Real	[0;inf]	75.0
4	Environment Temperature	Temperature	[C]	Real	[-inf;inf]	15.0
Outputs						
1	Fluid Temperature	Temperature	[C]	Real	[-inf;inf]	0
2	Load Flow Rate	Flow Rate	[kg/hr]	Real	[-inf;inf]	0
3	Excess Flow Temperature	Temperature	[C]	Real	[-inf;inf]	0
4	Excess Flow Rate	Flow Rate	[kg/hr]	Real	[-inf;inf]	0
5	Fluid Volume	Volume	[m^3]	Real	[-inf;inf]	0
6	Enthalpy Difference	Power	[kJ/hr]	Real	[-inf;inf]	0
7	Environment Losses	Power	[kJ/hr]	Real	[-inf;inf]	0
8	Internal Energy Change	Energy	[kJ]	Real	[-inf;inf]	0
9	Level Indicator	Dimensionless	[-]	Integer	[-inf;inf]	0

The tank has two operation modes, determined by the first parameter. For mode one, the tank recirculates the fluid if the tank has reached its maximum volume. For mode two, the tank diverts the fluid stream if the tank is full. The overall tank volume, minimum and maximum fluid volume, tank circumference, and cross-sectional area are all geometric properties of the tanks. These values will be determined based on the heat transfer fluid and system type, which will be discussed in the next chapter. The wetted loss coefficient is an overall loss coefficient associated with the section of the tank where the heat transfer fluid is present. Conversely, the dry loss coefficient is the overall loss coefficient associated with the section of the tank where heat transfer fluid is not present. Both of these coefficients depend on the type of heat transfer fluid being used. The fluid specific heat and density for the hot storage tank are taken at the design collector outlet temperature. In the case of the cold storage tank, the specific heat and density are determined from the design cycle outlet temperature. For all simulations, the initial fluid volume in the hot storage tank will be the minimum fluid volume and the initial temperature will be the design collector outlet temperature. For the cold tank, the initial fluid volume will be the maximum tank volume minus the minimum fluid volume of the hot tank, and the initial temperature will be the design cycle outlet temperature.

For the hot and cold tank, the inlet temperature and inlet flow rate are connected to the outputs of the collector field and Rankine cycle, respectively. The flow rate to load for both tanks is determined by the flow controller based on system demand. The environment temperature is determined from the weather data from Type 15.

The storage tank model outputs a fluid temperature based on the fluid present in the tank and accounts for mixing and losses to the environment. The load flow rate is determined from

the input value, except in cases where the tank has been depleted to the minimum fluid volume. The tank model will override any signals for flow demand to maintain the minimum fluid volume. The excess flow rate and temperature are determined based on the tank operation mode. The fluid volume output from the hot tank is used in the flow controller to control the flow demand from both tanks. The enthalpy difference output gives the enthalpy difference between the incoming and outgoing flows from the tank. The environment losses output gives the rate at which the tank losses energy to the environment. The internal energy change output gives the change in internal energy relative to the beginning of the simulation. Finally the level indicator is another output that measures the fluid volume. The level indicator returns a value of -1 if the tank is at minimum volume, 0 if the tank is somewhere between the minimum and maximum volume, and 1 if the tank is at maximum volume.

5.11 Simple Heating Thermostat (Type 1502-Existing)

The simple heating thermostat is used to determine if auxiliary heating is required to operate the cycle. In the case where the collector field is not heating enough heat transfer fluid to meet demand and there is insufficient volume in the hot storage tank, cold fluid is drawn from the cold storage tank and bypasses the collector field to be heated by the auxiliary heater to run the Rankine cycle. The thermostat is used to distinguish between hot and cold fluid entering the cycle and outputs a control signal to the auxiliary heater to turn on when the fluid is below a certain temperature. The parameters, inputs, and outputs for the simple heating thermostat are shown in Table 5.14.

Table 5.14 Simple Heating Thermostat Parameters, Inputs, and Outputs

Para.	Name	Dimension	Unit	Type	Range	Default
1	Number of Heating Stages	Dimensionless	[-]	Integer	[1;100]	1
2	Number of Oscillations Permitted	Dimensionless	[-]	Integer	[1;99]	5
3	Temperature Dead Band	Temperature Difference	[ΔC]	Real	[-inf;inf]	2.0
4	Number of Stage Exceptions	Dimensionless	[-]	Integer	[0;100]	0
5	Stage to Watch for Exception	Dimensionless	[-]	Integer	[0;100]	0
6	Affected Stage for Exception	Dimensionless	[-]	Integer	[0;100]	0
Inputs						
1	Fluid Temperature	Temperature	[C]	Real	[-inf;inf]	20.0
2	Lockout Signal	Dimensionless	[-]	Real	[-inf;inf]	0
3	Set Point Temperature for Stage	Temperature	[C]	Real	[-inf;inf]	20.0
Outputs						
1	Control Signal for Stage Heating	Dimensionless	[-]	Real	[0;1]	0
2	Conditioning Signal	Dimensionless	[-]	Real	[0;1]	0

The number of heating stages for all systems will always be one. The number of oscillations permitted works in a similar way as the N-stage differential controller discussed in section 5.4; this parameter is kept at the default value for all systems. The temperature dead band allows for the modeling of hysteresis effects; however, these effects are not present based on the control strategy, so the dead band is set to zero. The exception parameters are not used, so these parameters are left at zero.

The inlet fluid temperature is the outlet temperature from the hot side mixer. If this fluid temperature is less than the set point temperature, the thermostat will output a signal of one to indicate that heating is required. The set point temperature is the minimum allowable cycle input temperature, which is the lowest value in the range of the heat transfer fluid

specified in section 4.7. The lockout signal overrides the controller when a value greater than 0.5 is specified; this input is left set at zero. The conditioning signal returns a value of one if any of the stages are turned on. Since only one stage is used in these systems, it is identical to the control signal.

5.12 Auxiliary Heater (Type 6-Existing)

The auxiliary heater is a component that calculates the heating rate required to increase the temperature of a flowing fluid. The parameters, inputs, and outputs for this component are shown in Table 5.15.

Table 5.15 Table 5.15 Auxiliary Heater Parameters, Inputs, and Outputs

Para.	Name	Dimension	Unit	Type	Range	Default
1	Maximum Heating Rate	Power	[kJ/hr]	Real	[-inf;inf]	1000.0
2	Specific heat of fluid	Specific Heat	[kJ/kg-K]	Real	[0;inf]	4.19
3	Overall Loss Coefficient for Heater During Operation	Overall Loss	[kJ/hr-K]	Real	[0;inf]	0.0
4	Efficiency of Auxiliary Heater	Dimensionless	[-]	Real	[0;1]	1
Inputs						
1	Inlet Fluid Temperature	Temperature	[C]	Real	[-inf;inf]	20.0
2	Fluid Mass Flow Rate	Flow Rate	[kg/hr]	Real	[0;inf]	100.0
3	Control Function	Dimensionless	[-]	Integer	[0;1]	1
4	Set Point Temperature	Temperature	[C]	Real	[-273;inf]	60.0
5	Temperature of Surroundings	Temperature	[C]	Real	[-273;inf]	20.0
Outputs						
1	Outlet Fluid Temperature	Temperature	[C]	Real	[-inf;inf]	0
2	Outlet Fluid Flow Rate	Flow Rate	[kg/hr]	Real	[0;inf]	0
3	Required Heating Rate	Power	[kJ/hr]	Real	[-inf;inf]	0

4	Losses from the Auxiliary Heater	Power	[kJ/hr]	Real	[-inf;inf]	0
5	Rate of Energy Delivery to Fluid Stream	Power	[kJ/hr]	Real	[-inf;inf]	0

The maximum heating rate for all simulations is set to a high number to ensure that the heat transfer fluid can be heated to the minimum cycle temperature. The specific heat is calculated from the cold tank temperature. Since the fluid leaving the hot tank will never be below the minimum cycle temperature, the heat transfer fluid is only heated by the auxiliary heater when it bypasses the collector field when the hot tank has insufficient volume to supply the cycle flow. The loss coefficient for the heater is assumed to be zero, and the efficiency is assumed to be one. The auxiliary heater can represent several different types of heating, such as natural gas or electric heating. The results for the required heating rate can be manipulated afterwards to adjust for losses and efficiency based on a specific type of heating element.

The inlet fluid temperature and flow rate are taken from the outlet from the hot side mixer. The control function is the output from the thermostat. The auxiliary heater will heat the heat transfer fluid to the set point temperature when specified by the control function. The temperature of the surroundings is based on weather data from Type 15. The outlet fluid flow rate is the same as the inlet. The outlet temperature is the same as the inlet when the temperature is higher than the set point; when it is lower, it is the set point temperature. The losses from the heater are zero when the loss coefficient is zero. The required heating rate and rate of energy delivery to the fluid stream are the same when the efficiency is one and losses are zero.

5.13 Weather Data (Type 15-2-Existing)

The weather data component reads weather data files with various formats and outputs the information for other TRNSYS components to use. The parameters and used outputs are shown in Table 5.16.

Table 5.16 Weather Data Parameters and Utilized Outputs

Para.	Name	Dimension	Unit	Type	Range	Default
1	File Type	Dimensionless	[-]	Integer	[2;2]	2
2	Logical Unit	Dimensionless	[-]	Integer	[10;inf]	30
3	Tilted Surface Radiation Mode	Dimensionless	[-]	Integer	[1;5]	3
4	Ground Reflectance – no snow	Dimensionless	[-]	Real	[0;1]	0.2
5	Ground Reflectance – snow cover	Dimensionless	[-]	Real	[0;1]	0.7
6	Number of Surfaces	Dimensionless	[-]	Real	[1;99]	1
7	Tracking Mode	Dimensionless	[-]	Integer	[1;4]	1
8	Slope of Surface	Direction (Angle)	[degree]	Real	[-360;360]	0.0
9	Azimuth of Surface	Direction (Angle)	[degree]	Real	[-360;360]	0.0
Outputs						
1	Dry Bulb Temperature	Temperature	[C]	Real	[-inf;inf]	0
2	Wet Bulb Temperature	Temperature	[C]	Real	[-inf;inf]	10
3	Mains Water Temperature	Temperature	[C]	Real	[-inf;inf]	10
4	Wind Velocity	Velocity	[m/s]	Real	[0;inf]	0
5	Direct Normal Radiation	Flux	[kJ/hr-m^2]	Real	[0;inf]	0

The file type used for Type 15-2 is TMY2 data, which stands for Typical Meteorological Year. It is a collation of selected weather data for a specific location, generated from a data bank much longer than a year in duration. It is specially selected so that it presents the range

of weather phenomena from the location in question, while still giving annual averages that are consistent with the long-term averages for the location in question. The logical unit is the parameter through which the data reader will read the external weather file. The tilted surface radiation mode, ground reflectance, number of surfaces, tracking mode, slope of surface, and azimuth of surface are all parameters used to determine outputs that are not used in the simulations, and they are left at their default values.

The dry bulb temperature is the temperature of the air as measured by an ordinary thermometer. The wet bulb temperature is the temperature of an air-water vapor mixture that is measured with a thermometer that has a wetted measurement point. The wet-bulb temperature is used for calculations in the cooling tower. The mains water temperature is the temperature available from the water mains, which is used for the makeup water to the cooling tower. The wind velocity is used for losses in the collector field. The direct normal radiation the solar insolation measured at a given location on Earth with a surface element perpendicular to the Sun's rays. It does not include diffuse radiation, which is solar radiation that is scattered or reflected by atmospheric components in the sky.

5.14 Cooling Tower (Type 51b-Existing)

The cooling tower component calculated the parasitic fan power required to supply cooling water to the condenser in the Rankine cycle. The parameters, inputs, and outputs are shown in Table 5.17.

Table 5.17 Cooling Tower Parameters, Inputs, and Outputs

Para.	Name	Dimension	Unit	Type	Range	Default
1	Calculation Mode	Dimensionless	[-]	Integer	[1;1]	1
2	Flow Geometry	Dimensionless	[-]	Integer	[1;2]	1
3	Number of Tower Cells	Dimensionless	[-]	Integer	[1;8]	1

4	Maximum Cell Flow Rate	Volumetric Flow Rate	[m^3/hr]	Real	[0;inf]	40.0
5	Fan Power at Maximum Flow	Power	[kW]	Real	[0;inf]	1.0
6	Minimum Cell Flow Rate	Volumetric Flow Rate	[m^3/hr]	Real	[0;inf]	10.0
7	Sump Volume	Volume	[m^3]	Real	[-1;inf]	1.0
8	Initial Sump Temperature	Temperature	[C]	Real	[-inf;inf]	15.0
9	Mass Transfer Constant	Dimensionless	[-]	Real	[0.5;5]	1.36
10	Mass Transfer Exponent	Dimensionless	[-]	Real	[-1.1;-0.35]	-0.94
11	Print Performance Results?	Dimensionless	[-]	Integer	[1;2]	1
Inputs						
1	Water Inlet Temperature	Temperature	[C]	Real	[-inf;inf]	20.0
2	Inlet Water Flow Rate	Flow Rate	[kg/hr]	Real	[0;inf]	100.0
3	Dry Bulb Temperature	Temperature	[C]	Real	[-inf;inf]	15.0
4	Wet Bulb Temperature	Temperature	[C]	Real	[-inf;inf]	12.0
5	Sump make-up Temperature	Temperature	[kJ/hr]	Real	[-inf;inf]	10.0
6	Relative Fan Speed for Cell	Dimensionless	[-]	Real	[-1.0;1.0]	0.85
Outputs						
1	Sump Temperature	Temperature	[C]	Real	[-inf;inf]	0
2	Sump Flow Rate	Flow Rate	[kg/hr]	Real	[-inf;inf]	0
3	Fan Power Required	Power	[kW]	Real	[-inf;inf]	0
4	Heat Rejection Rate	Power	[kJ/hr]	Real	[-inf;inf]	0
5	Cell Outlet Temperature	Temperature	[C]	Real	[-inf;inf]	0
6	Water Loss Rate	Flow Rate	[kg/hr]	Real	[-inf;inf]	0
7	Outlet Air Dry Bulb	Temperature	[C]	Real	[-inf;inf]	0
8	Outlet Air Wet Bulb	Temperature	[C]	Real	[-inf;inf]	0

9	Outlet Humidity Ratio	Dimensionless	[-]	Real	[-inf;inf]	0
10	Outlet Air Flow Rate	Flow Rate	[kg/hr]	Real	[-inf;inf]	0
11	Change in Internal Energy	Energy	[kJ]	Real	[-inf;inf]	0

The calculation mode only has one possible value, so this parameter remains unchanged. The flow geometry allows a choice between counterflow geometry (1) or crossflow geometry (2). Counterflow geometry is used for all simulations. For the cooling tower model, the cooling tower parameters and inputs are taken from the cooling tower at the SEGs plant modeled by Patnode, which was also a 30 MW plant. There are two tower cells used for every simulation. The maximum cell flow rate, fan power at maximum flow, minimum cell flow rate, sump volume, initial sump temperature, mass transfer constant, and mass transfer exponent are identical to the Patnode model (2006).

The water inlet temperature is taken from the cooling water outlet temperature from the Rankine cycle, and the inlet flow rate is the same as the outlet flow rate from the cooling tower, which is the design cooling water flow rate specified in chapter 3. The dry and wet bulb temperatures are taken from the weather data in Type 15. The sump make-up temperature is assumed to be the mains water temperature for the location, which is determined from the weather data file. The relative fan speed is assumed to be 0.85 for both cells. The outputs utilized in the simulation are the sump temperature, the sump flow rate, and the required fan power. The sump temperature and flow rate are the cooling water inputs to the Rankine cycle, and the fan power required is added to the parasitic power losses from the system.

5.15 Dual Flow Controller (Type 989-New)

The dual loop system has a different controller due to the fact that the proposed dual loop system only stores molten salt, and uses the molten salt to heat Dowtherm A when the collector field doesn't produce enough flow rate to supply the power cycle. Figures 5.21 and 5.22 show the layout of the dual loop system.

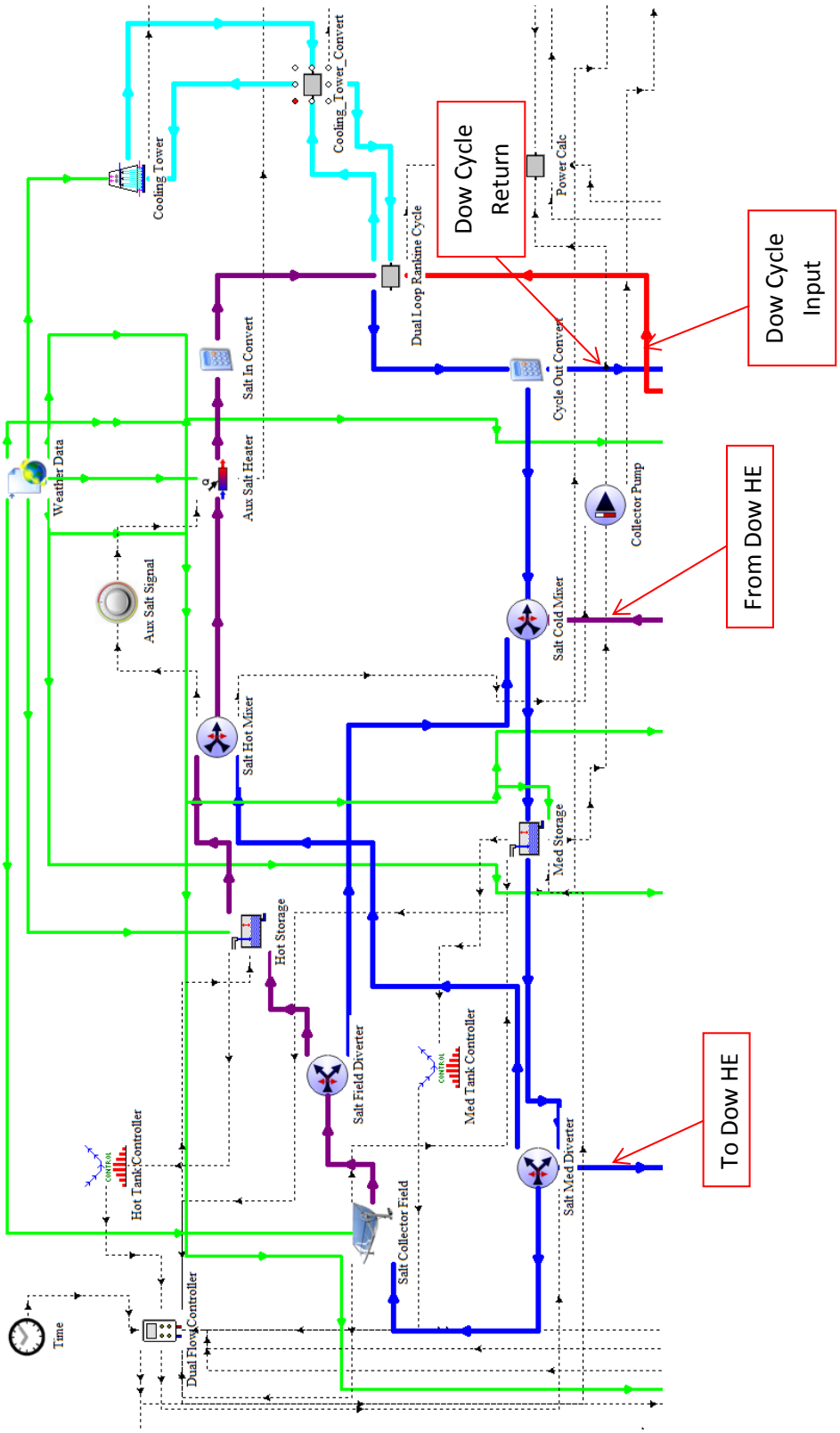

Figure 5.21 Dual Loop System Layout (Salt Loop and Power Block)

The salt loop portion of the dual loop system has a layout that is similar to the single loop systems. The design outlet temperature for the salt portion is the same as the temperature from the single loop system. The bottom half of the dual loop layout is shown in Figure 5.22.

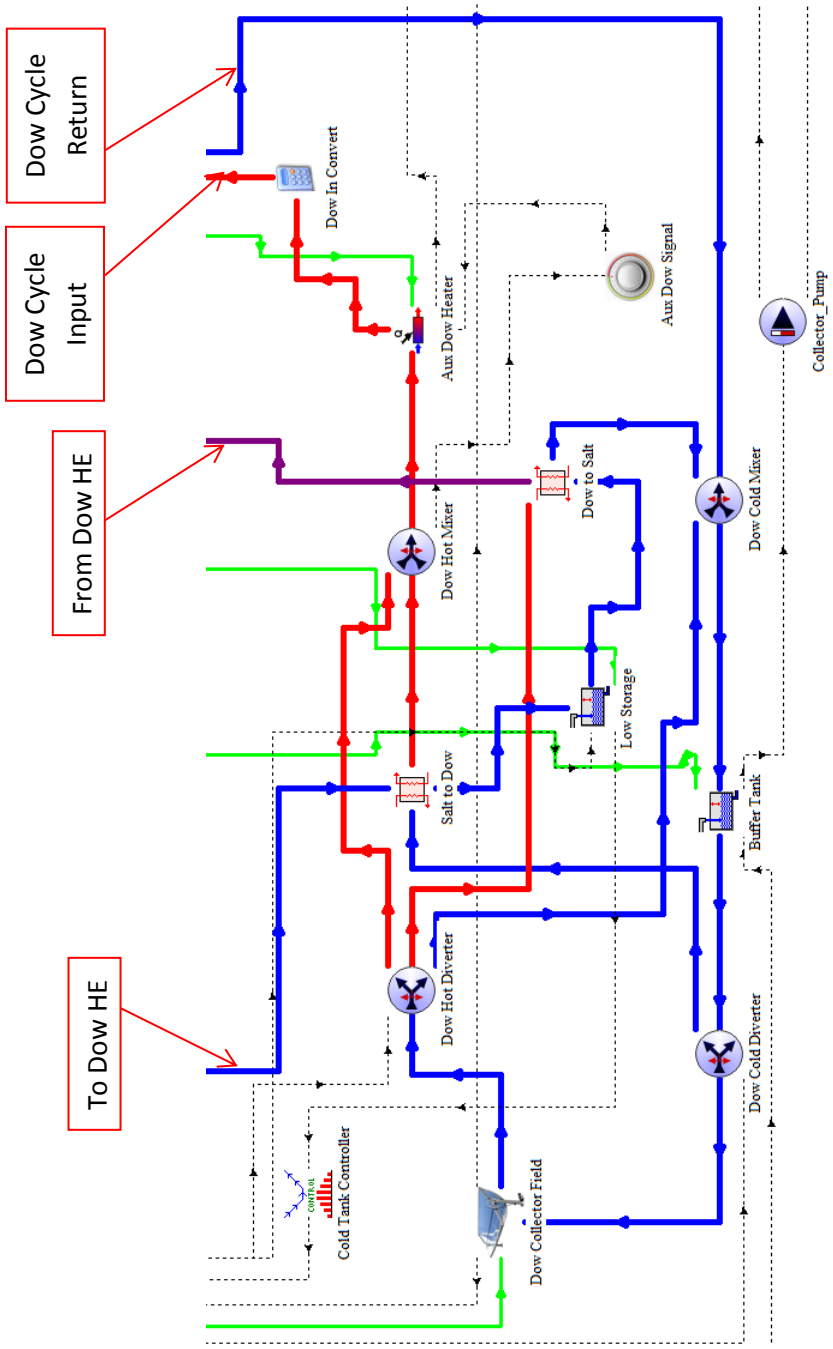

Figure 5.22 Dual Loop System Layout (Dowtherm A Loop)

The dual flow controller works with the same principles as the flow controller from section 5.6. A table with the parameters, inputs, and outputs is shown in Table 5.18.

Table 5.18 Flow Controller Parameters, Inputs, and Outputs

Parameters	Name	Dimension	Unit	Type	Range	Default
1	$Hour_{Start}$	Time	[hr]	Real	[0;24]	6
2	$Hour_{End}$	Time	[hr]	Real	[0;24]	21
3	$Set\ Flow_{Salt}$	Flow Rate	[kg/s]	Real	[0;inf]	150.0
4	$Set\ Flow_{Dow}$	Flow Rate	[kg/s]	Real	[0;inf]	384.0
5	$Dow\ Temp\ Lim$	Temperature	[C]	Real	[0;inf]	0
Inputs						
1	$Hour$	Time	[hr]	Real	[0;24]	0
2	$Control_{Signal,Hot}$	Dimensionless	[-]	Real	[0;1]	0
3	$Control_{Signal,Med}$	Dimensionless	[-]	Real	[0;1]	0
4	$Control_{Signal,Cold}$	Dimensionless	[-]	Real	[0;1]	0
5	$Collector_{Flow,salt}$	Flow Rate	[kg/hr]	Real	[0;inf]	0
6	$Collector_{Flow,Dow}$	Flow Rate	[kg/hr]	Real	[0;inf]	0
7	$Collector_{Temp,Dow}$	Temperature	[C]	Real	[0;inf]	0
8	$Med\ Tank\ Temp$	Temperature	[C]	Real	[0;inf]	0
Outputs						
1	$Flow_{Demand,HT}$	Flow Rate	[kg/hr]	Real	[0;inf]	0
2	$Flow_{Demand,MT}$	Flow Rate	[kg/hr]	Real	[0;inf]	0
3	$Flow_{Demand,HT}$	Flow Rate	[kg/hr]	Real	[0;inf]	0
4	$Bypass\ Flow_{Salt}$	Flow Rate	[kg/hr]	Real	[0;inf]	0
5	$Bypass\ Flow_{Dow}$	Flow Rate	[kg/hr]	Real	[0;inf]	0
6	$Dow_{Overflow}$	Flow Rate	[kg/hr]	Real	[0;inf]	0
7	$Salt_{Demand} from\ Dow$	Flow Rate	[kg/hr]	Real	[0;inf]	0
8	Dow_{Demand}	Flow Rate	[kg/hr]	Real	[0;inf]	0

The parameters $Hour_{Start}$ and $Hour_{End}$ correspond to the times between which the power cycle is in operation. Between these two hours, the flow rates to the power cycle are the design flow rates for the power cycle. For all other hours during the day, the flow rates to the power cycle are zero. The set flows are the mass flow rates sent to the power block. The hour input is the hour of the day output from Type 21. The control signal inputs are the

signal outputs from the volume controllers for each storage tank, Type 973. The collector flow is the flow rate specified by the collector model for both fields, Type 850.

The flow demand from the storage tanks are determined from the time of day and control signal from the volume controllers. The salt bypass flow is the amount of flow required to bypass the collector field to be heated by an auxiliary heater, Type 6, to meet the cycle demand. If the hot control signal is one, meaning the volume of the hot salt storage tank is depleted, the flow demand from the tanks are as follows

$$Flow_{Demand,MT} = Set\ Flow_{Salt} + Collector\ Flow_{Salt} \tag{5.27}$$

$$Flow_{Demand,HT} = 0 \tag{5.28}$$

$$Bypass\ Flow_{Salt} = Set\ Flow_{Salt} \tag{5.29}$$

If the hot control signal is zero, there is sufficient volume in the hot storage tank to supply the cycle flow, and the flow demand from the tanks are as follows

$$Flow_{Demand,MT} = Collector\ Flow_{Salt} \tag{5.30}$$

$$Flow_{Demand,HT} = Set\ Flow_{Salt} \tag{5.31}$$

$$Bypass\ Flow_{Salt} = 0 \tag{5.32}$$

There are three methods with which the Dowtherm A fluid can be heated before being sent to the power block. If the Dowtherm A collector field produces a mass flow rate exactly equal to the set flow rate for Dowtherm A, then there is no bypass flow and the Dowtherm A is

routed directly to the power block. If the Dowtherm A collector field produces a flow rate lower than the set flow rate of the cycle and there is sufficient volume in the medium salt storage tank, then bypass flow is sent to the heat exchanger between molten salt and Dowtherm A. In this scenario, Dowtherm A is heated using the stored thermal energy in the medium salt storage tank. In order to determine the mass flow rate of salt required to heat the Dowtherm flow rate to the cycle temperature in the heat exchanger, an EES model was created to determine the flow rates of salt required depending on the mass flow rate of Dowtherm A and the temperature of the molten salt in the medium storage tank. The transport properties of Dowtherm A were assumed to be constant in the heat exchanger at the average temperature of Dowtherm A in the heat exchanger.

$$T_{avg,Dow} = \frac{T_{in,Dow} + T_{out,Dow}}{2} \tag{5.33}$$

The transport properties of the molten salt are also assumed to be constant in the heat exchanger; therefore, the average temperature is calculated to evaluate the properties in the heat exchanger.

$$T_{avg,Salt} = \frac{T_{in,Salt} + T_{out,Salt}}{2} \tag{5.34}$$

The capacitance rate of the Dowtherm A is the product of the mass flow rate of the Dowtherm A and the specific heat capacity of the Dowtherm A. The mass flow rate of Dowtherm A is the bypass flow. The specific heat capacity of the Dowtherm in the heat exchanger is determined using the "CP" function in EES.

$$\dot{C}_{cold} = \dot{m}_{Dow} c_p\left('Dowtherm'_A, T = T_{avg,Dow}\right) \tag{5.35}$$

Similar to equation 5.35, the capacitance rate of the molten salt is calculated from the mass flow rate of the molten salt and the specific heat capacity of the molten salt. The mass flow rate of the molten salt is the calculated variable based on the other inputs and heat exchanger relationships.

$$\dot{C}_{hot} = \dot{m}_{salt} c_p('Salt(60NaNO3\_40KNO3)', T = T_{avg,salt}) \tag{5.36}$$

The minimum capacitance rate in the heat exchanger is defined as the lowest capacitance of the two fluids in the heat exchanger.

$$\dot{C}_{min} = Minimum(\dot{C}_{cold}, \dot{C}_{hot}) \tag{5.37}$$

The maximum capacitance rate in the superheater is defined as the highest capacitance of the two fluids in the heat exchanger.

$$\dot{C}_{max} = Maximum(\dot{C}_{cold}, \dot{C}_{hot}) \tag{5.38}$$

$\dot{C}_r$ is the heat capacity ratio in the heat exchanger, which is calculated as the ratio between the minimum and maximum capacitance rate.

$$\dot{C}_r = \frac{\dot{C}_{min}}{\dot{C}_{max}} \tag{5.39}$$

An overall UA (heat transfer coefficient-area product) for the heat exchanger is specified in the component. For this model, several UA values were used to determine the optimum heat exchanger conductance. The heat transfer rate in the heat exchanger was calculated using equations 5.40-5.42.

$$\dot{Q}_{HE} = \dot{m}_{Dow}(h_{Dow,out} - h_{Dow,in}) \tag{5.40}$$

$$\dot{Q}_{HE} = \dot{m}_{salt}\left(h_{salt,in} - h_{salt,out}\right) \tag{5.41}$$

$$\dot{Q}_{HE} = \varepsilon_{HE}\dot{C}_{min}\left(T_{salt,in} - T_{Dow,in}\right) \tag{5.42}$$

The effectiveness of a counter flow heat exchanger is calculated using equation 5.43, if the heat capacity ratio is less than 1, which is the case for this heat exchanger.

$$\varepsilon_{HE} = \frac{1 - e^{-NTU_{HE}(1-C_r)}}{1 - C_r e^{-NTU_{HE}(1-C_r)}} \tag{5.43}$$

The number of transfer units for the heat exchanger, NTU_{HE}, is calculated using equation 3.13, which is the ratio of the overall heat exchanger conductance, UA_{HE}, and the minimum capacitance rate.

$$NTU_{HE} = \frac{UA_{HE}}{\dot{C}_{min}} \tag{5.44}$$

The salt flow rate required to heat a Dowtherm A fluid stream is plotted for various overall heat exchanger conductance values in Figure 5.23 with the inlet salt temperature assumed to be 400°C.

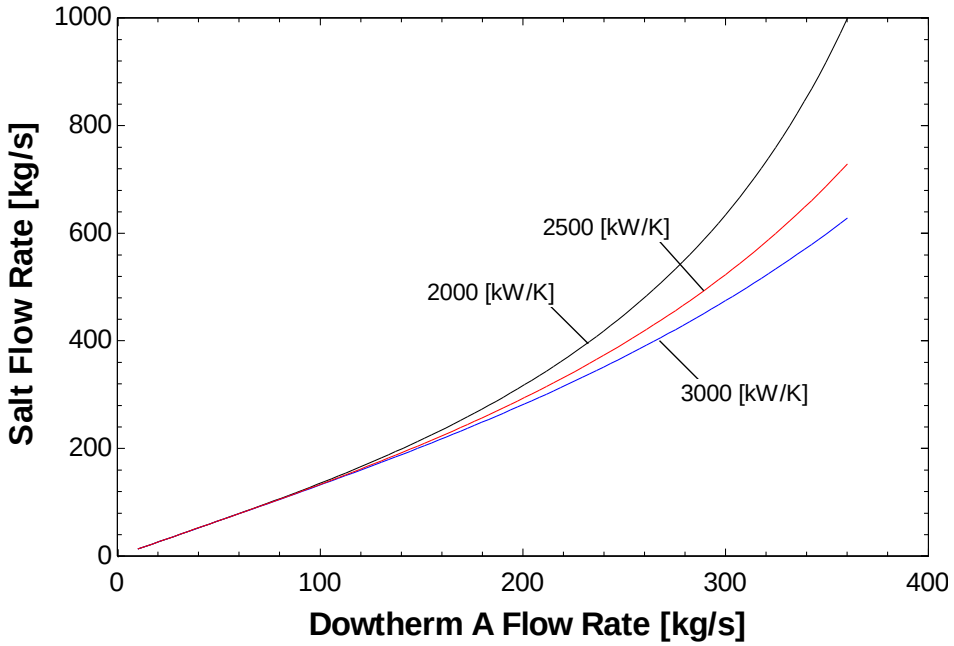

Figure 5.23 Required Salt Flow Rate vs. Dowtherm A Flow Rate

For the system, the overall heat exchanger conductance is assumed to be 3000 [kW/K]. After setting the overall heat exchanger conductance value, the heat exchanger was run at a range of flow rates of Dowtherm A (0 [kg/s] to 360 [kg/s]) and salt inlet temperatures (400°C to 440°C). Using this data a correlation was developed using the linear regression tool in EES (2014) shown in Equation 5.45.

$$Salt\ Demand = 13069 + 10.683 \cdot Dow_{Flow} + 0.00079618 \cdot Dow_{Flow}^2 - 63.323 \cdot T_{salt,tank} + 0.076661 \cdot T_{salt,tank}^2 - 0.023332 \cdot Dow_{Flow} \cdot T_{salt,tank} \quad (5.45)$$

The statistical fit data for equation 5.45 is shown in Table 5.19

Table 5.19 Statistical Fit Data For Molten Salt to Dowtherm A Heat Exchanger Correlation

Number of Points	990
RMS	3.11E01
Bias	-1.49E-13
R^2	94.18%

This correlation is used in the dual flow controller to determine the amount of molten salt needed from the medium storage tank to the heat exchanger between Dowtherm A and molten salt. The molten salt is routed to the cold storage tank after being sent through this heat exchanger. If there is insufficient volume in the medium storage tank, the Dowtherm A fluid stream is heated using the auxiliary heating (Type-6). If the Dowtherm A collector field produces a flow rate greater than the cycle flow, then the extra flow is sent to a different heat exchanger where Dowtherm A is used to heat molten salt in the cold storage tank, which is then sent to the medium salt storage tank. The salt flow rate that could be heated to 394°C with a Dowtherm A fluid stream is plotted for various overall heat exchanger conductance values in Figure 5.24.

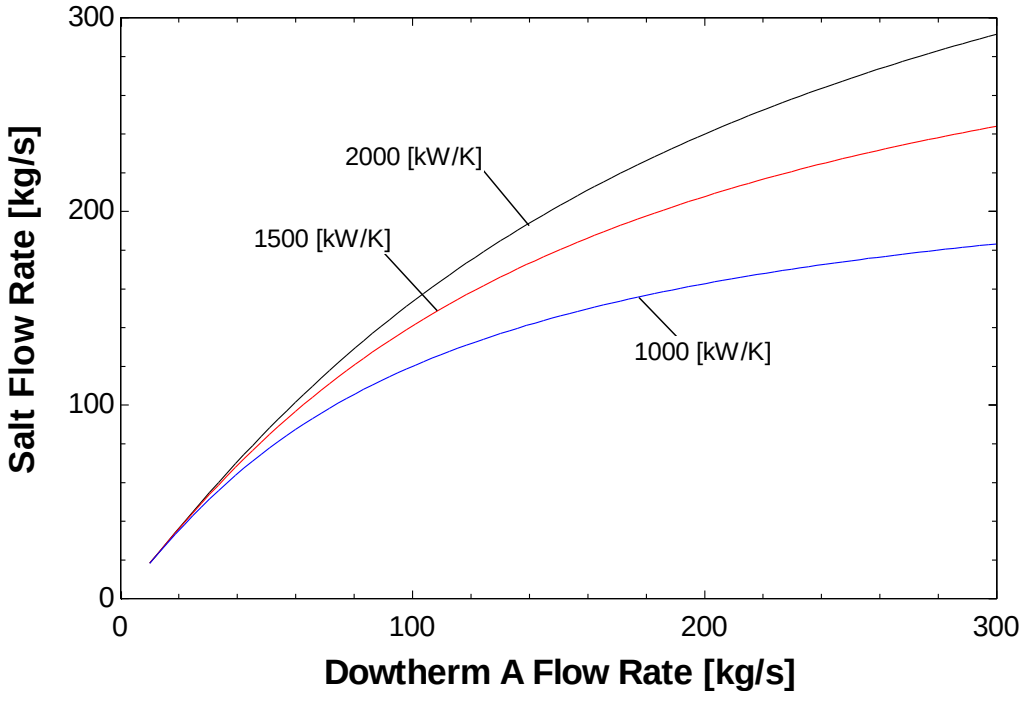

Figure 5.24 Salt Flow Rate vs. Dowtherm A overflow rate

The overall heat exchanger conductance was chosen to be 2000 [kW/K]. Equations 5.33 through 5.44 apply for this heat exchanger except that Dowtherm A is the heating fluid and

the molten salt is the cooling fluid. This model is simpler because the Dowtherm A overflow rate will always be at the specified collector outlet temperature, which is 397°C. Therefore, the salt flow rate from the cold temperature tank is only dependent on the overflow rate of Dowtherm A from the collector field.

$$Salt\ Demand = 1.0235 + 1.9060 \cdot Dow_{Overflow} - 0.0058107 \cdot Dow_{Overflow}^{2} \quad (5.46)$$

Table 5.20 Statistical Fit Data For Dowtherm A to Molten Salt Heat Exchanger Correlation

Number of Points	100
RMS	4.31
Bias	4.03E-17
R^2	99.06%

5.16 Counter Flow Heat Exchanger (Type 5b-Existing)

The counter flow heat exchanger model is a zero capacitance heat exchanger model which calculates outlet temperatures given hot and cold side inlet temperatures and flow rates and the overall heat transfer coefficient.

Table 5.21 Counter Flow Heat Exchanger Parameters, Inputs, and Outputs

Para.	Name	Dimension	Unit	Type	Range	Default
1	Counter Flow Mode	Dimensionless	[-]	Integer	[2;2]	2
2	Specific Heat of Source Side Fluid	Specific Heat	[kJ/kg-K]	Real	[0;inf]	4.19
3	Specific Heat of Load Side Fluid	Specific Heat	[kJ/kg-K]	Real	[0;inf]	4.19
Inputs						
1	Source Side Inlet Temperature	Temperature	[C]	Real	[-inf;inf]	20.0
2	Source Side Flow Rate	Flow Rate	[kg/hr]	Real	[0;inf]	100.0
3	Load Side Inlet Temperature	Temperature	[C]	Real	[-inf;inf]	20.0
4	Load Side Flow Rate	Flow Rate	[kg/hr]	Real	[0;inf]	100.0
5	Overall Heat Transfer Coefficient	Overall Loss Coefficient	[kJ/hr-K]	Real	[0;inf]	10.0
Output						
1	Source Side Outlet Temperature	Temperature	[C]	Real	[-inf;inf]	0
2	Source Side Flow Rate	Flow Rate	[kg/hr]	Real	[-inf;inf]	0
3	Load Side Outlet Temperature	Temperature	[C]	Real	[-inf;inf]	0
4	Load Side Flow Rate	Flow Rate	[kg/hr]	Real	[-inf;inf]	0
5	Heat Transfer Rate	Power	[kJ/hr]	Real	[-inf;inf]	0
6	Effectiveness	Dimensionless	[-]	Real	[-inf;inf]	0

The source and load side flow rates and temperatures are the flow rates and temperatures of molten salt and Dowtherm A. The overall heat transfer coefficient was set based on the EES heat exchanger model described in section 5.15.

Chapter 6 TRNSYS Annual Results

6.1 Introduction

The three TRNSYS simulations, the single loop of Dowtherm A, the single loop of molten salt (60% $NaNO_3$ / 40% KNO_3), and the Dual Loop, which utilizes both fluids, were run for an annual period to determine the performance of each cycle. The simulation location was Daggett, CA, using weather data for a typical meteorological year. The efficiency of each Rankine cycle power block using Dowtherm A, molten salt and a both fluids was determined using the EES models described in Chapter 3. The efficiency of the single loop of molten salt and the dual loop cycle were comparable to one another, due to the access to higher temperatures with the molten salt. However, the 2008 Schott collectors, which were used for these simulations, have greater losses at the molten salt operating temperatures than at the Dowtherm operating temperatures, which is a thermodynamic advantage for Dowtherm A. Molten salt has lower pumping losses due to its higher density, which gives it a thermodynamic advantage. The dual loop exhibits both of these fluids' advantages and disadvantages. In order to determine the balance of these advantages, annual simulations are used to determine how these factors will affect the thermodynamic performance of each system.

6.2 System Layouts

The single loop of Dowtherm layout is shown in Figure 6.1.

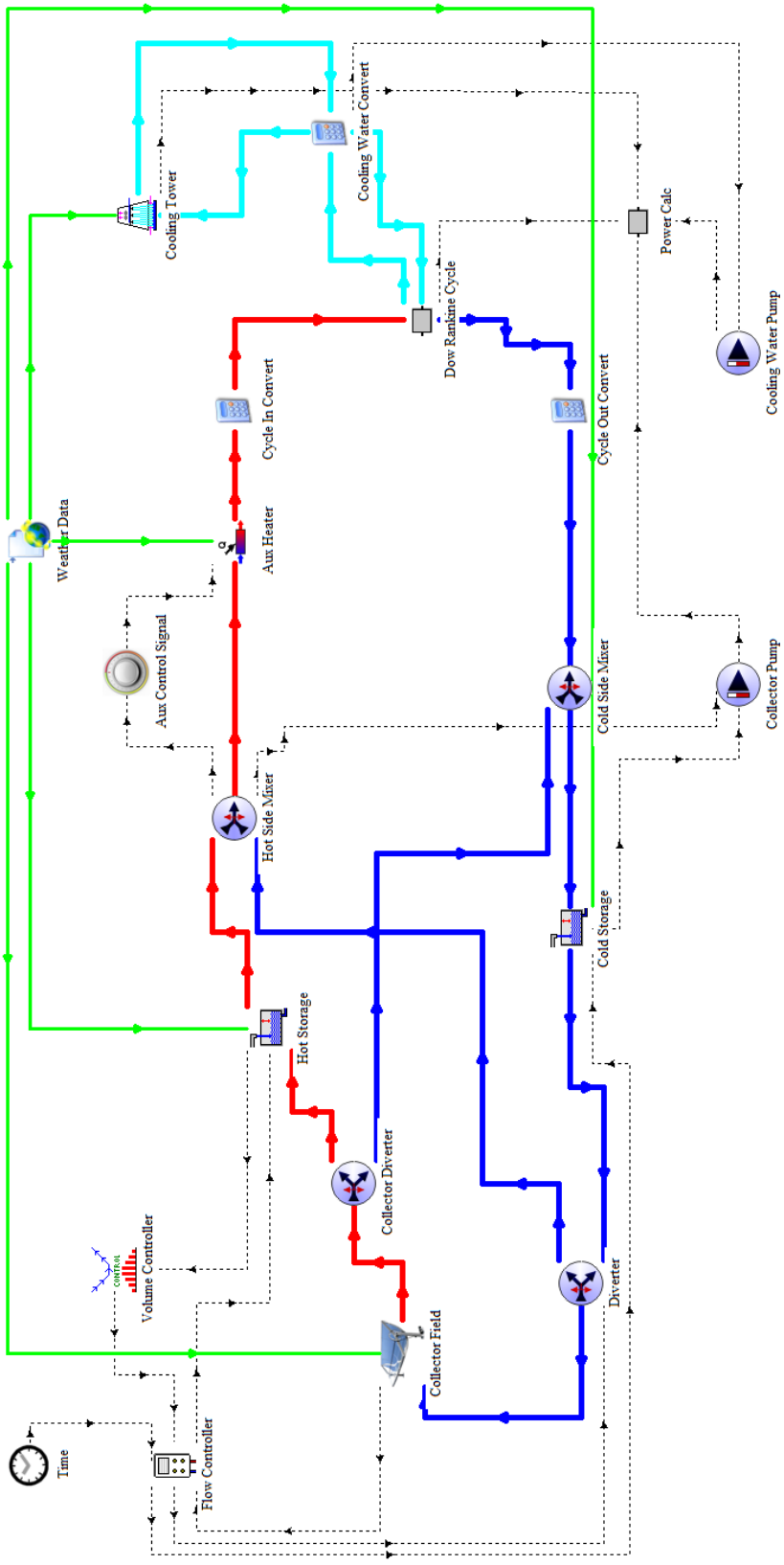

Figure 6.1 Single Loop Dowtherm System Layout

For each system, the power cycle hours of operation are 6:00 A.M. to 9:00 P.M. For the Dowtherm system, the design outlet temperature of the field is 397°C. The design field outlet temperature is slightly higher than the design cycle temperature because of thermal losses from the storage tank and piping. The collector field calculates the mass flow rate based on the ambient conditions and this design outlet temperature. If the collector field can produce a positive flow rate at the outlet temperature, the flow is routed to the hot storage tank. The cycle side of the system draws fluid from the hot storage tank if there is sufficient volume in the tank. If there is insufficient volume in the hot storage tank, fluid from the cold storage tank bypasses the collector field and is heated using an auxiliary heater. The outlet flow from the cycle is sent to the cold storage tank. The pumping losses for the heat transfer fluid and cooling water are calculated based on the flow rates of each fluid. The pumping losses and fan power losses from the cooling tower are subtracted from the power output from the cycle to get the net power output from the system.

The single loop of molten salt layout is shown in Figure 6.2

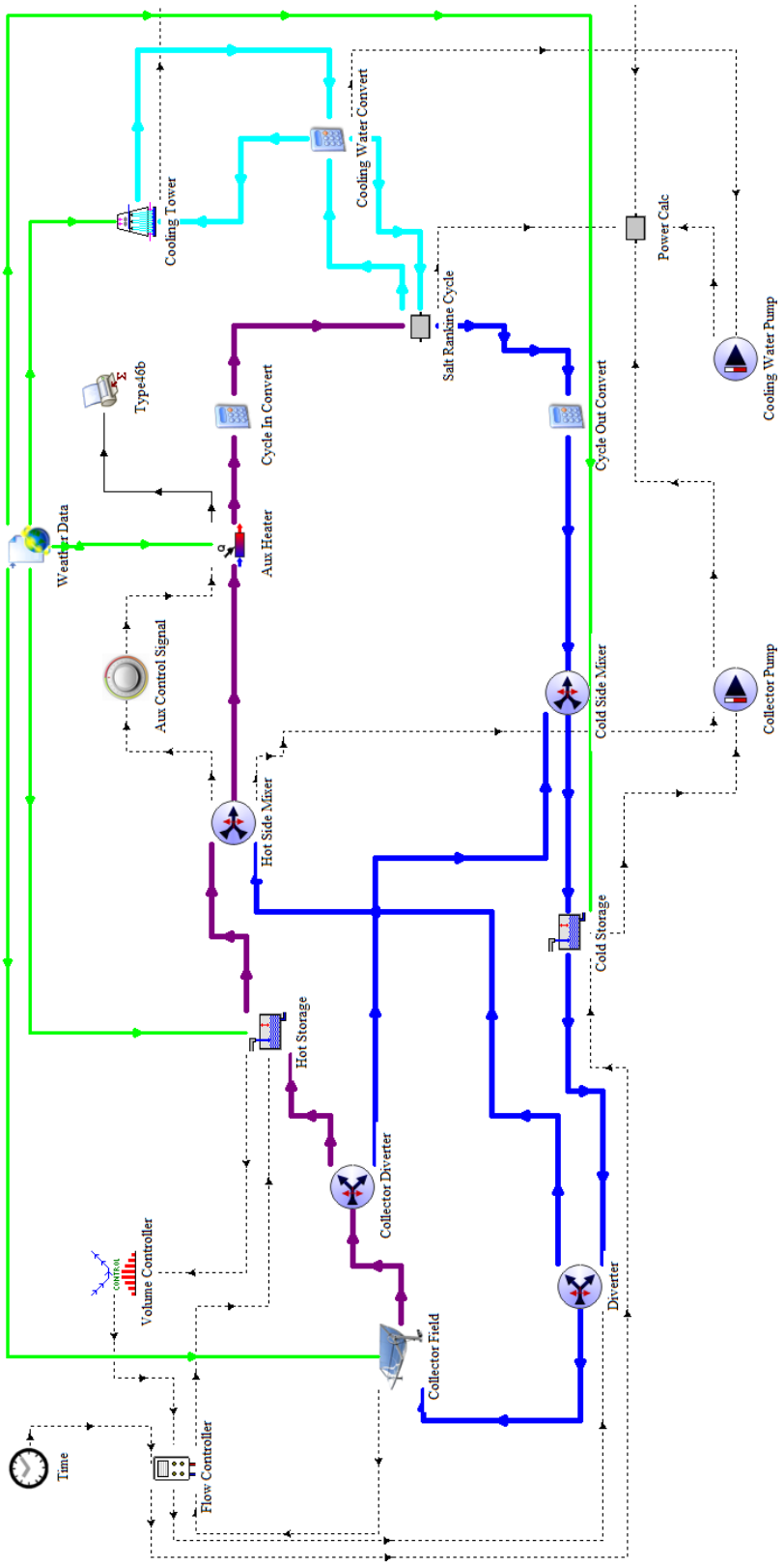

Figure 6.2 Single Loop Molten Salt Layout

The single loop of molten salt system works essentially the same way as the single loop of Dowtherm A system. However, the design outlet temperature of collector field for the single loop of salt system is 555°C. This value is higher than the design cycle temperature to account for thermal losses from the storage tank and piping.

The top half of the dual loop layout is shown in Figure 6.3.

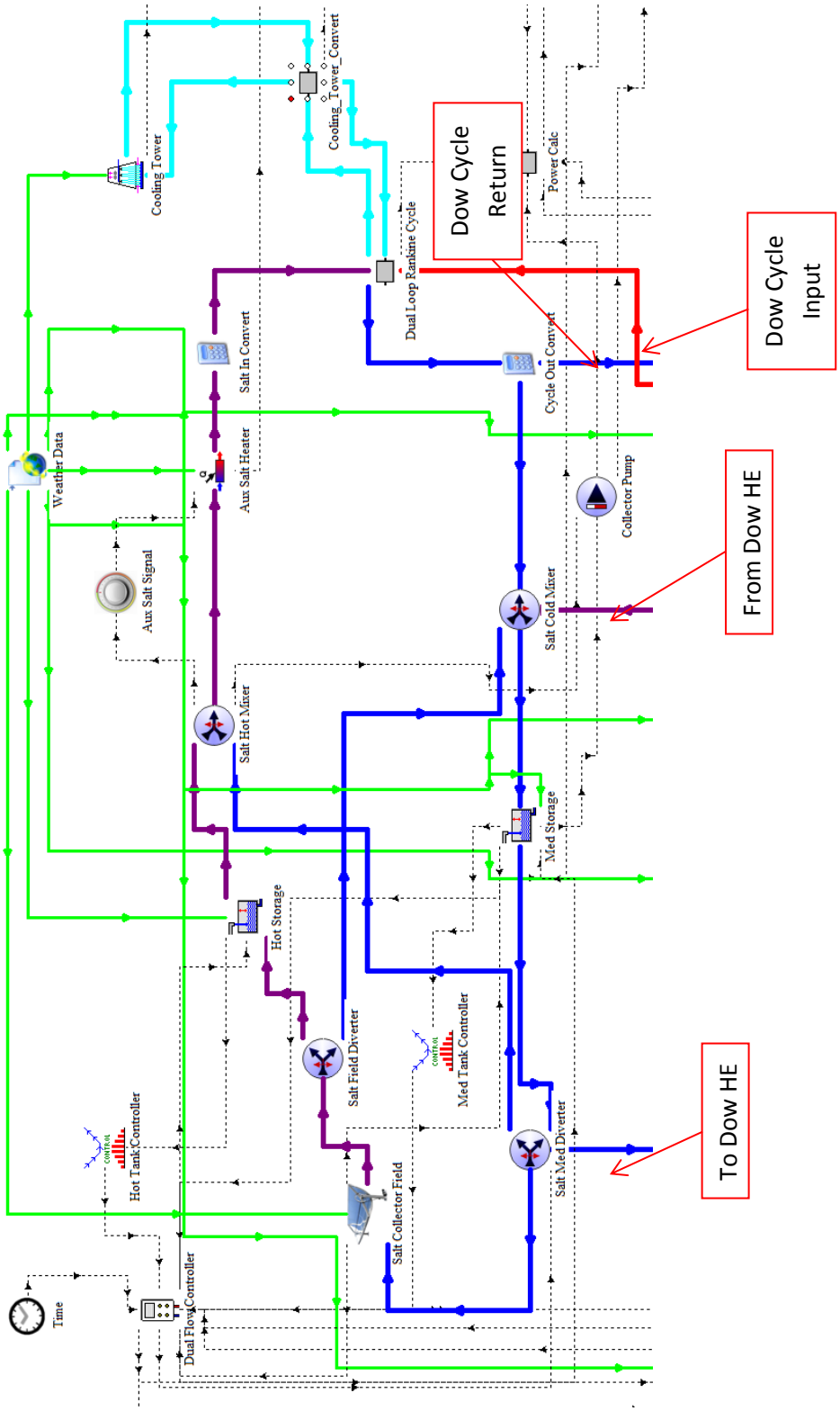

Figure 6.3 Dual Loop (Salt Loop and Power Block)

The salt loop portion of the dual loop system has a layout that is similar to the single loop systems. The design outlet temperature for the salt portion is the same as the temperature from the single loop system. The bottom half of the dual loop layout is shown Figure 6.4.

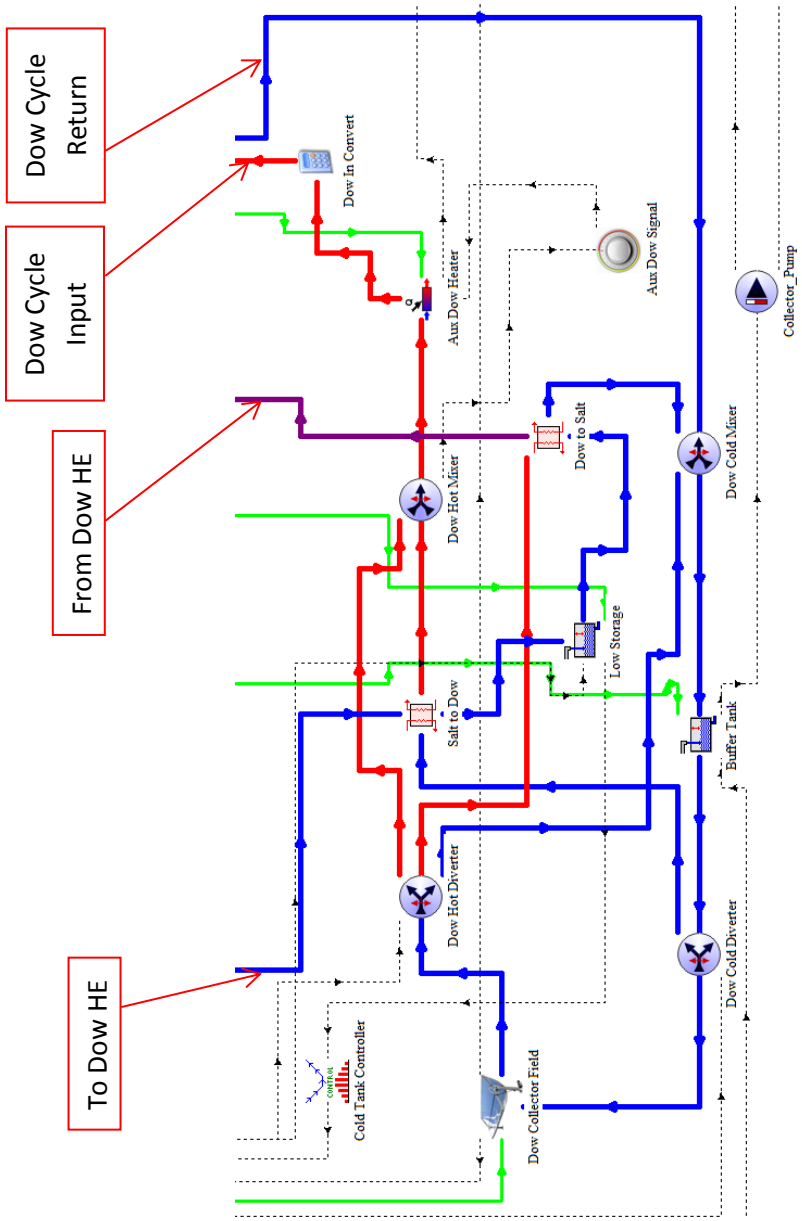

Figure 6.4 Dual Loop (Dowtherm Loop)

The Dowtherm loop does not have any built-in storage capacity. If the Dowtherm collector field does not produce sufficient flow rate for the cycle, additional flow is sent through a heat exchanger with molten salt drawn from the medium storage tank used as a heating fluid. The molten salt used to heat the Dowtherm is then sent to a low temperature storage tank. If there is insufficient storage from the medium salt storage, this flow is heated using auxiliary heating. In the case where Dowtherm collector field produces more flow rate than the cycle flow, molten salt is drawn from the cold storage tank, heated using the additional flow of Dowtherm, and sent back to the medium storage tank. All other aspects of the system operate the same as the single loop systems.

6.3 Collector Thermal Losses

The heat loss for the 2008 Schott collector is shown below. This curve was generated from experimentation performed by NREL (Buckholder 2009).

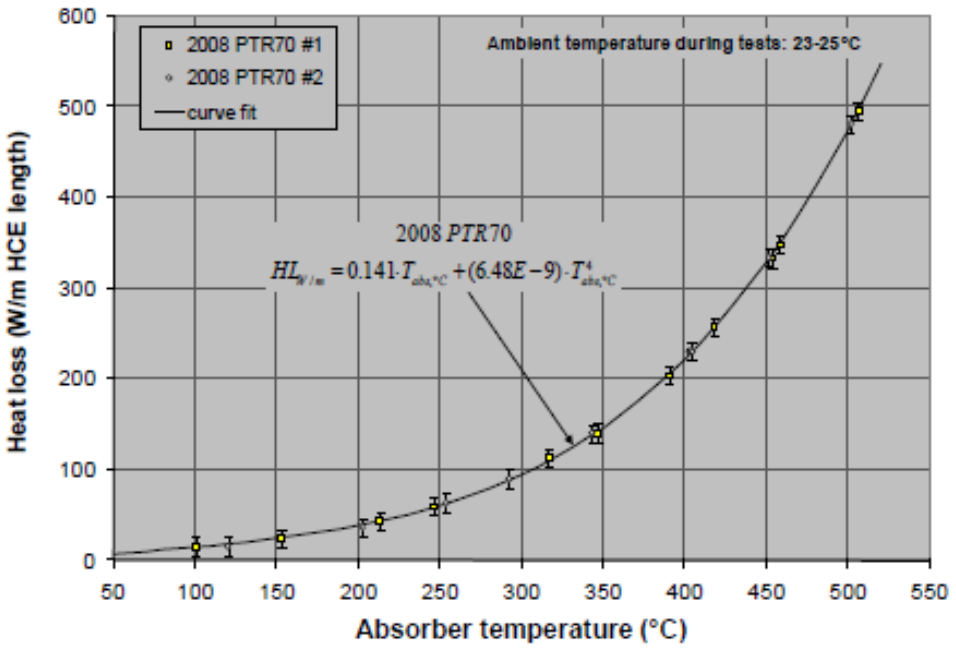

Figure 6.5 Heat Loss vs. Temperature for 2008 Schott Collector (Buckholder 2009)

The Dowtherm A operating temperatures are between 300°C and 400°C, and the molten salt operating temperatures are between 400°C and 550°C. Clearly, the heat losses for the molten salt will be much greater than that of Dowtherm for operation. A plot of the thermal losses for a typical summer week is shown in Figure 6.6.

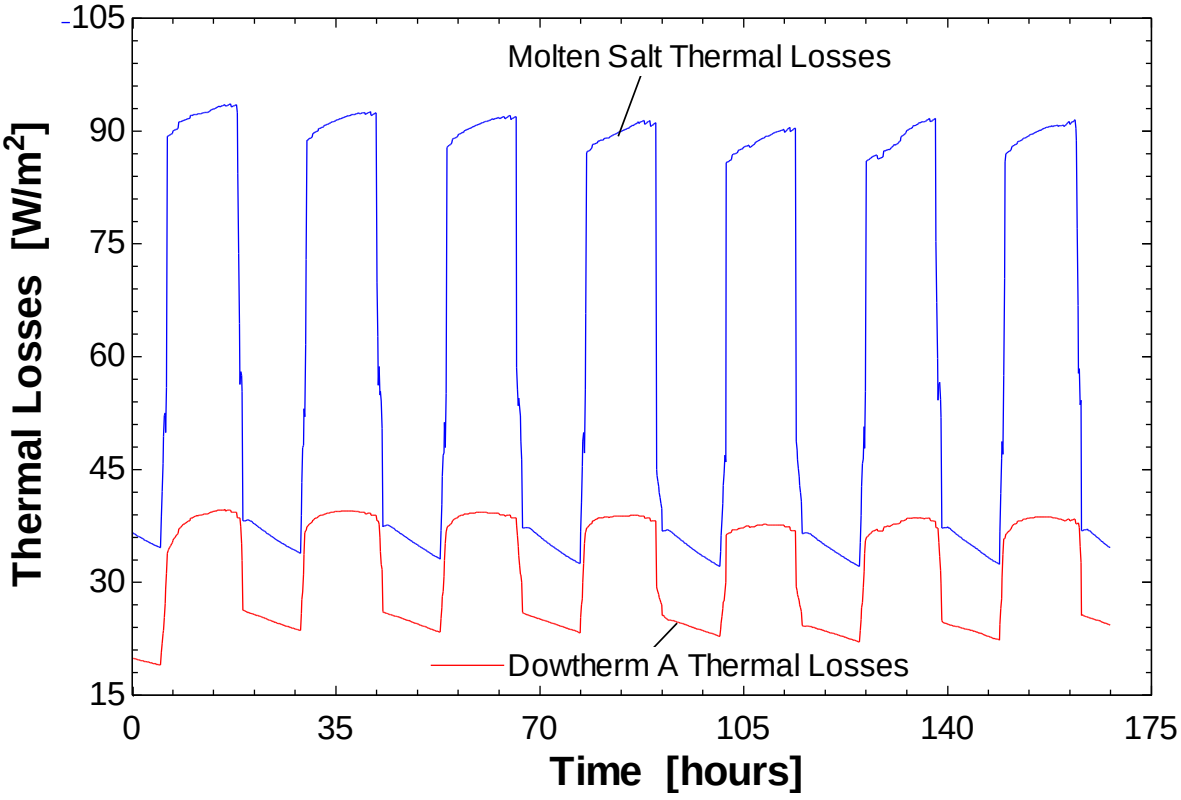

Figure 6.6 Collector Losses per unit area for a week in summer

During the collector field operation hours, the thermal losses for salt per unit area are more than double that of Dowtherm. For the annual simulations, the total thermal losses for each system are shown in Figure 6.7.

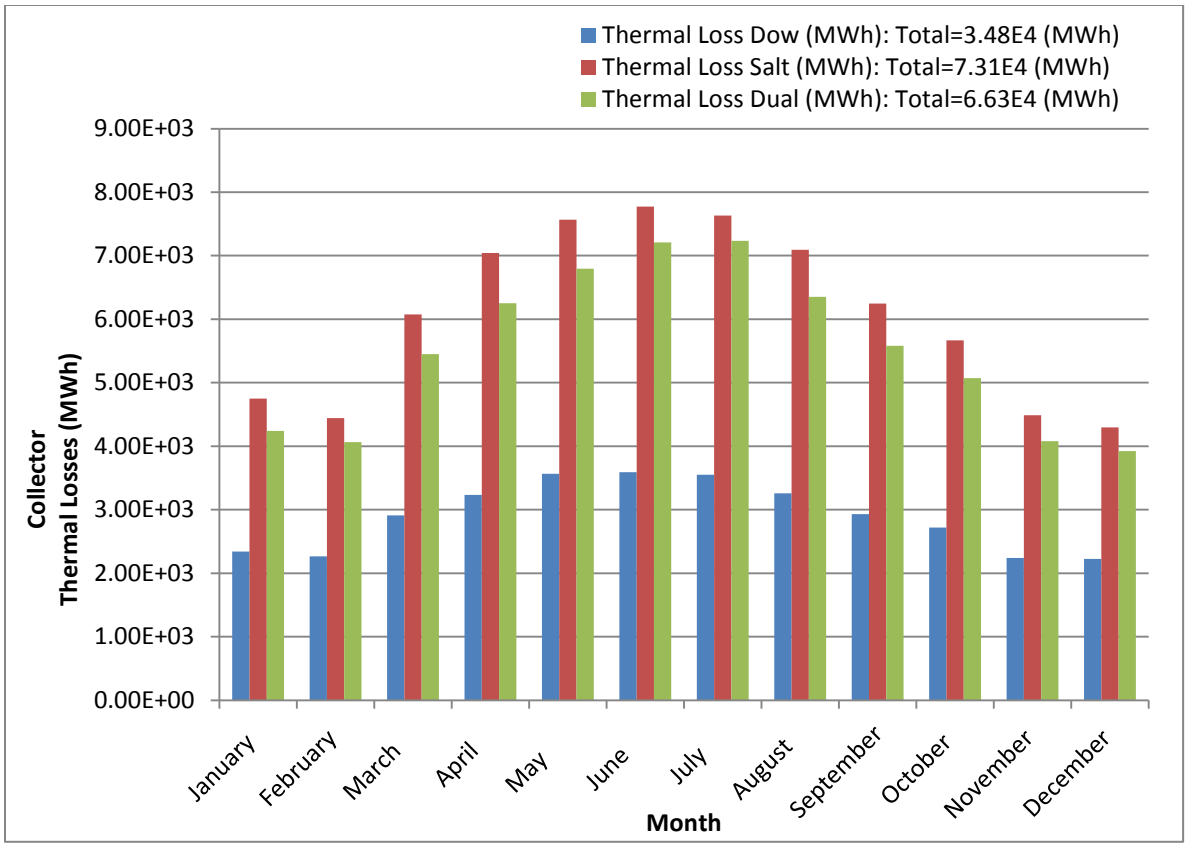

Figure 6.7 Collector Thermal Losses per month

The single loop of Dowtherm has the smallest thermal losses every month and annually, which is expected based on the information in Figure 6.5 and Figure 6.6. The dual loop system has lower collector losses than the single loop of salt, but is closer to the losses for salt than the losses for Dowtherm because the molten salt in the system enters the collector field at a higher temperature than in the single loop of salt system. For all hours of operation, the low temperature storage of salt in the single loop cycle is 70°C or more lower than the medium temperature storage in the dual loop system. Despite this, the dual loop system has an advantage regarding collector thermal losses by using Dowtherm in addition to molten salt.

6.4 Pump Losses

The parasitic pumping power required at design flow for the collector field for the SEGs power plant in Daggett, CA is 1.6 [MWe] (Patnode 2006). Therefore, at design, the parasitic pumping power is over 5% the design power output of the system. The pumping power requirement for each of these fluids must be analyzed to determine their effect on system outputs. The pumping power requirement is calculated using the correlations described in section 5.4. A plot of these correlations is shown again in Figure 6.8. The pumping power required for salt can be calculated based on the pumping power from the Dowtherm A generated from the System Advisory model. The derivation for Equation 6.1 is shown in section 5.4.

$$\frac{\dot{W}_{Dow}}{\dot{W}_{Salt}} = \frac{f_{fd,Dow}}{f_{fd,Salt}} \left(\frac{\rho_{Salt}}{\rho_{Dow}}\right)^2 \tag{6.1}$$

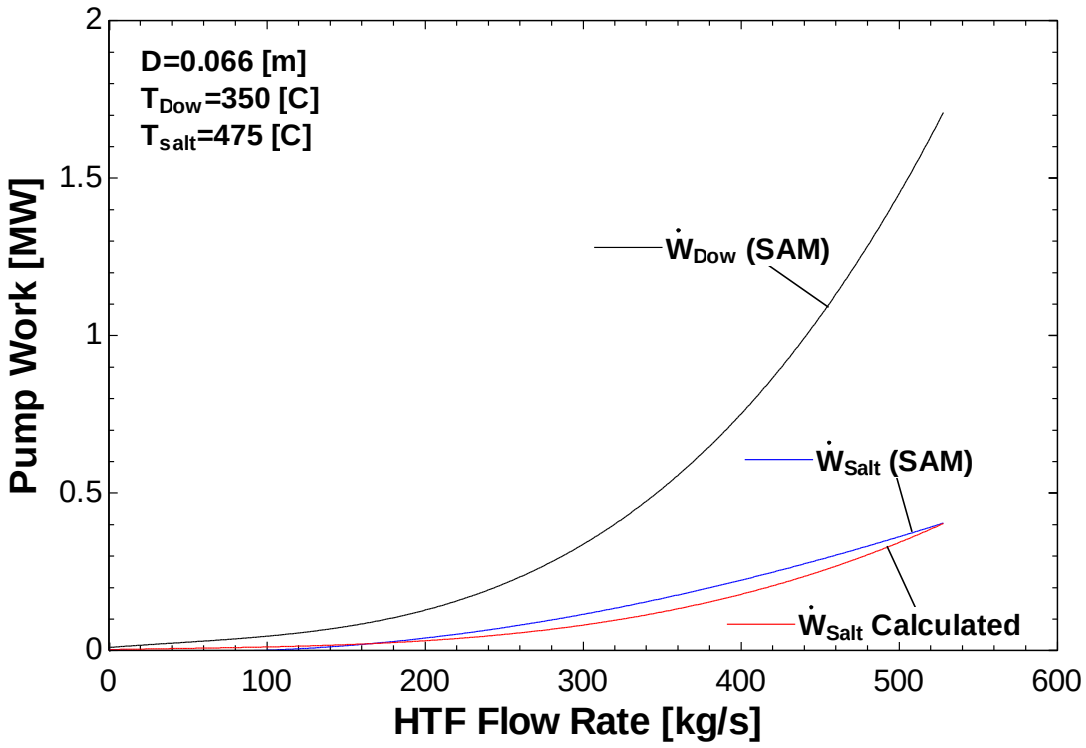

Figure 6.8 Pump Work vs. Mass Flow Rate

Based on the correlation generated from the System Advisory Model data and on equation 6.1, it is clear that the density of the fluid dominates the value of the pump work. The density of molten salt is approximately 1800 kg/s and the density of Dowtherm A is approximately 800 kg/s, so it is clear why the parasitic pumping power for Dowtherm is higher for the same mass flow rate. The study by Kearney (2003) corroborates this result. It states that the parasitic pumping losses using molten salt will be lower than an organic fluid in a parabolic trough solar field due to lower mass flow rates and a lower pressure drop.

The pumping losses for one year for each system are shown Figure 6.9.

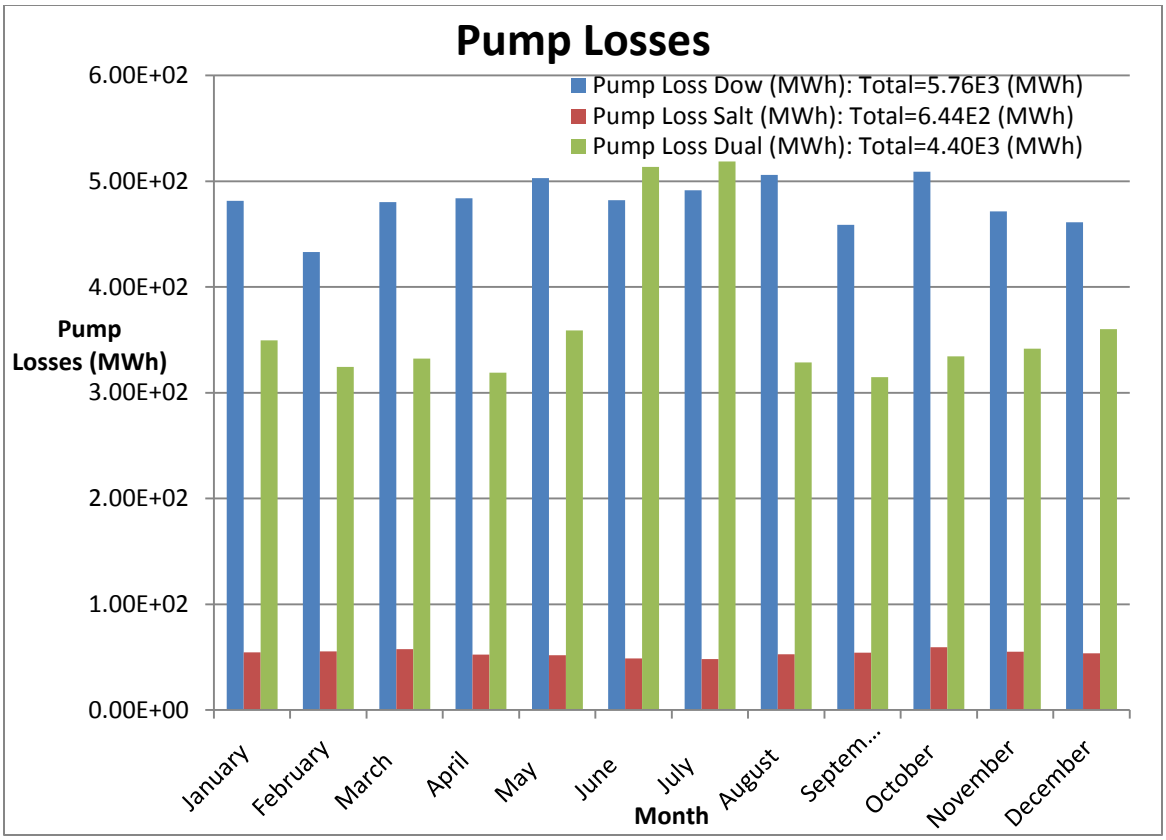

Figure 6.9 Pump Work per month

The pump work for the Dual loop system is between the two single loop cycles for most of the annual simulation. The exceptions are in June and July. For these months, the Dowtherm loop produces more flow rate than the power cycle requires. When this occurs, molten salt from the cold storage tank is heated using this excess flow and sent to the medium storage tank. However, in the summer months, the cold storage tank is quickly depleted. When this occurs, the excess flow of Dowtherm, which is not sent to the cycle, mixes with the Dowtherm returning from the power cycle. This increases the temperature of the Dowtherm entering the collector field. Since the outlet temperature of the collector field is fixed, the mass flow rate through the collector field increases, which acts like a positive

feedback loop and the excess Dowtherm flow continues to increase, thereby increasing pumping power. Figure 6.10 shows this effect.

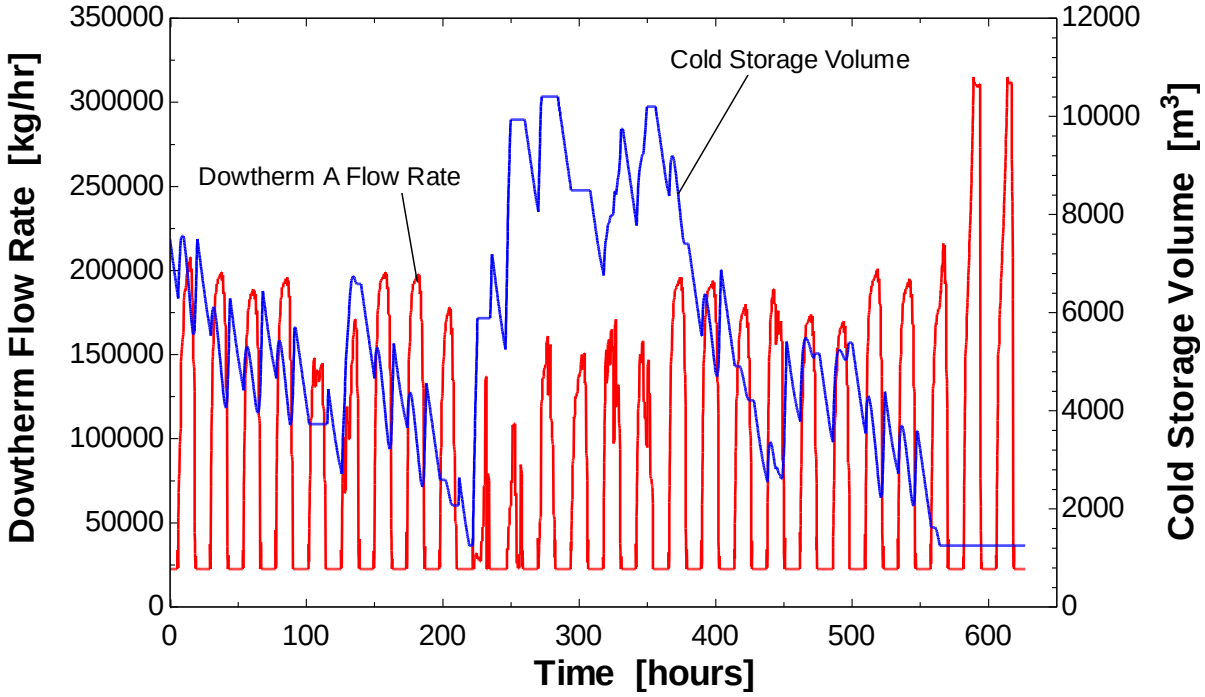

Figure 6.10 Dowtherm Collector Flow Rate vs. Time and Salt Cold Storage Volume vs. Time

The only way to combat this problem is to decrease the collector field area for the Dowtherm A to decrease the flow rate that can be produced by the field at the same outlet temperature. However, this has an overall detrimental effect to the system. If the Dowtherm A collector area is decreased by 20% and the molten salt collector area is increased by 20%, the auxiliary heating required increases by 6% and the net power output decreases 2.3%. This negative effect must be absorbed by the dual loop system for an optimum setup.

6.5 Auxiliary Heating

Auxiliary heating is used to heat the heat transfer fluid or fluids in each system so that the system can continue to produce power when thermal storage has been depleted. It is

assumed that each fluid can be heated with natural gas with the same efficiency. The auxiliary heating requirement for each fluid for each month is shown in Figure 6.11.

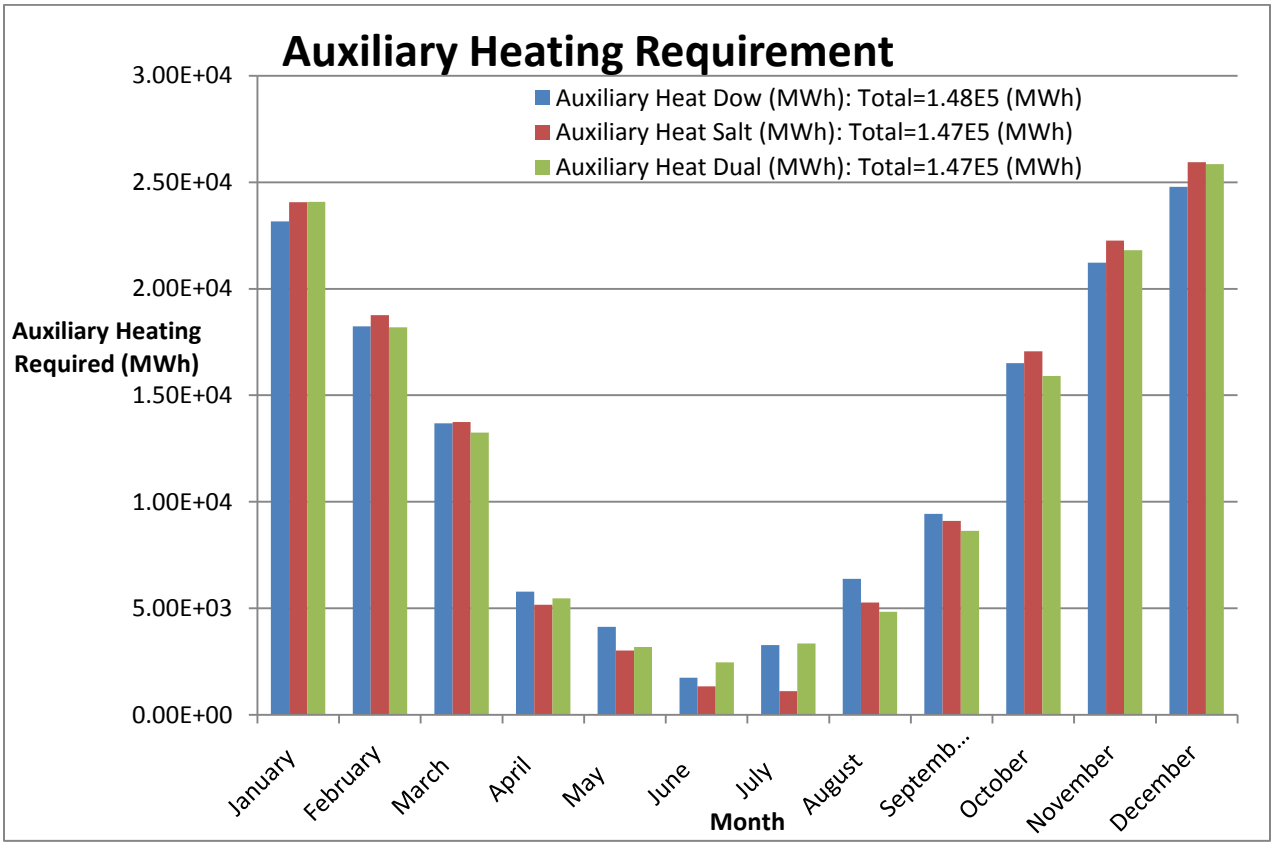

Figure 6.11 Heating Requirement per Month

The total auxiliary heating input was matched for every cycle. At first, the molten salt and the Dowtherm systems had the highest auxiliary heating requirement, but to ensure that Dual Loop system had the same access to natural gas heating, the parameters on the auxiliary heaters in the dual loop system were adjusted to match the auxiliary heating requirement. There are four different ways that auxiliary heating can be used in the dual loop system: the mass flow rate of Dowtherm can be increased, the temperature of Dowtherm can be increased, the mass flow rate of salt can be increased, or the temperature of salt can be increased. In order to determine which parameter had the most effect on increasing the

power output, the correlations from Section 4 were used. For a fixed value of auxiliary heating input, the effect of each one of these parameters is shown in the Table 6.1.

Table 6.1 Auxiliary Heating Parameters

Free Parameter	Dow Flow Rate (kg/s)	Dow Inlet Temperature (C)	Salt Flow Rate (kg/s)	Salt Inlet Temperature (C)	Power Output (MW)
Dow Inlet Temperature	358	**379.3**	150	520	26.2
Salt Inlet Temperature	358	363	150	**586.1**	26.04
Dow Flow Rate	**543.9**	363	150	520	26.03
Salt Flow Rate	358	363	**241.1**	520	22.74

In each case, all but one of these four parameters is held constant. The auxiliary heating input is held constant for each case. As shown, using auxiliary heating to increase the temperature of the Dowtherm has the most beneficial effect on power output. This would make sense because the Dowtherm is used for direct steam generation. If the Dowtherm has more energy, more steam can be generated in the power cycle. Increasing the flow rate of either fluid does not increase the power output as much as increasing the temperature. In addition, increasing the flow rate would also increase the parasitic pumping power.

The solar fraction can be defined in Equation 6.2.

$$SF = \frac{Q_{abs}}{Q_{abs} + Q_{aux}} \tag{6.2}$$

SF is the solar fraction; Q_{abs} is the radiation absorbed by the heat transfer fluid in the collector field, which includes thermal losses; Q_{aux} is the auxiliary heating supplied to the fluid. A plot of the solar fraction for each month is shown in Figure 6.12.

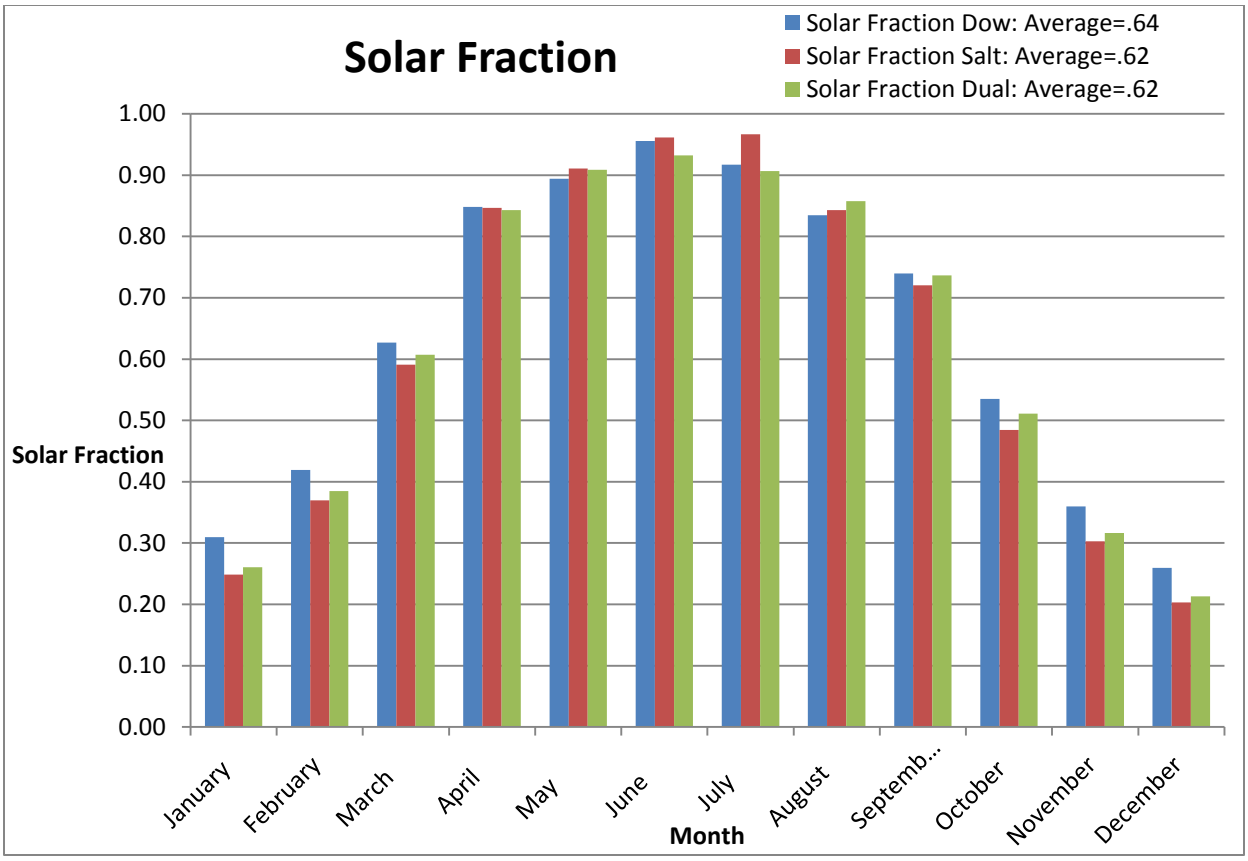

Figure 6.12 Solar Fraction per month

The solar fraction for Dowtherm is higher than the other two cycles due to lower thermal losses.

6.6 Results

To conclude this study, the net power and equipment usage are compared to determine the thermodynamic performance of each system over the course of a year. The net power output for each cycle is shown in Figure 6.13.

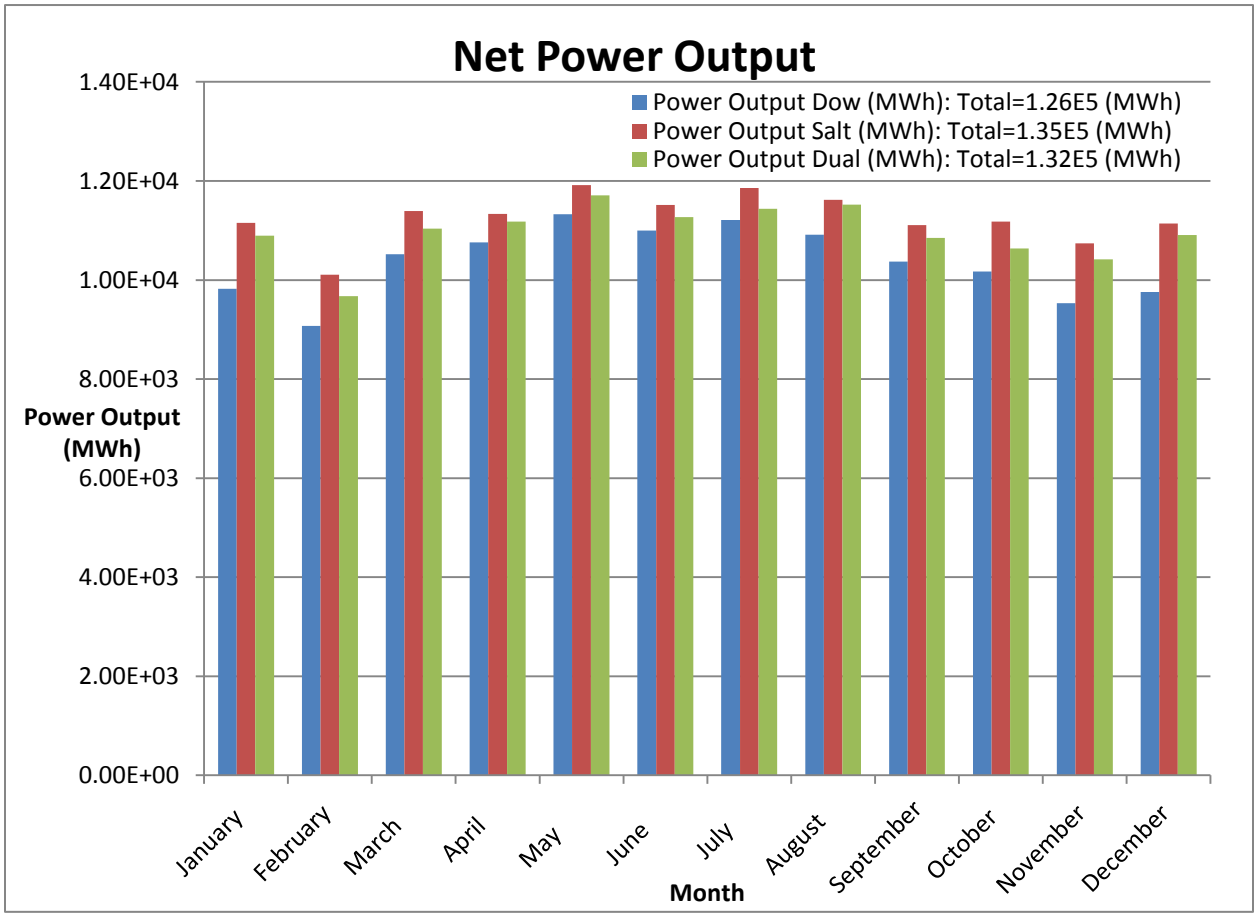

Figure 6.13 Net Power Output per month

According to Lang and Cuthbert (2011), the dual loop design has a better performance than a traditional single loop system containing an organic heat transfer fluid. Another study of dual loop also concludes that the dual loop system can reduce the levelized cost of electricity when compared to a single loop of organic fluid (Vogel 2014). Both of these studies conclude that utilizing molten salt as a second stage heating fluid can boost the power block

efficiency to 42%. All of these results are corroborated by this study. The dual loop system has an advantage in power cycle efficiency due to access to higher temperatures that increases the net power output for the same collector area. However, the molten salt system has the largest power output out of the three system designs, and this system type was not considered in the other two studies. The molten salt has a higher power output for the same temperatures as the dual loop due to the fact that the parasitic pumping power is significantly lower for salt than for Dowtherm A. Although the thermal losses for salt are higher, the loss of electrical energy in the form of pumping of Dowtherm A is far more significant. A comparison of the equipment uses for each system is shown in Table 6.2. The overall efficiency of the system is defined using equation 6.3.

$$\eta_{system} = \frac{\dot{W}_{net}}{\dot{Q}_{abs} + \dot{Q}_{aux}}$$

Table 6.2 System Comparison

	Collector Area (m^2)	Storage Volume (m^3)	Total UA (kW/K) (Does not include Condenser)	Net Power Output (MWh)	Overall System Efficiency
Single Loop Dow	200000	63500	2888	1.26E5	26.5%
Single Loop Salt	200000	30000	2746	1.35E5	28.9%
Dual Loop	200000	45000	3156	1.32E5	28.1%

Each system has roughly the same amount of total heat exchanger conductance (UA). However, this does not directly translate to the same amount of heat exchanger area. For the same Reynolds number for Dowtherm A and molten salt, the Nusselt numbers for both fluids are approximately the same. However, the thermal conductivity of salt is six times greater than Dowtherm, which means, if the Reynolds number is the same for each fluid in a heat

exchanger, the convective heat transfer coefficient for salt will be six times greater than that of Dowtherm. This means that the actual amount of heat exchanger area used in the single loop salt system is significantly less than the other two systems. Heat exchanger cost is a consideration, and the reduction in heat exchanger surface area for the salt may not translate into corresponding cost savings because of the need to use corrosion resistant materials for molten salt. However, for the same collector area, smaller storage area, and smaller heat exchangers, molten salt has the best thermodynamic performance out of each of these systems. Further economic analysis is needed to quantify the cost impact of installing heat tracing, corrosion resistant storage tanks, piping, and heat exchangers, to determine the viability of using molten salt in a parabolic trough field.

References

Bartlett, Robert L. Steam Turbine Performance and Economics. New York: McGraw-Hill, 1958.

Burkholder, F., and C. Kutsher. "Heat Loss Testing of Schott's 2008 PTR70 Parabolic Trough Receiver." National Renewable Energy Laboratory, NREL. Print. TP-550-45633. May 2009.

"Dowtherm A: Heat Transfer Fluid." *Product Technical Data*. Dow Chemical Co., 15 Mar. 1997. Web. 9 Aug. 2013.

Duffie, John A., and Beckman, William A. Solar Engineering of Thermal Processes. 4th edition. New York: John Wiley and Sons, Inc., 2013.

El-Wakil, M. M. *Powerplant Technology*. New York: McGraw-Hill Primis Custom Pub., 2002. Print.

Engineering Equation Solver (EES). Middleton, WI: F-Chart Software, 2014. Available at http://www.fchart.com.

Forristall, Russell. "Heat Transfer Analysis and Modeling of a Parabolic Trough Solar Receiver Implemented in Engineering Equation Solver." National Renewable Energy Laboratory, NREL/TP-550-34169. October 2003.

Incropera, Frank P., and DeWitt, David P. Fundamentals of Heat and Mass Transfer. 5th edition. New York: John Wiley and Sons, Inc., 2002.

Kearney, D., D. Blake, and H. Price. "Assessment of a Molten Salt Heat Transfer Fluid in a Parabolic Trough Solar Field." *Journal of Solar Energy Engineering* 125 (2003): 170-76. American Society of Mechanical Engineers. April 2002.

Klein, Sanford A., and Gregory Nellis. *Thermodynamics*. New York: Cambridge UP, 2012. Print.

Lang, Christoph, and John Cuthbert. "Evaluation of Dual Loop Design for Parabolic Trough." (2012): n. pag. Web.

Logan, Earl, and Ramenendra Roy. *Handbook of Turbomachinery*. New York: M. Dekker, 2003. Print.

"Molten Salts Properties." *Archimede Solar Energy*. http://www.archimedesolarenergy.it/molten_salt.htm. Web. 06 Dec. 2014.

Nellis, Gregory, and Sanford A. Klein. *Heat Transfer*. Cambridge: Cambridge UP, 2009. Print.

Angela, Patnode M. *Simulation and Performance Evaluation of Parabolic Trough Solar Power Plants*. Thesis. University of Wisconsin-Madison, 2006.

Price, Henry (Microsoft Excel program). Excelergy. Last updated 2005.

TRNSYS – A Transient System Simulation Program. Madison, WI: University of Wisconsin-Madison Solar Energy Laboratory. Available at http://sel.me.wisc.edu/trnsys/.

Solel UVAC (Website). "Solel #5 – the Only Proven and Cost Effective Parabolic Trough." Available at http://solel.com/products/pgeneration/tkey_fields/. Last accessed December 6, 2014.

Stodola, A., and Loewenstein, Louis C. Steam and Gas Turbines. Volume I. New York: McGraw-Hill Book Company, 1945.

System Advisor Model. Computer software. *Sytem Advisor Model (SAM)*. Vers. 1.14. National Renewable Energy Labratory, 14 Jan. 2014. Web. 10 Oct. 2014.

Vogel, A. K., H. Reiling, T. P. Fluri, and W. J. Platzer. "High Temperature in Line Focusing Systems." *AASRI Conference on Circuit and Signal Processing*. Proc. of SolarPACES, UK, London. AASRI Procedia, 30 June 2014. Web. 30 Sept. 2014.

Appendix A

Molten Salt Properties

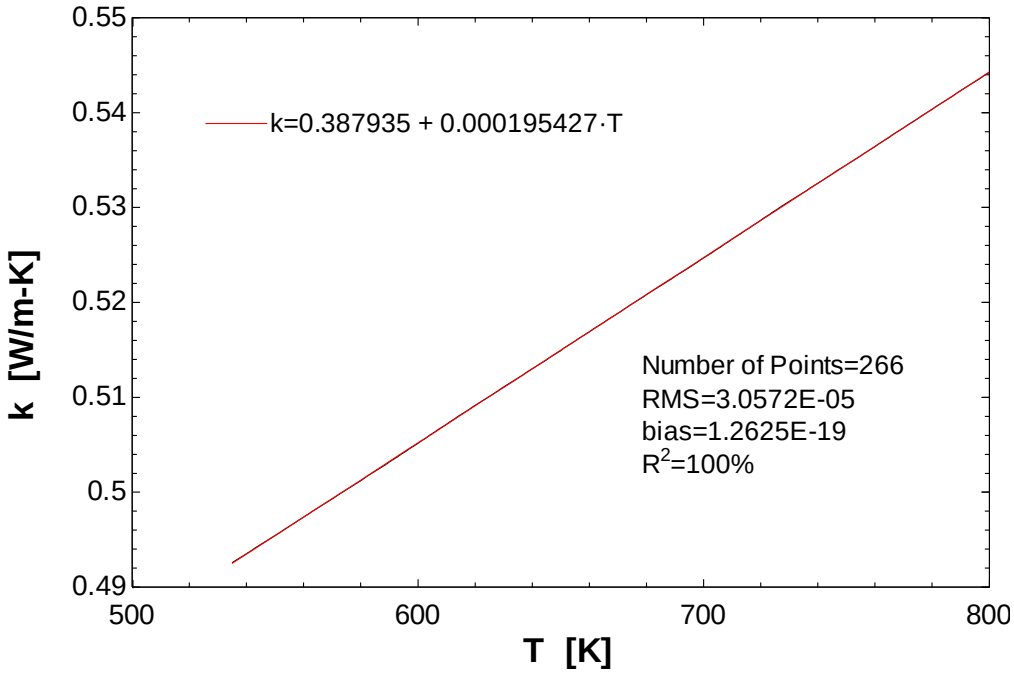

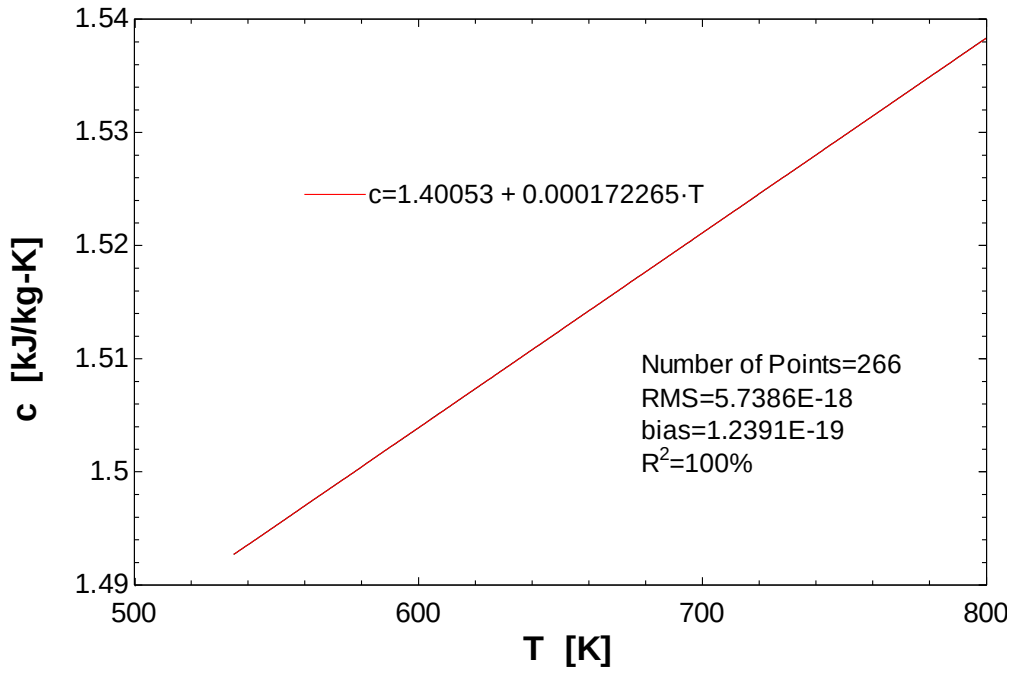

Figure A2 Molten Salt Conductivity

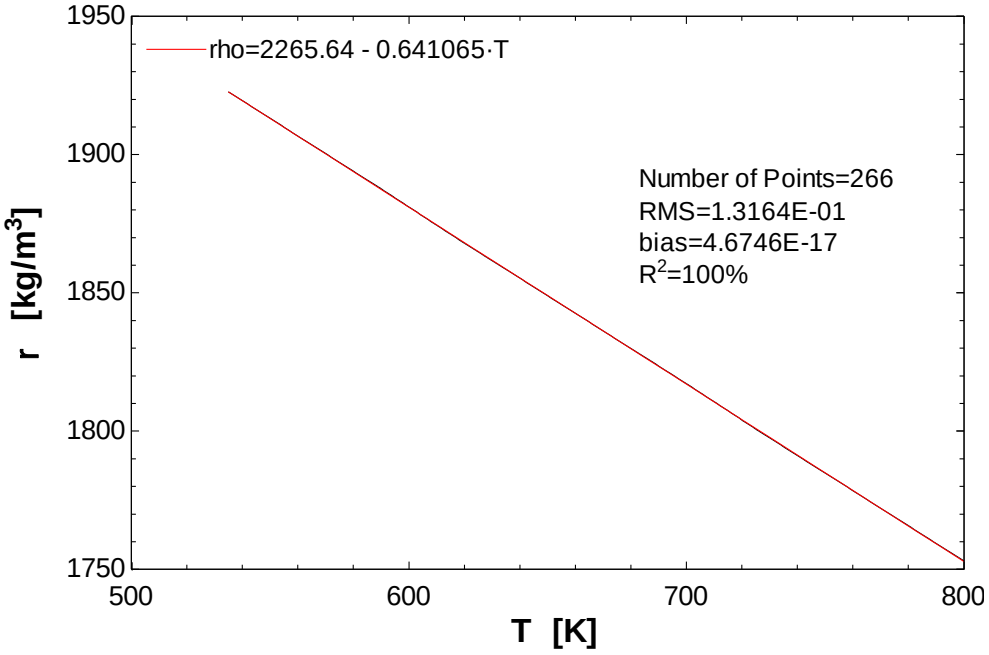

Figure A3 Molten Salt Density

Cellular Glass Properties

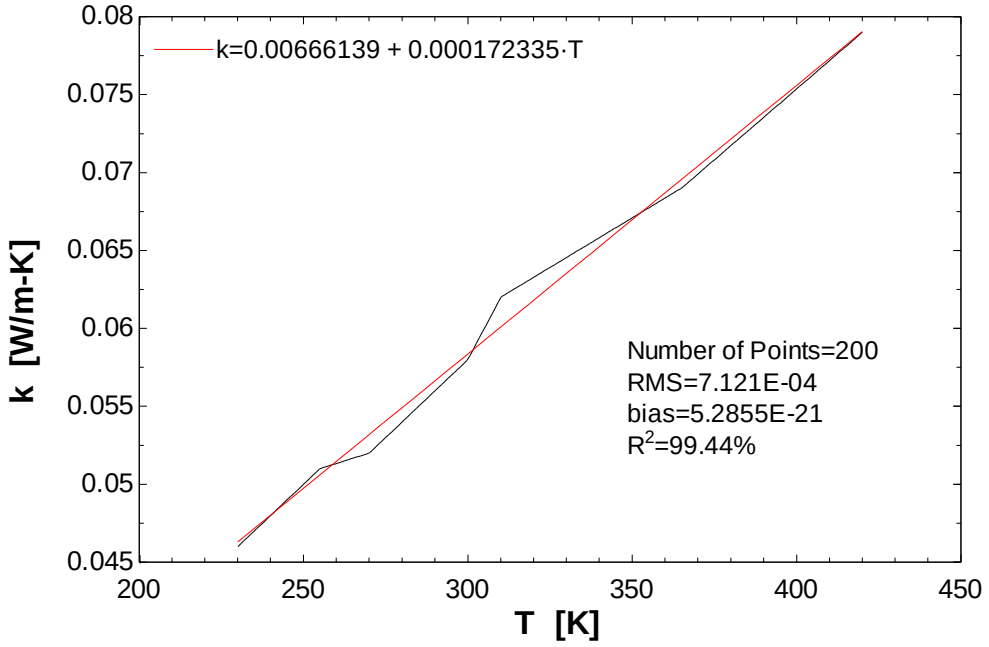

Figure A4 Cellular Glass Conductivity

Aluminum Casing Properties

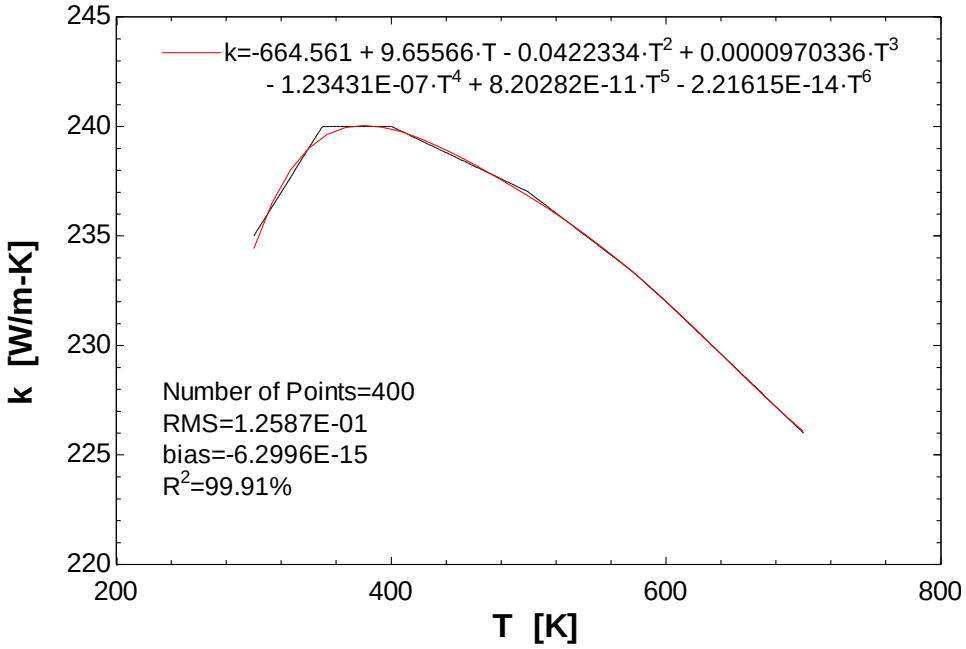

Figure A5 Aluminum Casing Conductivity

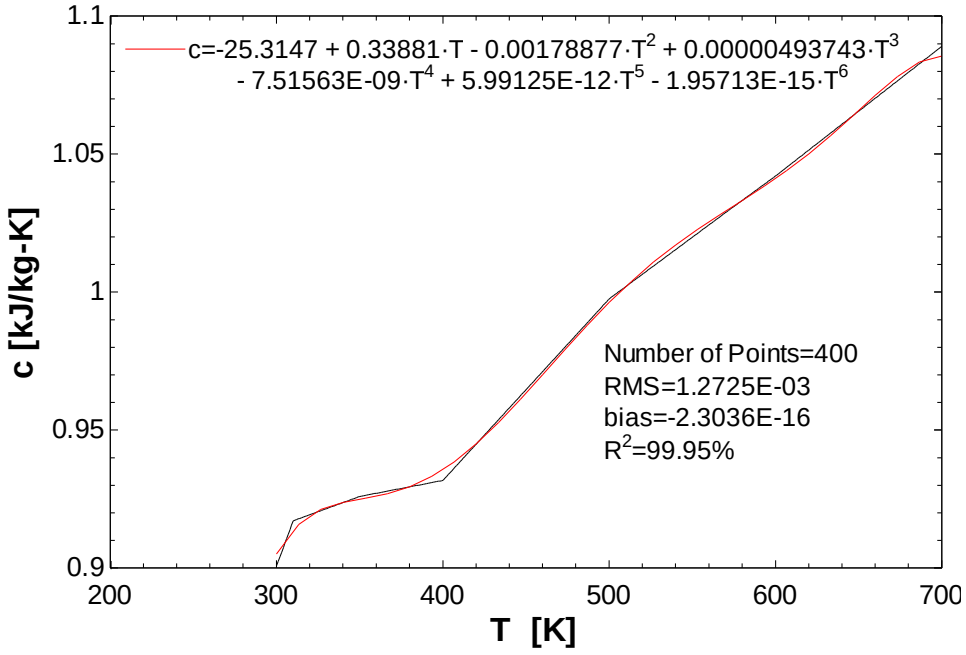

Figure A6 Aluminum Casing Specific Heat

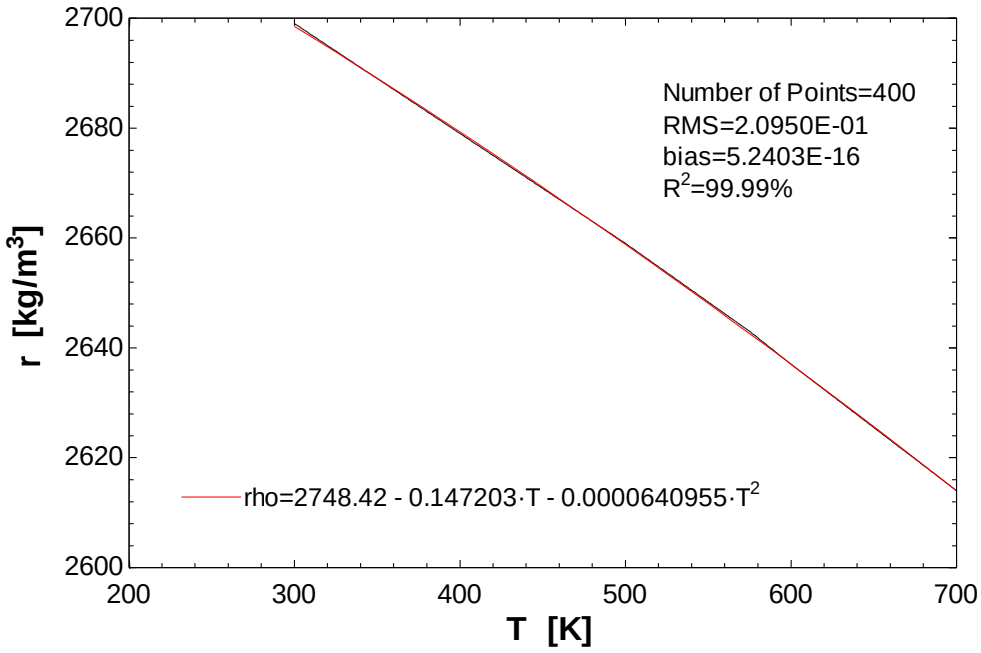

Figure A7 Aluminum Casing Density

Appendix B

Program Name	Software	Description
HCE Freezing Model	EES	Program used to model the time scale for freezing to begin in the heat collection element
Return Pipe Model	EES	Program used to model the time scale for freezing to begin in components connected to the heat collection element
Single Loop Design	EES	Program used to model the steam Rankine cycle design condition for the single loop of Dowtherm A
Single Loop MS Design	EES	Program used to model the steam Rankine cycle design condition for the single loop of molten salt (60% $NaNO_3$ / 40% KNO_3)
Dual Loop Design	EES	Program used to model the steam Rankine cycle design condition for the dual loop system utilizing both Dowtherm A and molten salt (60% $NaNO_3$ / 40% KNO_3)
Boiling UA	EES	Program used to determine the validity of using the scaling law outlined in Section 4.3 for the boiler
Preheater UA	EES	Program used to determine the validity of using the scaling law outlined in Section 4.3 for the preheater and other heat exchangers
Single Loop Off Design	EES	Program used to model the steam Rankine cycle off design conditions for the single loop of Dowtherm A
Single Loop MS Off Design	EES	Program used to model the steam Rankine cycle off design conditions for the single loop of molten salt (60% $NaNO_3$ / 40% KNO_3)
Dual Loop Off Design	EES	Program used to model the steam Rankine cycle off design conditions for the dual loop system utilizing both Dowtherm A and molten salt (60% $NaNO_3$ / 40% KNO_3)
Type850	Fortran Source	Program used to model the collectors field described in section 5.3. (This program was modified from Patnode)
Flow Controller	Type Studio	Program used to create type component described in section 5.6
Dual Flow Controller	Type Studio	Program used to create type component described in section 5.15
Flow Diverter	Type Studio	Program used to create type component described in section 5.8

Flow Mixer	Type Studio	Program used to create type component described in section 5.7
Flow Mixer Triple	Type Studio	Program used to create type component similar to the type component described in section 5.7
Collector Pump	Type Studio	Program used to create type component described in section 5.4
Collector Diverter	Type Studio	Program used to create type component described in section 5.9
Cooling Water Pump	Type Studio	Program used to create type component similar to the type component described in section 5.4
Single Loop Dowtherm	Type Studio	Program used to create type component associated with the single loop of Dowtherm A off design correlations listed in Table 4.2
Single Loop Salt	Type Studio	Program used to create type component associated with the single loop of molten salt off design correlations listed in Table 4.3
Dual Loop	Type Studio	Program used to create type component associated with the dual loop off design correlations listed in Table 4.4
Single Loop Dow	TRNSYS	Program that models the performance of the single loop of Dowtherm A system described in section 6.2
Single Loop MS	TRNSYS	Program that models the performance of the single loop of molten salt system described in section 6.2
Dual Loop	TRNSYS	Program that models the performance of the dual loop system described in section 6.2